

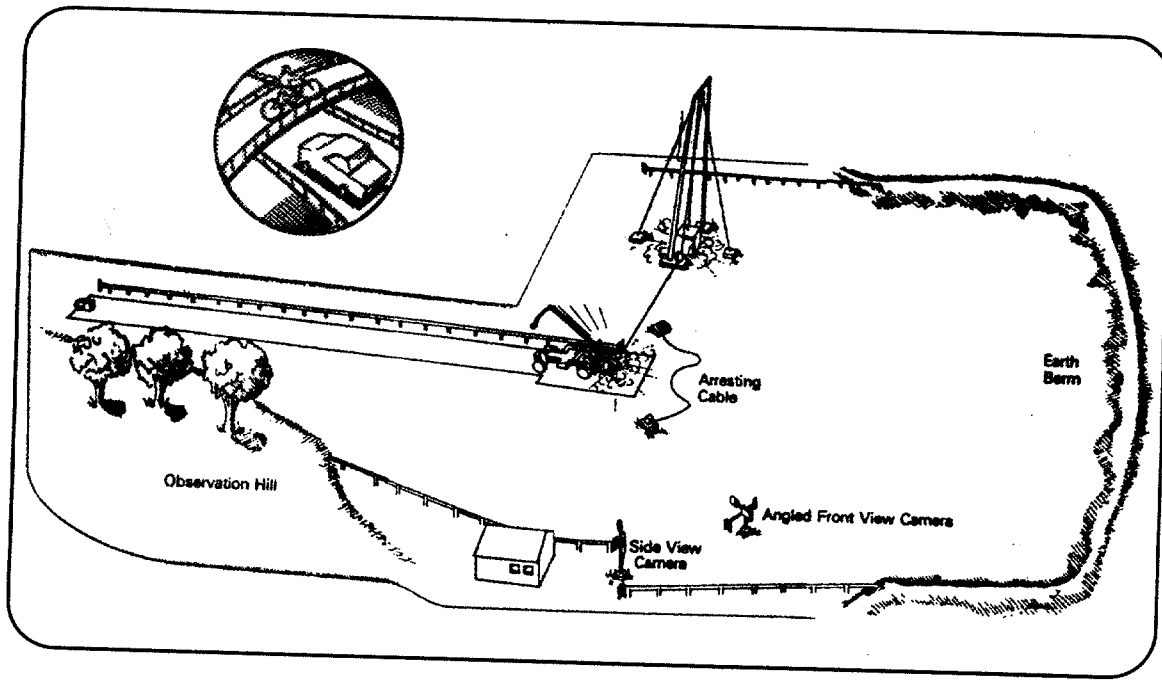
Crush Characteristics of the 1997 Geo

Metro, FOIL Test Numbers: 98F010

Through 98F015 and 99S001

PUBLICATION NO. FHWA-RD-01-047

MARCH 2001



FOIL



U.S. Department of Transportation
Federal Highway Administration

Research, Development, and Technology
Turner-Fairbank Highway Research Center
6300 Georgetown Pike
McLean, VA 22101-2296



FOREWORD

This report documents the results from six crash tests between 1997 Geo Metro two-door hatchbacks and the FOIL 300K rigid pole. The Federal Highway Administration (FHWA) has invested many resources in the development of finite element models (FEM) of passenger vehicles, pickup trucks, and roadside safety hardware. Computer simulations using these FEMs of collisions between the vehicles and roadside safety hardware are used to investigate the behavior of and improve the safety performance of roadside safety hardware. An essential step for developing the FEM is to validate the models by comparing data from simulation output with data collected from full-scale vehicle crash tests with roadside safety hardware. The FHWA's Federal Outdoor Impact Laboratory (FOIL) was used to conduct these five frontal-collision and one broadside collision rigid pole tests. The data from these tests will be used to develop and validate FEM of the Geo Metro. The nominal test speed for each test was 35 km/h and the nominal test weight of each vehicle was 820 kg.

This report (FHWA-RD-01-047) contains test data, photographs taken with high-speed film, and a summary of the test results.

This report will be of interest to all State departments of transportation; FHWA headquarters; region and division personnel; and highway safety researchers interested in the crashworthiness of roadside safety hardware.



Michael Trentacoste, Director
Office of Safety and Traffic
Operations Research and Development

NOTICE

This document is disseminated under the sponsorship of the Department of Transportation in the interest of information exchange. The United States Government assumes no liability for its contents or use thereof. This report does not constitute a standard, specification, or regulation.

The United States Government does not endorse products or manufacturers. Trade and manufacturers' names appear in this report only because they are considered essential to the object of the document.



Technical Report Documentation Page

1. Report No. FHWA-RD-01-047	2. Government Accession No.	3. Recipient's Catalog No.	
4. Title and Subtitle CRUSH CHARACTERISTICS OF THE 1997 GEO METRO, FOIL TEST NUMBERS: 98F010 THROUGH 98F015 AND 99S001		5. Report Date	
7. Author(s) Christopher M. Brown		6. Performing Organization Code	
9. Performing Organization Name and Address MiTech Incorporated 8484 Georgia Avenue, Suite 950 Silver Spring, MD 20910		8. Performing Organization Report No.	
12. Sponsoring Agency Name and Address Office of Safety and Traffic Operations R&D Federal Highway Administration 6300 Georgetown Pike McLean, VA 22101-2296		10. Work Unit No. (TRAIS) 3A5f3142	
		11. Contract or Grant No. DTFH61-99-F-00104	
15. Supplementary Notes Contracting Officer's Technical Representative (COTR) Charles McDevitt		13. Type of Report and Period Covered Final Report, Jan. to May 1999	
16. Abstract			
<p>This report contains the test procedures followed and test results from five frontal and one broadside crash test between 1997 Geo Metros and the FOIL instrumented 300K rigid pole. The tests were conducted at the Federal Highway Administration's (FHWA) Federal Outdoor Impact Laboratory (FOIL) located at the Turner-Fairbank Highway Research Center (TFHRC) in McLean, Virginia. The target test speed for each test was 35 km/h and the target test weight (no dummy was used for these tests) was 820 kg. The crush profile, electronic data, and high-speed film from these tests will aid computer simulation engineers in developing and validating finite element models of the Geo Metro and roadside safety hardware. The data will also be used to redesign the reusable honeycomb nose of the FOIL bogie vehicle to resemble the crush stroke of the Geo Metro.</p>			
17. Key Words Geo Metro, crush profile, force, acceleration, energy, FOIL, rigid pole, broadside, frontal full-scale testing		18. Distribution Statement No restrictions. This document is available to the public through the National Technical Information Service, Springfield, VA 22161.	
19. Security Classif (of this report) Unclassified	20. Security Classif. (of this page) Unclassified	21. No. of Pages 203	22. Price



Table of Contents

	<u>Page</u>
INTRODUCTION	1
MATRIX	2
VEHICLE	2
RIGID POLE TEST DEVICE	3
INSTRUMENTATION	
Speed trap.	15
Transducer data.	15
High-speed photography.	15
.	19
DATA ANALYSIS	
Speed trap.	19
Transducer data package.	19
High-speed photography.	22
.	22
RESULTS	23
CONCLUSIONS	24
APPENDIX A. VEHICLE CRUSH MEASUREMENTS	32
APPENDIX B. TEST PHOTOGRAPHS	38
APPENDIX C. DATA PLOTS	62
REFERENCES	195



List of Figures

<u>Figure</u>	<u>Page</u>
1. Vehicle properties for test 98F010.	5
2. Vehicle properties for test 98F011.	6
3. Vehicle properties for test 98F012.	7
4. Vehicle properties for test 98F014.	8
5. Vehicle properties for test 98F015.	9
6. Vehicle properties for test 99S001.	10
7. Sketch of test vehicle engine compartment and target frontal impact locations	11
8. Overhead sketch of 1997 Geo Metro including target side impact location	12
9. Sketch of FOIL rigid pole frontal configuration	13
10. Sketch of FOIL rigid pole, side impact configuration	14
11. Camera placement and test setup for the five frontal impact tests, tests 98F010 through 98F015	20
12. Camera placement and test setup for the broadside test, test 99S001	21
13. Peak force vs. delta velocity, five frontal Geo Metro crash tests	29
14. Force vs. displacement, five frontal Geo Metro crash tests	30
15. Energy vs. displacement, five frontal Geo Metro crash tests	31
16. Vehicle deformation sketch, test 98F010.	32
17. Vehicle deformation sketch, test 98F011.	33
18. Vehicle deformation sketch, test 98F012.	34
19. Vehicle deformation sketch, test 98F014.	35
20. Vehicle deformation sketch, test 98F015.	36
21. Vehicle deformation sketch, test 99S001.	37
22. Photographs during the test, test 98F010	38
23. Pre-test photographs, test 98F010	39
24. Post-test photographs, test 98F010	40
25. Additional post-test photographs, test 98F010.	41
26. Photographs during the test, test 98F011	42
27. Pre-test photographs, test 98F011	43
28. Post-test photographs, test 98F011	44
29. Additional post-test photographs, test 98F011.	45
30. Photographs during the test, test 98F012	46
31. Pre-test photographs, test 98F012	47
32. Post-test photographs, test 98F012	48
33. Additional post-test photographs, test 98F012.	49
34. Photographs during the test, test 98F014	50
35. Pre-test photographs, test 98F014	51
36. Post-test photographs, test 98F014	52
37. Additional post-test photographs, test 98F014.	53
38. Photographs during the test, test 98F015	54



List of Figures (continued)

<u>Figure</u>	<u>Page</u>
39. Pre-test photographs, test 98F015	55
40. Post-test photographs, test 98F015	56
41. Additional post-test photographs, test 98F015.	57
42. Photographs during the test, test 99S001	58
43. Pre-test photographs, test 99S001	59
44. Post-test photographs, test 99S001	60
45. Additional post-test photographs, test 99S001.	61
46. C.g. acceleration vs. time, X-axis, test 98F010.	62
47. C.g. velocity vs. time, X-axis, test 98F010.	63
48. C.g. displacement vs. time, X-axis, test 98F010.	64
49. C.g. force vs. displacement, X-axis, test 98F010	65
50. C.g. energy vs. displacement, X-axis, test 98F010.	66
51. C.g. acceleration vs. time, Y-axis, test 98F010.	67
52. C.g. acceleration vs. time, Z-axis, test 98F010.	68
53. Rigid pole, force vs. time, test 98F010.	69
54. Rigid pole, acceleration vs. time, test 98F010	70
55. Rigid pole, velocity vs. time, test 98F010	71
56. Rigid pole, displacement vs. time, test 98F010	72
57. Rigid pole, force vs. displacement, test 98F010.	73
58. Rigid pole, energy vs. displacement, test 98F010	74
59. Impact force height vs. displacement, test 98F010	75
60. Top of engine acceleration vs. time, X-axis, test 98F010	76
61. Bottom of engine acceleration vs. time, X-axis, test 98F010	77
62. Left control arm acceleration vs. time, X-axis, test 98F010	78
63. Right control arm acceleration vs. time, X-axis, test 98F010	79
64. Instrument panel acceleration vs. time, X-axis, test 98F010	80
65. Pitch rate and angle vs. time, test 98F010	81
66. Roll rate and angle vs. time, test 98F010.	82
67. Yaw rate and angle vs. time, test 98F010	83
68. C.g. acceleration vs. time, X-axis, test 98F011.	84
69. C.g. velocity vs. time, X-axis, test 98F011.	85
70. C.g. displacement vs. time, X-axis, test 98F011.	86
71. C.g. force vs. displacement, X-axis, test 98F011	87
72. C.g. energy vs. displacement, X-axis, test 98F011.	88
73. C.g. acceleration vs. time, Y-axis, test 98F011.	89
74. C.g. acceleration vs. time, Z-axis, test 98F011.	90
75. Rigid pole, force vs. time, test 98F011.	91
76. Rigid pole, acceleration vs. time, test 98F011	92
77. Rigid pole, velocity vs. time, test 98F011	93
78. Rigid pole, displacement vs. time, test 98F011	94
79. Rigid pole, force vs. displacement, test 98F011.	95
80. Rigid pole, energy vs. displacement, test 98F011	96



List of Figures (continued)

<u>Figure</u>	<u>Page</u>
81. Impact force height vs. displacement, test 98F011. . .	97
82. Top of engine acceleration vs. time, X-axis, test 98F011	98
83. Bottom of engine acceleration vs. time, X-axis, test 98F011	98
84. Left control arm acceleration vs. time, X-axis, test 98F011	99
85. Right control arm acceleration vs. time, X-axis, test 98F011	100
86. Instrument panel acceleration vs. time, X-axis, test 98F011	101
87. Pitch rate and angle vs. time, test 98F011	102
88. Roll rate and angle vs. time, test 98F011.	103
89. Yaw rate and angle vs. time, test 98F011	104
90. C.g. acceleration vs. time, X-axis, test 98F012.	105
91. C.g. velocity vs. time, X-axis, test 98F012.	106
92. C.g. displacement vs. time, X-axis, test 98F012.	107
93. C.g. force vs. displacement, X-axis, test 98F012	108
94. C.g. energy vs. displacement, X-axis, test 98F012	109
95. C.g. acceleration vs. time, Y-axis, test 98F012.	110
96. C.g. acceleration vs. time, Z-axis, test 98F012.	111
97. Rigid pole, force vs. time, test 98F012.	112
98. Rigid pole, acceleration vs. time, test 98F012	113
99. Rigid pole, velocity vs. time, test 98F012	114
100. Rigid pole, displacement vs. time, test 98F012	115
101. Rigid pole, force vs. displacement, test 98F012	116
102. Rigid pole, energy vs. displacement, test 98F012	117
103. Impact force height vs. displacement, test 98F012	118
104. Top of engine acceleration vs. time, X-axis, test 98F012	119
105. Bottom of engine acceleration vs. time, X-axis, test 98F012	120
106. Left control arm acceleration vs. time, X-axis, test 98F012	121
107. Right control arm acceleration vs. time, X-axis, test 98F012	122
108. Instrument panel acceleration vs. time, X-axis, test 98F012	123
109. Pitch rate and angle vs. time, test 98F012.	124
110. Roll rate and angle vs. time, test 98F012	125
111. Yaw rate and angle vs. time, test 98F012.	126
112. C.g. acceleration vs. time, X-axis, test 98F014	127
113. C.g. velocity vs. time, X-axis, test 98F014	128
114. C.g. displacement vs. time, X-axis, test 98F014	129
115. C.g. force vs. displacement, X-axis, test 98F014	130
116. C.g. energy vs. displacement, X-axis, test 98F014	131
117. C.g. acceleration vs. time, Y-axis, test 98F014	132
	133



List of Figures (continued)

<u>Figure</u>	<u>Page</u>
118. C.g. acceleration vs. time, Z-axis, test 98F014 . . .	134
119. Rigid pole, force vs. time, test 98F014	135
120. Rigid pole, acceleration vs. time, test 98F014	136
121. Rigid pole, velocity vs. time, test 98F014.	137
122. Rigid pole, displacement vs. time, test 98F014	138
123. Rigid pole, force vs. displacement, test 98F014	139
124. Rigid pole, energy vs. displacement, test 98F014.	140
125. Impact force height vs. displacement, test 98F014	140
126. Top of engine acceleration vs. time, X-axis, test 98F014	141
127. Bottom of engine acceleration vs. time, X-axis, test 98F014	142
128. Left control arm acceleration vs. time, X-axis, test 98F014	143
129. Right control arm acceleration vs. time, X-axis, test 98F014	144
130. Pitch rate and angle vs. time, test 98F014.	145
131. Roll rate and angle vs. time, test 98F014	146
132. Yaw rate and angle vs. time, test 98F014.	147
133. C.g. acceleration vs. time, X-axis, test 98F015	148
134. C.g. velocity vs. time, X-axis, test 98F015	149
135. C.g. displacement vs. time, X-axis, test 98F015	150
136. C.g. force vs. displacement, X-axis, test 98F015	151
137. C.g. energy vs. displacement, X-axis, test 98F015.	152
138. C.g. acceleration vs. time, Y-axis, test 98F015	153
139. C.g. acceleration vs. time, Z-axis, test 98F015	154
140. Rigid pole, force vs. time, test 98F015	155
141. Rigid pole, acceleration vs. time, test 98F015.	156
142. Rigid pole, velocity vs. time, test 98F015.	157
143. Rigid pole, displacement vs. time, test 98F015.	158
144. Rigid pole, force vs. displacement, test 98F015	159
145. Rigid pole, energy vs. displacement, test 98F015	160
146. Impact force height vs. displacement, test 98F015.	161
147. Top of engine acceleration vs. time, X-axis, test 98F015	162
148. Bottom of engine acceleration vs. time, X-axis, test 98F015	163
149. Left control arm acceleration vs. time, X-axis, test 98F015	164
150. Right control arm acceleration vs. time, X-axis, test 98F015.	165
151. Pitch rate and angle vs. time, test 98F015.	166
152. Roll rate and angle vs. time, test 98F015.	167
153. Yaw rate and angle vs. time, test 98F015	168
154. C.g. acceleration vs. time, Y-axis, test 99S001	169
155. C.g. velocity vs. time, Y-axis, test 99S001	170
156. C.g. displacement vs. time, Y-axis, test 99S001	171
	172



List of Figures (continued)

<u>Figure</u>	<u>Page</u>
157. C.g. force vs. displacement, Y-axis, test 99S001 . . .	173
158. C.g. energy vs. displacement, Y-axis, test 99S001 . . .	174
159. C.g. acceleration vs. time, X-axis, test 99S001 . . .	175
160. Cg acceleration vs. time, Z-axis, test 99S001 . . .	176
161. Rigid pole, force vs. time, test 99S001	176
162. Rigid pole, acceleration vs. time, test 99S001	177
163. Rigid pole, velocity vs. time, test 99S001	178
164. Rigid pole, displacement vs. time, test 99S001	179
165. Rigid pole, force vs. displacement, test 99S001	180
166. Rigid pole, energy vs. displacement, test 99S001	181
167. Outer door-skin, acceleration vs. time, test 99S001 .	182
168. Interior of door, acceleration vs. time, test 99S001 .	183
169. Top of engine acceleration vs. time, Y-axis, test 99S001 .	184
170. Top of engine acceleration vs. time, X-axis, test 99S001 .	185
171. Seat track acceleration vs. time, Y-axis, test 99S001 .	186
172. Passenger side roof-sill acceleration vs. time, Y-axis, test 99S001 .	187
173. Passenger side floor-sill acceleration vs. time, Y-axis, test 99S001 .	188
174. Acceleration vs. time, above rear axle, Y-axis, test 99S001 .	189
175. Acceleration vs. time, above rear axle, X-axis, test 99S001 .	190
176. Pitch rate and angle vs. time, test 99S001	191
177. Roll rate and angle vs. time, test 99S001	192
178. Yaw rate and angle vs. time, test 99S001	193
	194



List of Tables

Table

	<u>Page</u>
1. Test matrix for Geo Metro crash tests.	2
2. Inertial properties of 1997 Geo Metro.	3
3. Summary of instrumentation and channel assignments for tests 98F010 through 98F015 (frontal tests)	16
4. Summary of instrumentation and channel assignments for broadside crash test 99S001	17
5. Summary of camera placement	19
6. Summary of results from six 1997 Geo Metro/rigid pole tests	26
7. Summary of sensor output, maximum and minimum values for tests 98F010 through 98F015 (frontal testing).	27
8. Summary of sensor output for test 99S001 (broadside test).	28



INTRODUCTION

The Federal Highway Administration (FHWA) has invested many resources in the development of finite element models (FEM) of passenger vehicles, pickup trucks, and roadside safety hardware. Computer simulations using these FEMs of collisions between the vehicles and roadside safety hardware are used to investigate the behavior of and improve the safety performance of roadside safety hardware. An essential step for developing the FEM is to validate the vehicle models by comparing data from simulation output with data collected from full-scale vehicle crash tests.

The following report outlines the test procedures and test results from a series of six crash tests conducted at the Federal Outdoor Impact Laboratory (FOIL) located at the Turner-Fairbank Highway Research Center (TFHRC) in McLean, Virginia. Each of the six tests involved a 1997 Geo Metro striking the FOIL instrumented rigid pole. The vehicles collided with the rigid pole in either a frontal or broadside orientation. The rigid pole was used to ensure that the total initial energy was consumed by vehicle deformation. The vehicles used for this study were 1997 Geo Metro LSi two-door coupes (4-cylinder model) which is the recommended 820C test vehicle described in the National Cooperative Highway Research Program Report 350 (NCHRP Report 350)⁽¹⁾. The nominal vehicle weight (820 kg) and initial velocity (35 km/h) were held constant for each test. Five frontal impacts and one broadside collision were conducted. The impact location along the vehicles' front end was changed for each of the five frontal tests. This was done to obtain crush profile data at various locations across the vehicle front end. The objectives of these tests were to:

- Provide electronic data, high-speed film coverage, and analysis from full-scale vehicle collisions to the FEM community (specifically the NCAC) to aid in the development and validation of a Geo Metro FEM. Both a frontal and broadside FEM will be validated with the data collected during these tests.
- Collect baseline frontal crush profile or characteristic data to be used to develop a new crushable honeycomb nose for the FOIL breakaway bogie vehicle. The current honeycomb nose was developed to replicate the crush characteristics of a 1979 Volkswagen Rabbit's front left quarter point.

Vehicle crush characteristic data plots for each impact location and data plots generated from each sensor output are presented in Appendix C. Vehicle crush characteristic properties are presented as graphs of force vs. displacement, energy vs. displacement, peak force vs. delta velocity, and displacement vs. time. These plots profile the stiffness of the vehicle at a given impact location. In addition to the crush profile data



plots, data plots from each sensor affixed to the test vehicles and rigid pole are included. The sensor data plots include but are not limited to acceleration vs. time, force vs. time, and velocity vs. time. The data plots were generated from vehicle center-of-gravity (c.g.) accelerometer data, rigid pole load cell data, and vehicle component (engine, caliper, etc.) accelerometer data.

MATRIX

Five frontal collisions and one broadside collision between a Geo Metro and the FOIL rigid pole were conducted. The five frontal-impact tests provided crush characteristic data for five different locations along the Geo Metro front end. One broadside crash test provided side crush profile data at one specific location. The crash tests were conducted by accelerating the Geo Metros to a target speed of 35 km/h prior to striking the FOIL rigid pole. The target weight of the Geo Metros was 820 kg. A dummy was not used for this test program. Table 1 outlines the matrix for the six Geo Metro tests.

Table 1. Test matrix for Geo Metro crash tests.

Test number	Target weight	Target speed	Test device	Vehicle impact location/angle
98F010	820 kg	35 km/h	Rigid pole	Left hard point, 470 mm left of center / 0°
98F011	820 kg	35 km/h	Rigid pole	Midway between vehicle center and left hard pt., 230 mm left of center / 0°
98F012	820 kg	35 km/h	Rigid pole	Vehicle center / 0°
98F014	820 kg	35 km/h	Rigid pole	Midway between vehicle center and right hard pt., 230 mm right of center / 0°
98F015	820 kg	35 km/h	Rigid pole	Right hard point, 470 mm right of center / 0°
99S001	820 kg	35 km/h	Rigid pole	Broadside, mid-door 1,060 mm behind front axle / 90°

VEHICLE

The test vehicles used were 1997 Geo Metro LSi two-door hatch backs with automatic transmissions. Prior to each test each vehicle was drained of all fluids and its curb weight recorded. The vehicle's inertial properties were then measured



using the FOIL inertial measurement device (IMD). The vehicles were stripped of certain components (spare tire, rear seat, shifter linkage, etc.) and instrumented with data acquisition equipment, sensors, and vehicle guidance equipment. The final vehicle test weight was determined and the vehicle's inertial properties were measured a second time as instrumented. The target vehicle test weight for each vehicle was 820 kg. No components were removed from the vehicle's engine compartment. A dummy was not used for this test program. Table 2 summarizes the test vehicles' inertial properties and figures 1 through 6 are sketches of the vehicles' physical parameters. Figure 7 is a sketch of a typical Geo Metro engine compartment depicting the location of significant substructures (frame, battery, engine block, etc.) and includes each target impact location (frontal only). Figure 8 illustrates an overhead view of the Geo Metro.

Table 2. Inertial properties of 1997 Geo Metro.

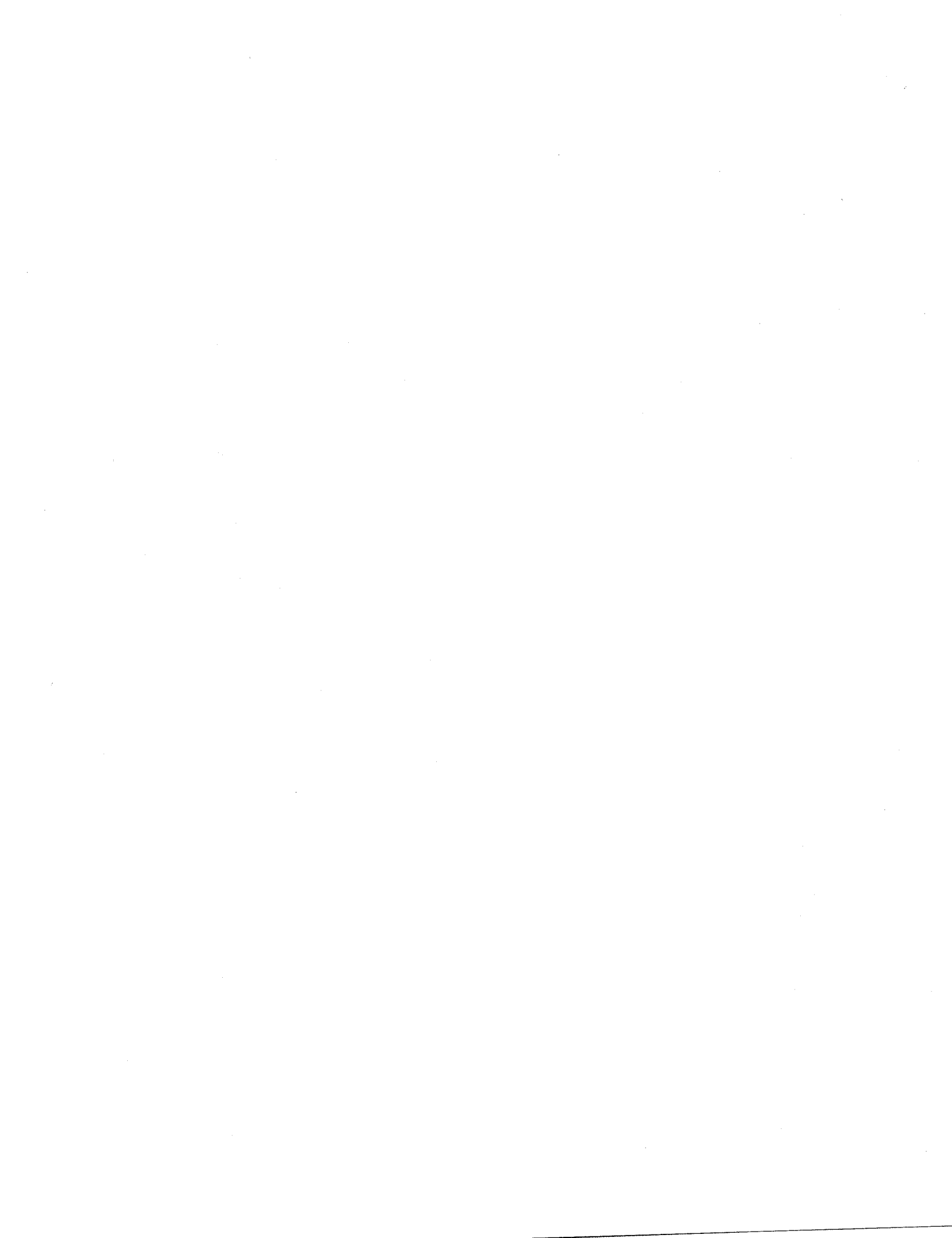
Test Number	Weight (kg)	Height (mm)*	Long.cg ** (mm)	Pitch kg•m ²	Roll kg•m ²	Yaw kg•m ²	Bumper Height (mm)	Wheel Base (m)
Curb Weight Configuration								
98F010	819	547	842	944	250	1,122	457	2.4
98F011	820	542	843	1,016	235	1,125	457	2.4
98F012	825	540	843	1,019	234	1,122	457	2.4
98F014	820	541	840	977	199	1,145	457	2.4
98F015	823	531	842	968	265	1,089	457	2.4
99S001	820	552	845	996	214	1,135	457	2.4
Test Configuration								
98F010	830	540	830	825	230	1,125	457	2.4
98F011	832	540	832	971	233	1,082	457	2.4
98F012	837	544	855	1,054	209	1,145	457	2.4
98F014	831	540	842	987	193	1,142	457	2.4
98F015	834	528	830	998	247	1,089	457	2.4
99S001	820	537	859	988	203	1,069	457	2.4

* Height of vehicle center-of-gravity.

** Longitudinal center-of-gravity, distance behind front axle.

RIGID POLE TEST DEVICE

The rigid pole was designed to record vehicle crush characteristic data for both frontal and broadside collisions. The rigid pole was installed on the FOIL runway with the pole



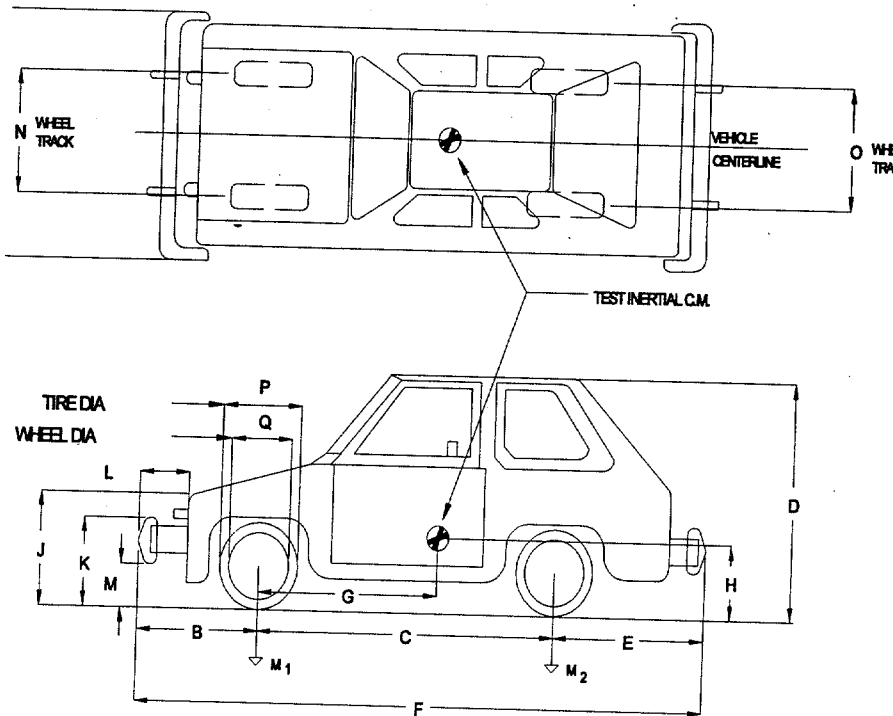
centerline aligned with the appropriate vehicle impact location. For five tests, the rigid pole was configured in the frontal impact configuration consisting of a 305-mm-diameter solid semi-circular steel impact face attached to two 890-kN load cells. The broadside test configuration of the rigid pole consisted of four 255-mm diameter solid steel impact faces. Each face was attached to two load cells (eight load cells total). Due to the vehicles' low roof height, the top two load cells (top impact face) were not used during the broadside test. The frontal and side impact configurations of the rigid pole are shown in figures 9 and 10, respectively.



DATE: 9-30-98 TEST NO: 98F010 TIRE PRESSURE: 35 psi MAKE: GEO
 MODEL: METRO YEAR: 1997 ODOMETER: 33,000 GVW: 832
 TIRE SIZE: VIN NUMBER: 2C1MR2294V6730262 TREAD TYPE:
 MASS DISTRIBUTION: CURB: LF 263 LF 264 LR 147 RR 145
 TEST INERTIAL: LF 268 RF 265 LR 150 RR 148

DESCRIBE ANY DAMAGE TO VEHICLE PRIOR TO TEST:

NONE



ENGINE TYPE: 1.3L 4 CYL.

ENGINE CID:

TRANSMISSION TYPE:

AUTO

MANUAL

OPTIONAL EQUIPMENT:

AIR CONDITIONING

Radio

DUMMY DATA:

TYPE: N.A.

MASS: N.A.

SEAT POSITION: N.A.

GEOMETRY

A <u>1525</u>	E <u>591</u>	J <u>679</u>	N <u>1385</u>	R <u></u>
B <u>830</u>	F <u>3783</u>	K <u>502</u>	O <u>1351</u>	S <u></u>
C <u>2363</u>	G <u>830</u>	L <u>106</u>	P <u>564</u>	T <u></u>
D <u>1413</u>	H <u>540</u>	M <u>409</u>	Q <u>361</u>	U <u></u>

MASS	CURB	TEST INERTIAL	GROSS STATIC
M ₁	<u>527</u>	<u>533</u>	<u>533</u>
M ₂	<u>292</u>	<u>298</u>	<u>298</u>
M _T	<u>819</u>	<u>831</u>	<u>831</u>

1 psi = 6.89 kPa

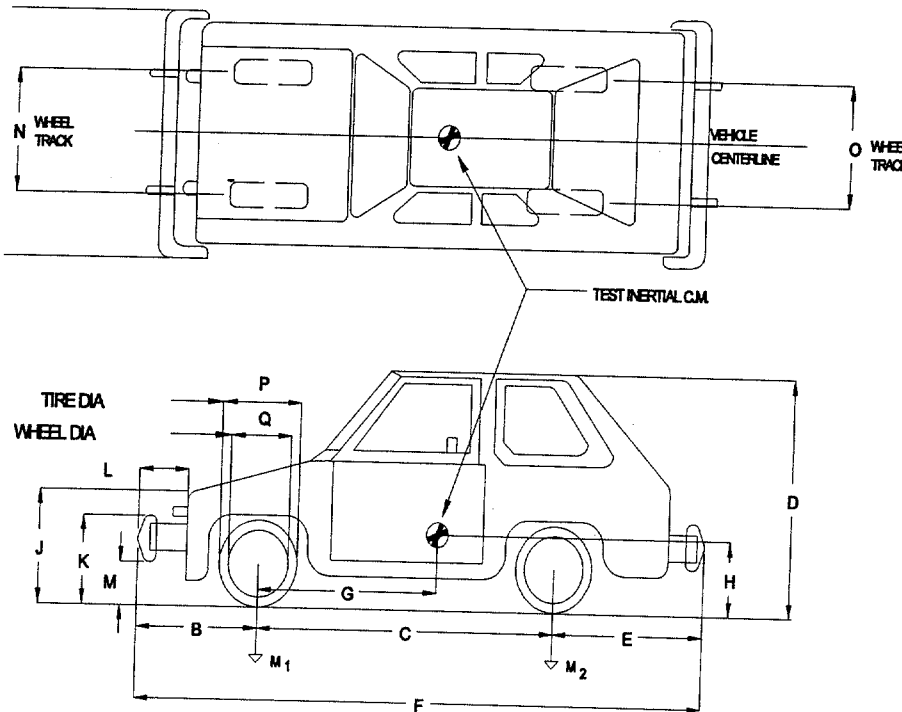
Figure 1. Vehicle properties for test 98F010.



DATE: 10-13-98 TEST NO: 98F011 TIRE PRESSURE: 35 psi MAKE: GEO
 MODEL: METRO YEAR: 1997 ODOMETER: 33,000 GVW: 832
 TIRE SIZE: VIN NUMBER: 2C1MR2296V6702091 TREAD TYPE:
 MASS DISTRIBUTION: CURB: LF 269 LF 259 LR 148 RR 145
 TEST INERTIAL: LF 274 RF 258 LR 152 RR 148

DESCRIBE ANY DAMAGE TO VEHICLE PRIOR TO TEST:

NONE



ENGINE TYPE: 1.3L 4 CYL

ENGINE CID:

TRANSMISSION TYPE:

AUTO

MANUAL

OPTIONAL EQUIPMENT:

AIR CONDITIONING

Radio

DUMMY DATA:

TYPE: N.A.

MASS: N.A.

SEAT POSITION: N.A.

GEOMETRY

A <u>1525</u>	E <u>591</u>	J <u>679</u>	N <u>1385</u>	R <u></u>
B <u>830</u>	F <u>3783</u>	K <u>502</u>	O <u>1351</u>	S <u></u>
C <u>2363</u>	G <u>832</u>	L <u>106</u>	P <u>564</u>	T <u></u>
D <u>1413</u>	H <u>540</u>	M <u>409</u>	Q <u>361</u>	U <u></u>

MASS	CURB	TEST INERTIAL	GROSS STATIC
M ₁	<u>528</u>	<u>532</u>	<u>532</u>
M ₂	<u>293</u>	<u>300</u>	<u>300</u>
M _t	<u>821</u>	<u>832</u>	<u>832</u>

1 psi = 6.89 kPa

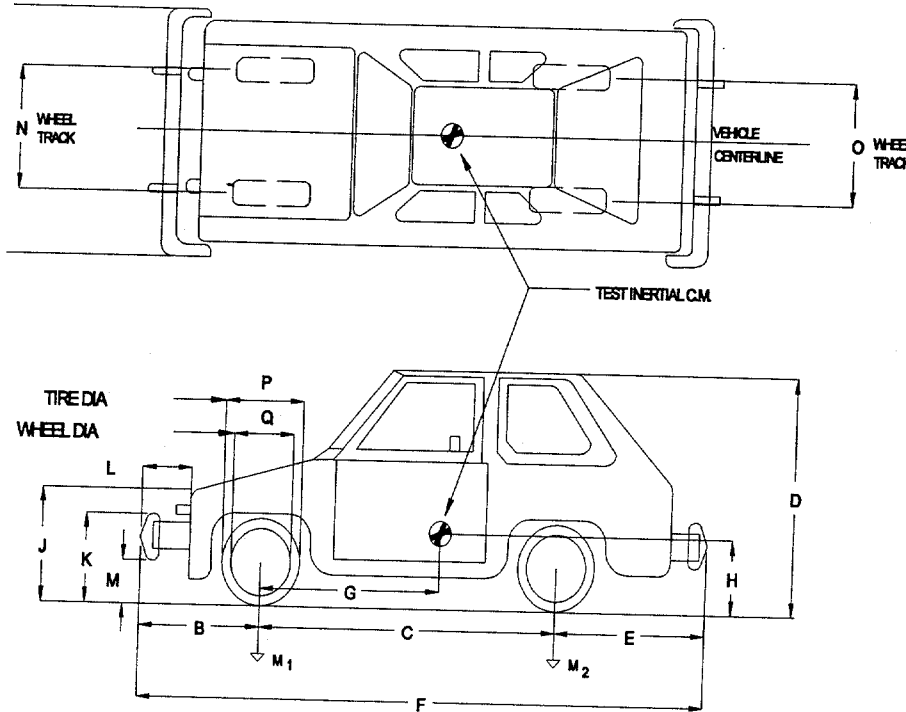
Figure 2. Vehicle properties for test 98F011.



DATE: 10-26-98 TEST NO: 98F012 TIRE PRESSURE: 35 psi MAKE: GEO
 MODEL: METRO YEAR: 1997 ODOMETER: 33,000 GVW: 827
 TIRE SIZE: VIN NUMBER: 2C1MR2294V6750060 TREAD TYPE:
 MASS DISTRIBUTION: CURB: LF 271 LF 260 LR 147 RR 147
 TEST INERTIAL: LF 269 RF 266 LR 152 RR 150

DESCRIBE ANY DAMAGE TO VEHICLE PRIOR TO TEST:

NONE



ENGINE TYPE: 1.3L 4 CYL.

ENGINE CID:

TRANSMISSION TYPE:

AUTO

MANUAL

OPTIONAL EQUIPMENT:

AIR CONDITIONING

Radio

DUMMY DATA:

TYPE: N.A.

MASS: N.A.

SEAT POSITION: N.A.

GEOMETRY

A	E <u>591</u>	J <u>679</u>	N <u>1385</u>	R
B <u>830</u>	F <u>3783</u>	K <u>502</u>	O <u>1351</u>	S
C <u>2363</u>	G <u>855</u>	L <u>106</u>	P <u>564</u>	T
D <u>1413</u>	H <u>544</u>	M <u>409</u>	Q <u>361</u>	U

MASS	CURB	TEST INERTIAL	GROSS STATIC
M ₁	<u>531</u>	<u>535</u>	<u>535</u>
M ₂	<u>294</u>	<u>302</u>	<u>302</u>
M _T	<u>825</u>	<u>837</u>	<u>837</u>

1 psi = 6.89 kPa

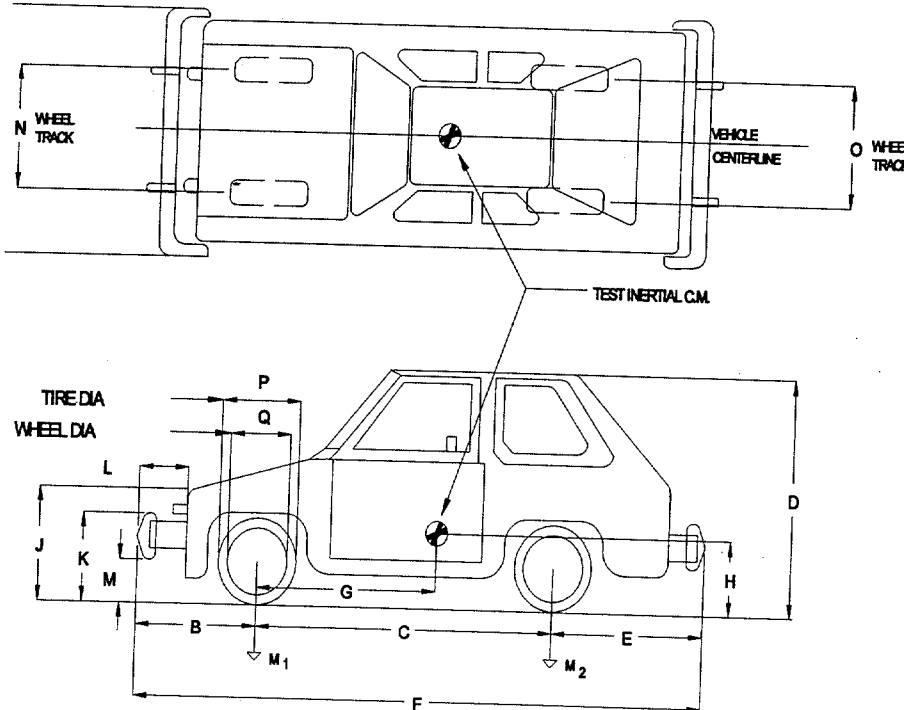
Figure 3. Vehicle properties for test 98F012.



DATE: 11-05-98 TEST NO: 98F014 TIRE PRESSURE: 35 psi MAKE: GEO
 MODEL: METRO YEAR: 1997 ODOMETER: 33,000 GVW: 827
 TIRE SIZE: VIN NUMBER: 2C1MR2295V6745109 TREAD TYPE:
 -
 MASS DISTRIBUTION: CURB: LF 270 LF 259 LR 144 RR 147
 TEST INERTIAL: LF 275 RF 261 LR 146 RR 145

DESCRIBE ANY DAMAGE TO VEHICLE PRIOR TO TEST:

NONE



ENGINE TYPE: 1.3L 4 CYL.

ENGINE CID:

TRANSMISSION TYPE:

AUTO

MANUAL

OPTIONAL EQUIPMENT:

AIR CONDITIONING

Radio

DUMMY DATA:

TYPE: N.A.

MASS: N.A.

SEAT POSITION: N.A.

GEOMETRY

A <u>1525</u>	E <u>591</u>	J <u>679</u>	N <u>1385</u>	R <u></u>
B <u>830</u>	F <u>3783</u>	K <u>502</u>	O <u>1351</u>	S <u></u>
C <u>2363</u>	G <u>842</u>	L <u>106</u>	P <u>564</u>	T <u></u>
D <u>1413</u>	H <u>540</u>	M <u>409</u>	Q <u>361</u>	U <u></u>

MASS	CURB	TEST INERTIAL	GROSS STATIC
M ₁	<u>529</u>	<u>536</u>	<u>536</u>
M ₂	<u>291</u>	<u>291</u>	<u>291</u>
M _T	<u>820</u>	<u>827</u>	<u>827</u>

1 psi = 6.89 kPa

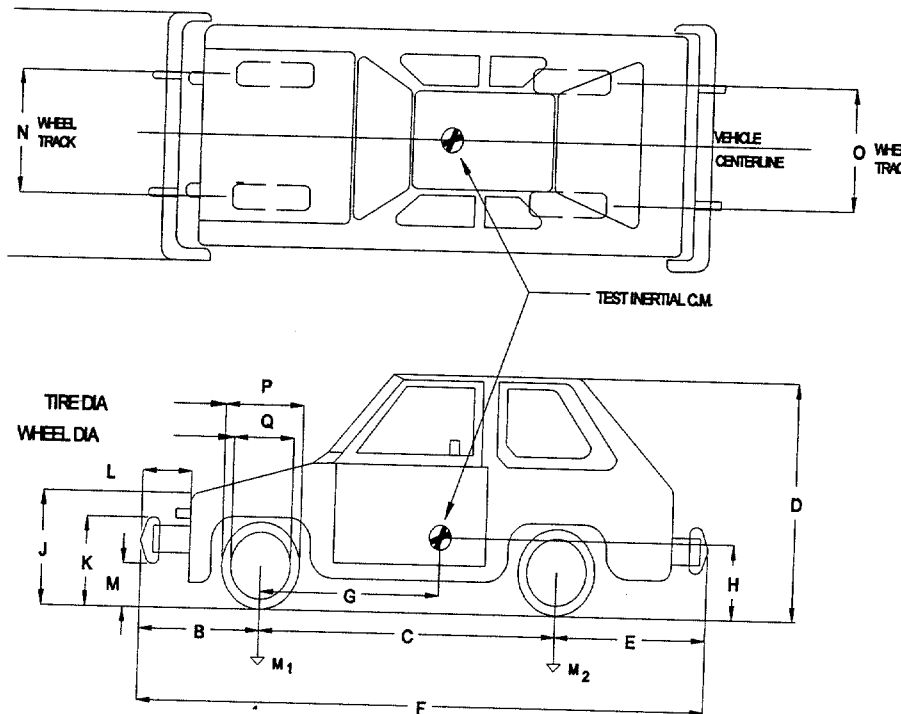
Figure 4. Vehicle properties for test 98F014.



DATE: 11-23-98 TEST NO: 98F015 TIRE PRESSURE: 35 psi MAKE: GEO
 MODEL: METRO YEAR: 1997 ODOMETER: 33,000 GVW: 834
 TIRE SIZE: VIN NUMBER: 2C1MR2293V6757971 TREAD TYPE:
 MASS DISTRIBUTION: CURB: LF 266 LF 263 LR 152 RR 142
 TEST INERTIAL: LF 270 RF 264 LR 150 RR 150

DESCRIBE ANY DAMAGE TO VEHICLE PRIOR TO TEST:

NONE



ENGINE TYPE: 1.3L 4 CYL.

ENGINE CID:

TRANSMISSION TYPE:

AUTO

MANUAL

OPTIONAL EQUIPMENT:

AIR CONDITIONING

Radio

DUMMY DATA:

TYPE: N.A.

MASS: N.A.

SEAT POSITION: N.A.

GEOMETRY

A <u>1525</u>	E <u>591</u>	J <u>679</u>	N <u>1385</u>	R <u></u>
B <u>830</u>	F <u>3783</u>	K <u>502</u>	O <u>1351</u>	S <u></u>
C <u>2363</u>	G <u>830</u>	L <u>106</u>	P <u>564</u>	T <u></u>
D <u>1413</u>	H <u>528</u>	M <u>409</u>	Q <u>361</u>	U <u></u>

MASS	CURB	TEST INERTIAL	GROSS STATIC
M ₁	<u>529</u>	<u>534</u>	<u>534</u>
M ₂	<u>294</u>	<u>300</u>	<u>300</u>
M _T	<u>823</u>	<u>834</u>	<u>834</u>

1 psi = 6.89 kPa

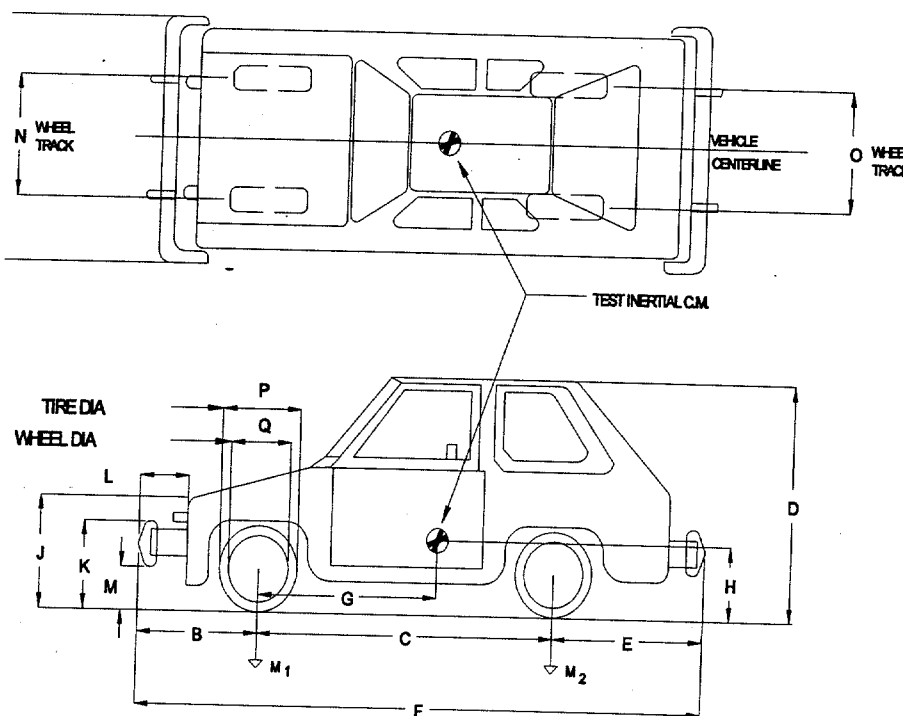
Figure 5. Vehicle properties for test 98F015.



DATE: 1-27-99 TEST NO: 99S001 TIRE PRESSURE: 35 psi MAKE: GEO
 MODEL: METRO YEAR: 1997 ODOMETER: 33,000 GVW: 830 kg
 TIRE SIZE: VIN NUMBER: 2C1MR2293V6727806 TREAD TYPE:
 MASS DISTRIBUTION: CURB: LF 275 RF 252 LR 146 RR 147
 TEST INERTIAL: LF 274 RF 254 LR 151 RR 150

DESCRIBE ANY DAMAGE TO VEHICLE PRIOR TO TEST:

NONE



ENGINE TYPE: 1.3L 4 CYL.

ENGINE CID:

TRANSMISSION TYPE:

AUTO

MANUAL

OPTIONAL EQUIPMENT:

AIR CONDITIONING

RADIO

DUMMY DATA:

TYPE: N.A.

MASS: N.A.

SEAT POSITION: N.A.

GEOMETRY

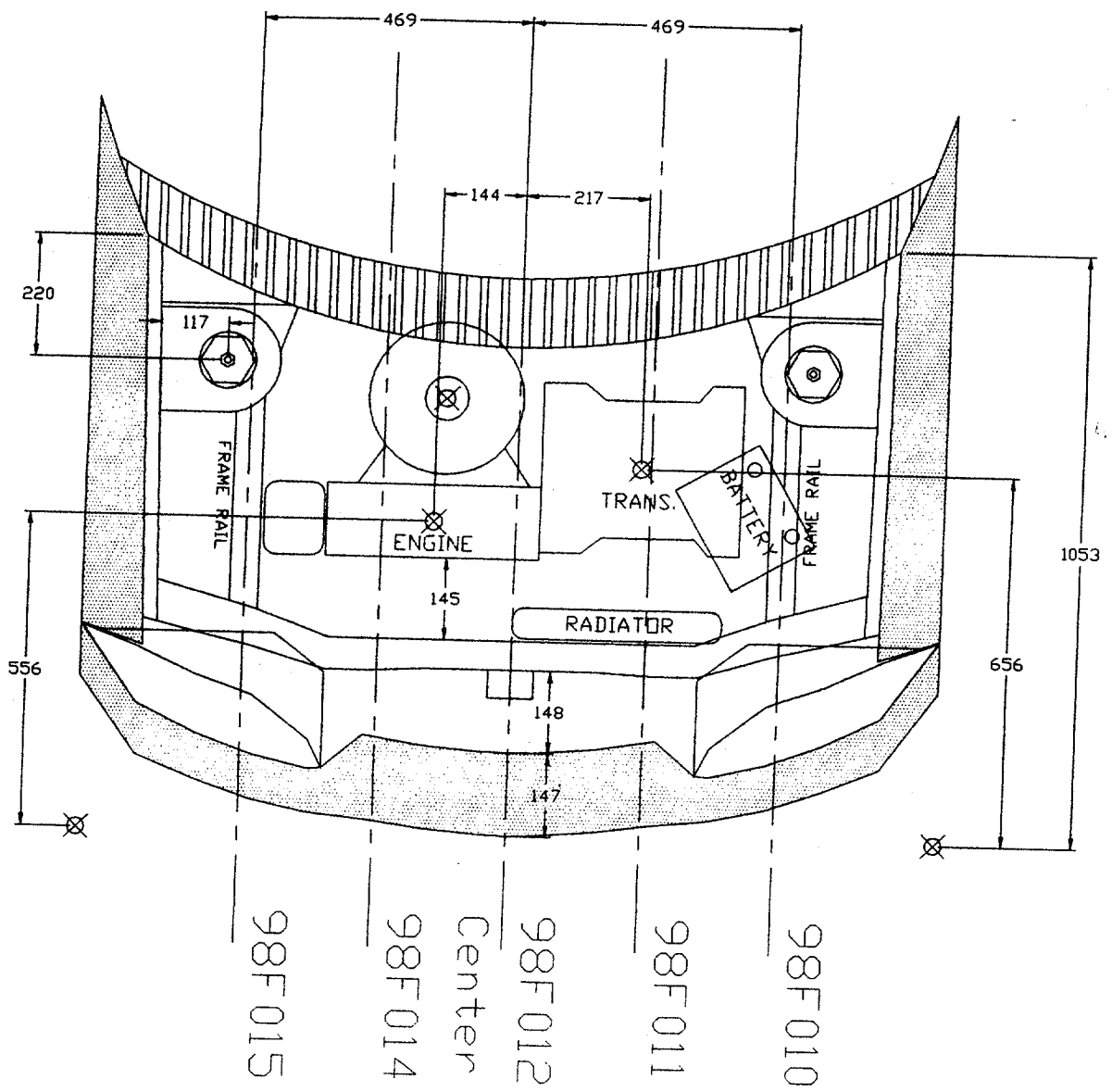
A <u>1525</u>	E <u>591</u>	J <u>679</u>	N <u>1385</u>	R <u></u>
B <u>830</u>	F <u>3783</u>	K <u>502</u>	O <u>1351</u>	S <u></u>
C <u>2363</u>	G <u>859</u>	L <u>106</u>	P <u>564</u>	T <u></u>
D <u>1413</u>	H <u>537</u>	M <u>409</u>	Q <u>361</u>	U <u></u>

MASS	CURB	TEST INERTIAL	GROSS STATIC
M ₁	<u>527</u>	<u>528</u>	<u>528</u>
M ₂	<u>293</u>	<u>301</u>	<u>301</u>
M _T	<u>820</u>	<u>829</u>	<u>829</u>

1 psi = 6.89 kPa

Figure 6. Vehicle properties for test 99S001.

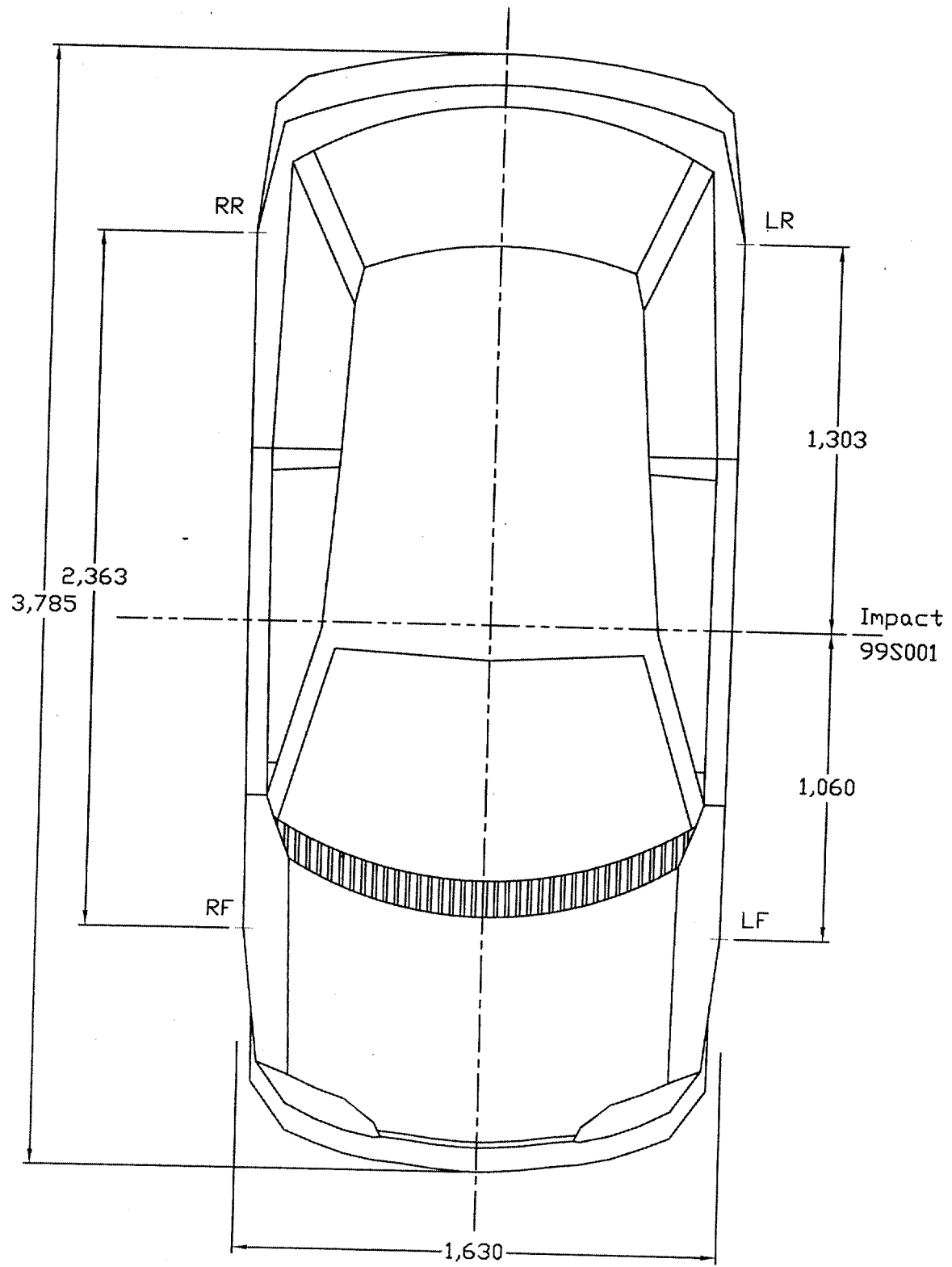




All dimensions in mm.

Figure 7. Sketch of test vehicle engine compartment and target frontal impact locations.





All dimensions in mm.

Figure 8. Overhead sketch of 1997 Geo Metro including target side impact location.



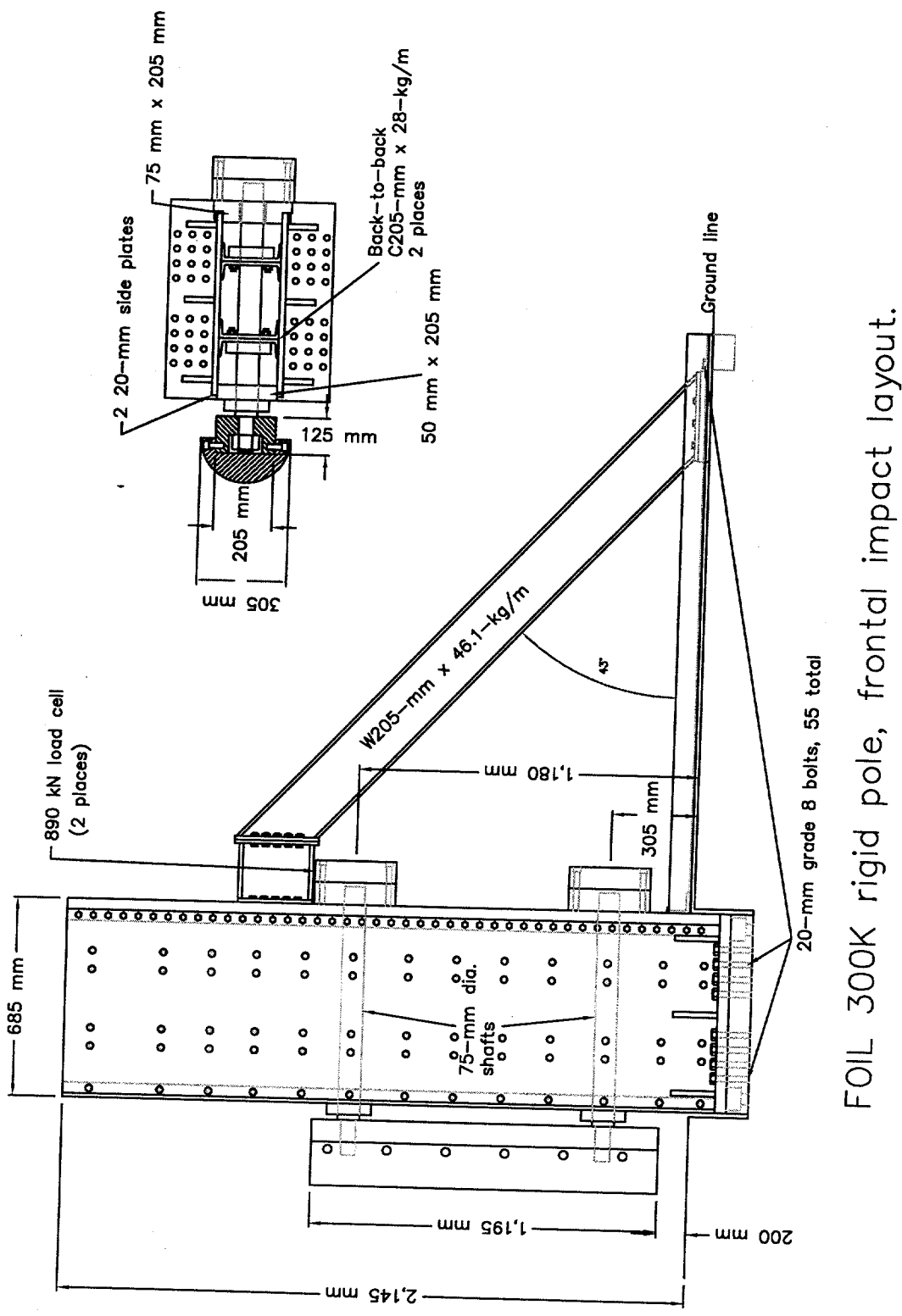
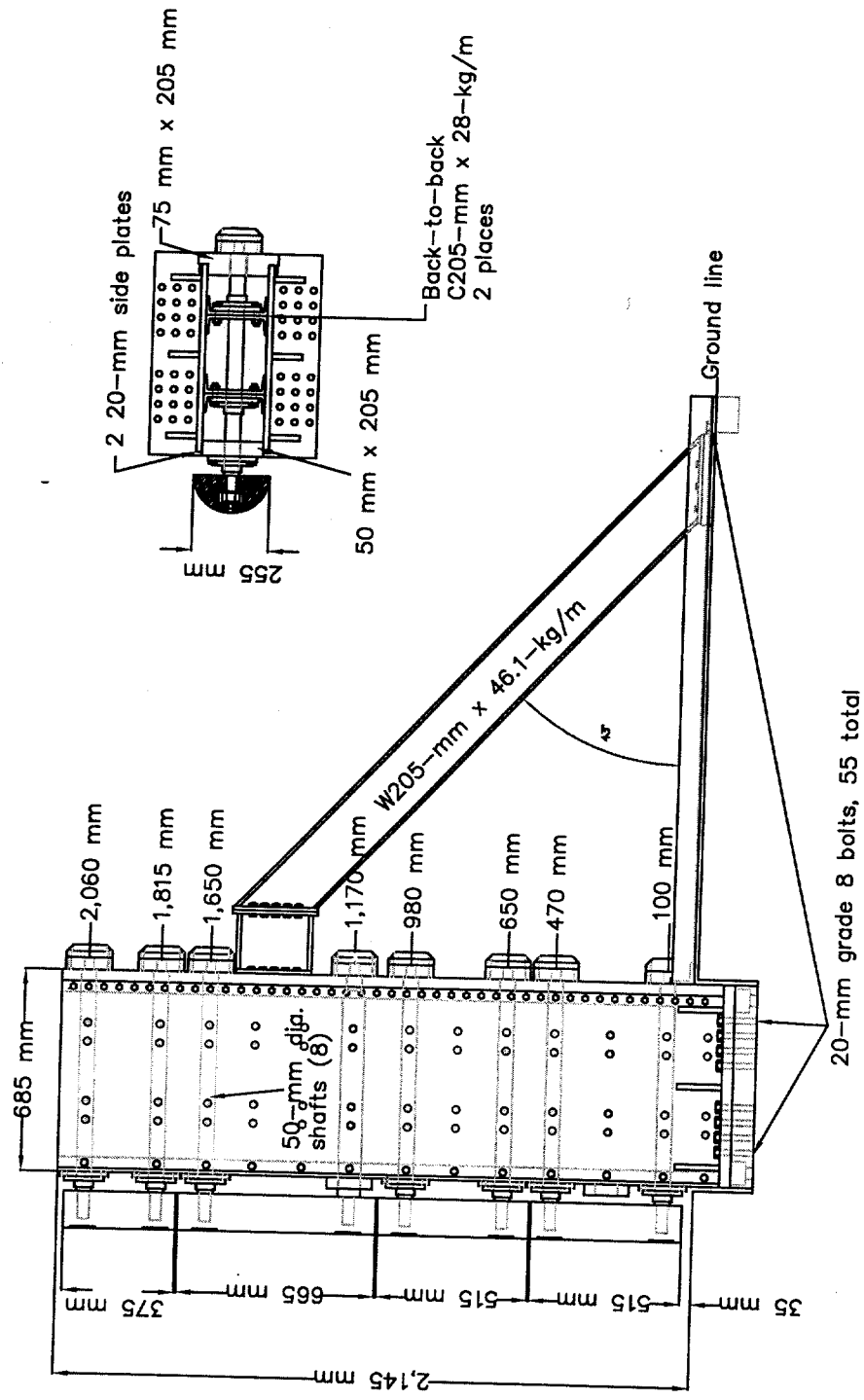


Figure 9. Sketch of FOIL rigid pole frontal configuration.





FOIL 300K rigid pole, side impact layout.

Figure 10. Sketch of FOIL rigid pole, side impact configuration.



INSTRUMENTATION

For each test, speed-trap, accelerometer, load-cell, and high-speed film data were collected to measure frontal and side crush characteristic data or force-deflection data of the 1997 Geo Metro.

Speed trap. For the five frontal impact tests, a speed trap was used to determine each vehicle's speed just prior to contact with the rigid pole. The center of the speed trap was placed approximately 3.7 m before the rigid pole. The speed trap consisted of a set of five contact switches fastened to the runway at 0.3-m intervals. As the vehicles passed over the switches, electronic pulses were recorded on analog tape.

For the broadside crash test, a single micro switch was fastened to the main FOIL side impact monorail at a location just prior to when the vehicle exited the monorail. As the vehicle passed over the switch, each wheel on the main side impact guidance carriage closed the micro switch. The wheels of the monorail carriage were spaced 1,015 mm apart. Two electronic pulses from the micro switch closures were recorded on analog tape. The monorail speed trap was used only to determine monorail exit speed. The vehicle speed just prior to contacting the rigid pole was determined from high-speed film.

Transducer data. The instrumentation used during the five frontal impact tests consisted of the two load cells attached to the rigid pole, a tri-axial accelerometer, and a tri-axial rate transducer at the vehicle's c.g. In addition to the pole and c.g. instrumentation, the Geo Metros were instrumented as described in Federal Motor Vehicle Safety Standard (FMVSS) 208.⁽²⁾ The data from the transducers were recorded by two data acquisition systems: the DSPT onboard data acquisition system (ODAS III) and an umbilical cable tape recorder system. Table 3 describes the instrumentation used during the frontal crash tests. A three dimensional sensor location is included in table 3. The location coordinates were referenced from the right-front wheel hub, which was 265 mm above ground.

The c.g. instrumentation used during the broadside crash test remained as in the frontal tests. However, the FMVSS 208 sensors were relocated. The sensors were positioned to acquire data from locations more pertinent for broadside testing. Accelerometers were affixed to the driver seat track, inside the driver door, and to the passenger side roof and floor sills. Table 4 summarizes the instrumentation used for the broadside test. The sensor locations are also included. Sensor location coordinates in table 4 were referenced from the right front wheel hub (265 mm above ground).

The ODAS III is a self-contained system. The output from the sensors was filtered, digitally sampled, and digitally stored



within the ODAS units mounted directly to the test vehicle inside the occupant compartment. The ODAS units are factory set with a 4000-Hz analog filter and a digital sampling rate of 12,500 Hz. FMVSS 208 accelerometer (vehicle component data), c.g., and rate transducer data were collected via the ODAS III system.

The FOIL umbilical cable system utilizes a 90-m cable between vehicle transducers, rigid pole load cells, or other sensors and a rack of signal conditioning amplifiers. The output from the amplifiers was recorded on 25-mm magnetic tape via a Honeywell 5600E tape recorder. After the test, the tape is played back through anti-aliasing filters, then input to a Data Translation analog-to-digital converter (ADC). The sample rate was set to 5000 Hz. The umbilical cable system recorded c.g. acceleration data and rigid pole load-cell data.

Table 3. Summary of instrumentation and channel assignments for tests 98F010 through 98F015 (frontal tests).

ODAS III onboard data system				
Ch	Transducer	Maximum range	Data description	Location* (X,Y,Z) mm
1	Accelerometer	100 g	Vehicle c.g., X-axis	-819, 782, 106
2	Accelerometer	100 g	Vehicle c.g., Y-axis	-819, 782, 106
3	Accelerometer	100 g	Vehicle c.g., Z-axis	-819, 782, 106
4	Accelerometer	2000 g	Top of engine, X-axis	277, 684, 490
5	Accelerometer	2000 g	Bottom of engine, X-axis	115, 757, -17
6	Accelerometer	2000 g	Left front caliper, Y-axis	106, 1390, 26
7	Accelerometer	2000 g	Right front caliper, X-axis	107, 152, 25
8	Accelerometer	2000 g	Instrument panel, X-axis	-396, 773, 652
9	Rate transducer	500 °/s	Pitch rate, c.g.	-819, 782, 106
10	Rate transducer	500 °/s	Roll rate, c.g.	-819, 782, 106
11	Rate transducer	500 °/s	Yaw rate, c.g.	-819, 782, 106



Table 3. Summary of instrumentation and channel assignments for tests 98F010 through 98F015 (frontal tests) (continued).

Umbilical cable, tape recorder system.				
1	Accelerometer	100 g	Vehicle c.g., X-axis	-819,782,106
2	Accelerometer	100 g	Vehicle c.g., Y-axis	-819,782,106
3	Accelerometer	100 g	Vehicle c.g., Z-axis	-819,782,106
4	Load cell	222 kN	Pole force, X-axis	0,0,305**
5	Load cell	222, kN	Pole force, X-axis	0,0,1180**
11	Contact switch	1.5 V	Time of impact, T0	Not available
12	Contact switches	1.5 V	Runway speed trap	Not available
14	Generator	1.5 V	1 kHz reference signal	Not available

* Origin located at right front wheel hub (265 mm above ground)

**Vertical location only referenced from FOIL runway.

Table 4. Summary of instrumentation and channel assignments for broadside crash test 99S001.

ODAS III onboard data system				
Ch	Transducer	Maximum range	Data description	Location* (X,Y,Z) mm
1	Accelerometer	100 g	Vehicle c.g., X-axis	-800,741,135
2	Accelerometer	100 g	Vehicle c.g., Y-axis	-800,741,135
3	Accelerometer	100 g	Vehicle c.g., Z-axis	-800,741,135
4	Accelerometer	2000 g	Top of engine, X-axis	295,712,470
5	Accelerometer	2000 g	Top of engine, Y-axis	295,712,470
6	Accelerometer	2000 g	Driver seat, Y-axis	-1030,1400,100
7	Accelerometer	2000 g	Rear axle, X-axis	-1820,770,180

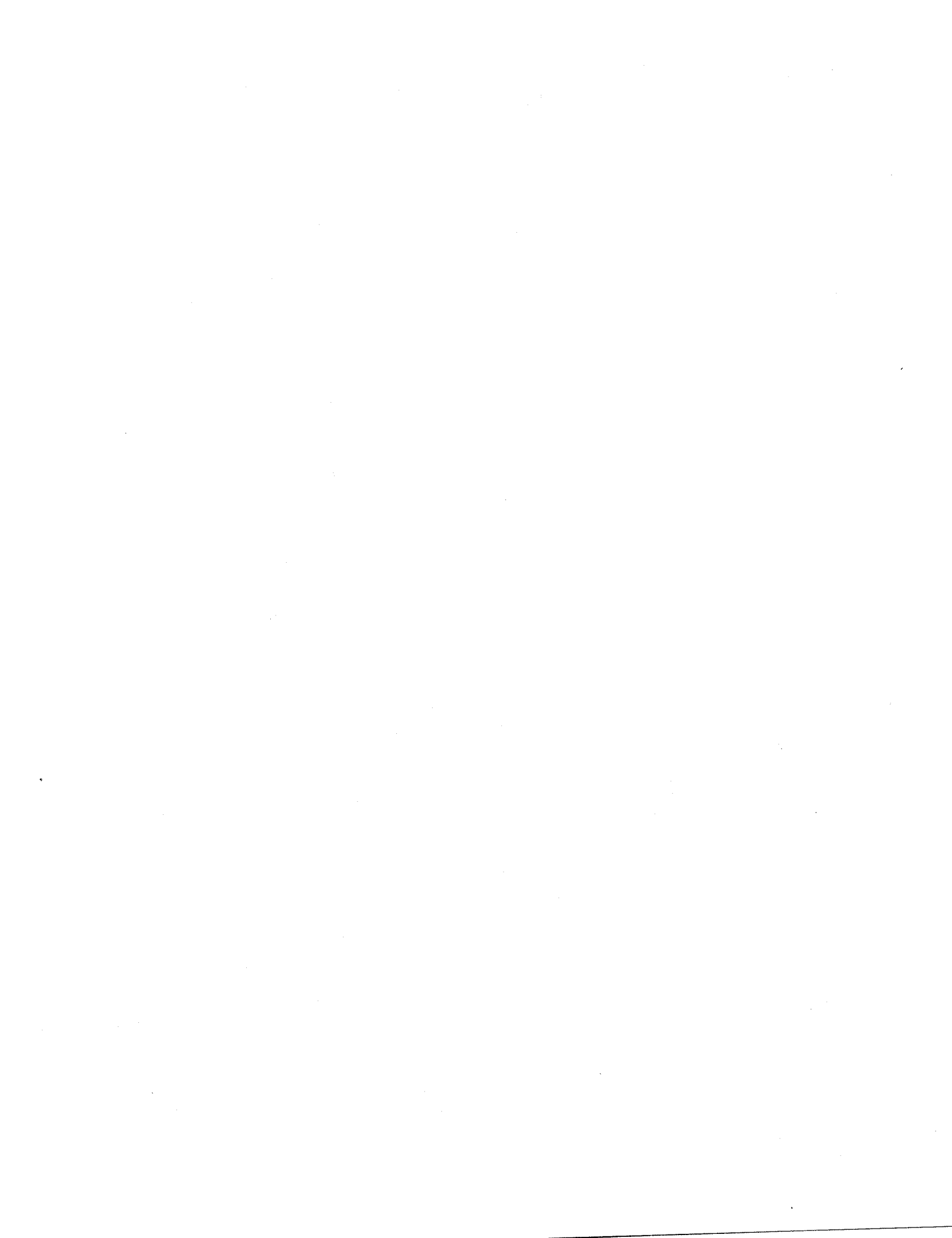


Table 4. Summary of instrumentation and channel assignments for broadside crash test 99S001 (continued).

8	Accelerometer	2000 g	Rear axle, Y-axis	-1820, 770, 180
9	Accelerometer	2000 g	right side floor	-1030, 171, 110
10	Accelerometer	2000 g	right side roof	-1030, 321, 1000
11	Rate transducer	500 °/s	Pitch rate, c.g.	-800, 741, 135
12	Rate transducer	500 °/s	Roll rate, c.g.	-800, 741, 135
13	Rate transducer	500 °/s	Yaw rate, c.g.	-800, 741, 135
Umbilical cable, tape recorder system.				
1	Accelerometer	100 g	Vehicle c.g., Y-axis	-800, 741, 135
2	Accelerometer	100 g	Vehicle c.g., Z-axis	-800, 741, 135
3	Accelerometer	200 g	Left door outer-skin	-1055, 1620, 315
4	Accelerometer	200 g	Left door inner brace	-1055, -1535, 315
5	Load cell	222 kN	Pole force, X-axis	0, 0, 100**
6	Load cell	222 kN	Pole force, X-axis	0, 0, 470**
7	Load cell	222 kN	Pole force, X-axis	0, 0, 650**
8	Load cell	222 kN	Pole force, X-axis	0, 0, 980**
9	Load cell	222 kN	Pole force, X-axis	0, 0, 1170**
10	Load cell	222 kN	Pole force, X-axis	0, 0, 1650**
11	Contact switch	1.5 V	Time of impact, T ₀	Not applicable
12	Micro switch	1.5 V	Monorail speed trap	Not applicable
14	Generator	1.5 V	1 kHz reference signal	Not applicable

* Origin located at right front wheel hub (265 mm above ground)

**Vertical location only referenced from FOIL runway.



High-speed photography. The crash tests were photographed using five high-speed cameras with an operating speed of 500 frames/s. All high-speed cameras used Kodak 2253 daylight film. The high-speed film was analyzed for impact speed and acceleration data. In addition to the high-speed cameras, one real-time camera loaded with Kodak 7239 daylight film and two 35-mm still cameras were used to document the test. Table 5 summarizes the cameras used and their respective placements. The camera numbers listed in table 5 are shown in figures 11 and 12. The figures depict the test facility layout for frontal and broadside rigid pole testing.

Table 5. Summary of camera placement.

Camera	Type	Film speed frames/s	Lens (mm)	Location
1	LOCAM II	500	75	Right 90° to impact
2	LOCAM II	500	50	Right 90° to impact
3	LOCAM II	500	50	Right side 45° to impact
4	LOCAM II	500	50	Left side 45° to impact
5	LOCAM II	500	10	Overhead
6	BOLEX	24	ZOOM	Documentary
7	CANNON AE-1	still	ZOOM	Documentary
8	CANNON AE-1	still	ZOOM	Documentary

DATA ANALYSIS

Data were collected via the FOIL analog tape recorder system, including speed-trap data, the FOIL ODAS III onboard data system, and high-speed film.

Speed trap. As the vehicles passed over the speed trap, tape switches or lone micro switch (side impact), electronic pulses were recorded to analog tape. The tape was played back through a Data Translation ADC inside a desktop computer. The time between pulses was then determined using the software provided with the ADC. For frontal impacts, the time intervals between the first pulse and each of the subsequent four pulses together with the distances between corresponding tape switches were entered into a computer spreadsheet and a linear regression was performed to determine the best-line fit of the data points. The impact velocity was then determined from the slope of the best-line fit of the displacement vs. time curve. For the broadside test, the monorail exit speed was calculated by dividing the distance



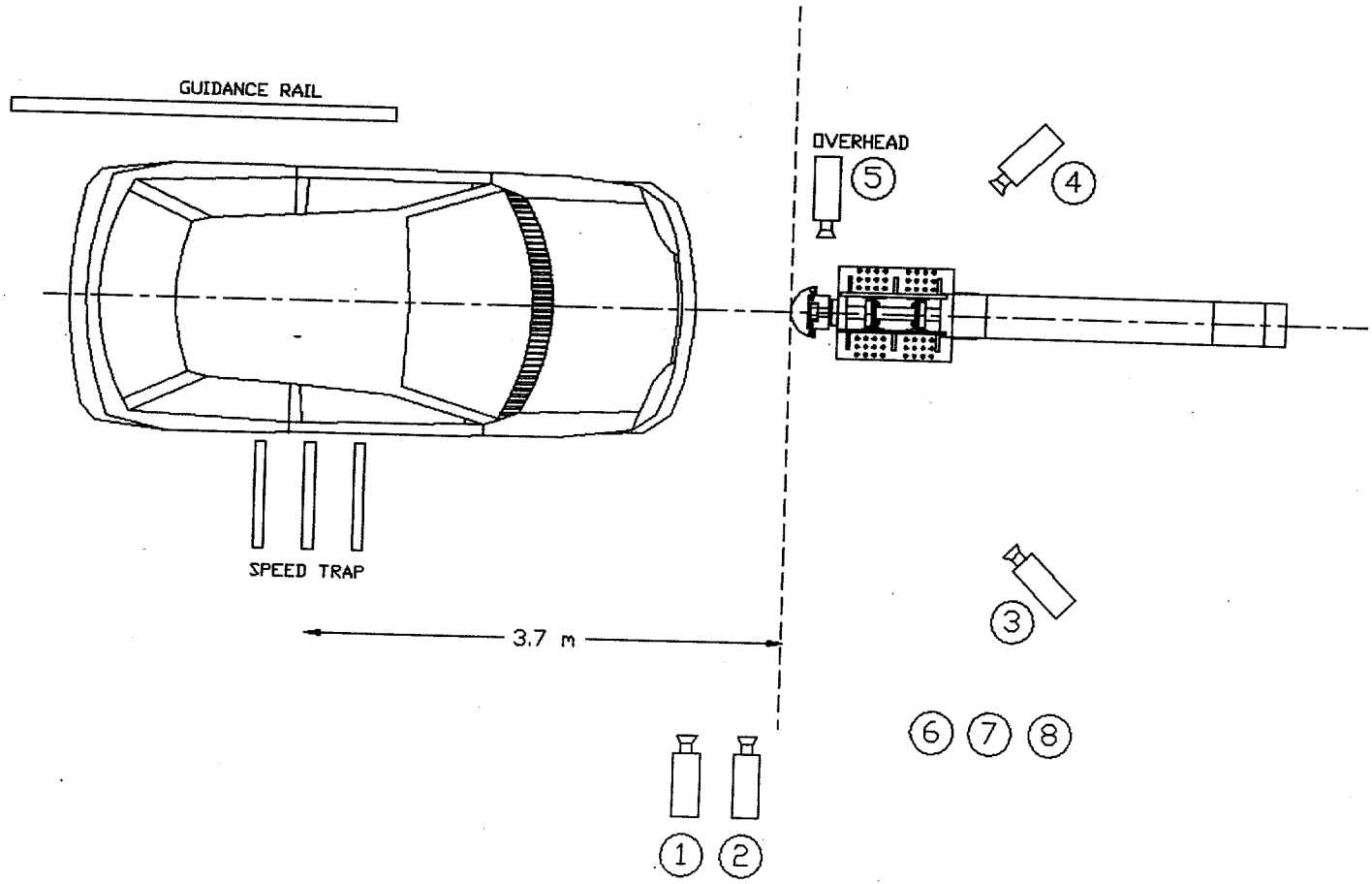


Figure 11. Camera placement and test setup for the five frontal impact tests, tests 98F010 through 98F015.



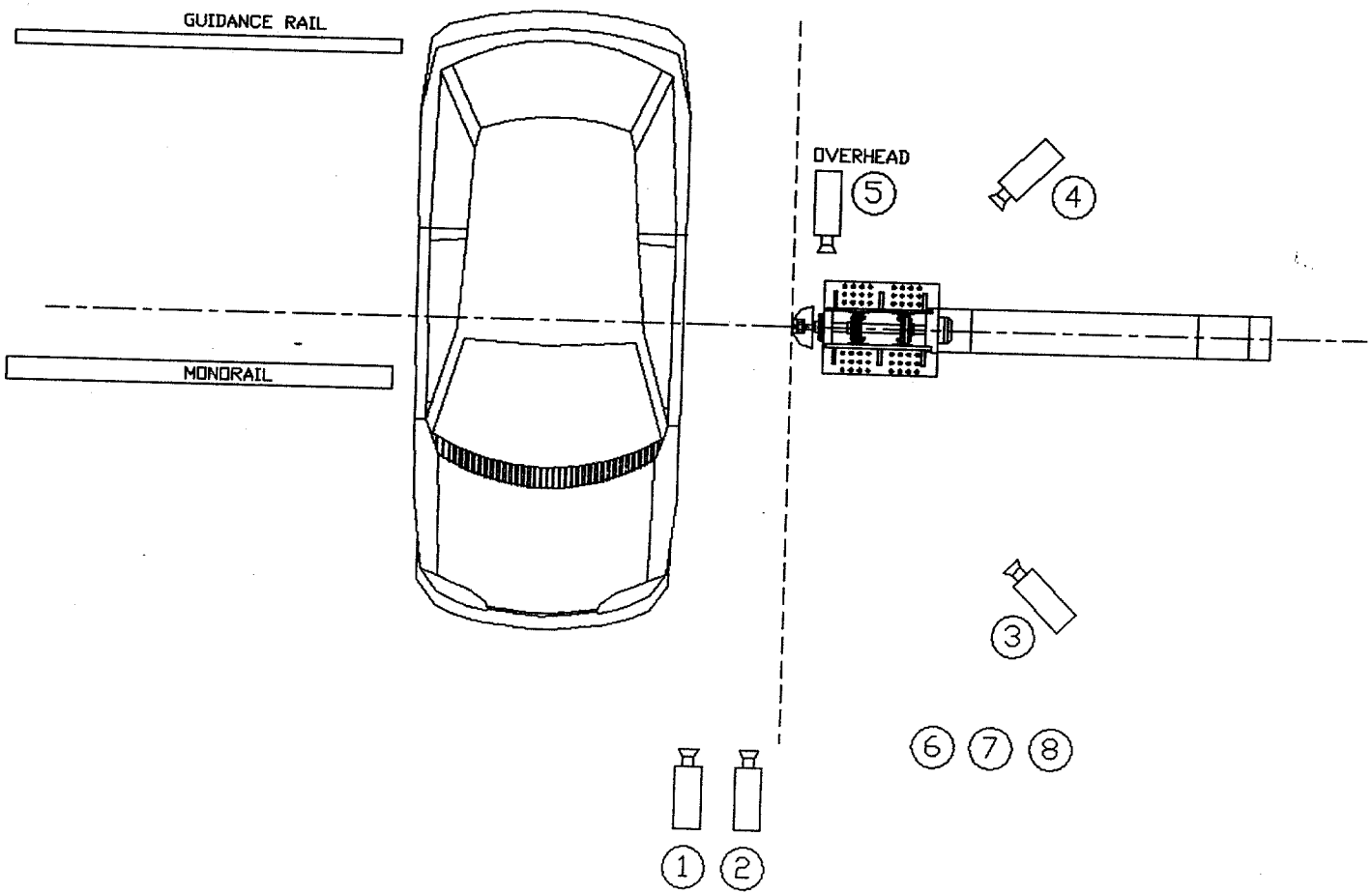


Figure 12. Camera placement and test setup for the broadside test, test 99S001.



between carriage wheels (1,015 mm) by the time between two electronic pulses recorded on magnetic tape.

Transducer data package. After the test, data from both data systems were converted to digital format and stored. The digital data from the tape recorder system and the ODAS III system were converted to the ASCII format, the zero bias was removed, and the data were digitally filtered using a digital Butterworth low-pass filter. The data from the crash tests were digitally filtered with a cutoff frequency of 300 Hz. The data were transferred to a spreadsheet for analysis.

The longitudinal (lateral for side impact) c.g. acceleration data were integrated twice to produce velocity and displacement traces. A force vs. time trace was generated by multiplying the acceleration data by the mass of the vehicle and plotting the product vs. time. The crush profile data plots were generated by plotting the force data with the displacement data. Integration of the force vs. displacement data yielded an energy vs. displacement trace. Acceleration vs. time traces were plotted for all FMVSS 208 accelerometers.

The load cells measured forces at two (frontal testing) or six (broadside test) separate locations on the rigid pole. The forces obtained were summed together to generate the entire force for the event. Using the force vs. time trace, an acceleration trace was produced by dividing the force vs. time trace by the mass of the vehicle. Velocity and displacement traces were generated by a single and double integration of the acceleration trace. A force vs. displacement trace was generated from the load-cell data. The force vs. displacement trace depicts the frontal crush characteristic of a vehicle for the given impact location. An energy vs. displacement trace was derived from integrating the force vs. displacement trace. The energy curve verifies the conservation of energy during the test and illustrates the amount of energy consumed for a given amount of deformation.

The load cells measured the forces on the rigid pole at two or six separate locations. Each pair of load cells was attached to a single, common rigid pole impact face. Using torque equations, a resultant load height on the rigid pole vs. displacement (crush) was generated. This plot is important because it depicts the location (height) on the vehicle that was producing the load. The resultant load height varied as the vehicle crushed inward. As contact between different structures in the vehicle occurred, the resultant load's vertical location shifted.

High-speed photography. Each crash event was recorded on 16-mm film by five high-speed cameras. The film from the camera perpendicular to the vehicle trajectory, with a 50-mm lens, was



analyzed for initial vehicle velocity. The overhead camera film was analyzed to determine vehicle displacement after contact, which can be used to measure vehicle deformation. Analysis of each crash event was performed using an NAC Film Motion Analyzer model 160-F in conjunction with a desktop personal computer. The motion analyzer digitized the 16-mm film, reducing the image to Cartesian coordinates. The Cartesian coordinate data were then imported into a computer spreadsheet for analysis. Using the Cartesian coordinate data, a displacement vs. time history of each test was obtained. A linear regression was performed on the first 20 data points of the displacement vs. time traces to determine the vehicles' impact velocities. The film was used to verify data obtained from the speed trap and rate transducer and could be used in the event of transducer malfunction. The film was used to observe roll, pitch, and yaw angular displacements. The speed trap, accelerometer, and load-cell data were the primary data systems.

RESULTS

Each vehicle was accelerated to within ± 1.7 km/h of the target impact speed (35 km/h) prior to striking the rigid pole.. The vehicles struck the rigid pole within ± 25 mm of the target impact location.

During each frontal test, different areas of the bumper, grill, hood, and fenders deformed after contact. The total amount of vehicle deformation varied depending on the vehicle substructure and engine compartment components at the specific impact location. Each vehicle rebounded away from the rigid pole with a small negative velocity. During the crash tests where the impact location was aligned with one of the front tires (98F010 and 98F015) the vehicles were unable to rebound as far or as fast due to the fender and wheel-well deformation against the tire. During contact with the rigid pole the vehicles rotated about the impact location. The magnitude and direction of the yaw was dependent on the distance between the vehicle centerline (lateral c.g.) and the impact location and on which side of the vehicles' centerline (left or right) the impact occurred.

For test 99S001, the Geo Metro was placed on the side impact monorail. The vehicle centerline was perpendicular to the rigid pole centerline. Prior to test execution the area of runway in front of the rigid pole was hosed down with water. This was done to minimize tire friction and therefore minimize the roll angle of the vehicle prior to striking the rigid pole. The vehicle exited the monorail at 38.8 km/h. The vehicle dropped from the monorail with the two left tire contacting the runway first followed by the right two tires. The vehicle slid across the wet runway and struck the rigid pole at the intended impact location with an



initial roll angle of 2.3° and an initial yaw angle of 90.0° . The impact speed was determined from high-speed film and was based on film analysis of the 15 frames (0.030 s) preceding contact with the rigid pole. The measured impact speed was 34.2 km/h. The vehicle slid into the pole with the driver door striking the pole first. The cross-section of the door collapsed causing the window to break. The floor-sill struck the pole and began to fold inwards. The roof-sill made contact with the pole last and buckled quickly, providing little resistance or stiffness. As the vehicle continued to collapse, the front and rear of the vehicle acted independently. The front and rear of the vehicle began to wrap around the pole. The yaw angle of the front and rear differed because the impact location essentially divided the vehicle into two sections. The rate transducer mounted inside the vehicle was located forward of the impact location and therefore measured the yaw rate and angle of the vehicle's front end. Data from sensors located at the c.g., to include accelerometers and rate transducers, may not accurately represent the event due to the severe buckling of the vehicle floor pan and tunnel.

Table 6 summarizes the results from the six Geo Metro crash tests. Table 7 and 8 list the peak values recorded by each sensor for each of the five frontal impact tests and the one broadside collision, respectively. Sketches of the test vehicles with static deflection measurements are presented in Appendix A. Photographs taken of the pre-test, during-test, and the post-test environment for each test are presented in Appendix B. Appendix C contains data plots of the data recorded by each sensor during each test. Crush profile data plots are included in Appendix C.

CONCLUSIONS

The results indicate that electronic data and high-speed film data were successfully recorded during six crash tests between Geo Metros and the FOIL rigid pole. The electronic data and film footage will aid computer simulation engineers to develop and validate FEMs of the Geo Metro and models of crash tests between Geo Metros and roadside safety devices.

The five frontal crash tests yielded crush profile data for five different locations along the Geo Metros' front end. One impact location will be selected as the location that the FOIL bogie vehicle's nose will replicate. The current bogie nose was modeled after a 1979 Volkswagen Rabbit's front left quarter point. The bogie vehicle is currently used to evaluate the safety performance of breakaway roadside safety hardware. Which location to be modeled will be based on a worst-case approach and/or guidance from NCHRP Report 350. The Geo Metro crush profile data are summarized as three data plots in figures 13, 14, and 15. These data plots were generated from load-cell data.



Because of the severe vehicle deformation, crush profile data plots used for this discussion were generated from the rigid pole load cells rather than from the vehicle c.g. accelerometers. Figure 13 helps illustrate the worst-case approach. Given the impact locations in tests 98F010 and 98F015, a roadside safety device designed to break away at 150,000 N would produce an occupant risk value (delta velocity value) higher than the recommended value outlined in *NCHRP Report 350* (5 m/s). The same device would produce an occupant risk value lower than 5 m/s when struck at the impact locations tested in tests 98F011, 98F012, and 98F014. Therefore it would be plausible that a roadside safety device that met the safety performance criteria when tested by a bogie vehicle modeled after tests 98F010 and/or 98F015 would also meet the safety performance criteria in all frontal impact scenarios. However, the standard safety performance evaluation test outlined in *NCHRP Report 350* is an 820C vehicle striking the breakaway device on the vehicle centerline. Off-center crash tests are considered optional for the high-speed test designations to observe possible vehicle instability induced by an off-center collision. The nose of the bogie vehicle may be modeled after any of the five tested locations; however, the nose is inserted into the bogie vehicle frame along the bogie centerline and therefore possible instability due to an off-center hit would not be observed using the bogie vehicle. From this reasoning, the FOIL bogie's crushable nose should replicate the Geo Metro centerline collision with the rigid pole.



Table 7. Summary of sensor output, maximum and minimum values for tests 98F010 through 98F015 (frontal testing).

ODAS III onboard data system										98F014 (+g) (-g)		98F015 (+g) (-g)	
Test number	98F010 (+g) (-g)			98F011 (+g) (-g)			98F012 (+g) (-g)			98F014 (+g) (-g)		98F015 (+g) (-g)	
Data description													
Vehicle c.g., A _x	4.5	43.5	9.8	41.1	9.2	59.2	5.6	37.2	3.6	3.6	30.3		
Vehicle c.g., A _y	9.8	18.7	8.7	15.3	17.2	16.9	15.9	9.3	15.0	10.6			
Vehicle c.g., A _z	16.6	18.8	24.5	50.8	1.2	1.7	12.5	23.6	16.8	11.6			
Top of engine, A _x	38.8	211.5	23.6	190.4	59.8	587.7	28.0	354.0	12.8	295.0			
Bottom engine, A _x	27.8	37.2	15.5	48.5	63.5	64.2	22.8	60.9	26.3	35.3			
Right front caliper, A _x	33.3	68.2	9.3	52.7	8.2	63.4	8.6	59.4	27.8	82.6			
Left front caliper, A _x	1345.8	535.1	19.1	87.6	8.9	47.1	8.7	50.7	25.8	46.9			
Instrument panel, A _x	33.9	55.4	9.2	53.3	35.1	70.5	NA	93.2	129.7	102.6			
Umbilical cable, tape recorder system.													
Vehicle c.g., A _x	4.9	49.9	9.9	44.8	5.8	63.8	8.5	39.0	3.0	31.6			
Vehicle c.g., A _y	8.7	16.7	8.1	13.2	12.5	13.3	20.3	9.5	10.1	15.4			
Vehicle c.g., A _z	18.3	18.0	23.9	41.5	20.0	42.3	12.4	19.8	16.3	10.7			
Pole force, F _x (1000 N)	2.4	170.0	2.5	268.0	1.9	245.0	4.5	194.0	2.2	152.0			



Table 7. Summary of sensor output, maximum and minimum values for tests 98F010 through 98F015 (frontal testing).

ODAS III onboard data system															
Test number	98F010 (+g) (-g)			98F011 (+g) (-g)			98F012 (+g) (-g)			98F014 (+g) (-g)			98F015 (+g) (-g)		
Data description															
Vehicle cg, A_x	4.5	43.5	9.8	41.1	9.2	59.2	5.6	37.2	3.6	3.6	30.3				
Vehicle cg, A_y	9.8	18.7	8.7	15.3	17.2	16.9	15.9	9.3	15.0	10.6					
Vehicle cg, A_z	16.6	18.8	24.5	50.8	1.2	1.7	12.5	23.6	16.8	11.6					
Top of engine, A_x	38.8	211.5	23.6	190.4	59.8	587.7	28.0	354.0	12.8	295.0					
Bottom engine, A_x	27.8	37.2	15.5	48.5	63.5	64.2	22.8	60.9	26.3	35.3					
Right front caliper, A_x	33.3	68.2	9.3	52.7	8.2	63.4	8.6	59.4	27.8	82.6					
Left front caliper, A_x	1345.8	535.1	19.1	87.6	8.9	47.1	8.7	50.7	25.8	46.9					
Instrument panel, A_x	33.9	55.4	9.2	53.3	35.1	70.5	NA	93.2	129.7	102.6					
Umbilical cable, tape recorder system.															
Vehicle cg, A_x	4.9	49.9	9.9	44.8	5.8	63.8	8.5	39.0	3.0	31.6					
Vehicle cg, A_y	8.7	16.7	8.1	13.2	12.5	13.3	20.3	9.5	10.1	15.4					
Vehicle cg, A_z	18.3	18.0	23.9	41.5	20.0	42.3	12.4	19.8	16.3	10.7					
Pole force, F_x (1000 N)	2.4	170.0	2.5	268.0	1.9	245.0	4.5	194.0	2.2	152.0					



Table 8. Summary of sensor output for test 99S001 (broadside test).

ODAS III onboard data system		
Data description	Maximum	
	(+g)	(-g)
Vehicle c.g., X-axis	16.3	14.0
Vehicle c.g., Y-axis	12.6	26.6
Vehicle c.g., Z-axis	16.2	42.8
Top of engine, X-axis	7.9	10.0
Top of engine, Y-axis	2.2	18.8
Driver seat, Y-axis	26.4	79.6
Rear axle, X-axis	23.0	19.9
Rear axle, Y-axis	27.4	20.2
Right side floor	2.7	14.9
Right side roof	0.9	7.4
Umbilical cable, tape recorder system.		
Vehicle c.g., Y-axis	9.2	28.3
Vehicle c.g., Z-axis	6.4	43.9
Left door outer-skin	126.4	201.6
Left door inner brace	236.9	104.8
Pole force, X-axis (1000 N)	0.3	102.2



Peak Force vs. Delta Velocity
1997 Geo Metro

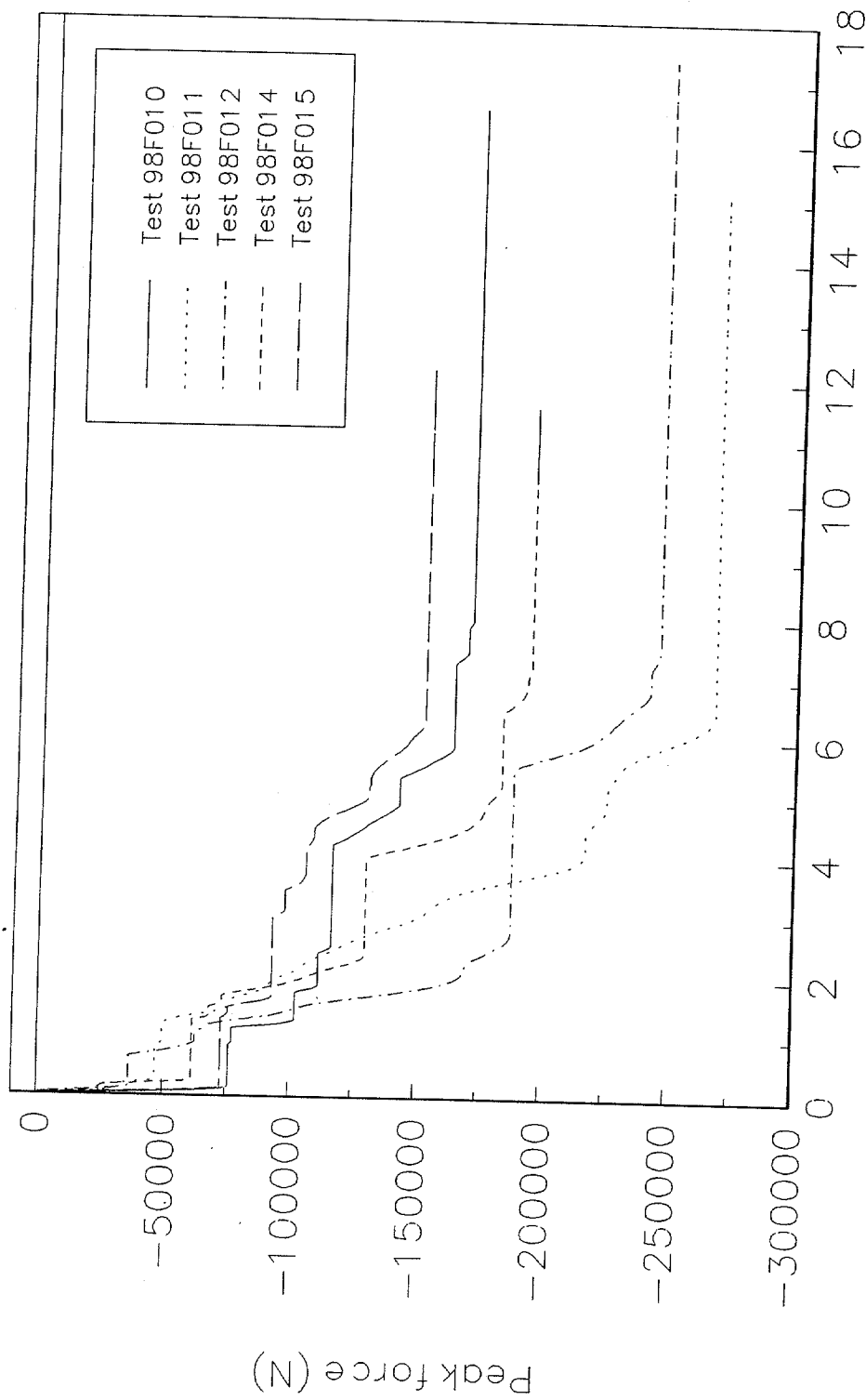


Figure 13. Peak force vs. delta velocity, five frontal Geo Metro crash tests.



Force vs. Displacement
1997 Geo Metro

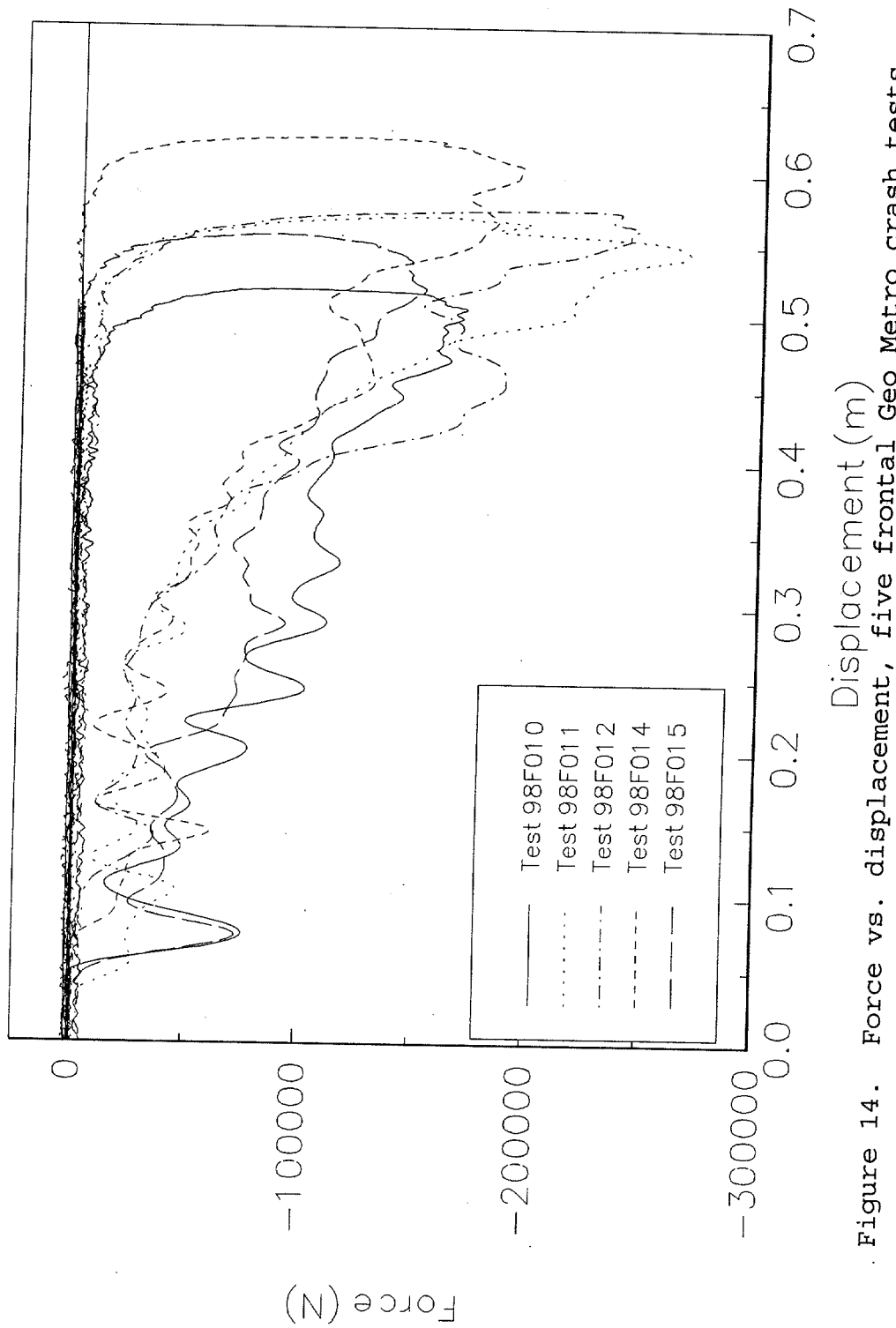


Figure 14. Force vs. displacement, five frontal Geo Metro crash tests.



Energy vs. Displacement
1997 Geo Metro

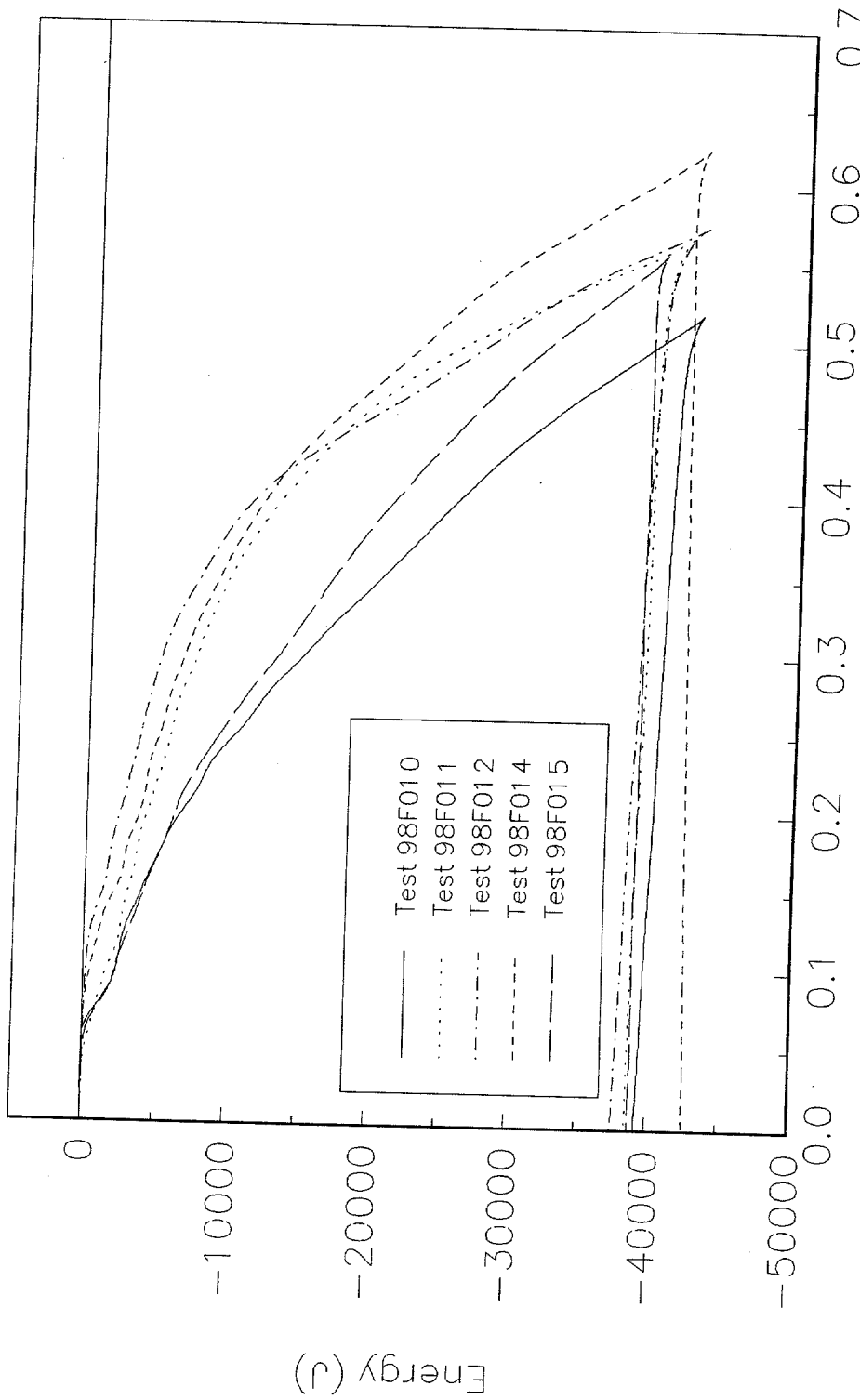
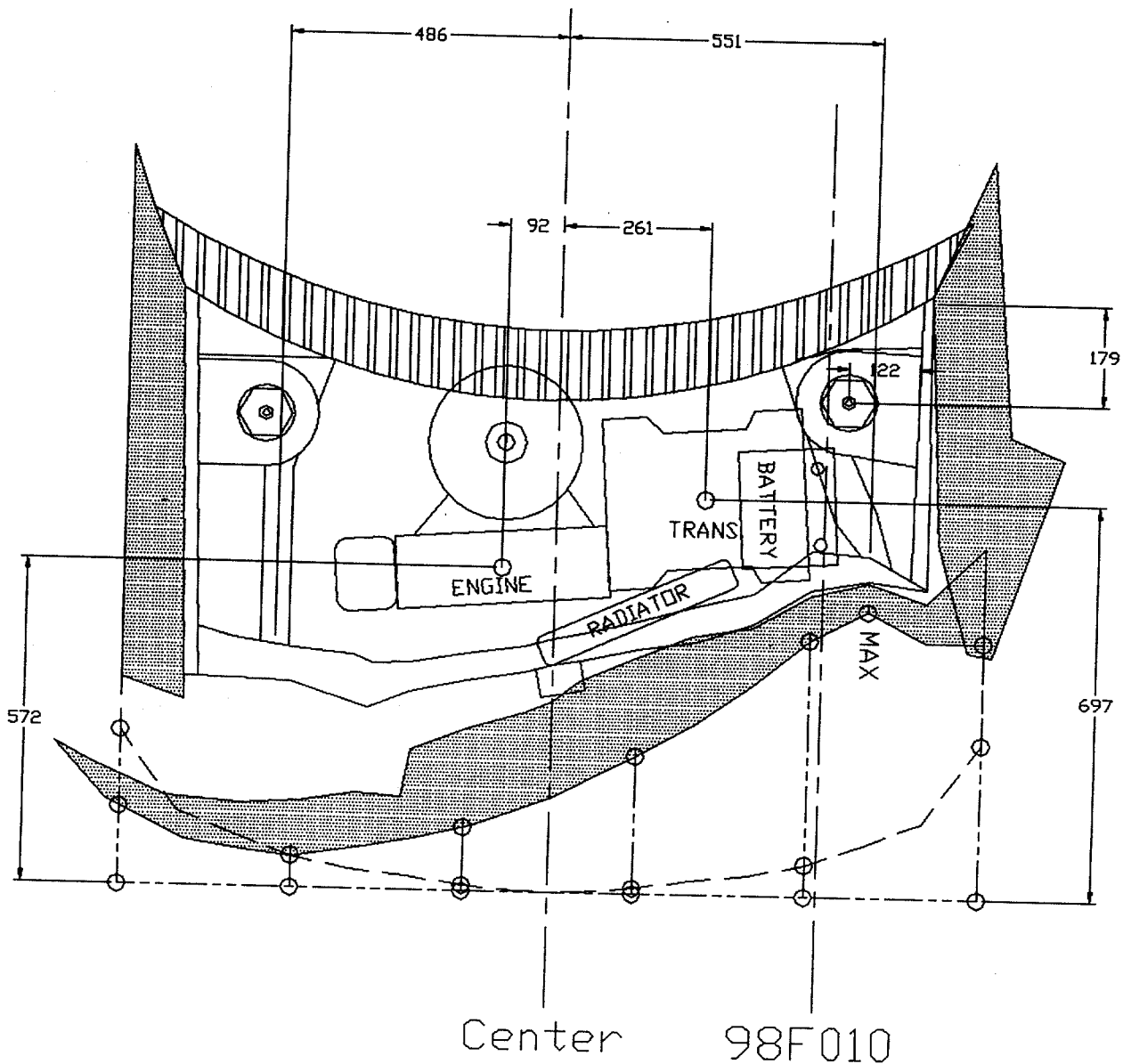


Figure 15. Energy vs. displacement, five front-end Geo Metro crash tests.



APPENDIX A. VEHICLE CRUSH MEASUREMENTS

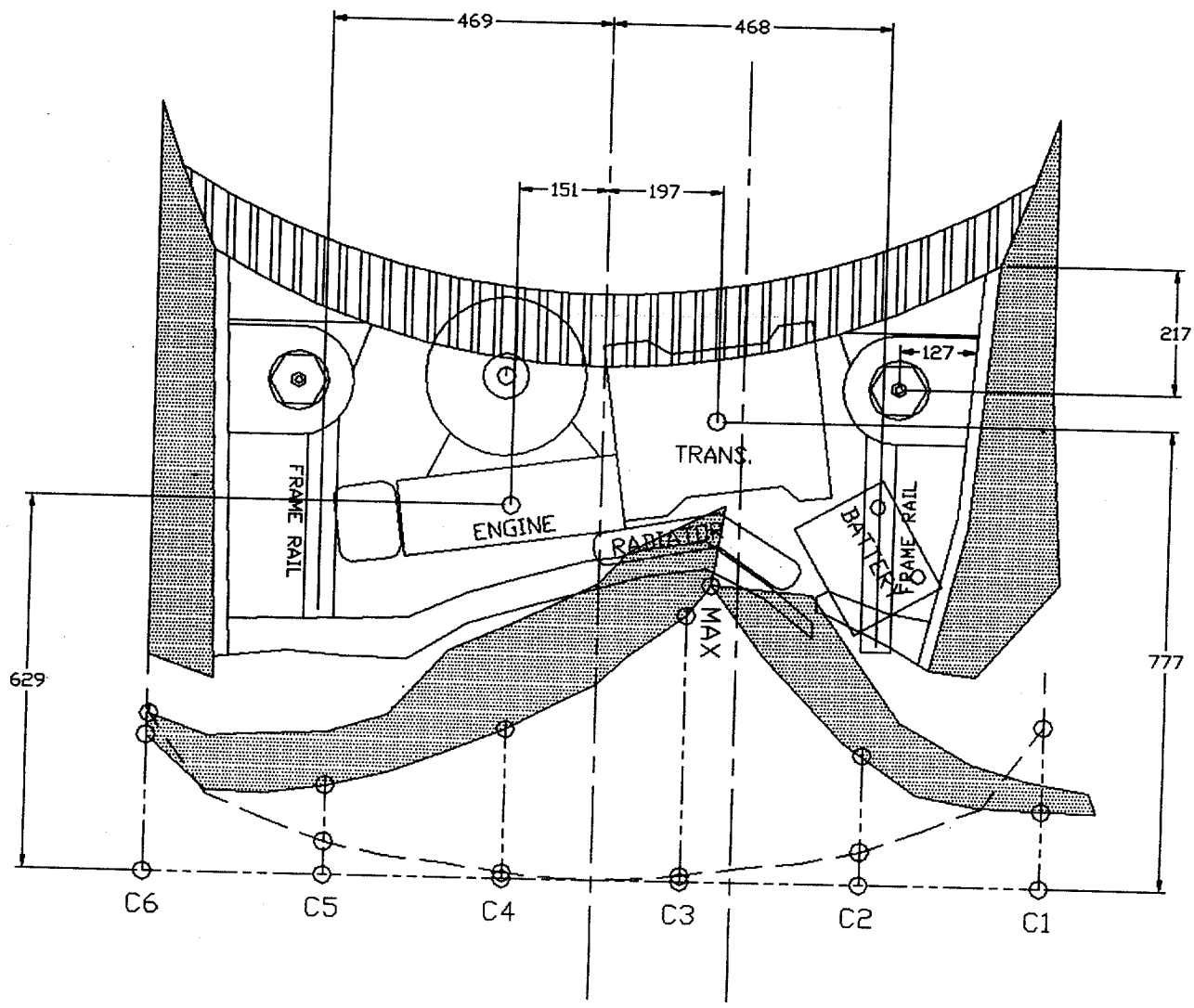


Crush

C1= 197mm C4= 89mm
 C2= 419mm C5= -12mm
 C3= 204mm C6=-133mm
 Max crush= 464mm L= 1448mm

Figure 16. Vehicle deformation sketch, test 98F010.





Center 98F011

Crush

C1= -107mm C4= 227mm

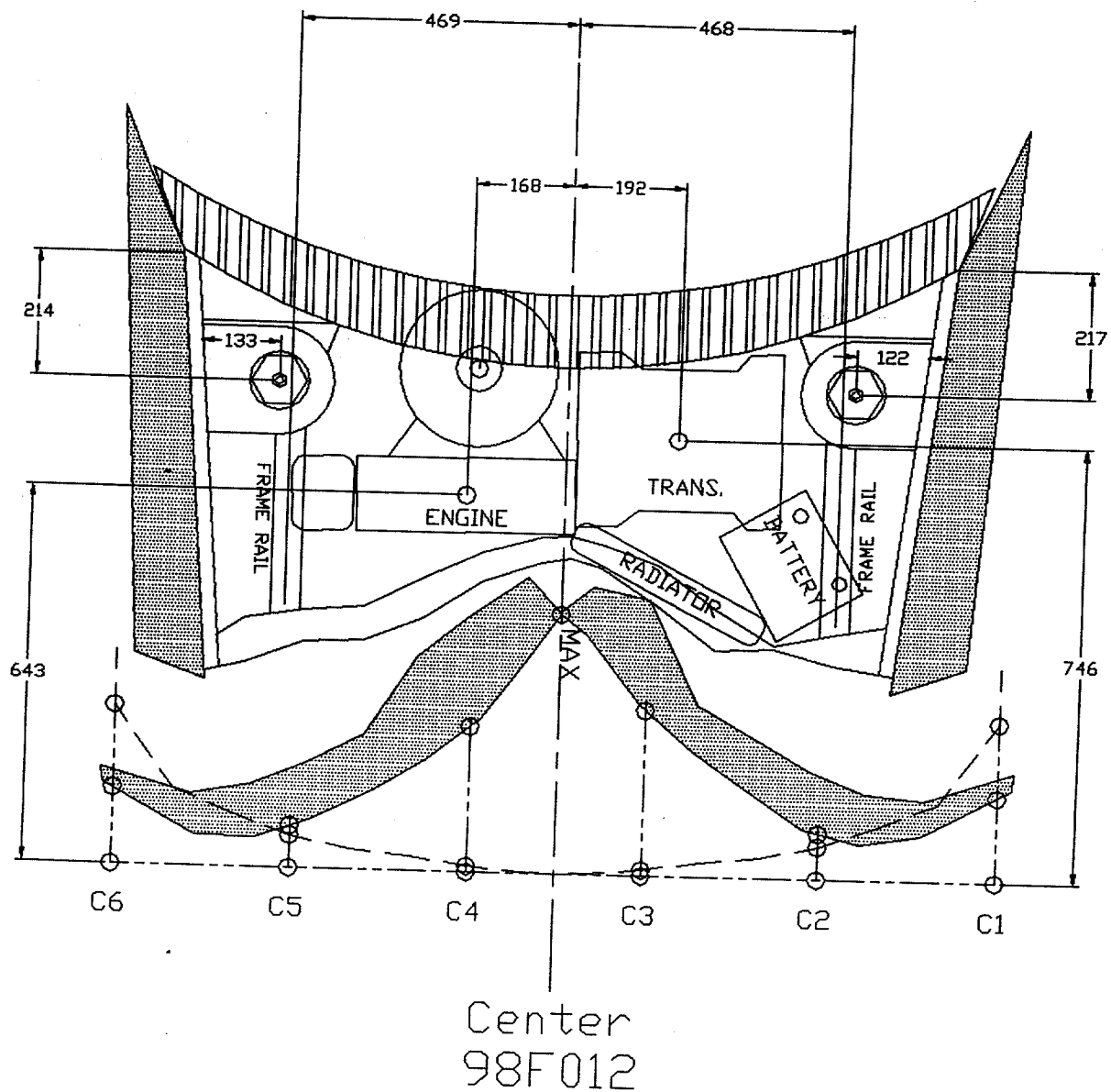
C2= 146mm C5= 53mm

C3= 459mm C6= -38mm

Max crush= 567mm L= 1448mm

Figure 17. Vehicle deformation sketch, test 98F011.



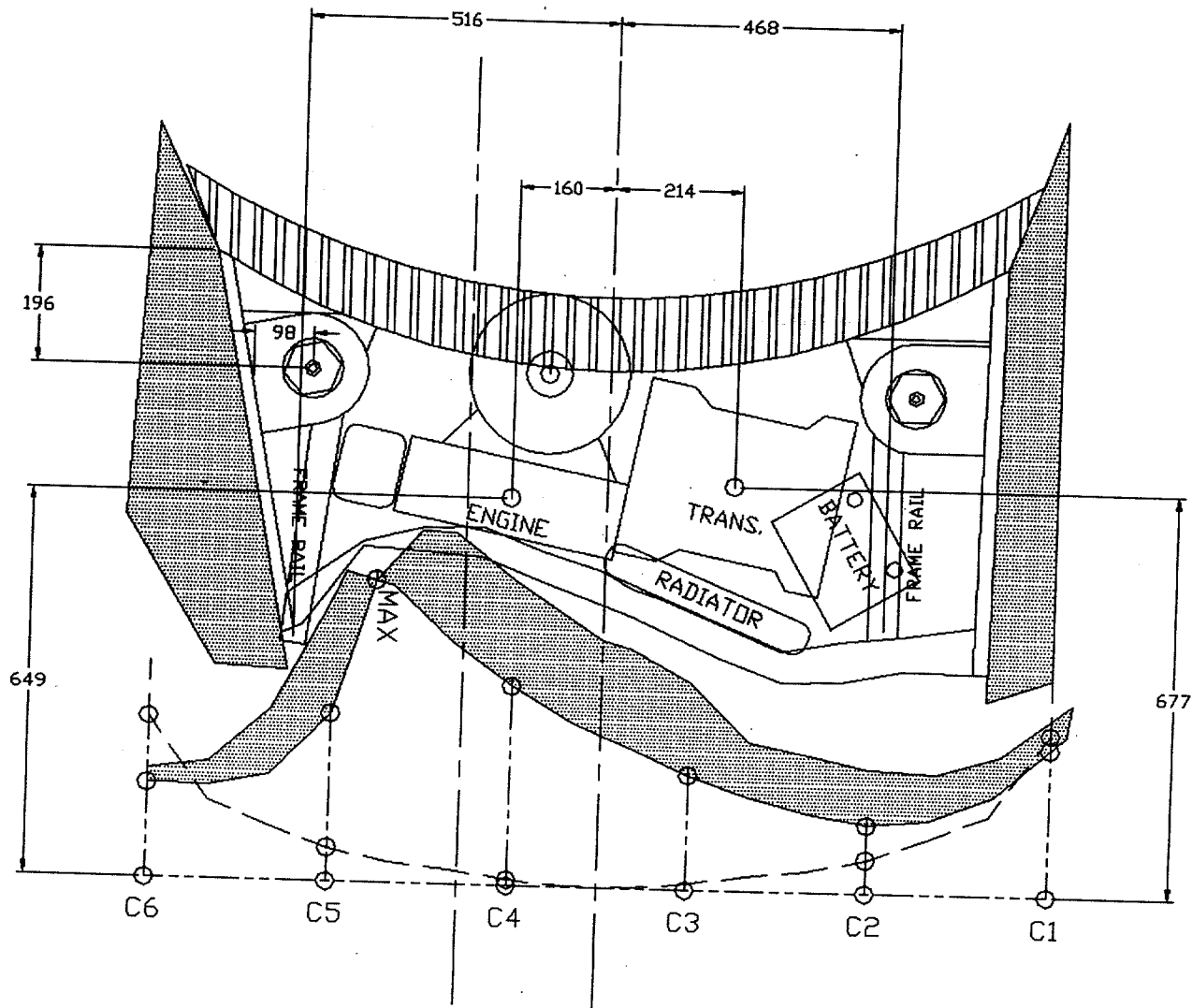


Crush

C1= -156mm C4= 151mm
 C2= 2mm C5= -27mm
 C3= 262mm C6= -111mm
 Max crush= 515mm L= 1448mm

Figure 18. Vehicle deformation sketch, test 98F012.





98F014 Center

Crush

$$C1 = -18\text{mm} \quad C4 = 307\text{mm}$$

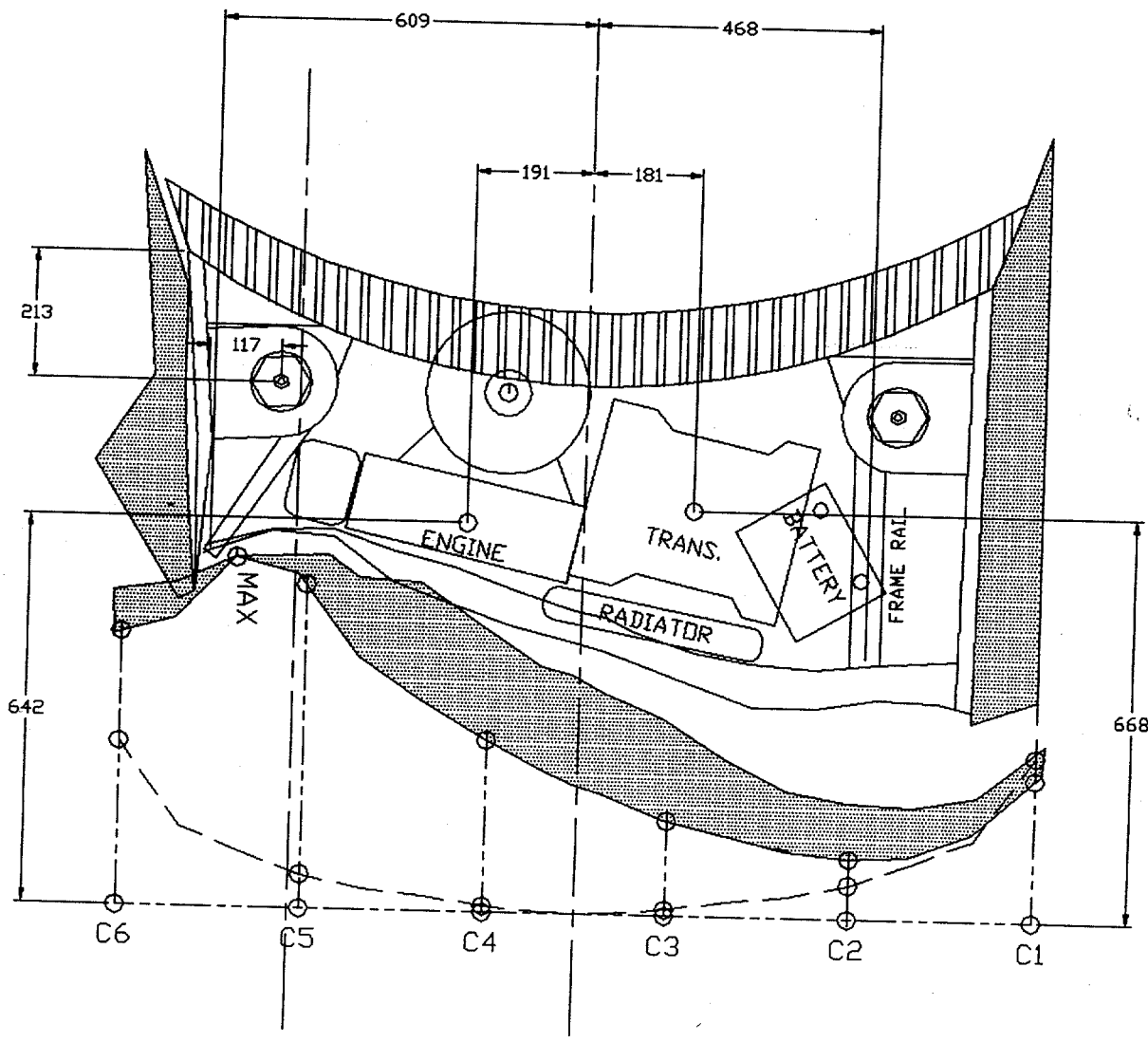
$$C2 = 32\text{mm} \quad C5 = 179\text{mm}$$

$$C3 = 155\text{mm} \quad C6 = -166\text{mm}$$

$$\text{Max crush} = 516\text{mm} \quad L = 1448\text{mm}$$

Figure 19. Vehicle deformation sketch, test 98F014.





98F015 Center

Crush

$$C1 = -29\text{mm} \quad C4 = 282\text{mm}$$

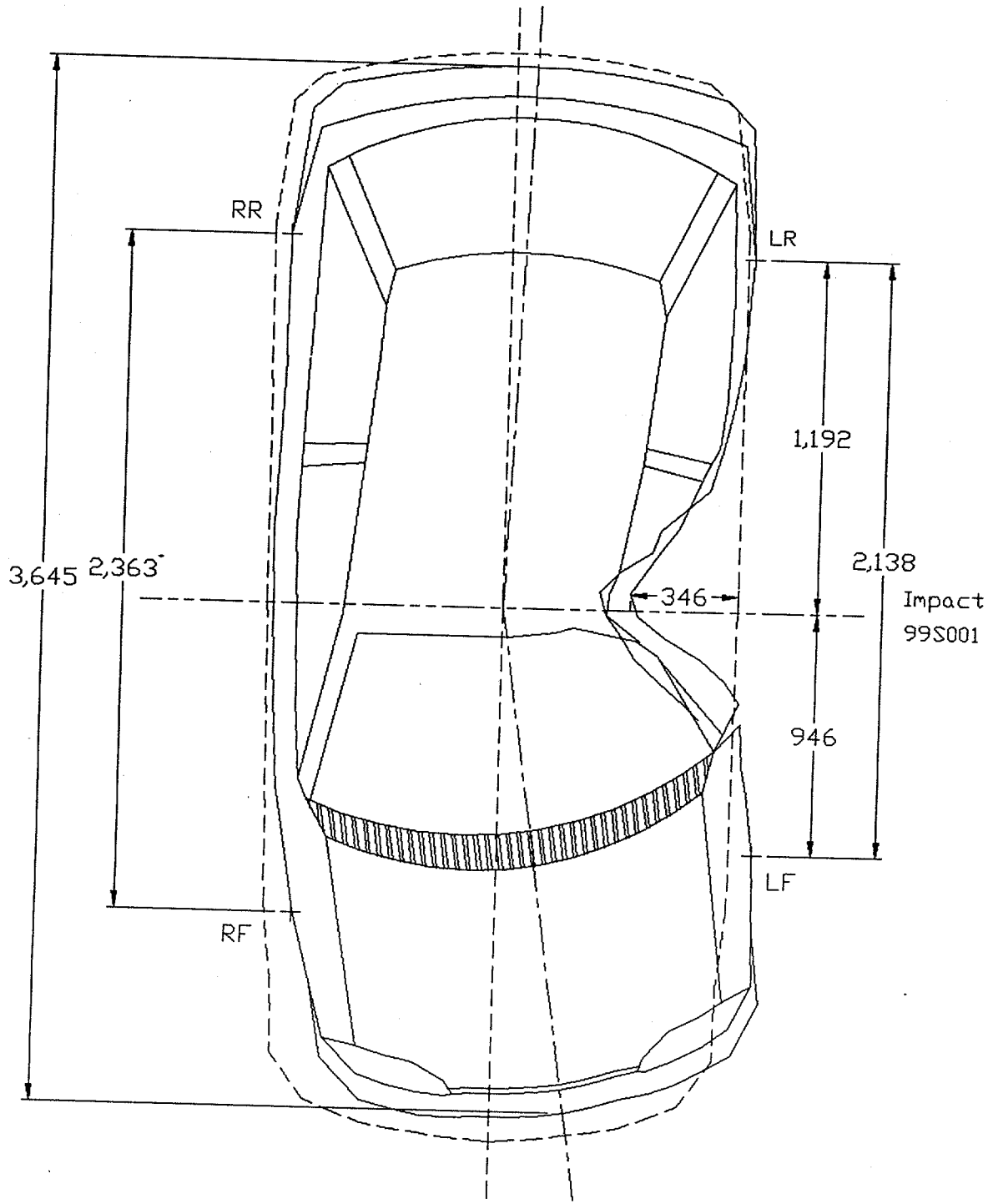
$$C2 = 36\text{mm} \quad C5 = 452\text{mm}$$

$$C3 = 153\text{mm} \quad C6 = 247\text{mm}$$

$$\text{Max crush} = 524\text{mm} \quad L = 1448\text{mm}$$

Figure 20. Vehicle deformation sketch, test 98F015.





All dimensions in mm.

Figure 21. Vehicle deformation sketch, test 99S001.



APPENDIX B. TEST PHOTOGRAPHS

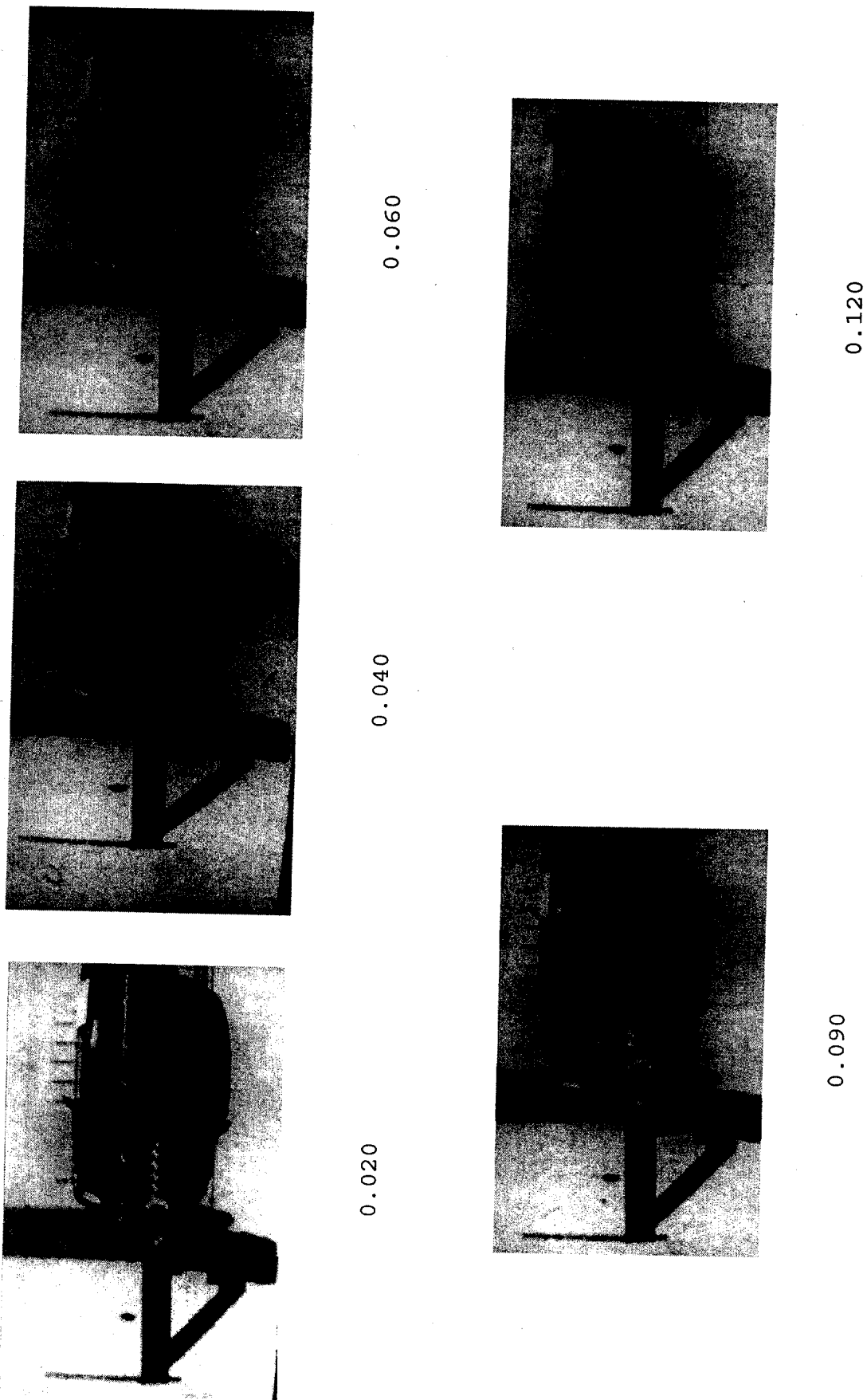


Figure 22. Photographs during the test, test 98F010.





Figure 23. Pre-test photographs, test 98F010.



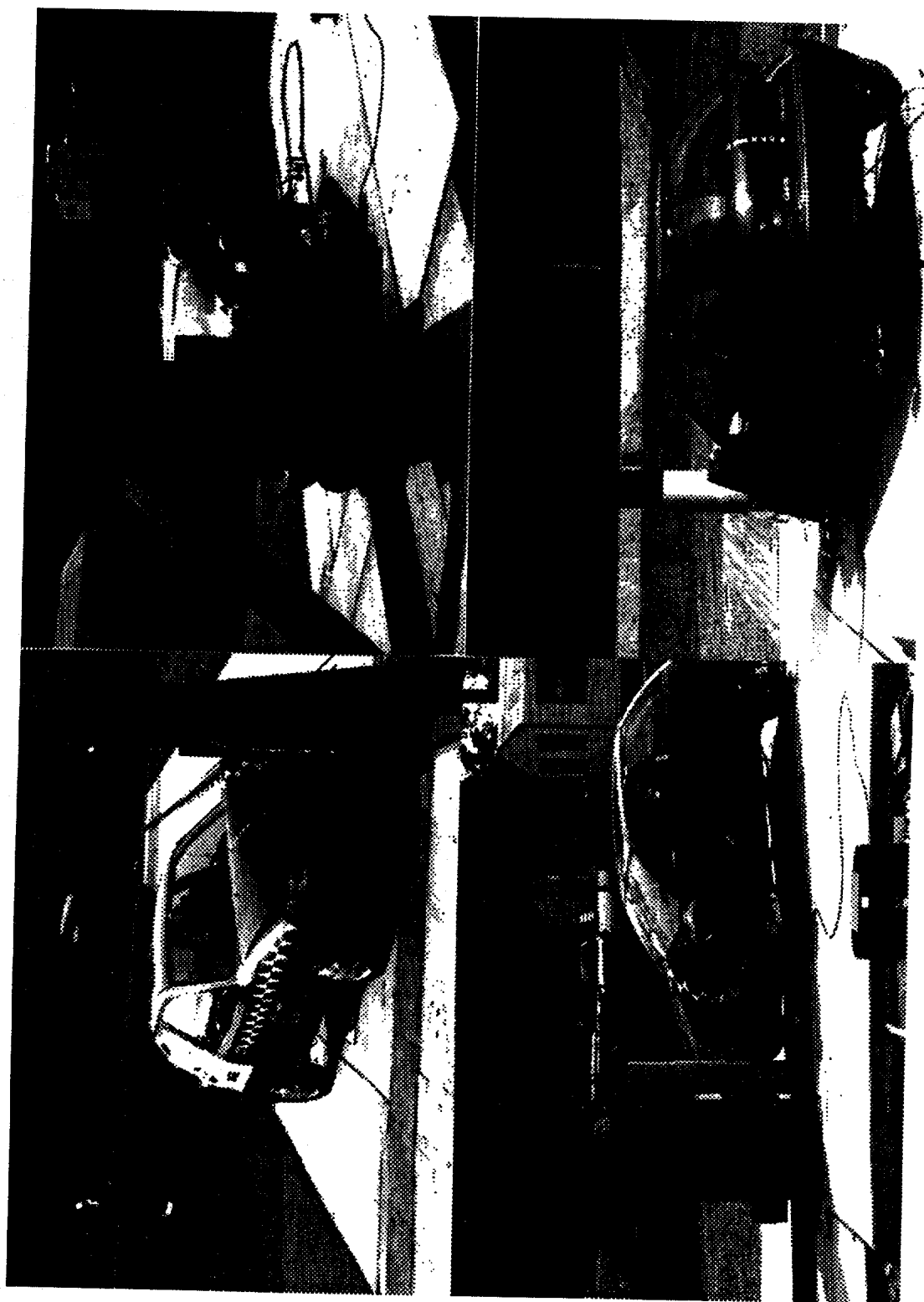


Figure 24. Post-test photographs, test 98F010.



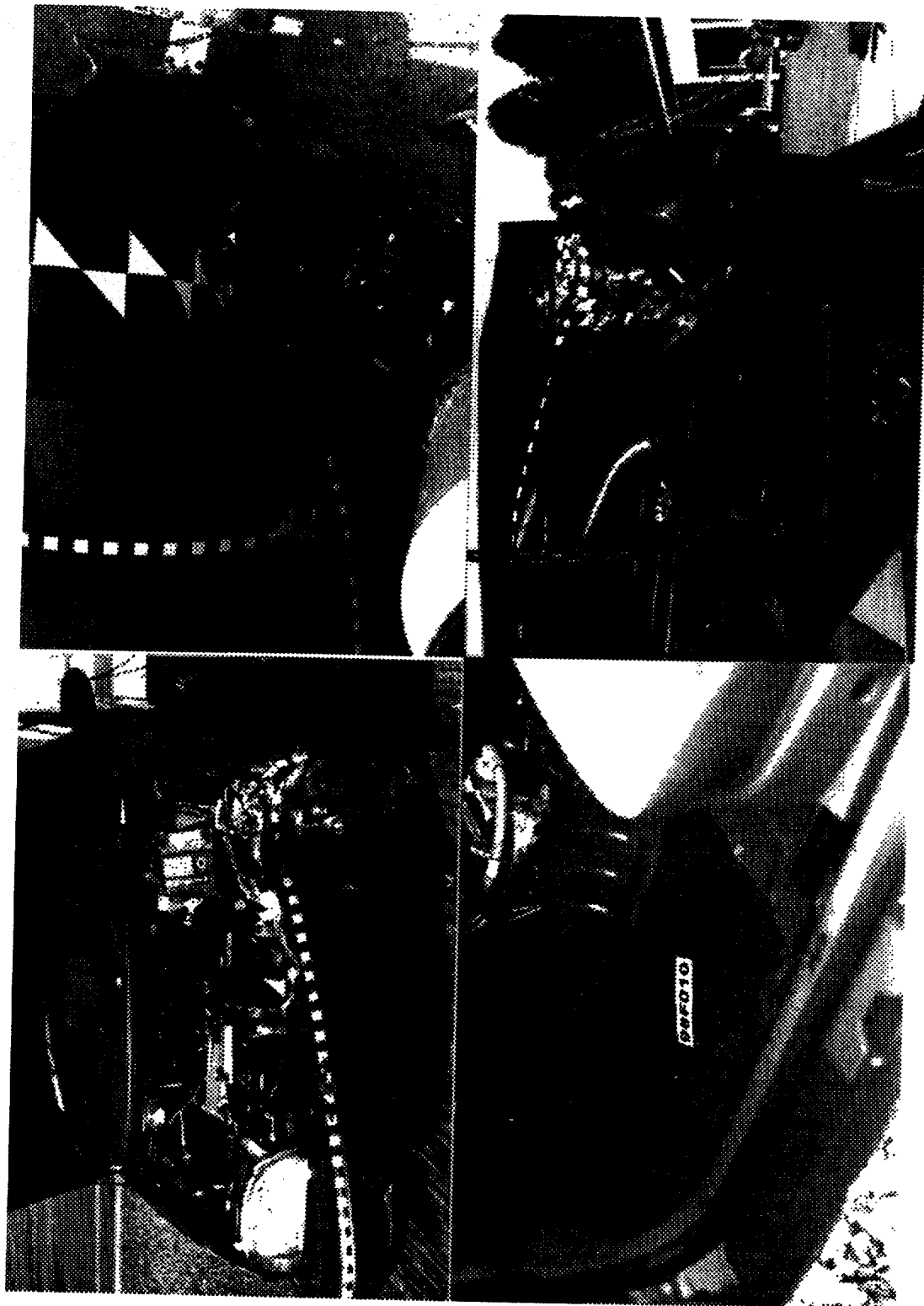


Figure 25. Additional post-test photographs, test 98F010.



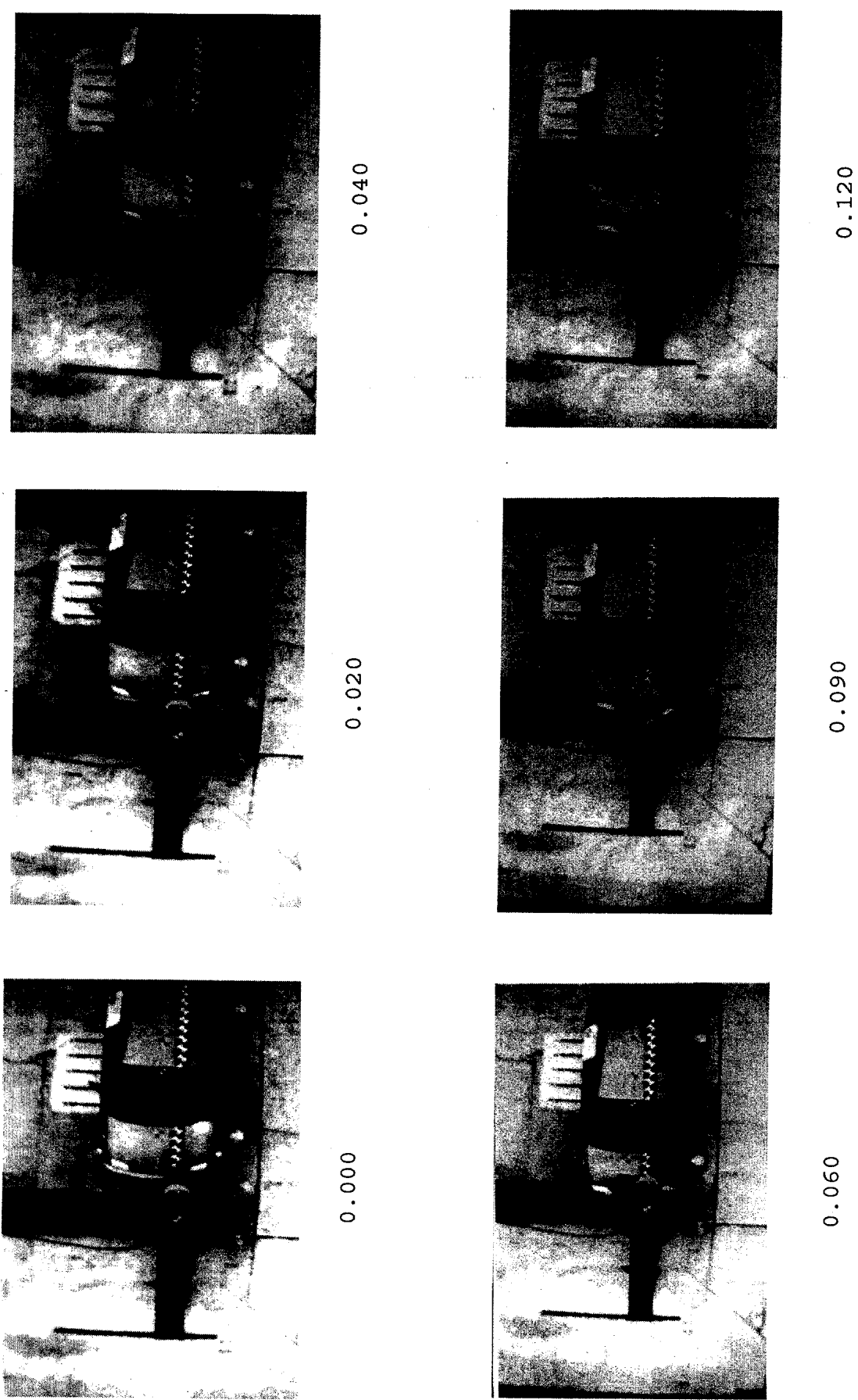
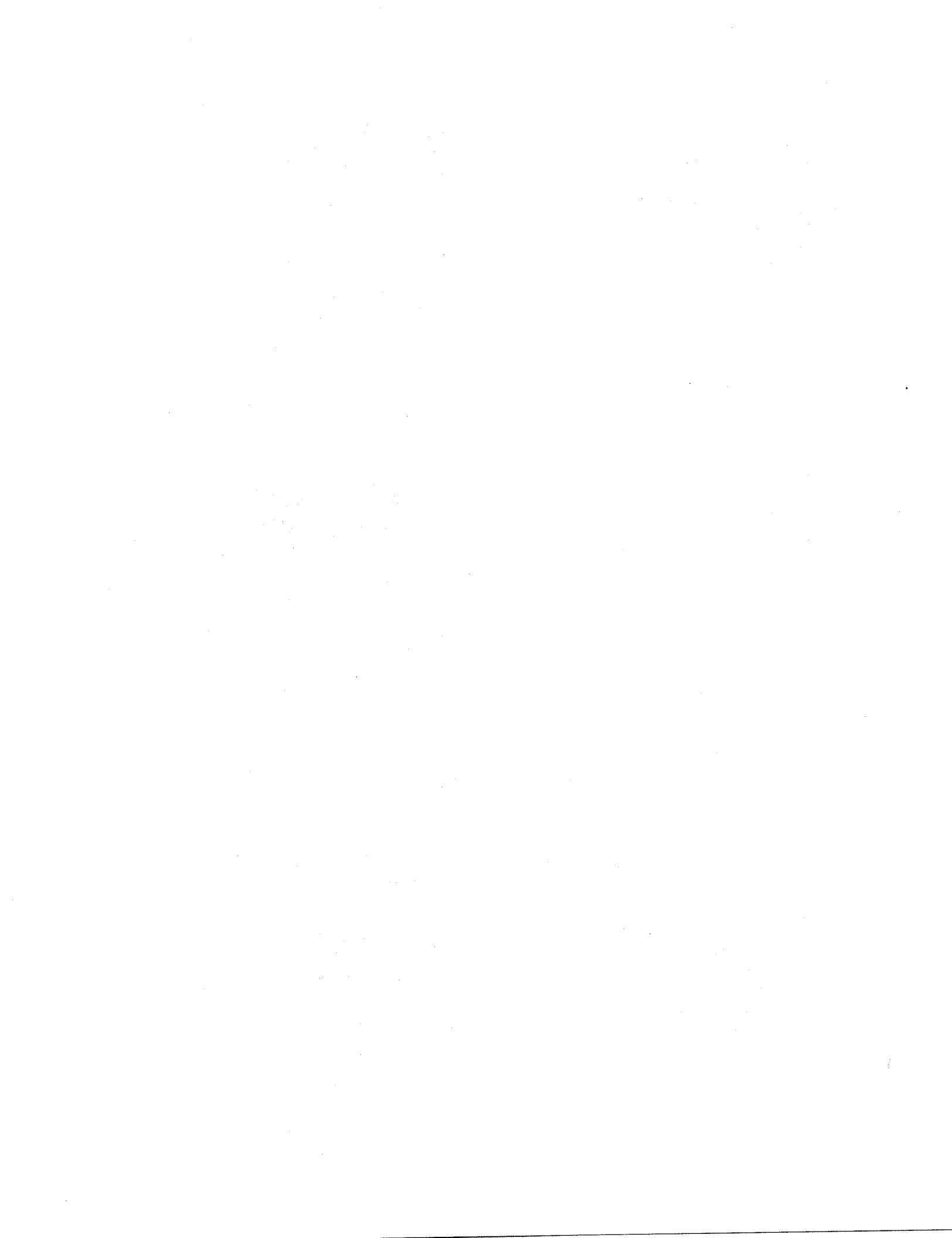


Figure 26. Photographs during the test, test 98F011.



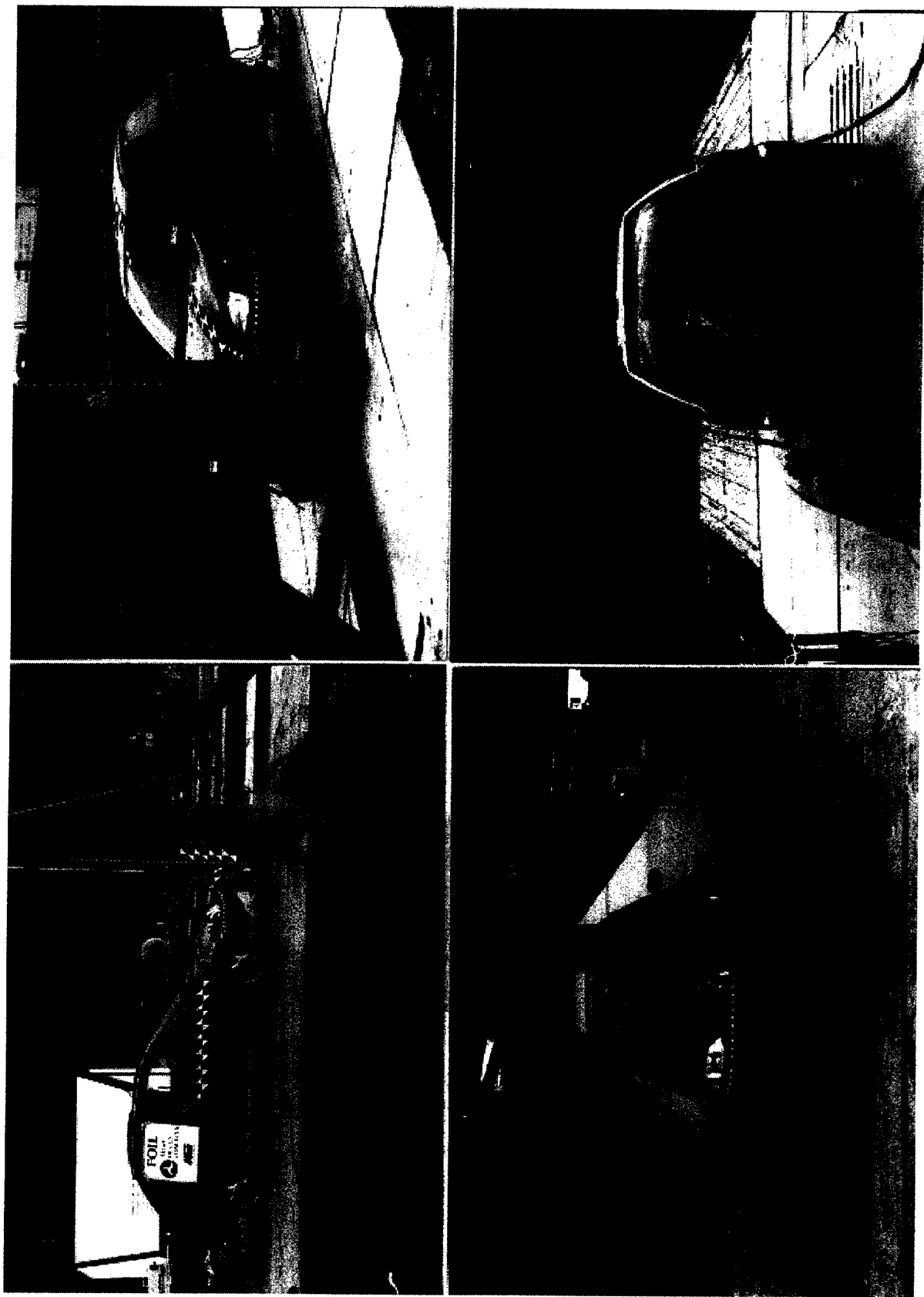


Figure 27. Pre-test photographs, test 98F011.



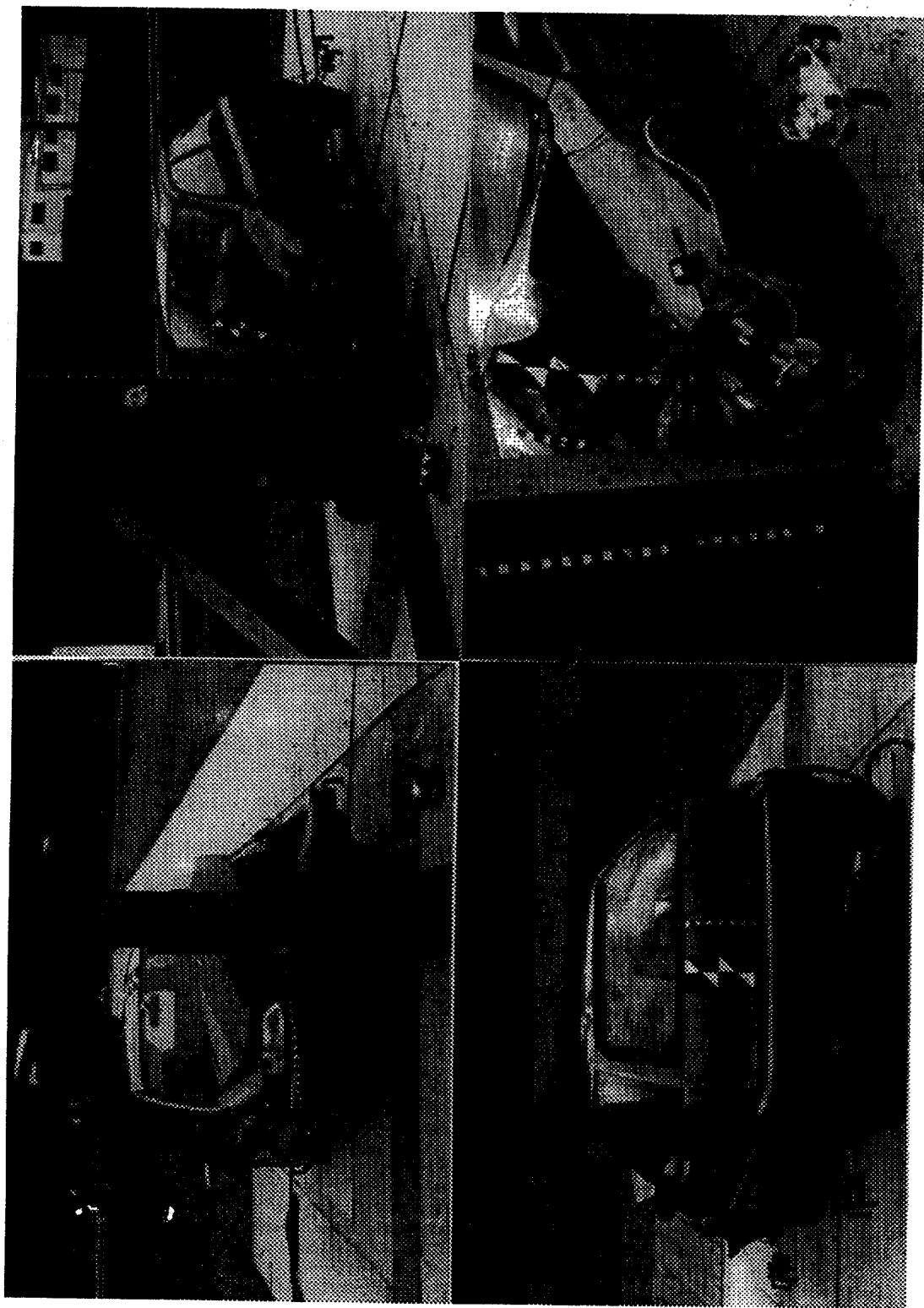
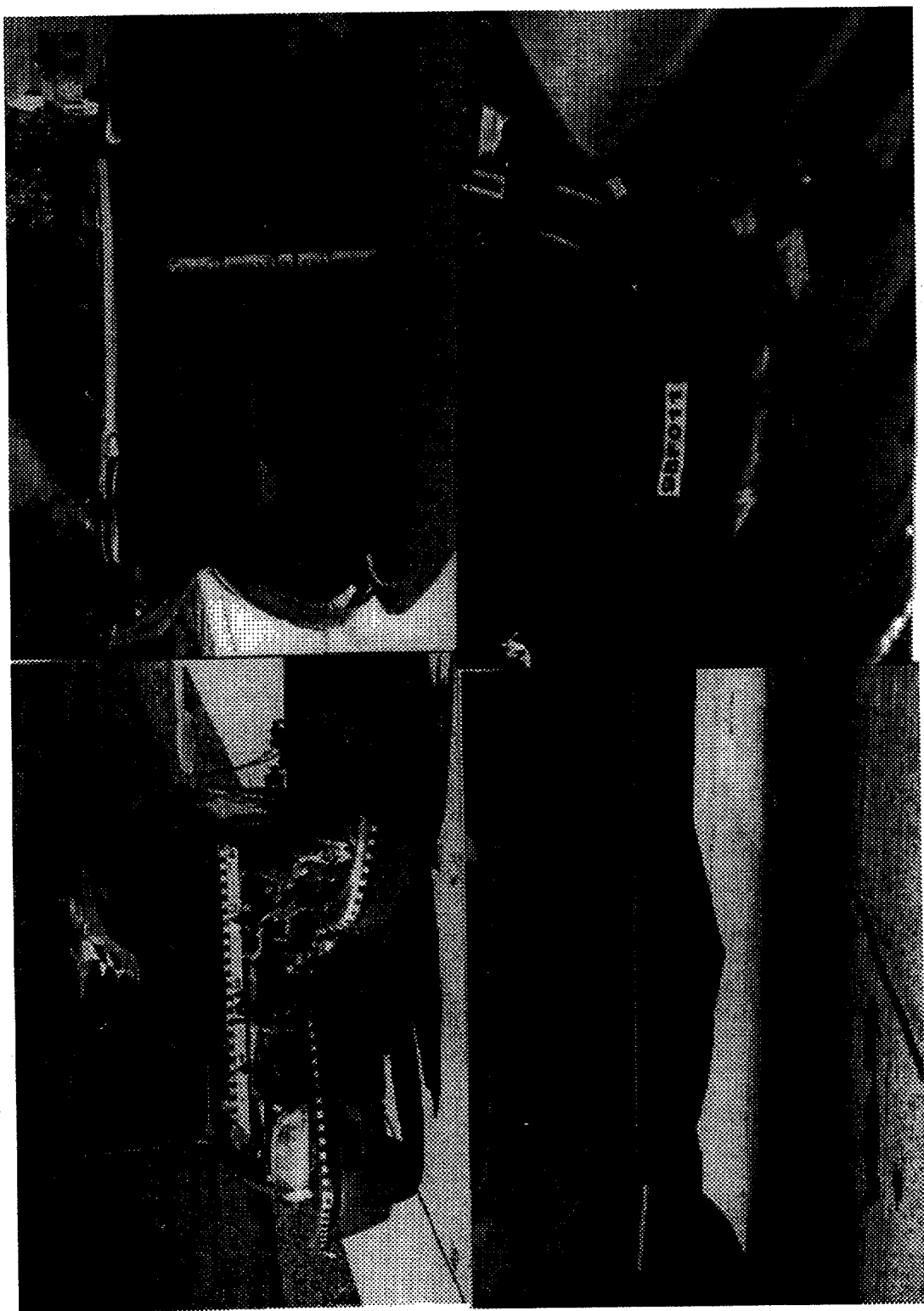


Figure 28 . Post-test photographs, test 98F011.



Figure 29. Additional post-test photographs, test 98F011.





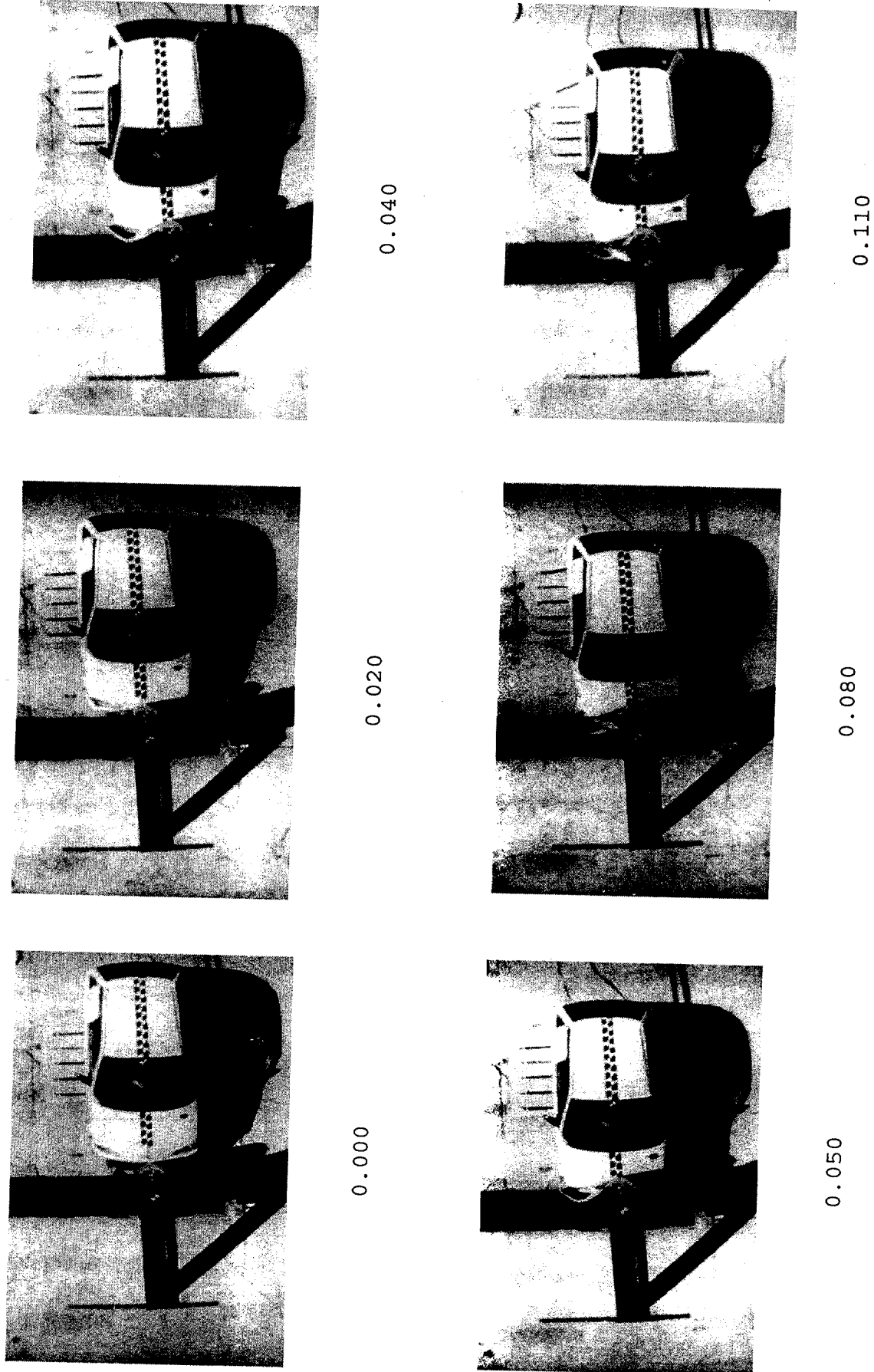


Figure 30. Photographs during the test, test 98F012.



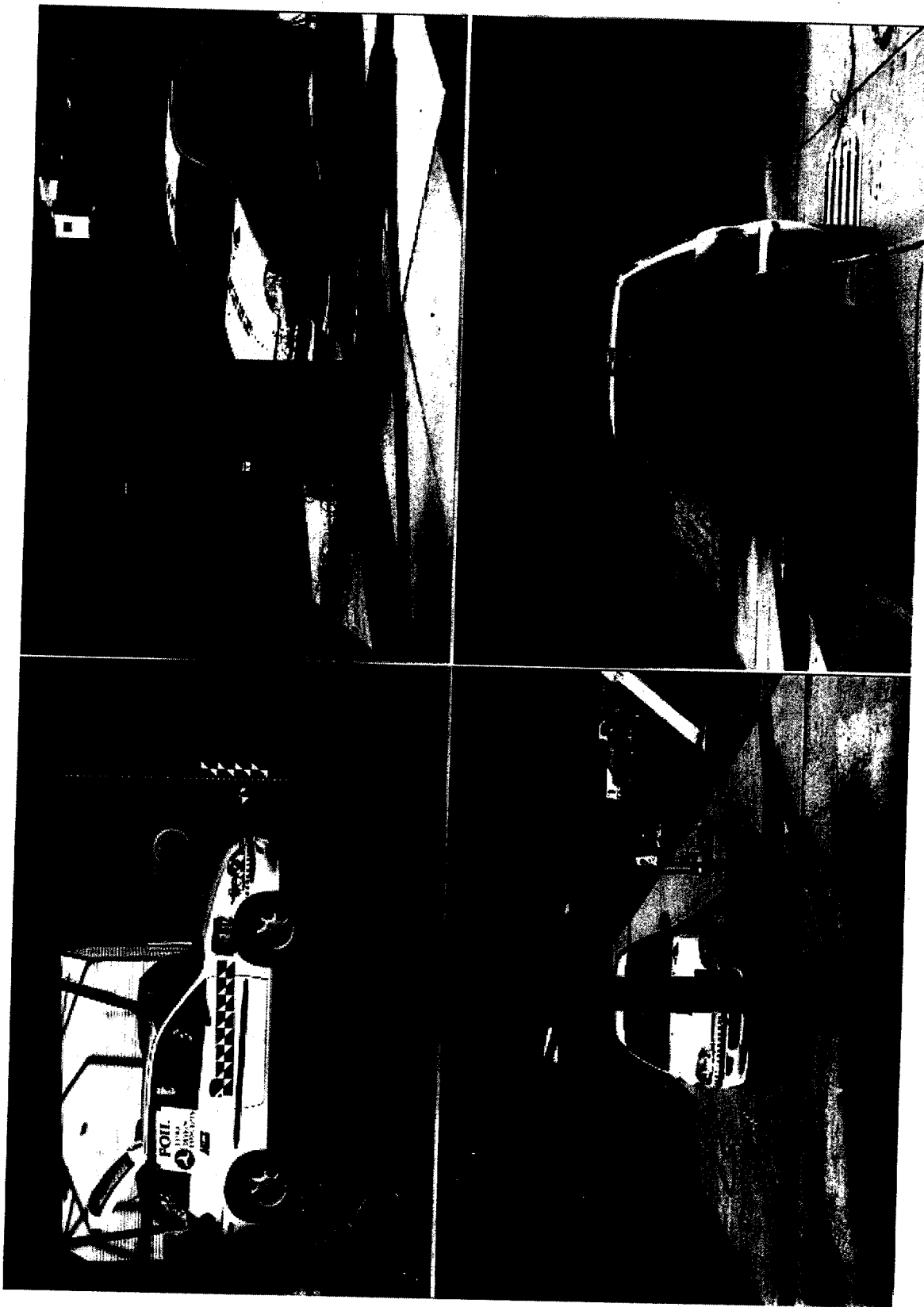


Figure 31. Pre-test photographs, test 98F012.



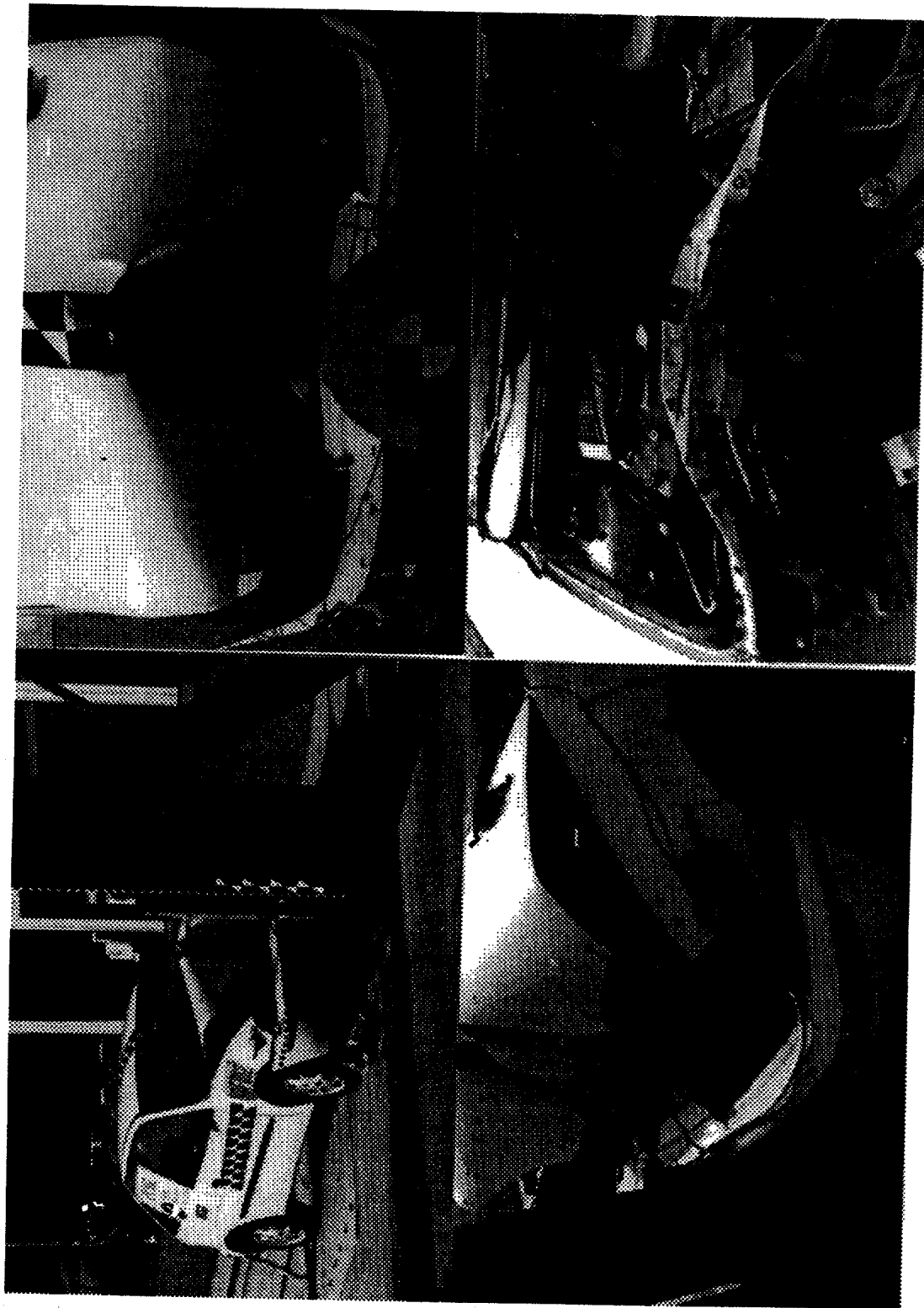


Figure 32. Post-test photographs, test 98F012.



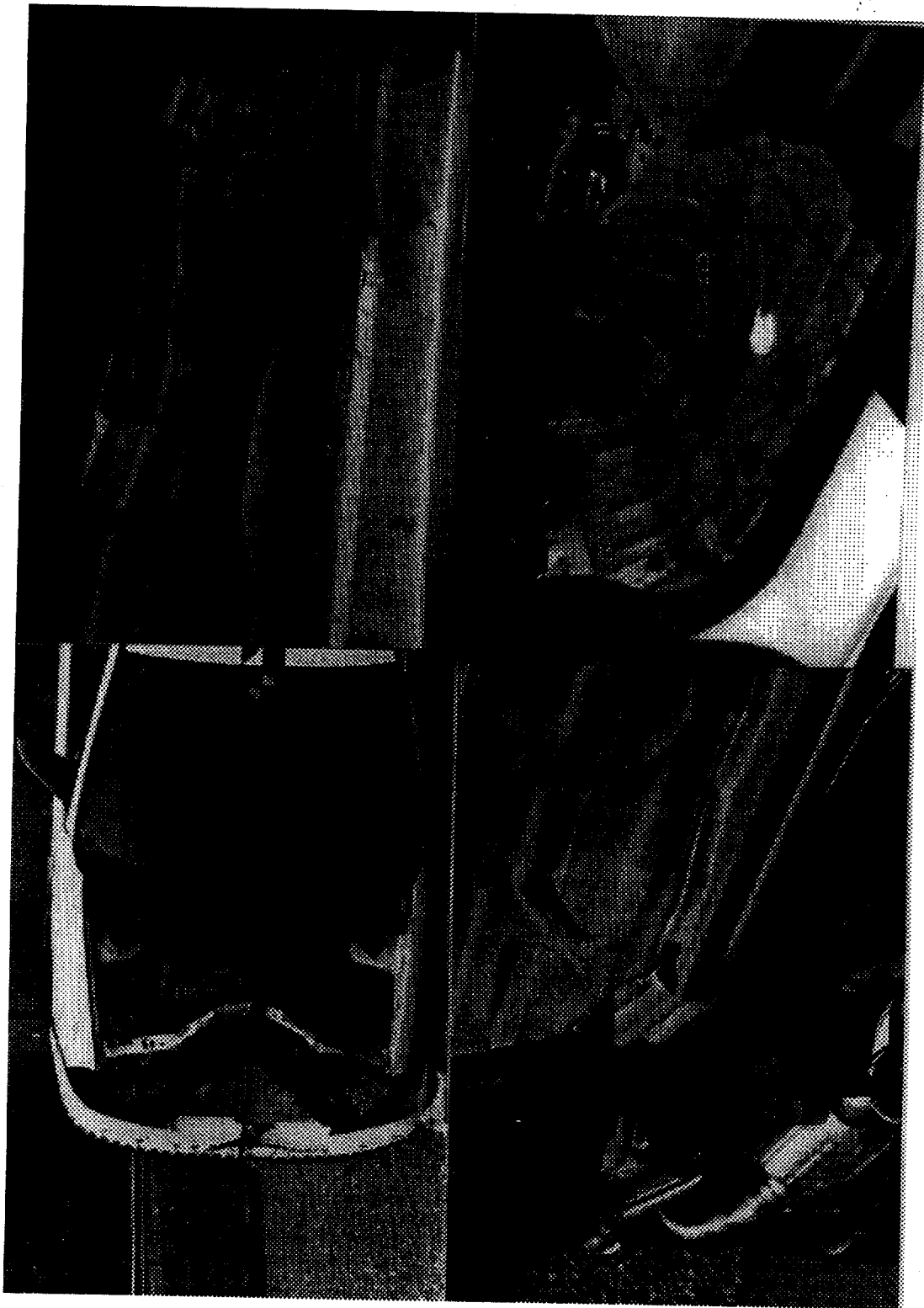


Figure 33 . Additional post-test photographs, test 98F012.



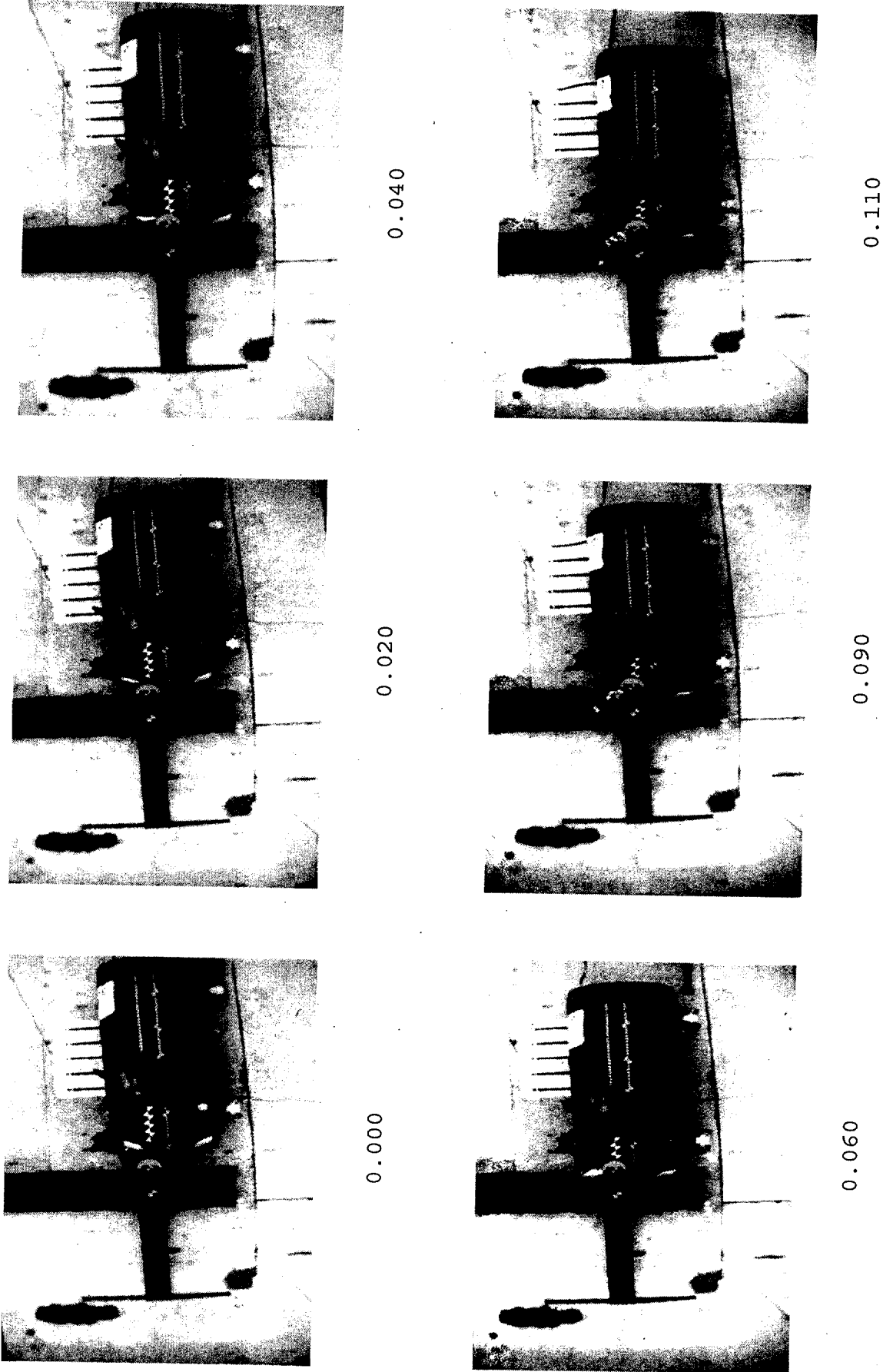


Figure 34. Photographs during the test, test 98F014.



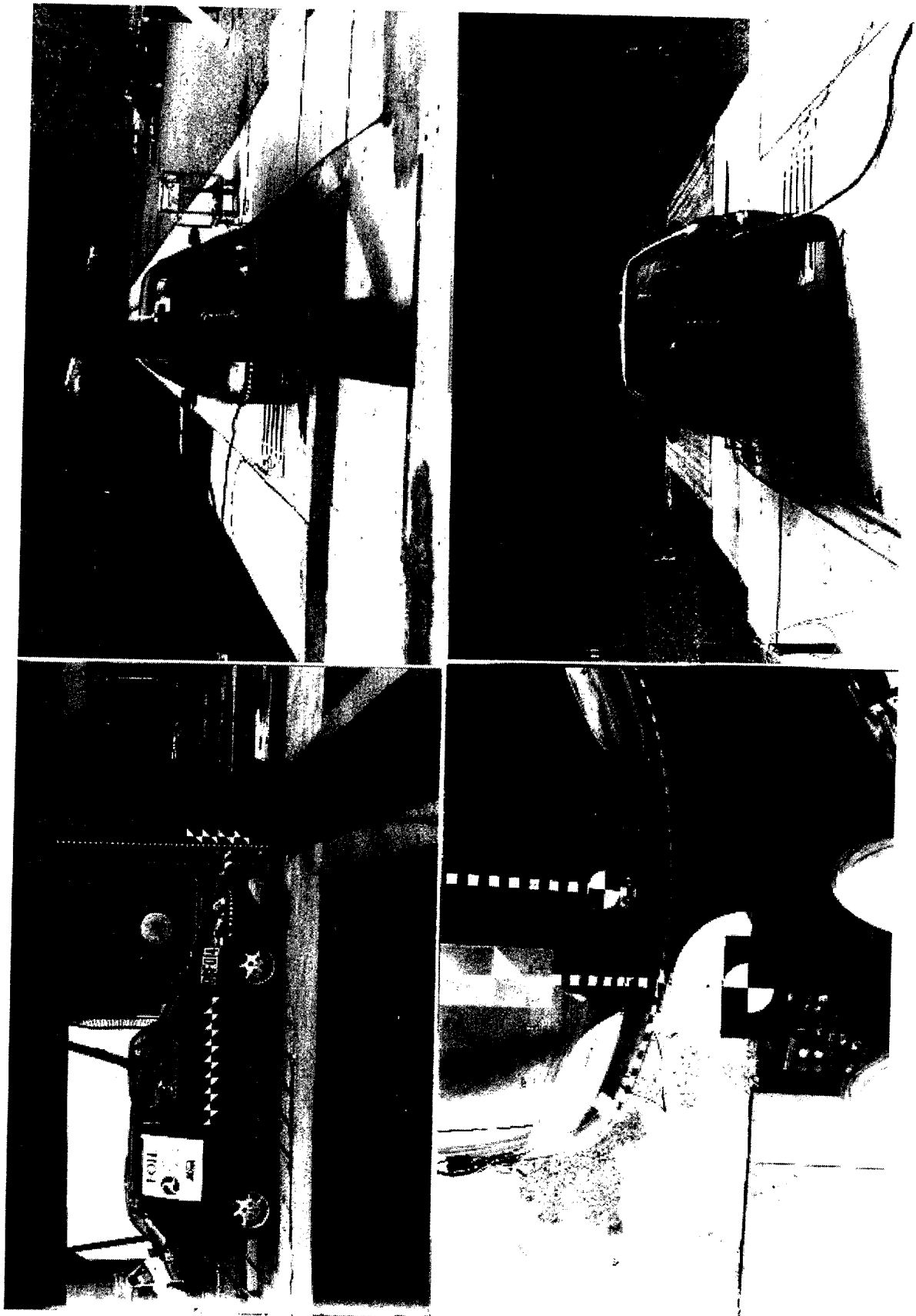


Figure 35. Pre-test photographs, test 98F014.



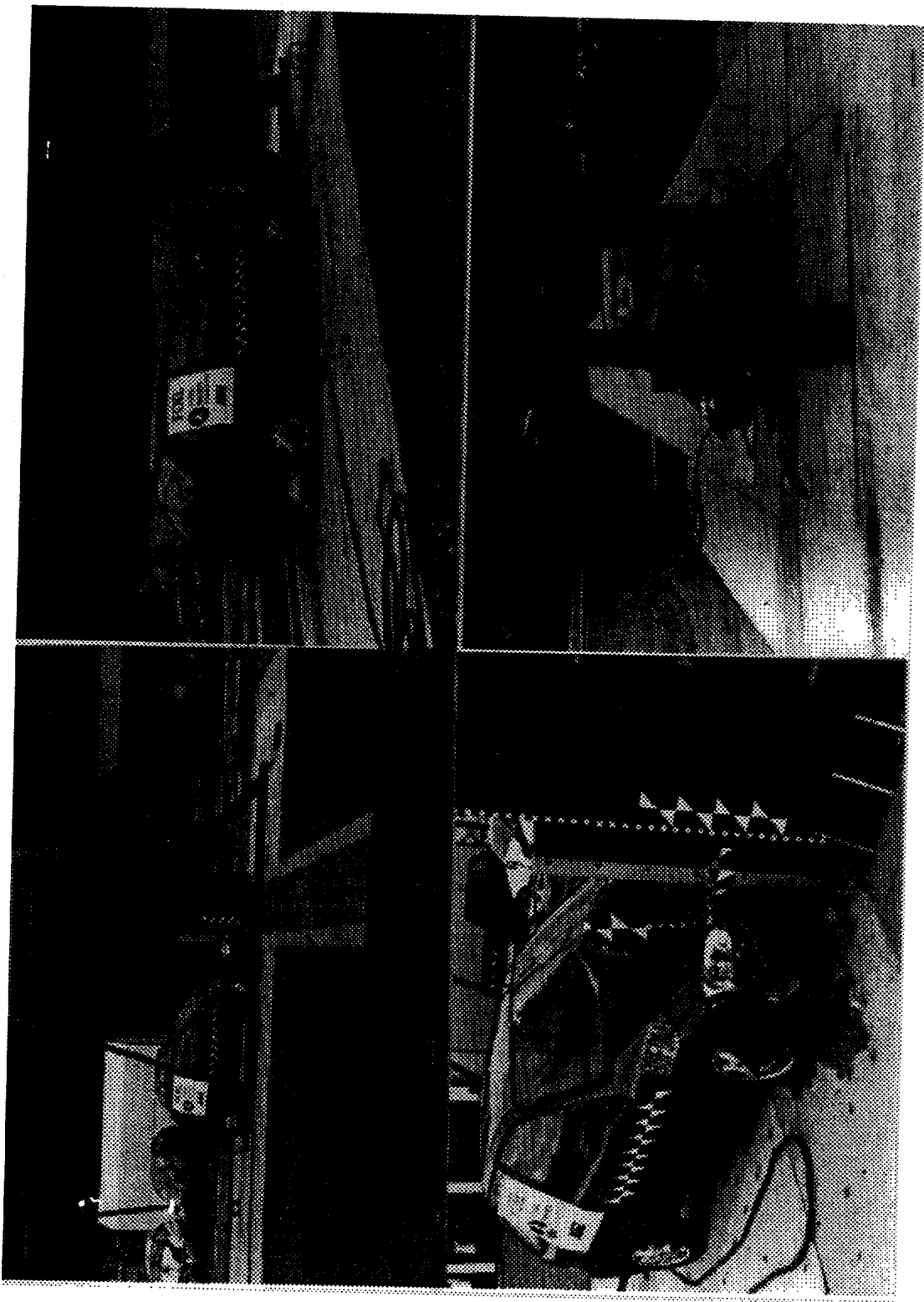


Figure 36. Post-test photographs, test 98F014.



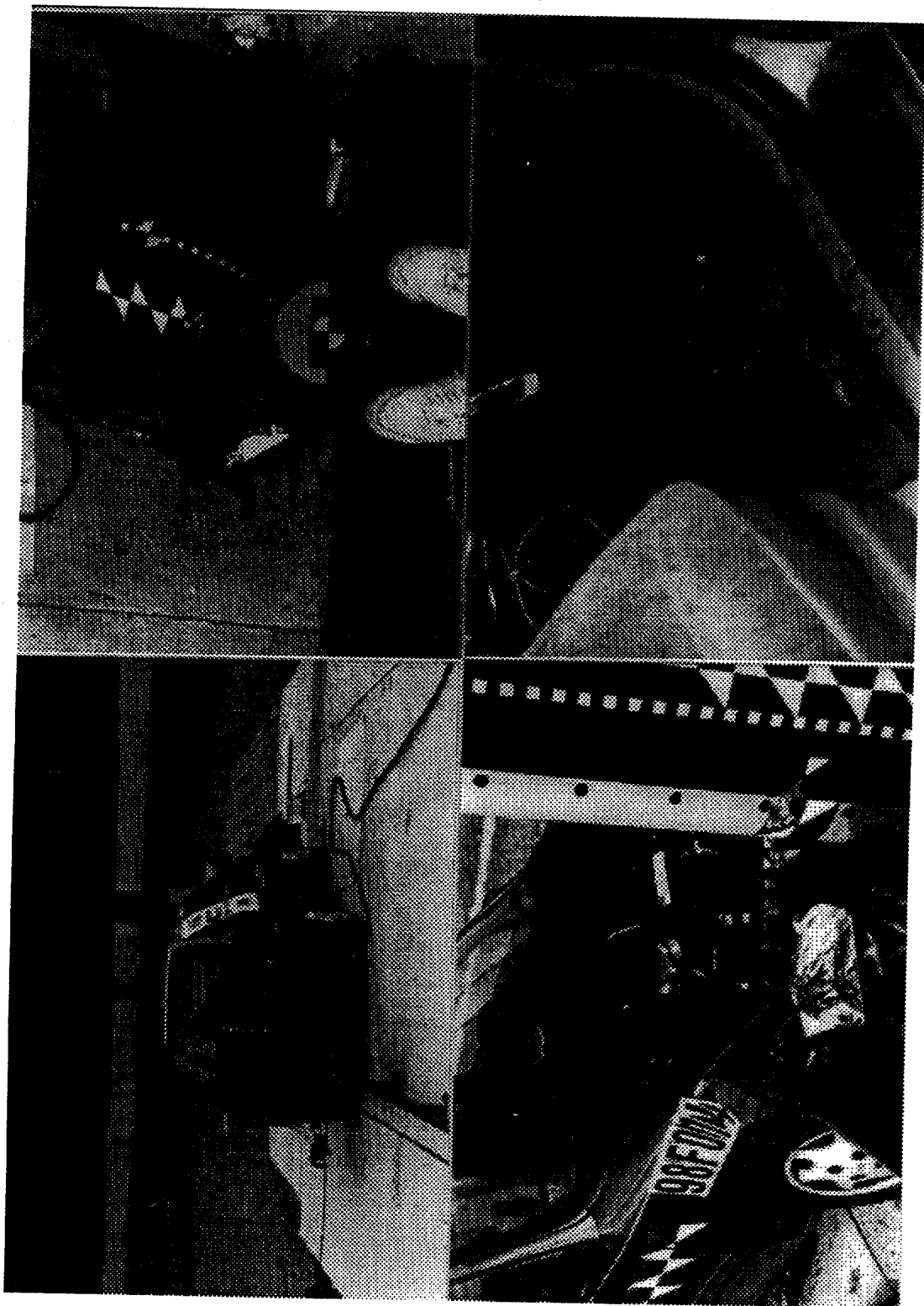


Figure 37. Additional post-test photographs, test 98F014.



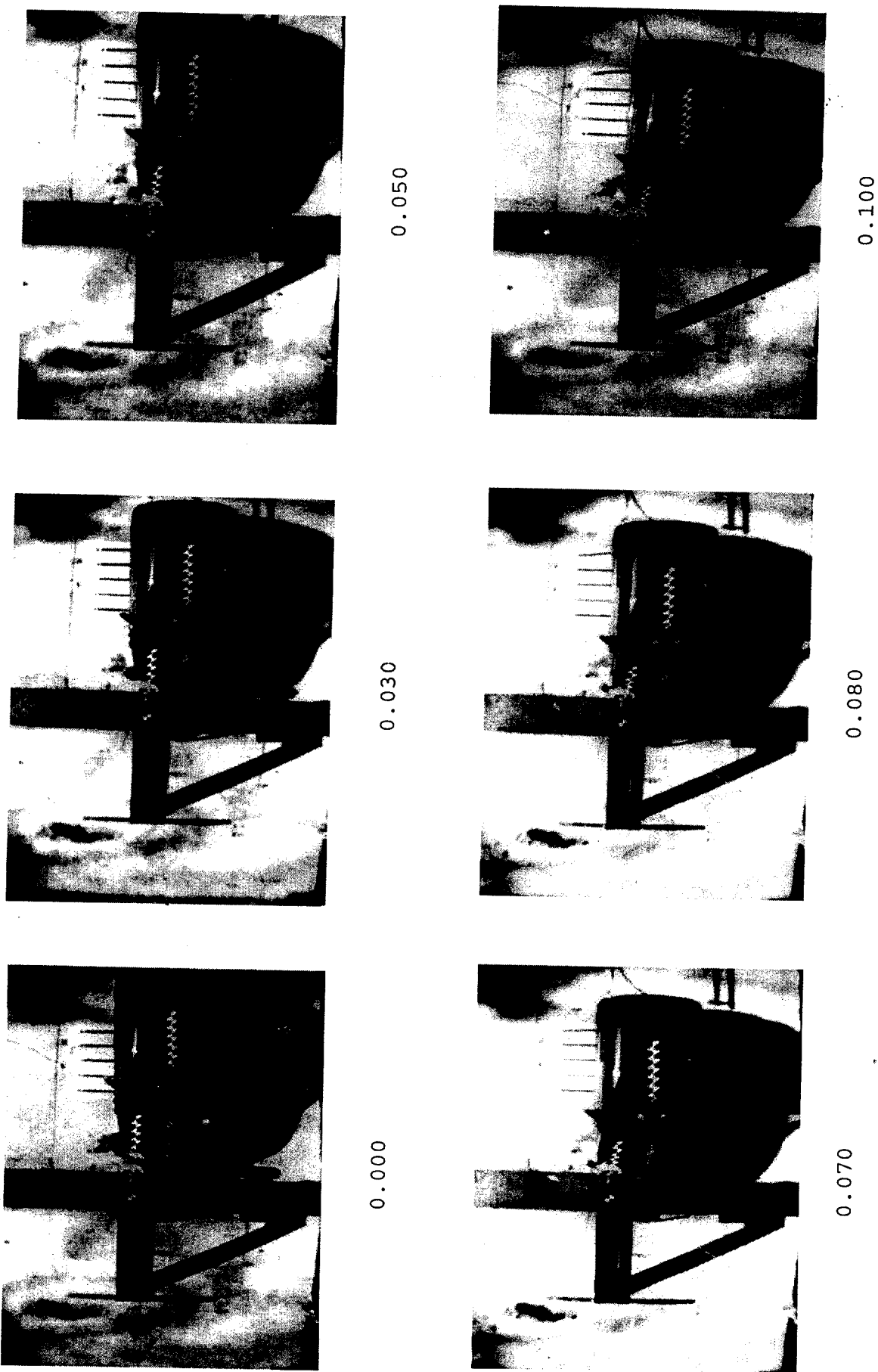


Figure 38. Photographs during the test, test 98F015.





Figure 39. Pre-test photographs, test 98F015.

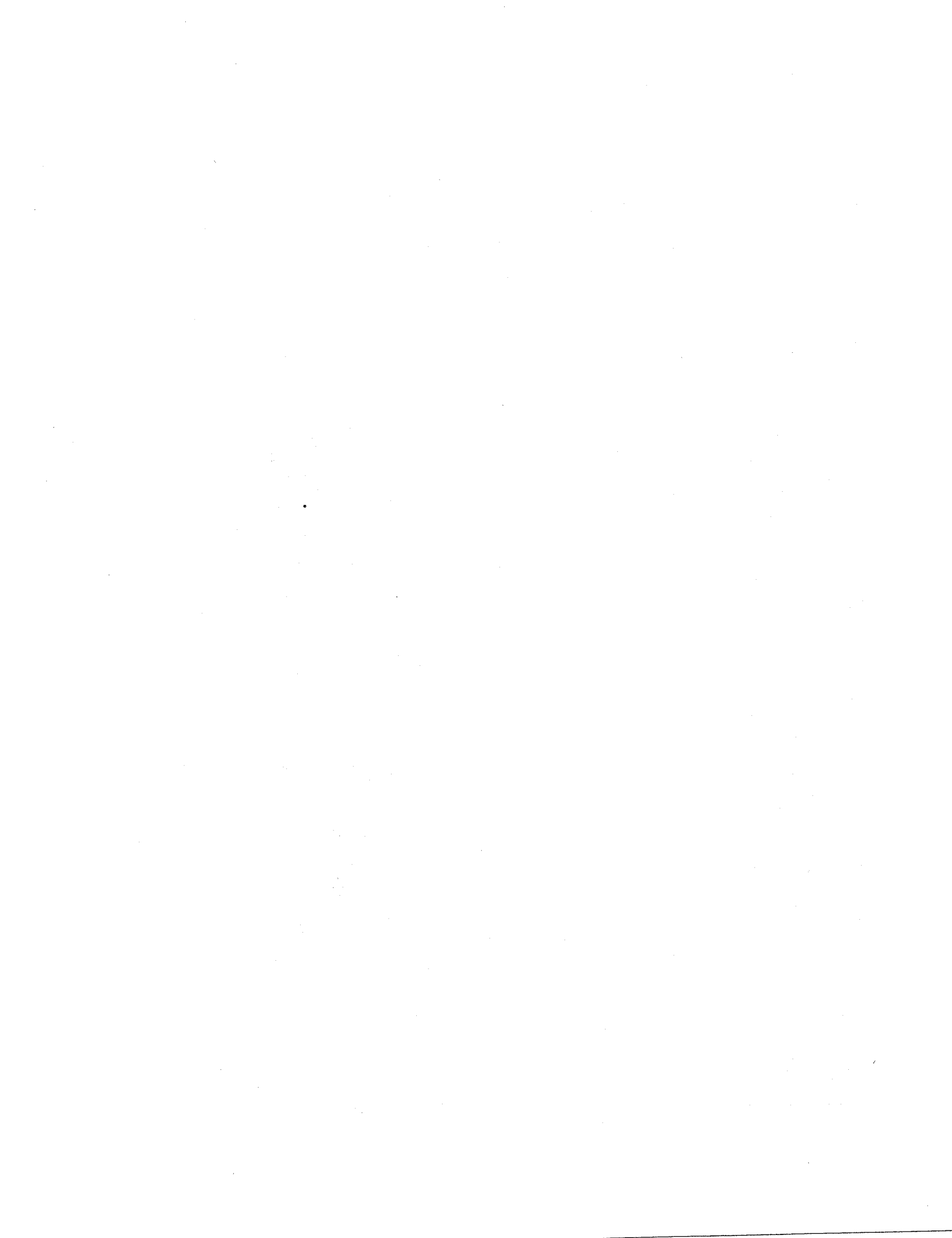
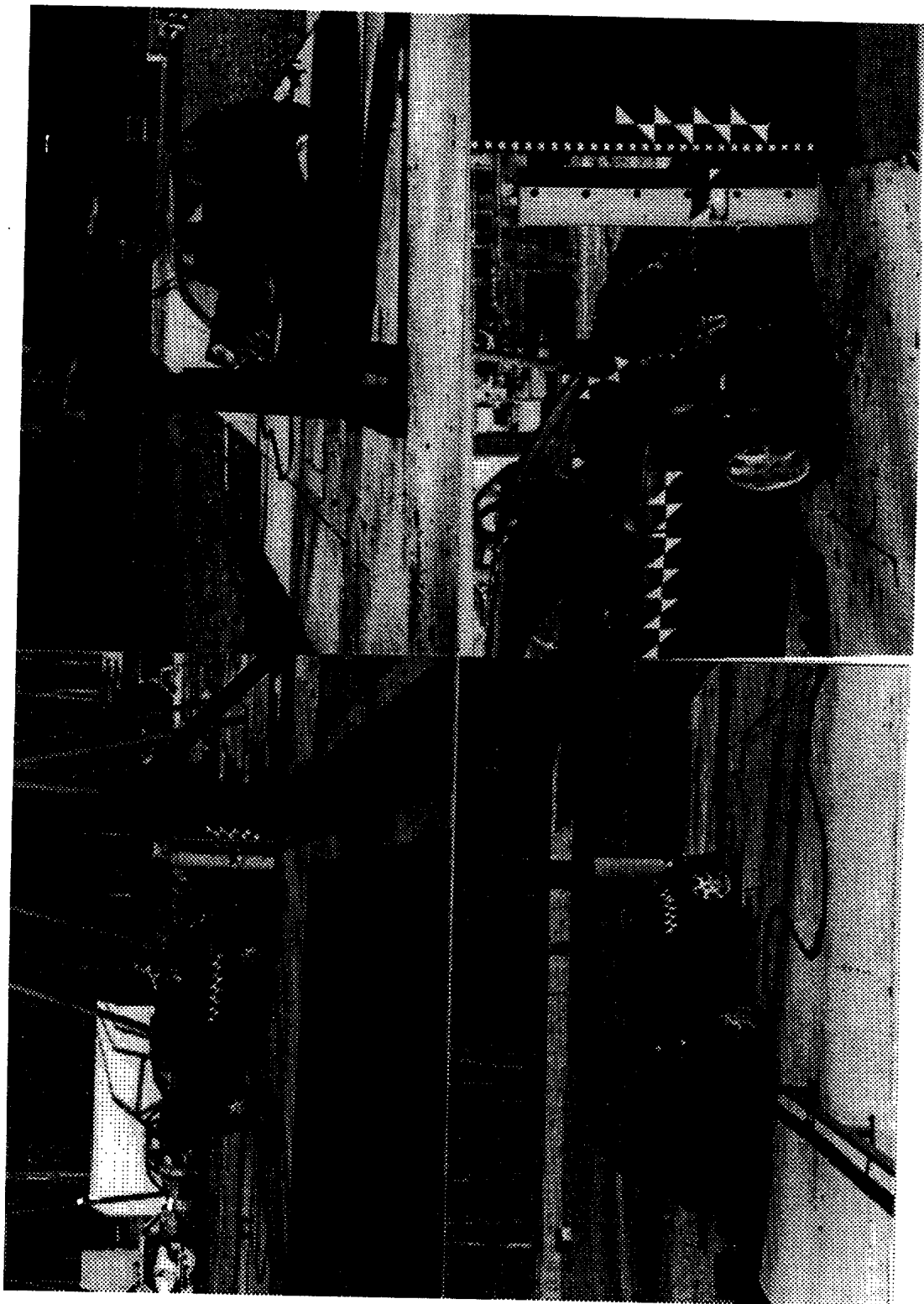


Figure 40. Post-test photographs, test 98F015.





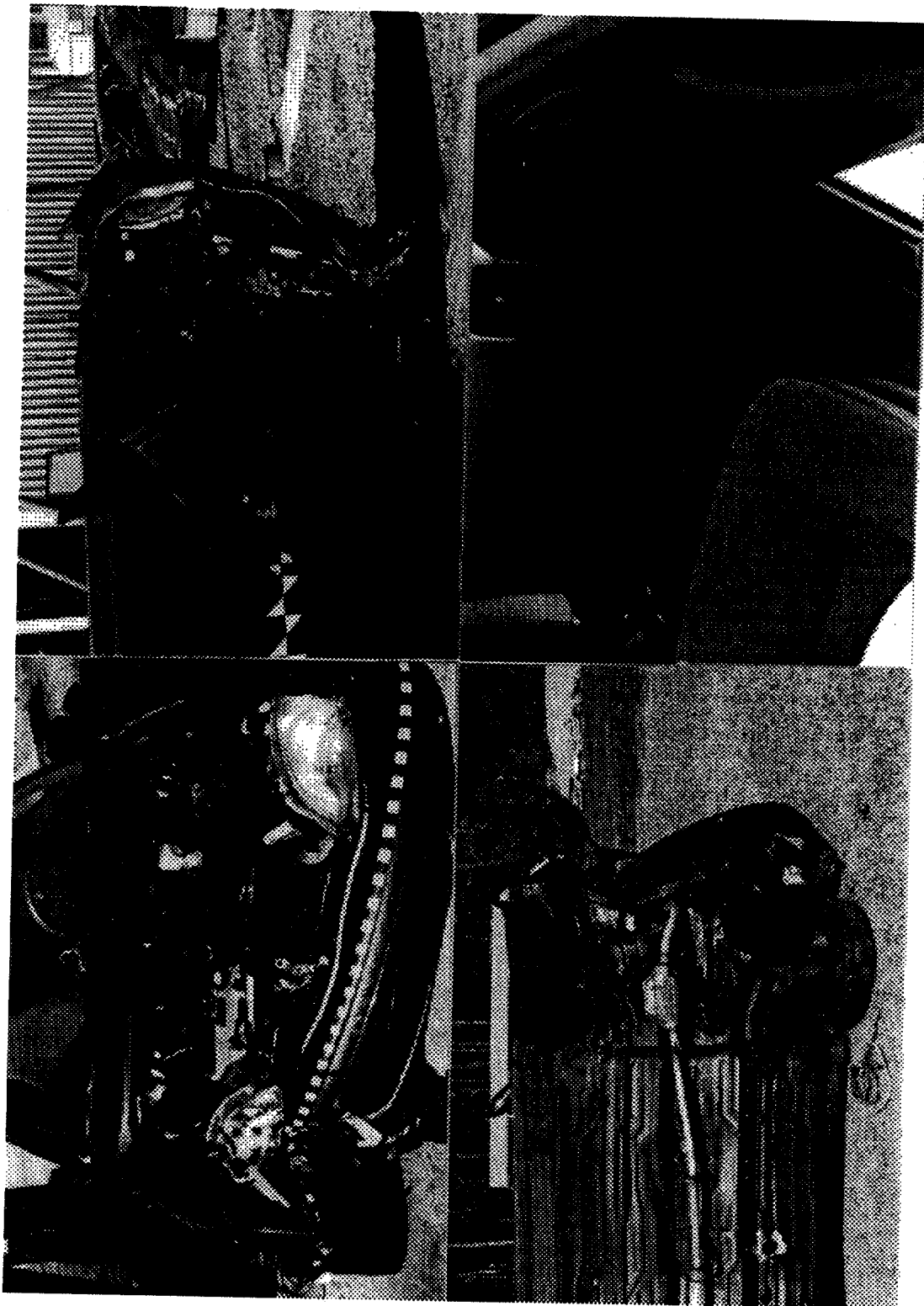
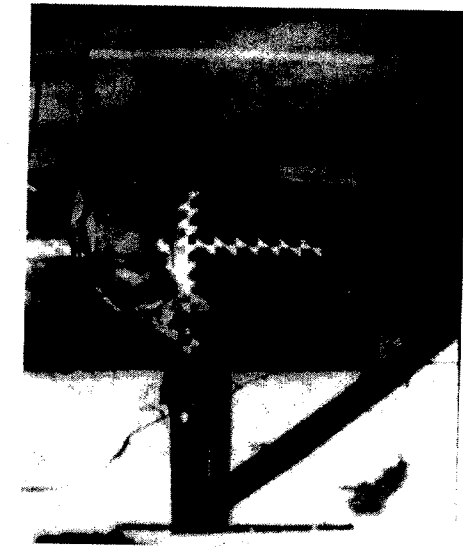


Figure 41. Additional post-test photographs, test 98F015.

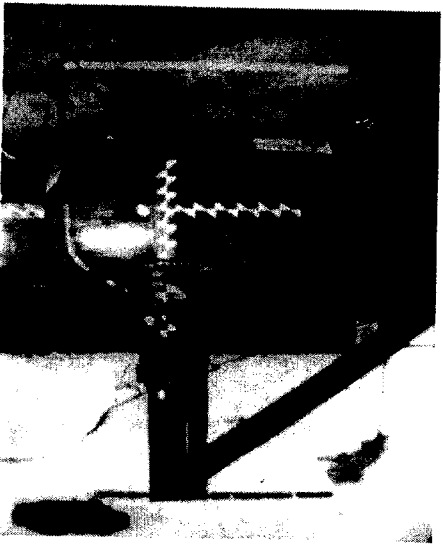




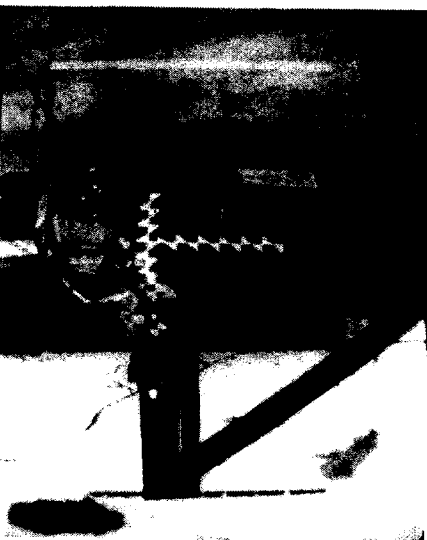
0.010



0.030



0.050



0.060



0.080



0.090

Figure 42. Photographs during the test, test 99S001.



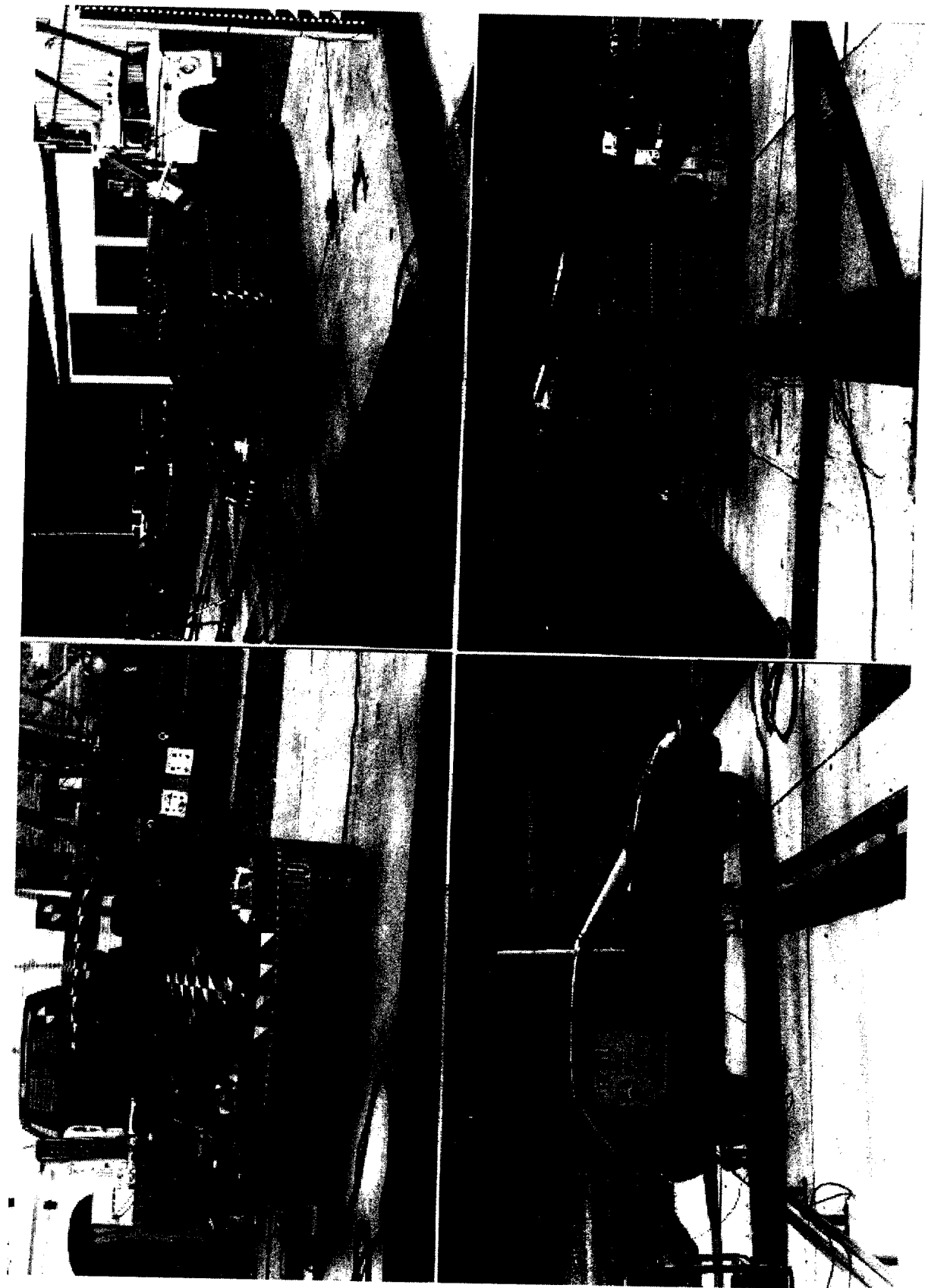


Figure 43. Pre-test photographs, test 99S001.



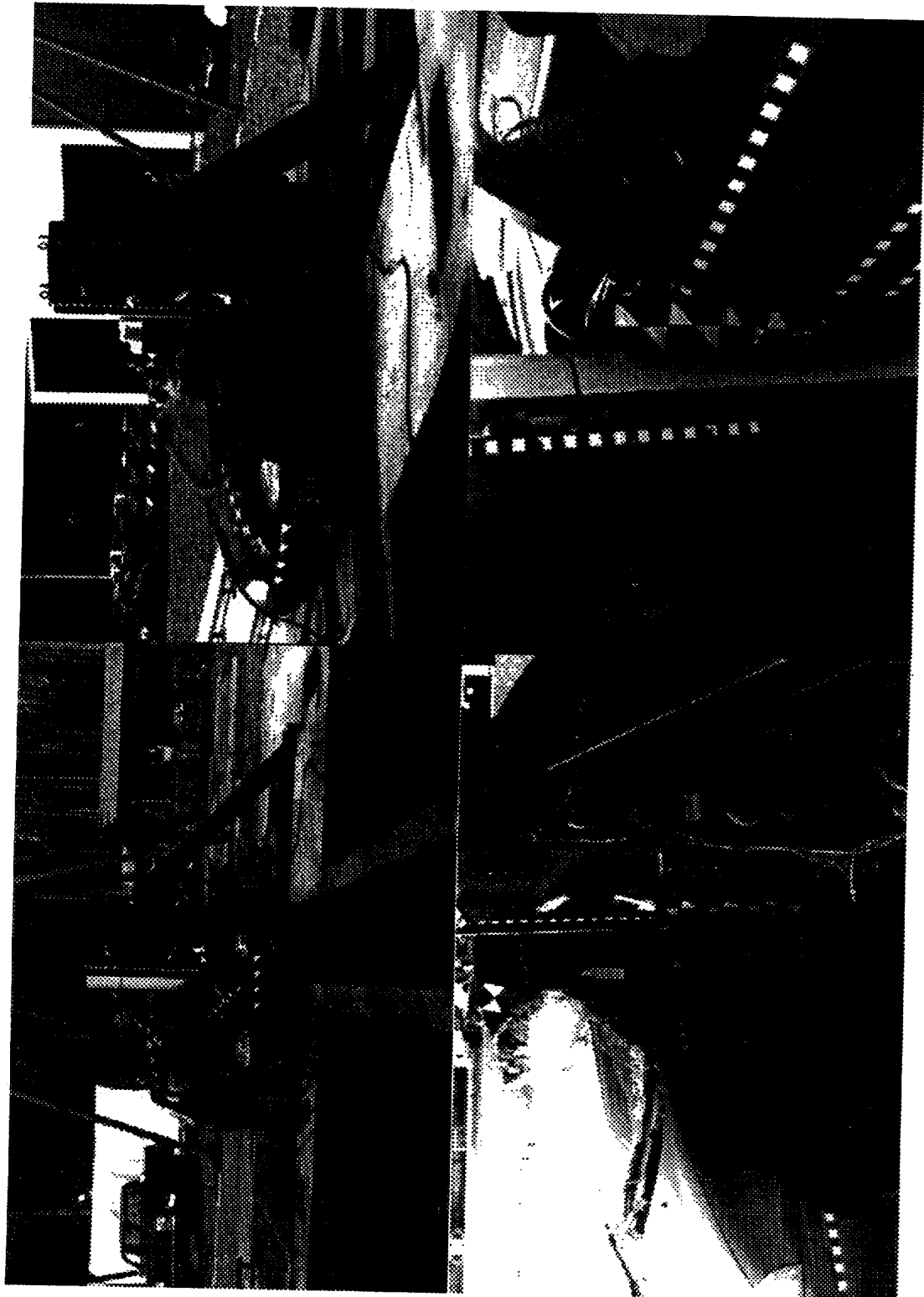


Figure 44. Post-test photographs, test 99S001.



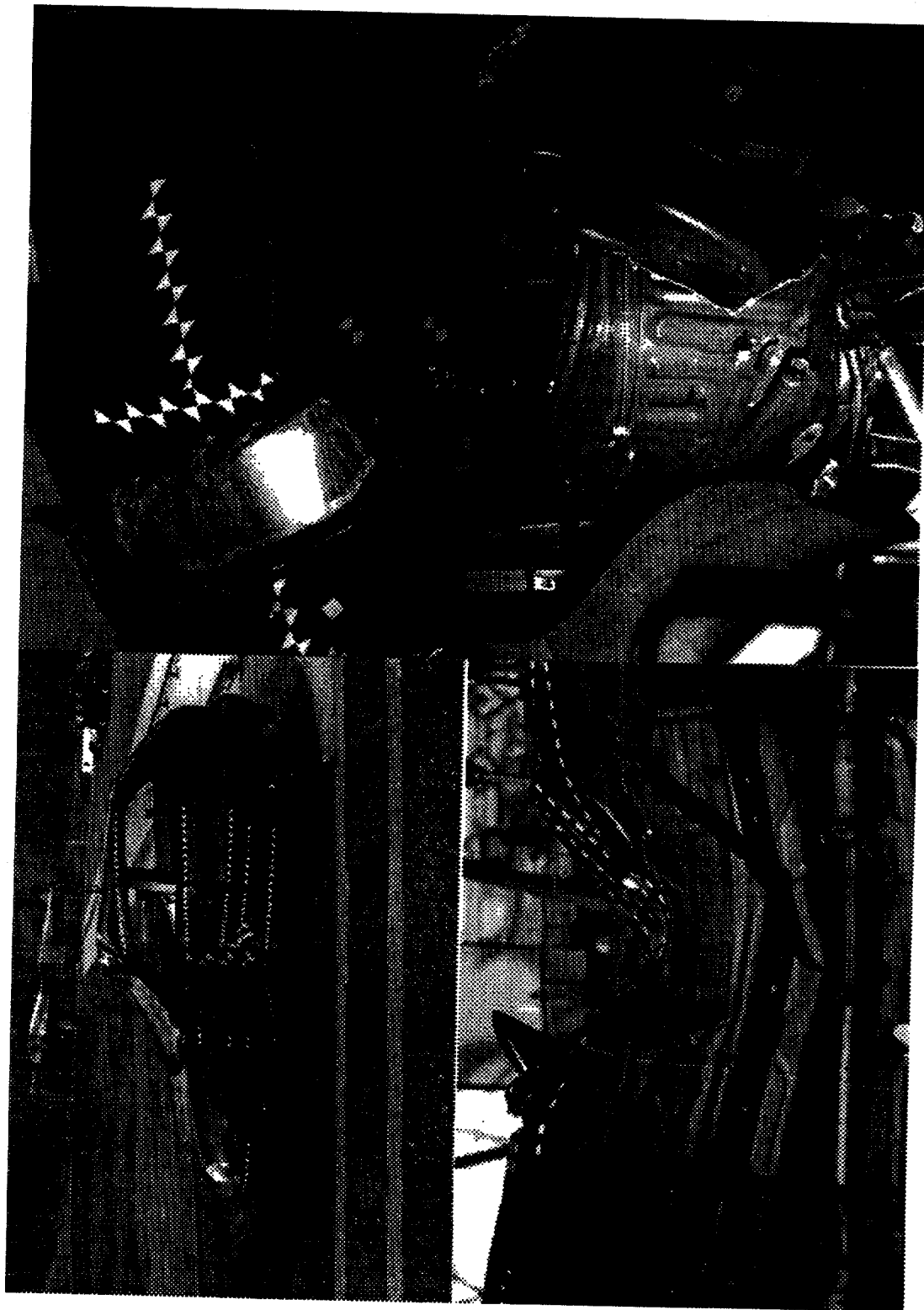


Figure 45. Additional post-test photographs, test 99S001.



Test No. 98F010
Cg acceleration vs. time, X-axis

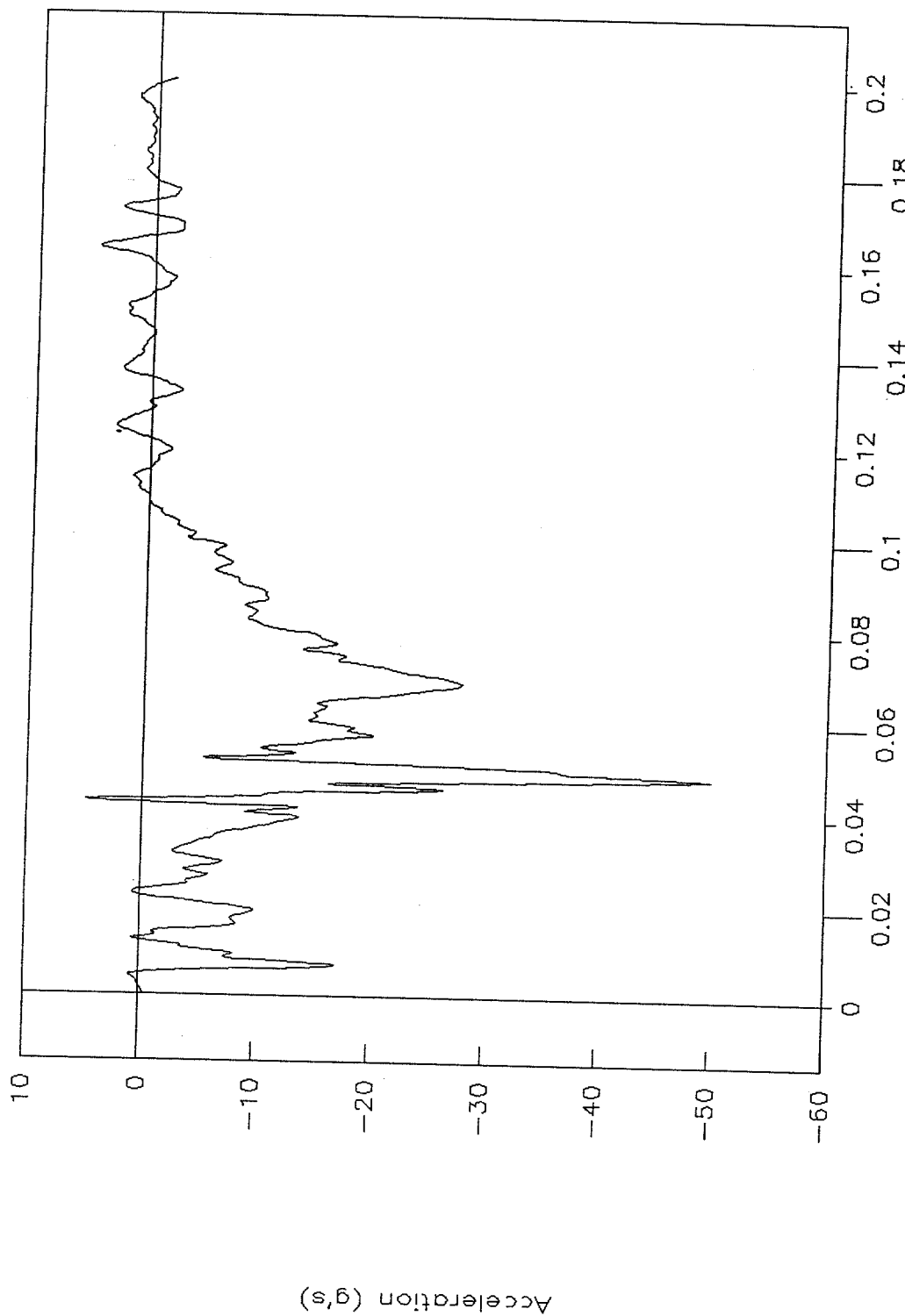


Figure 46. C.g. acceleration vs. time, X-axis, test 98F010.



Test No. 98F010
Cg velocity vs. time, X-axis

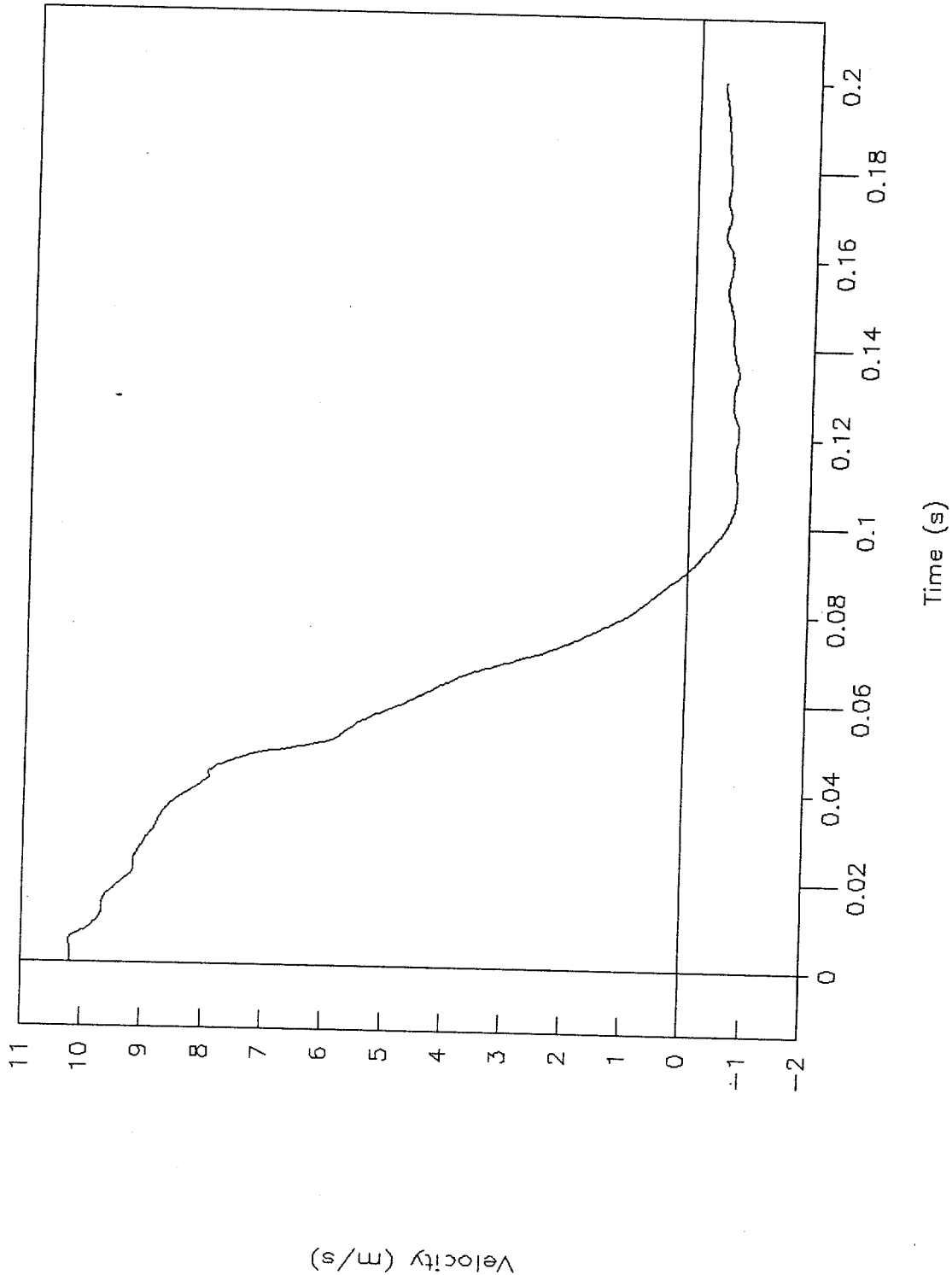


Figure 47. C.g. velocity vs. time, X-axis, test 98F010.



Test No. 98F010
Cg displacement vs. time, X-axis

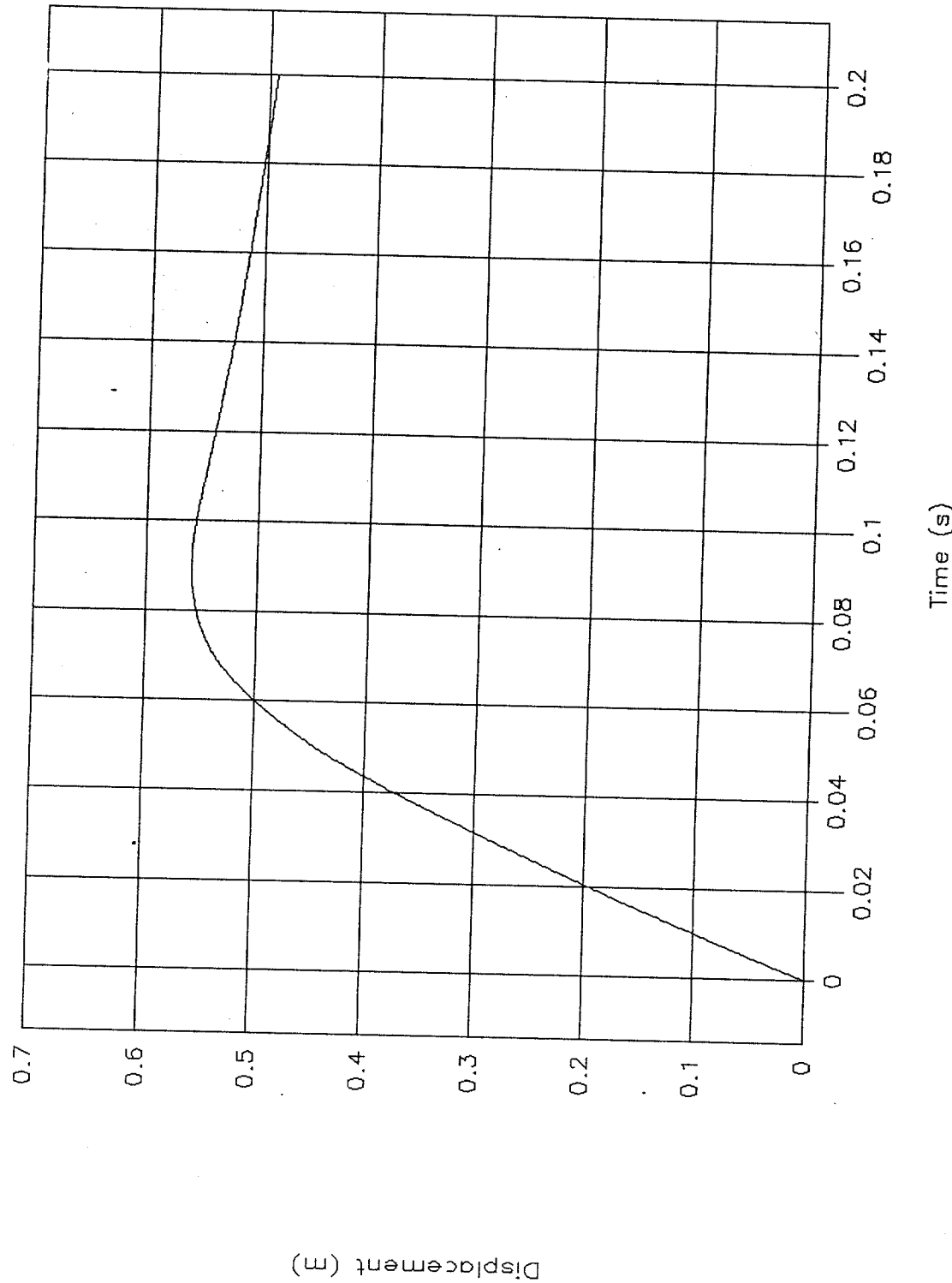


Figure 48. C.g. displacement vs. time, X-axis, test 98F010.



Test No. 98F010
Cg force vs. displacement, X-axis

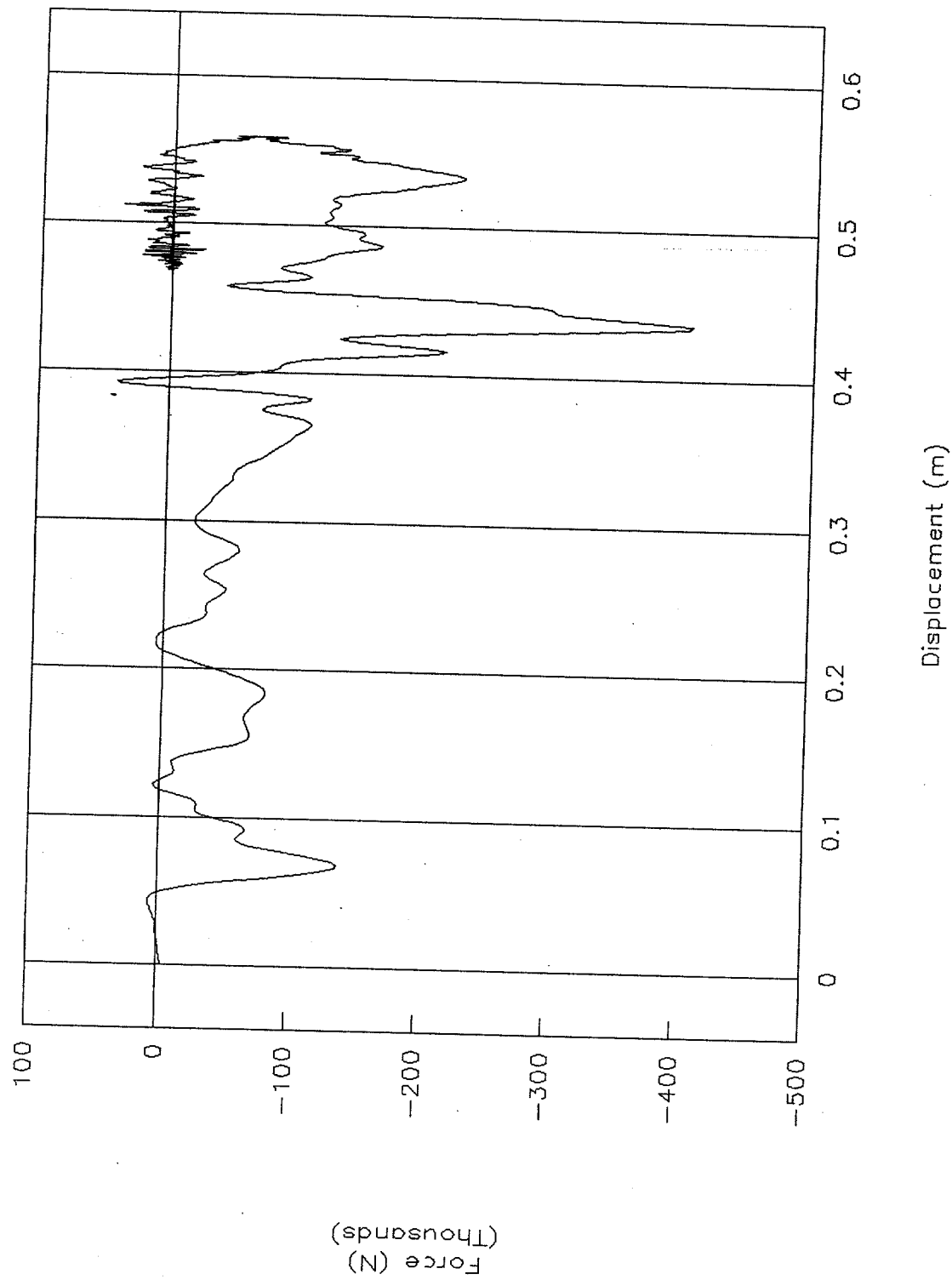


Figure 49. C.g. force vs. displacement, X-axis, test 98F010.



Test No. 98F010
Cg energy vs. displacement, X-axis

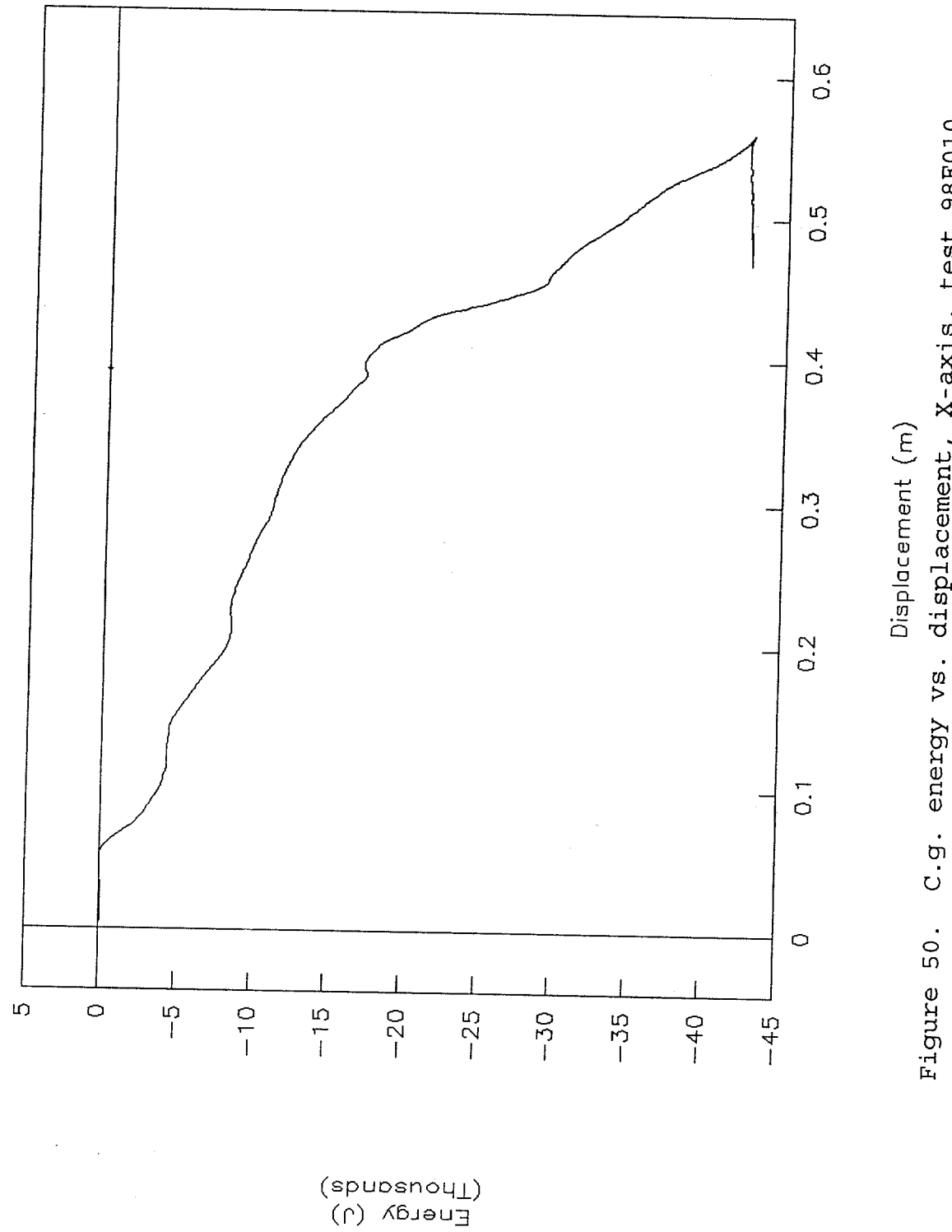


Figure 50. C.g. energy vs. displacement, X-axis, test 98F010.



Test No. 98F010
Cg acceleration vs. time, Y-axis

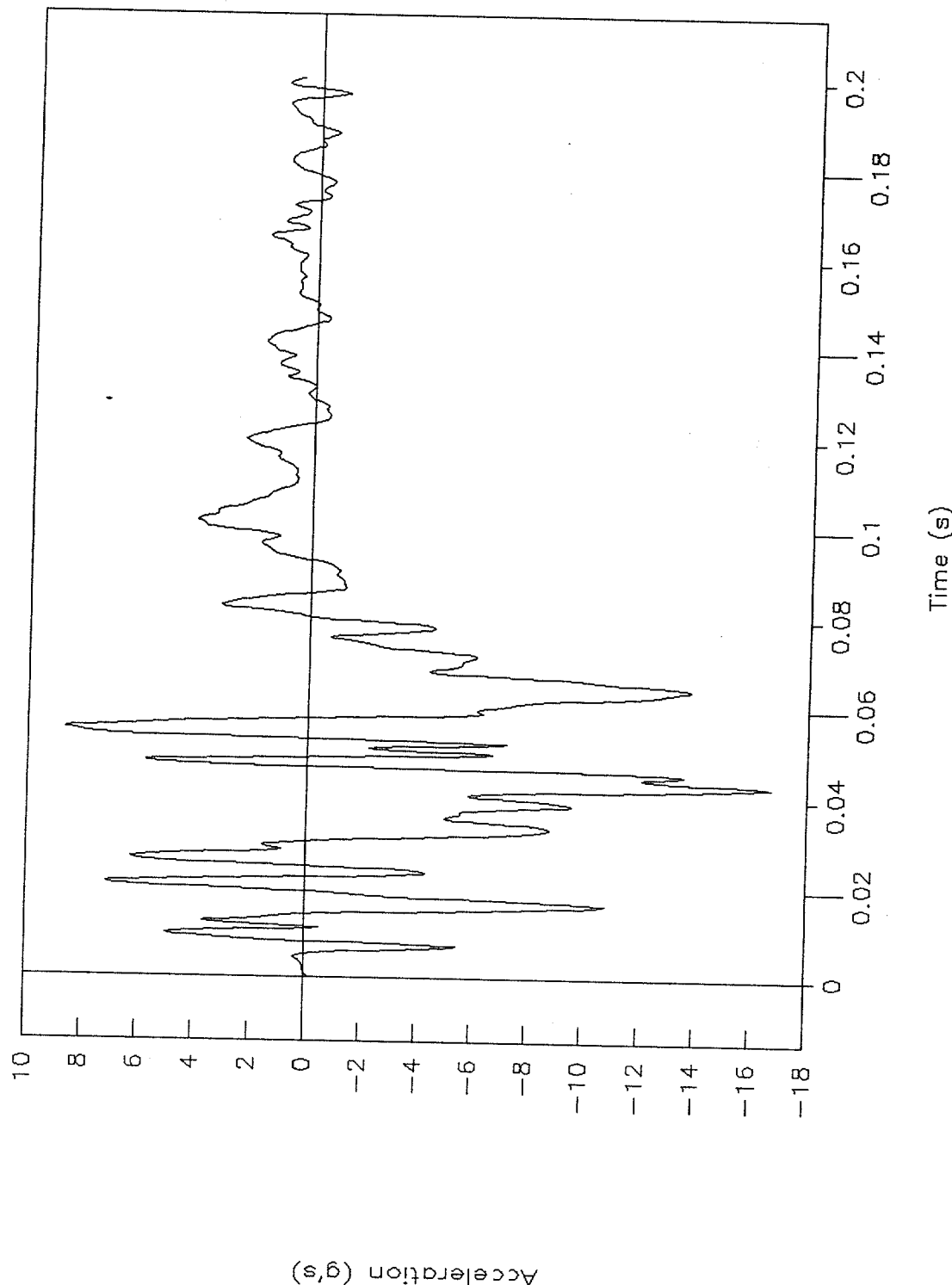


Figure 51. C.g. acceleration vs. time, Y-axis, test 98F010.



Test No. 98F010
Cg acceleration vs. time, Z-axis

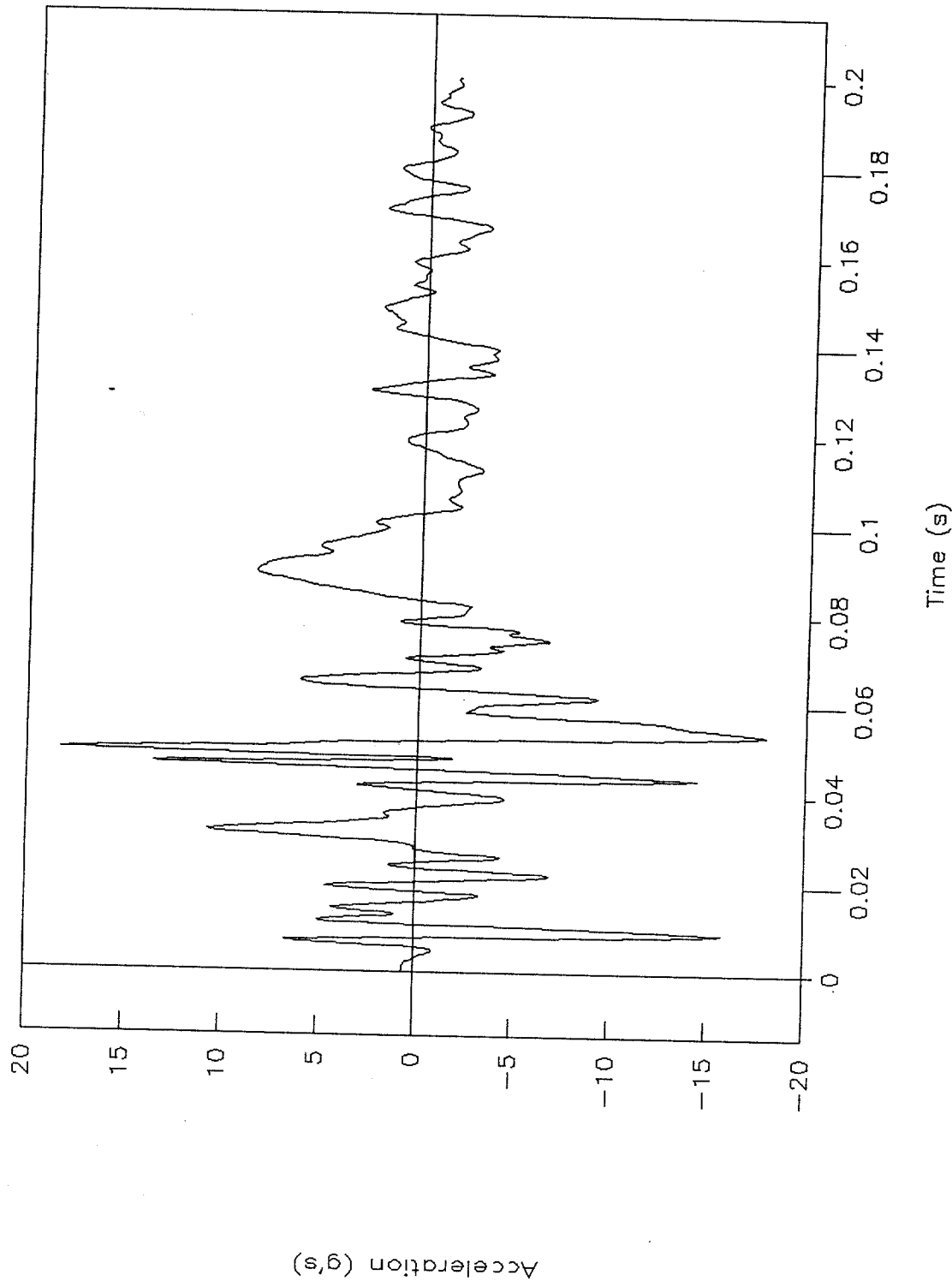


Figure 52. C.g. acceleration vs. time, Z-axis, test 98F010.



Test No. 98F010
Rigid pole, force vs. time

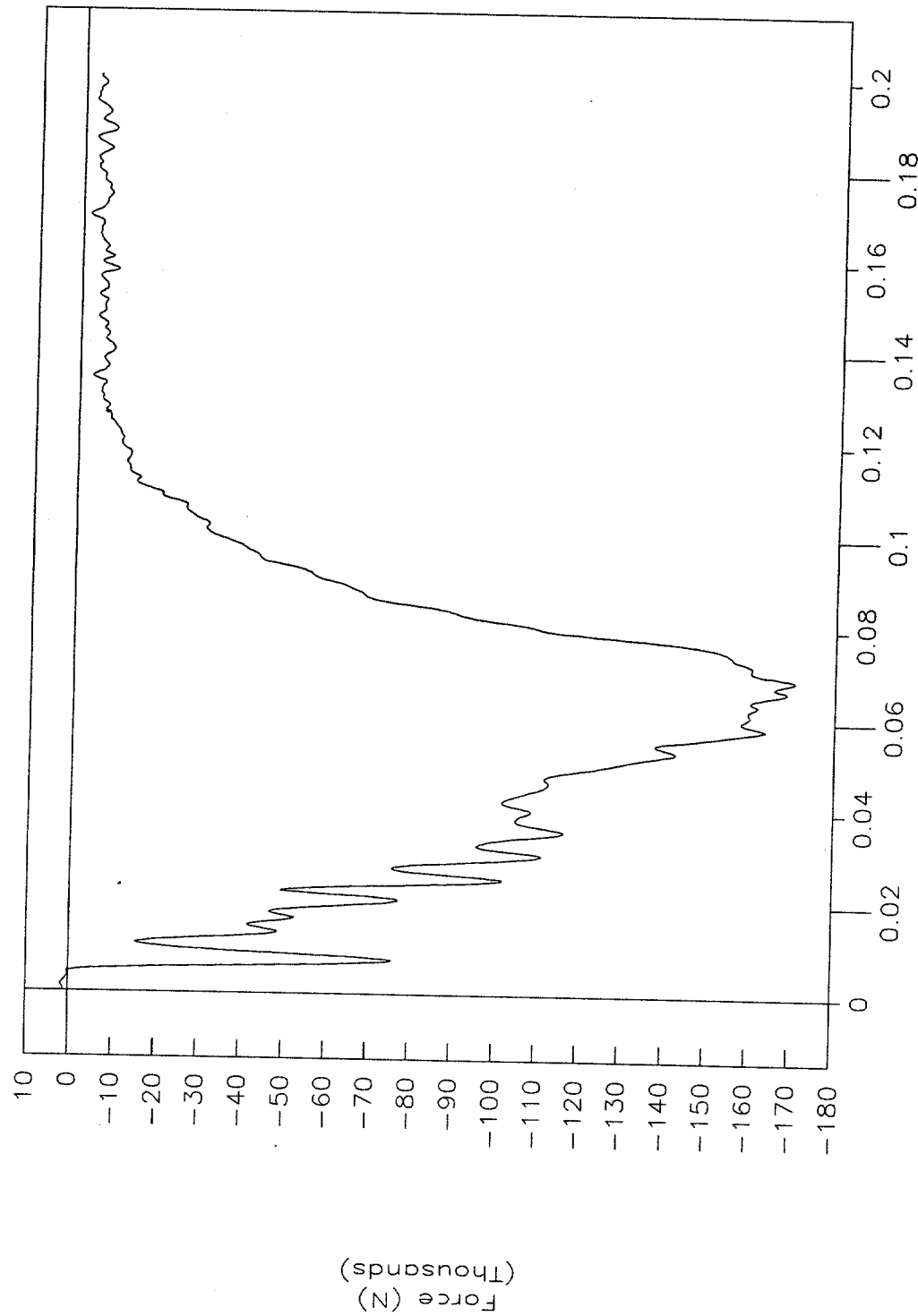


Figure 53. Rigid pole, force vs. time, test 98F010.



Test No. 98F010
Rigid pole, acceleration vs. time

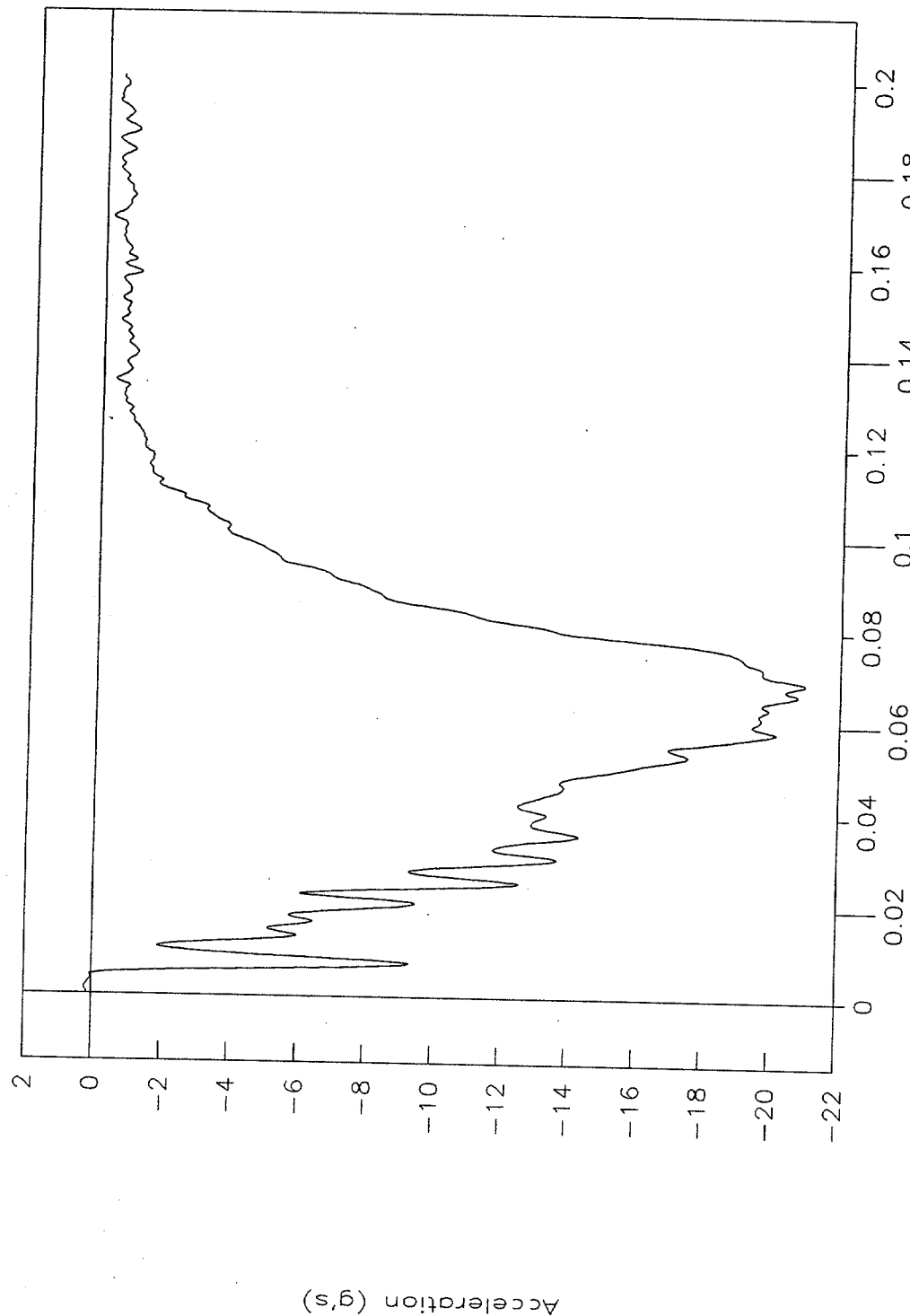


Figure 54. Rigid pole, acceleration vs. time, test 98F010.



Test No. 98F010
Rigid pole, velocity vs. time

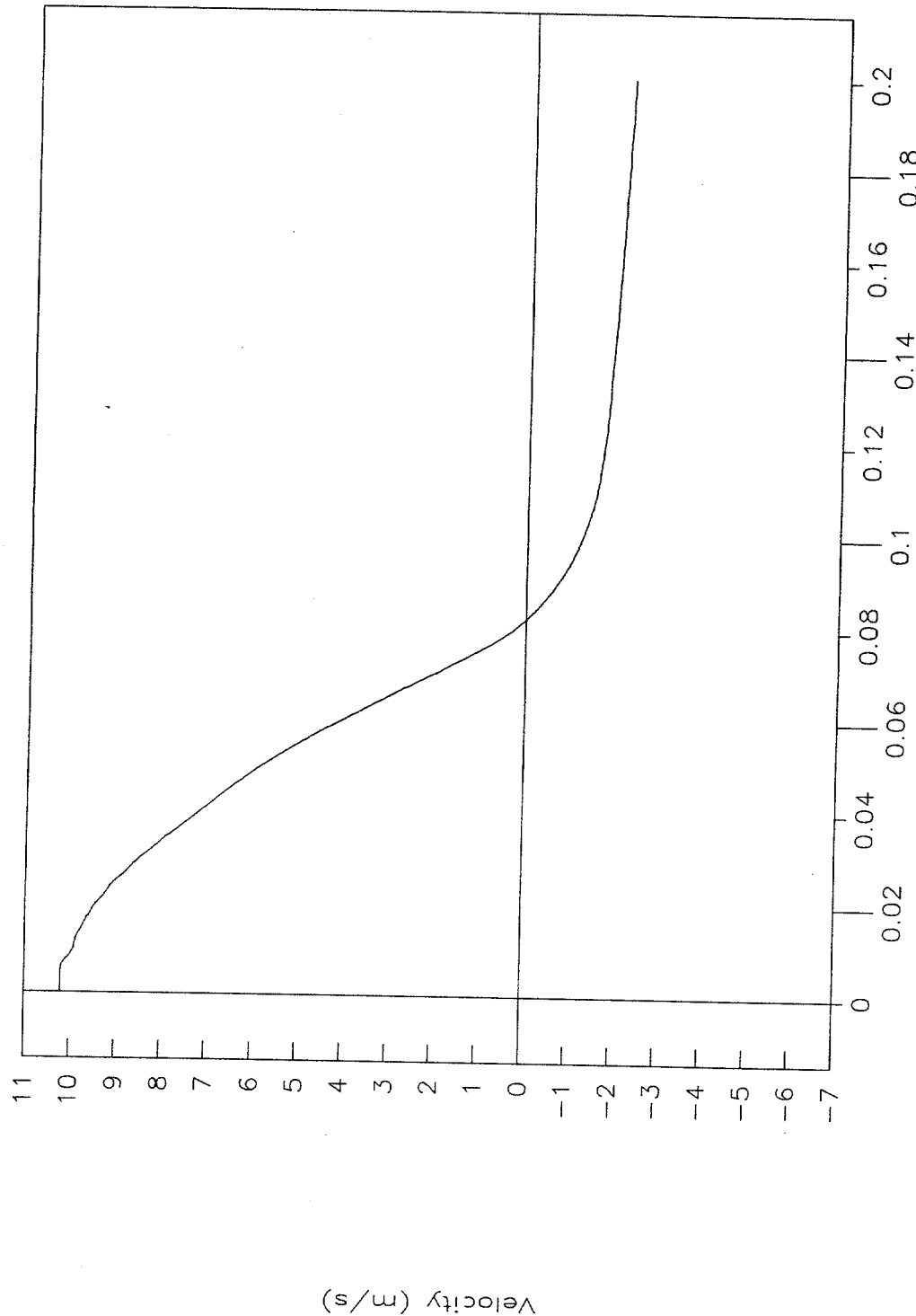


Figure 55. Rigid pole, velocity vs. time, test 98F010.



Test No. 98F010
Rigid pole, displacement vs. time

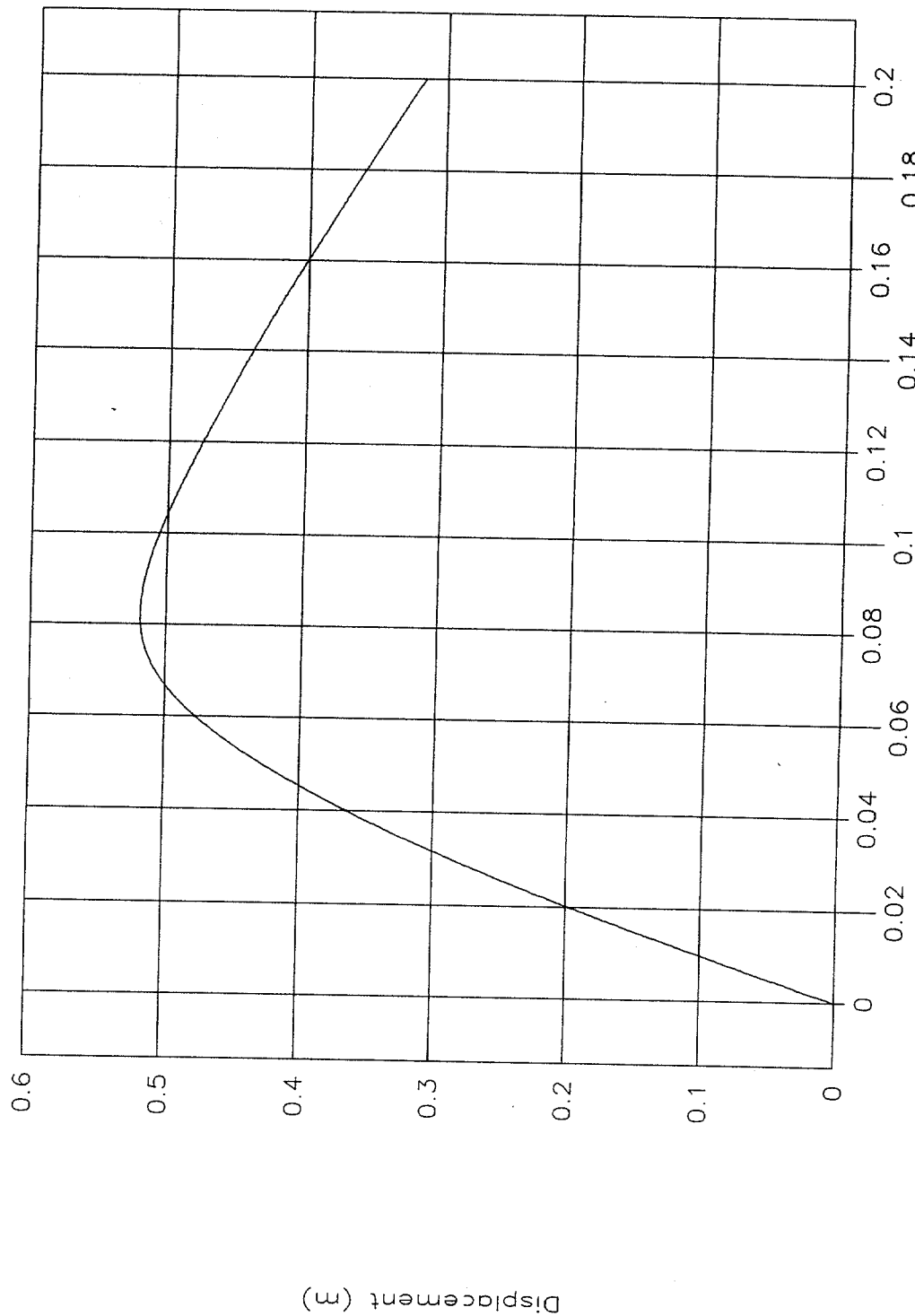


Figure 56. Rigid pole, displacement vs. time, test 98F010.



Test No. 98F010
Rigid pole, force vs. displacement

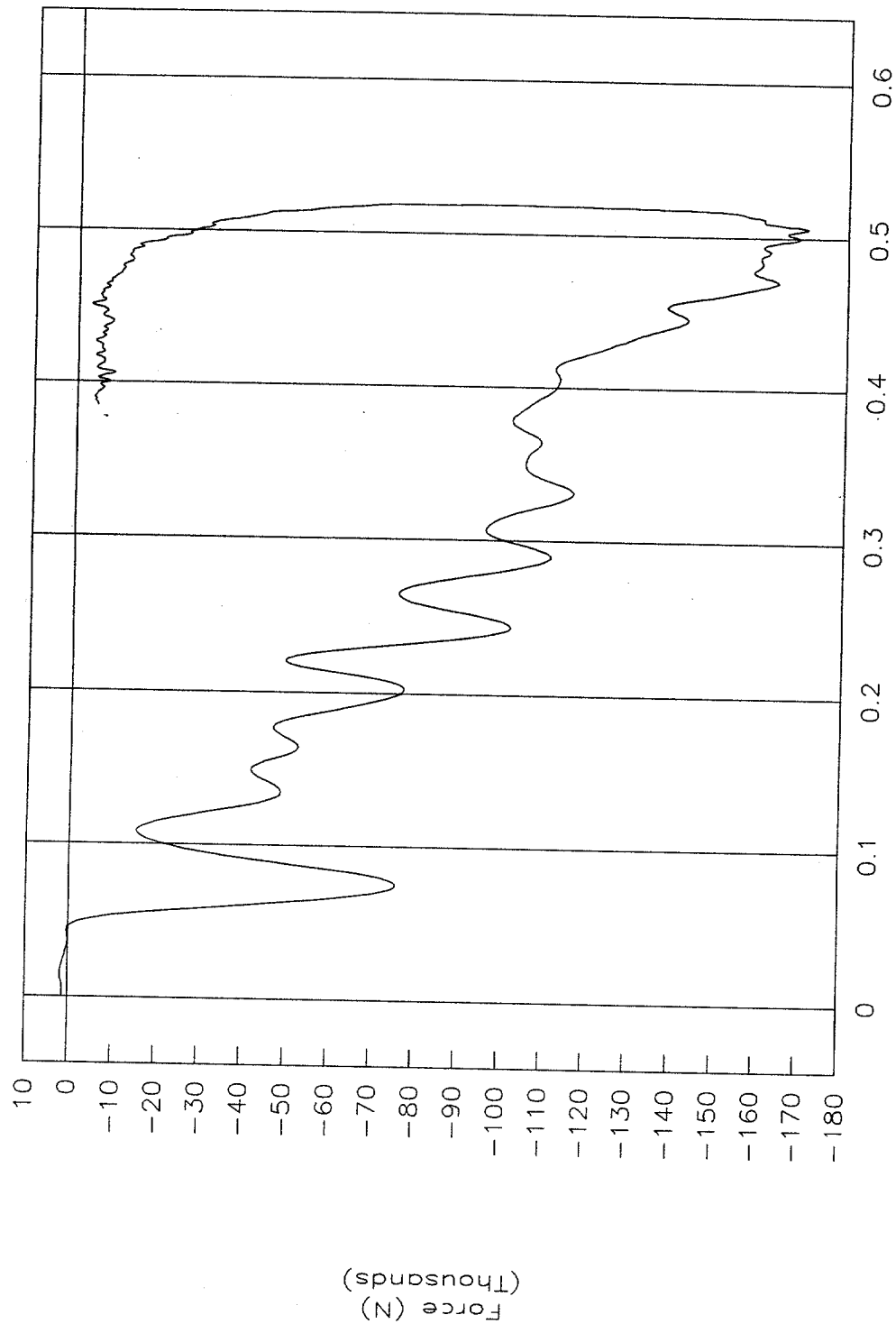


Figure 57. Rigid pole, force vs. displacement, test 98F010.



Test No. 98F010
Rigid pole, energy vs. displacement

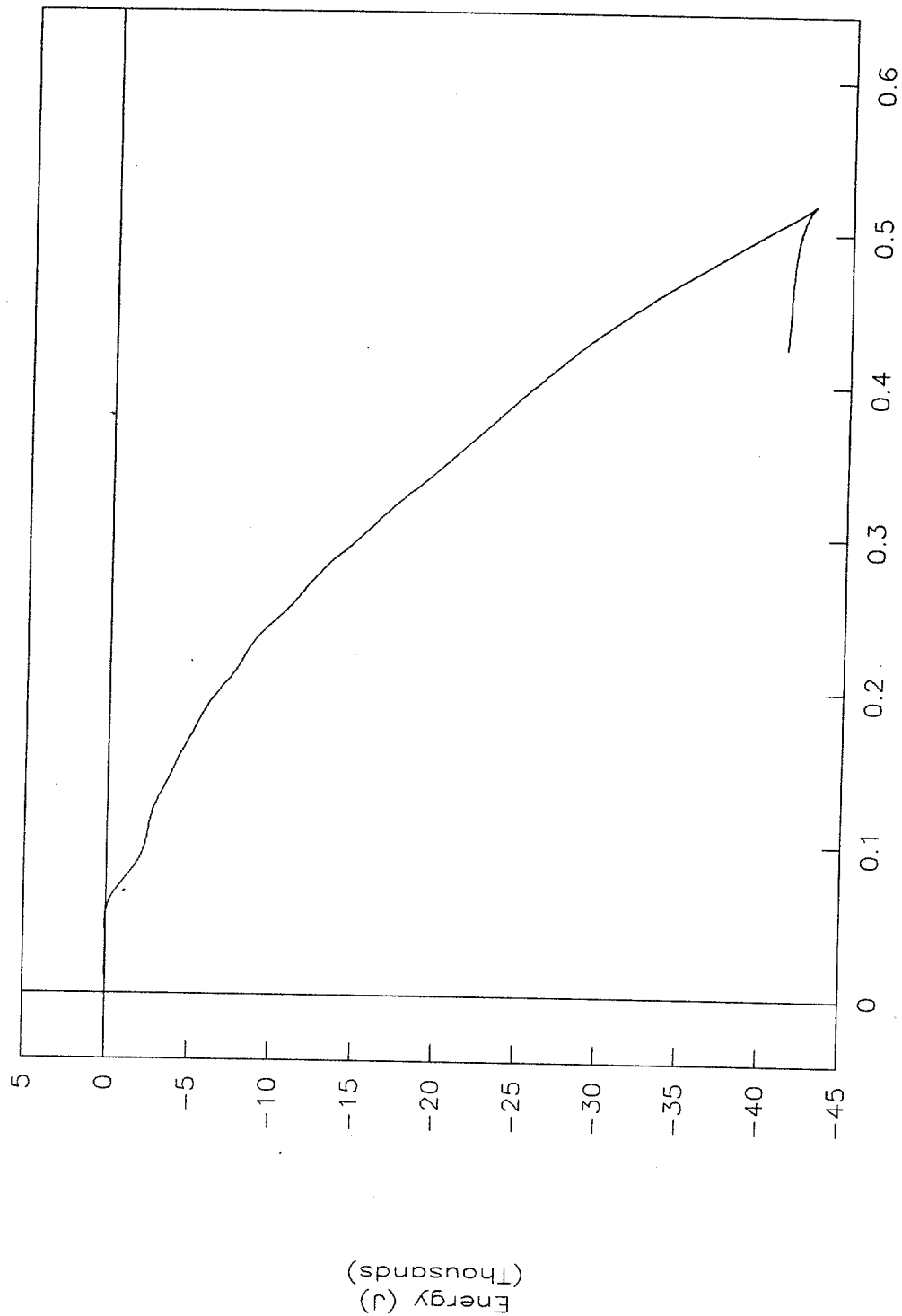


Figure 58. Rigid pole, energy vs. displacement, test 98F010.



Test No. 98F010
Impact force height vs. displacement

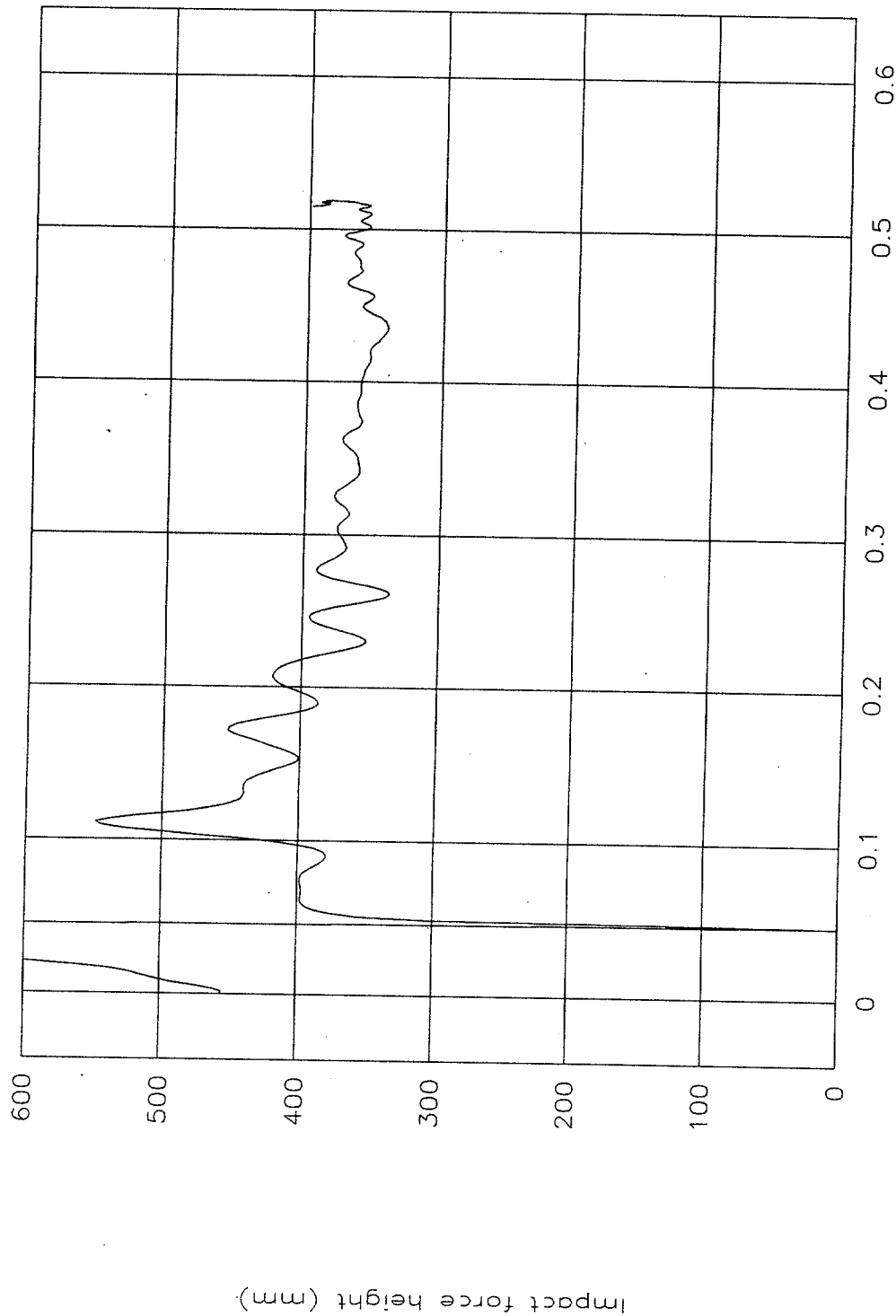


Figure 59. Impact force height vs. displacement, test 98F010.



Test No. 98F010
Top of engine, X-axis

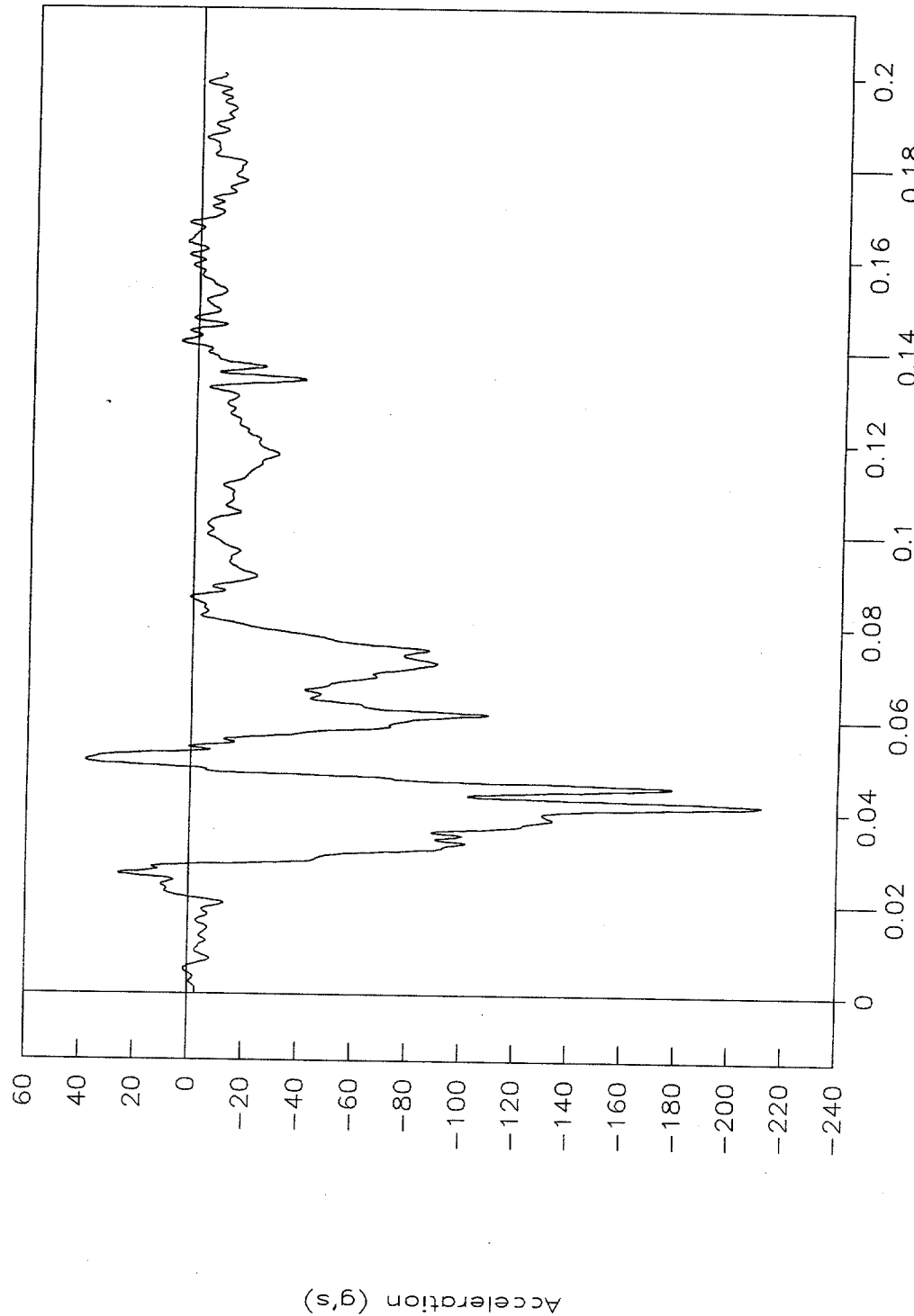


Figure 60. Top of engine acceleration vs. time, X-axis, test 98F010.



Test No. 98F010
Bottom of engine, X-axis

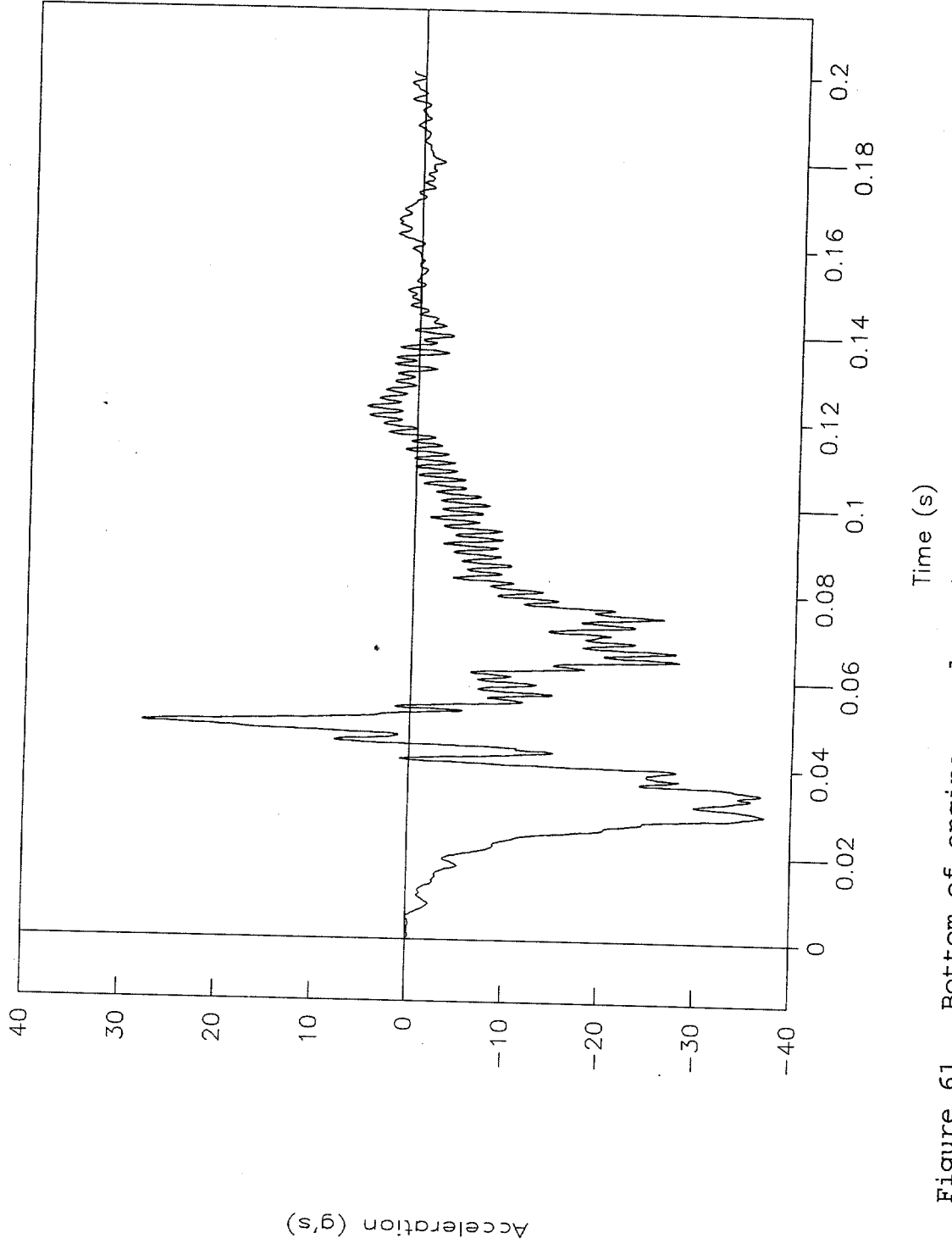


Figure 61. Bottom of engine acceleration vs. time, X-axis, test 98F010.



Test No. 98F010
Left control arm, X-axis

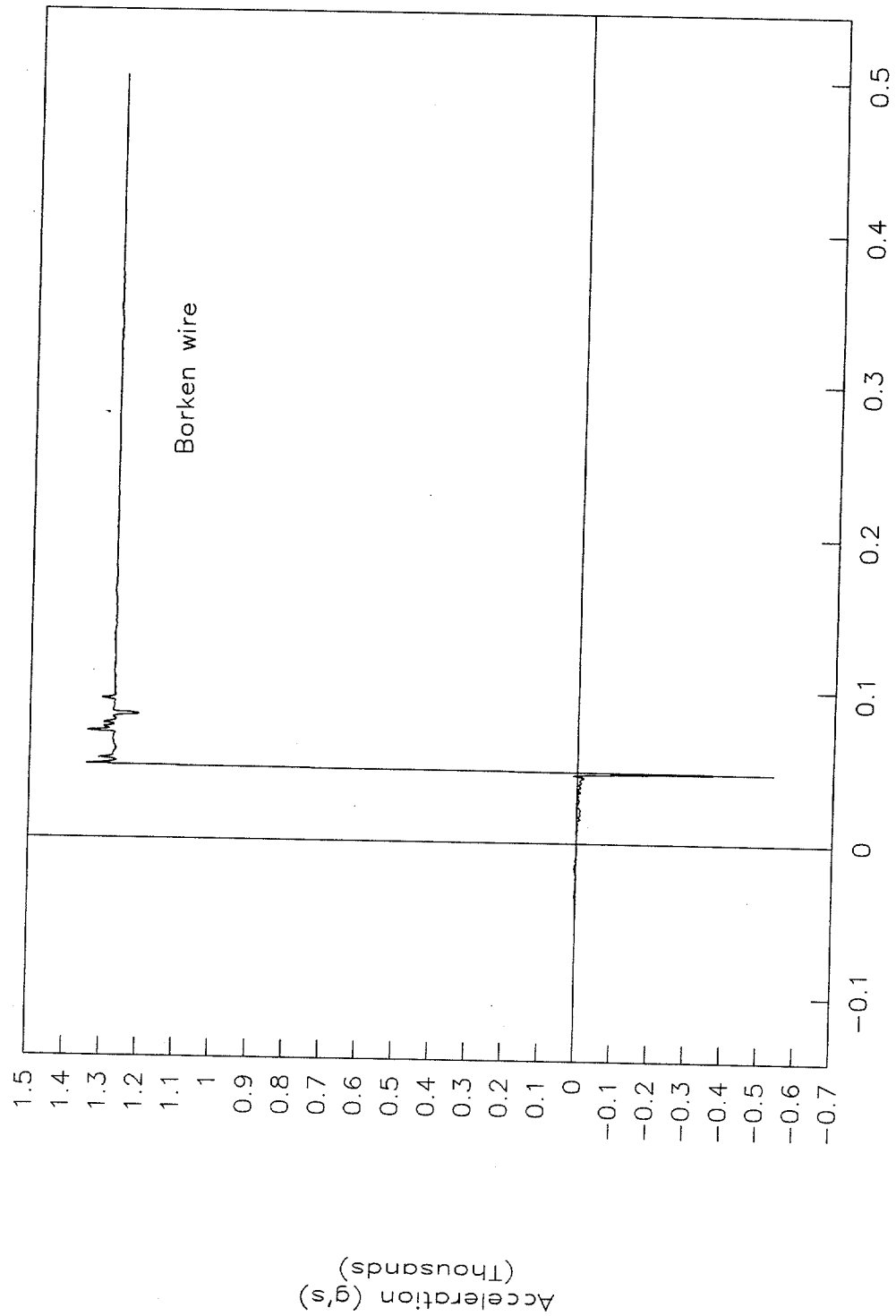
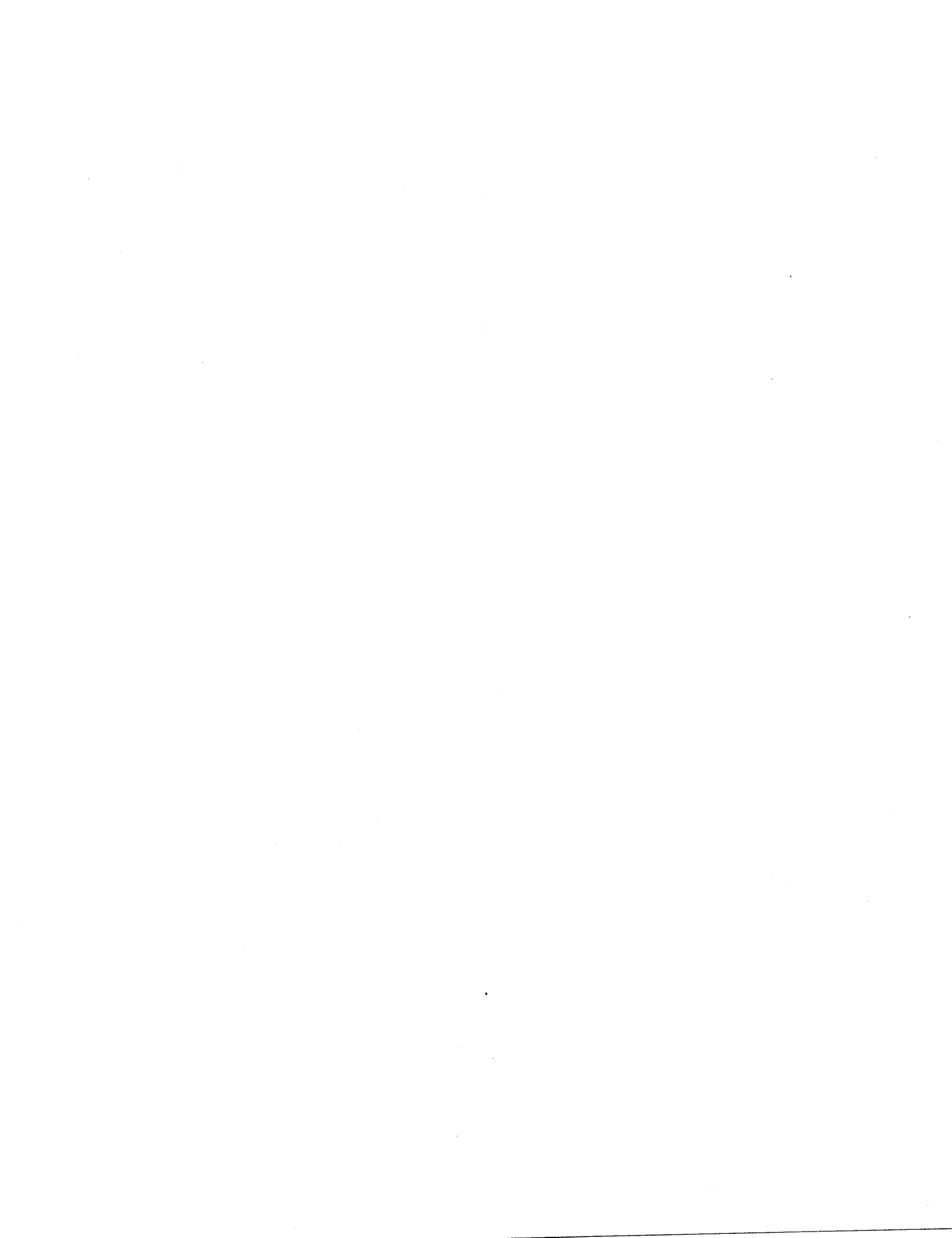


Figure 62. Left control arm acceleration vs. time, X-axis, test 98F010.



Test No. 98F010
Right control arm, X-axis

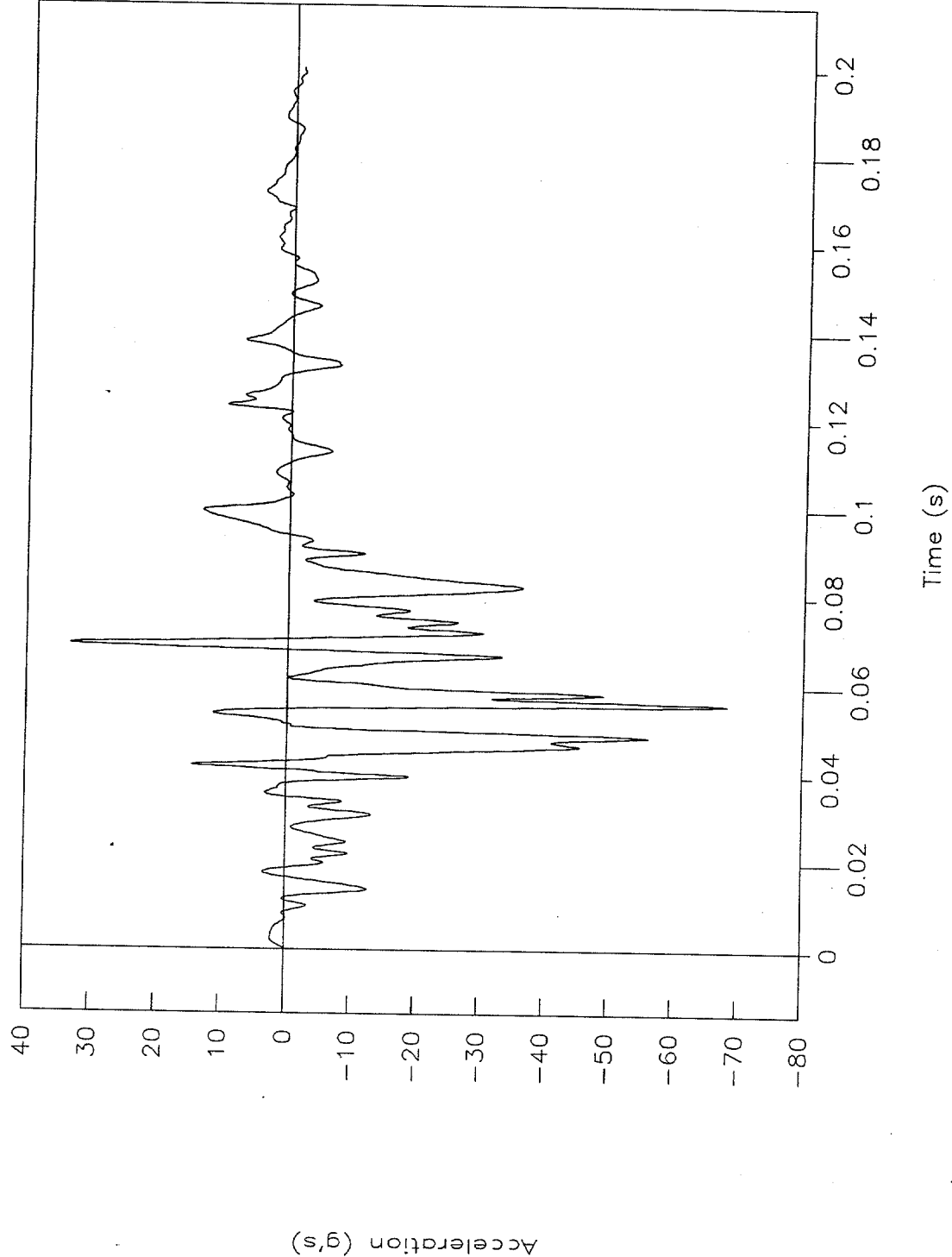


Figure 63. Right control arm acceleration vs. time, X-axis, test 98F010.



Test No. 98F010

Instrument panel, X-axis

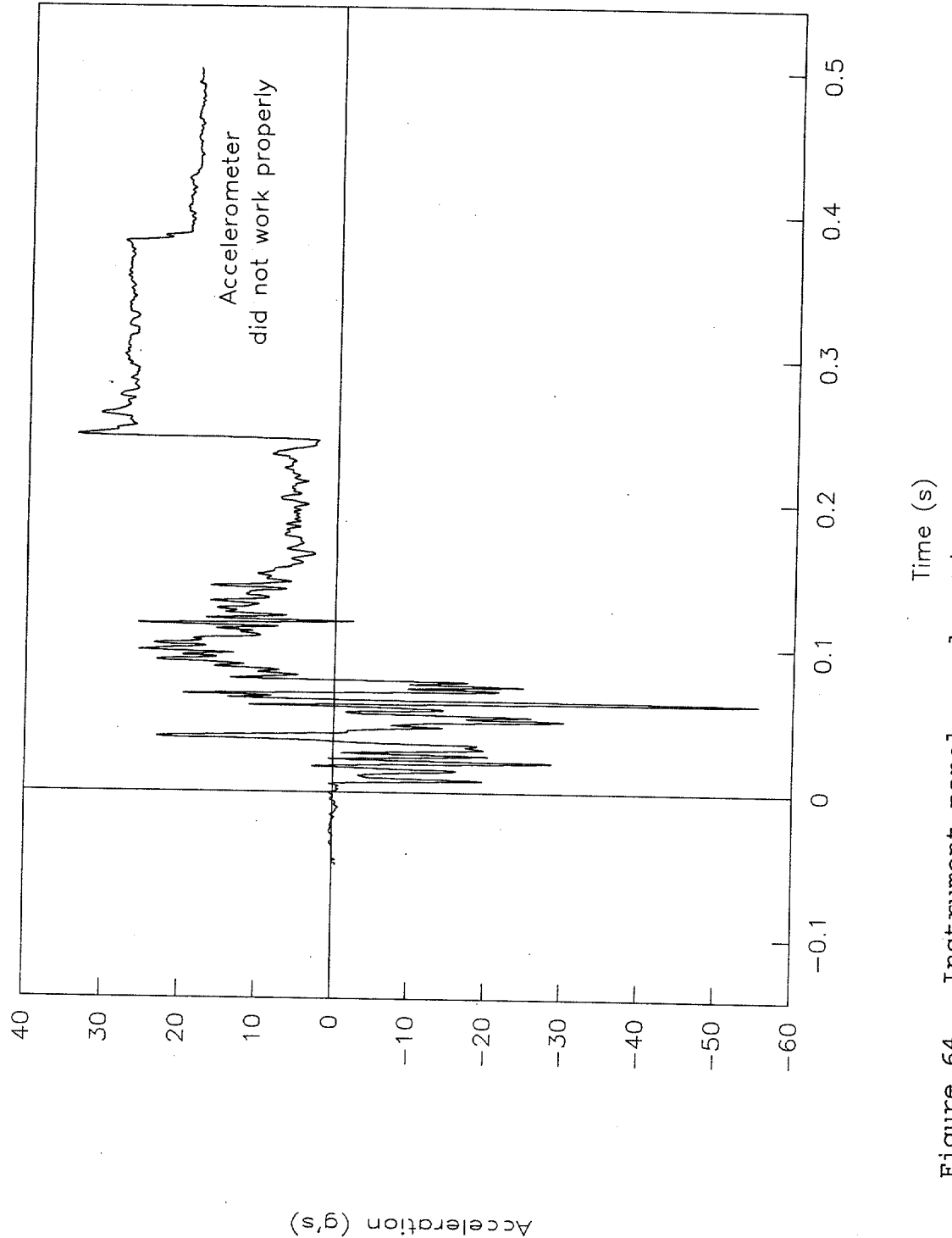


Figure 64. Instrument panel acceleration vs. time, X-axis, test 98F010.



Test No. 98F010
Pitch rate and angle vs. time

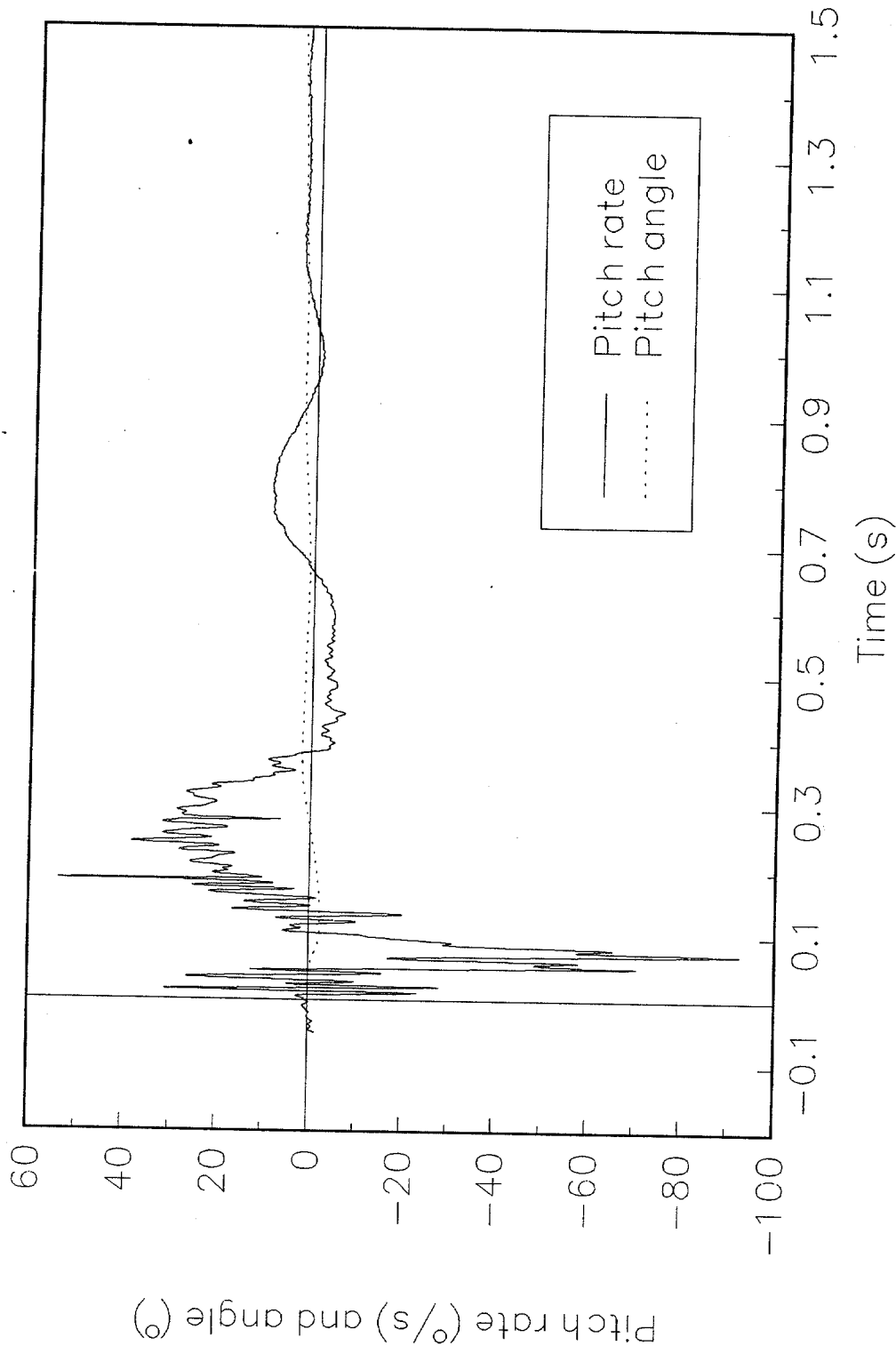


Figure 65. Pitch rate and angle vs. time, test 98F010.



Test No. 98F010
Roll rate and angle vs. time

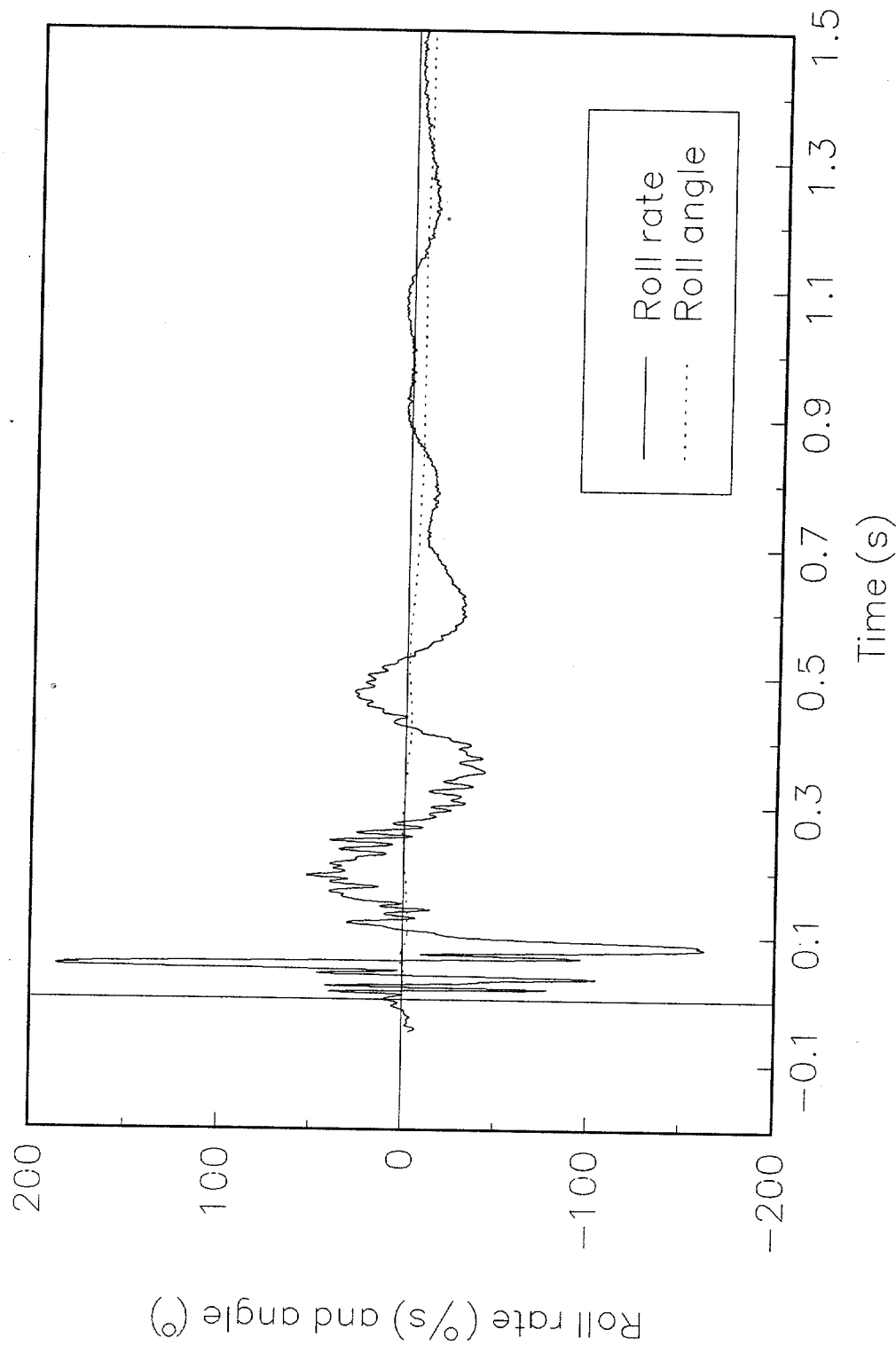


Figure 66. Roll rate and angle vs. time, test 98F010.



Test No. 98F010
Yaw rate and angle vs. time

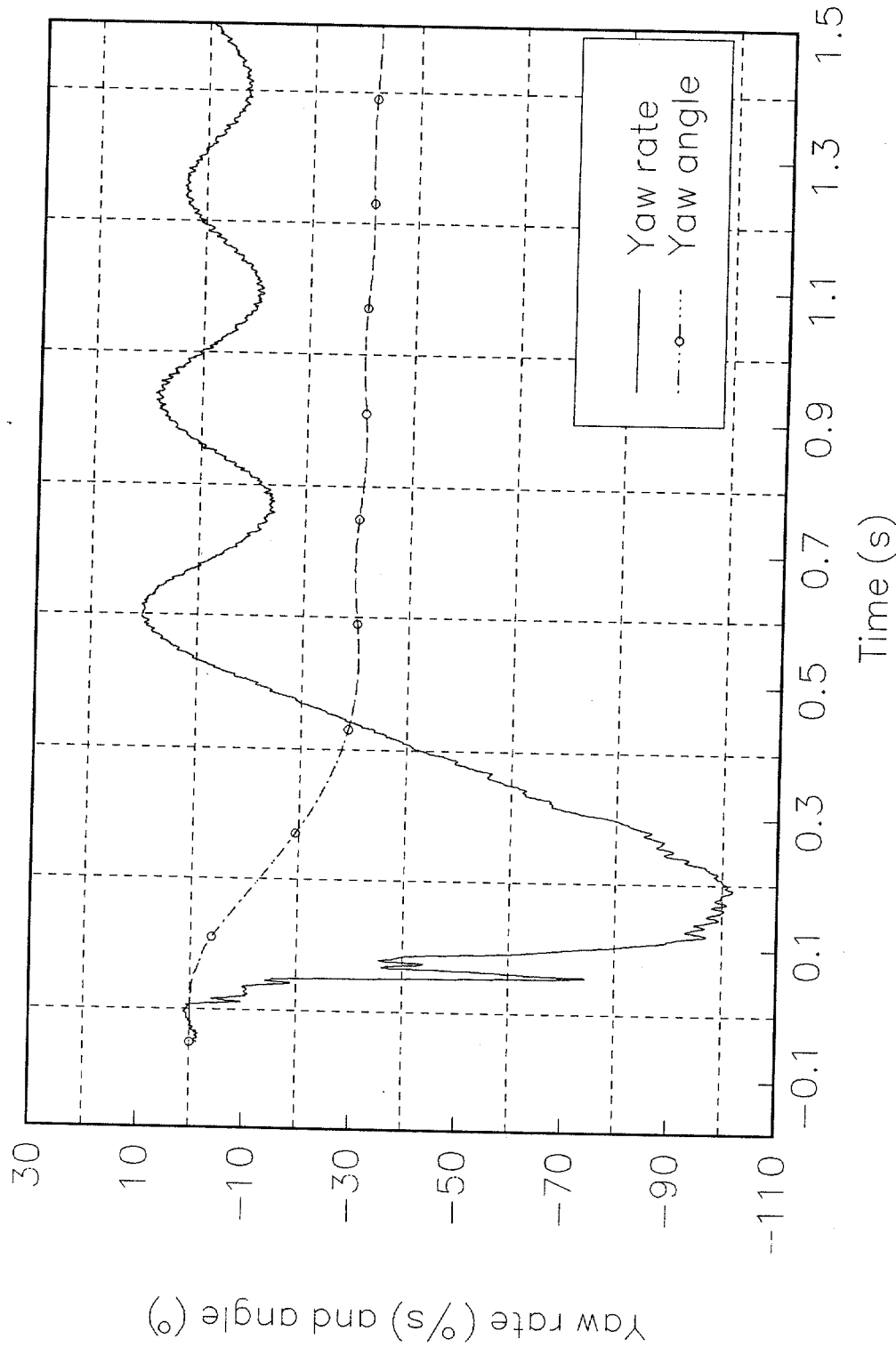


Figure 67. Yaw rate and angle vs. time, test 98F010.



Test No. 98F011
Cg acceleration vs. time, X-axis

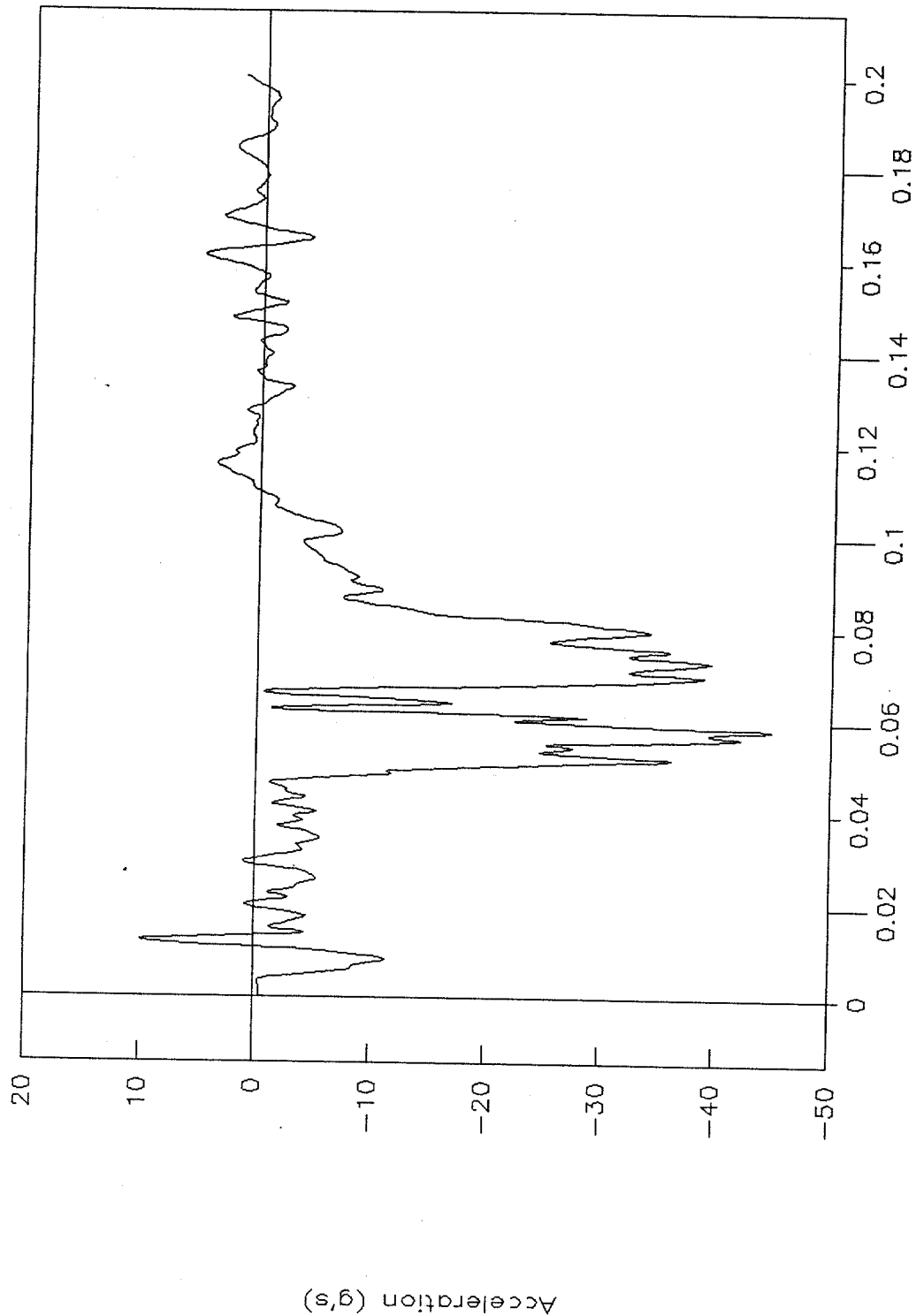


Figure 68. C.g. acceleration vs. time, X-axis, test 98F011.



Test No. 98F011

Cg velocity vs. time, X-axis

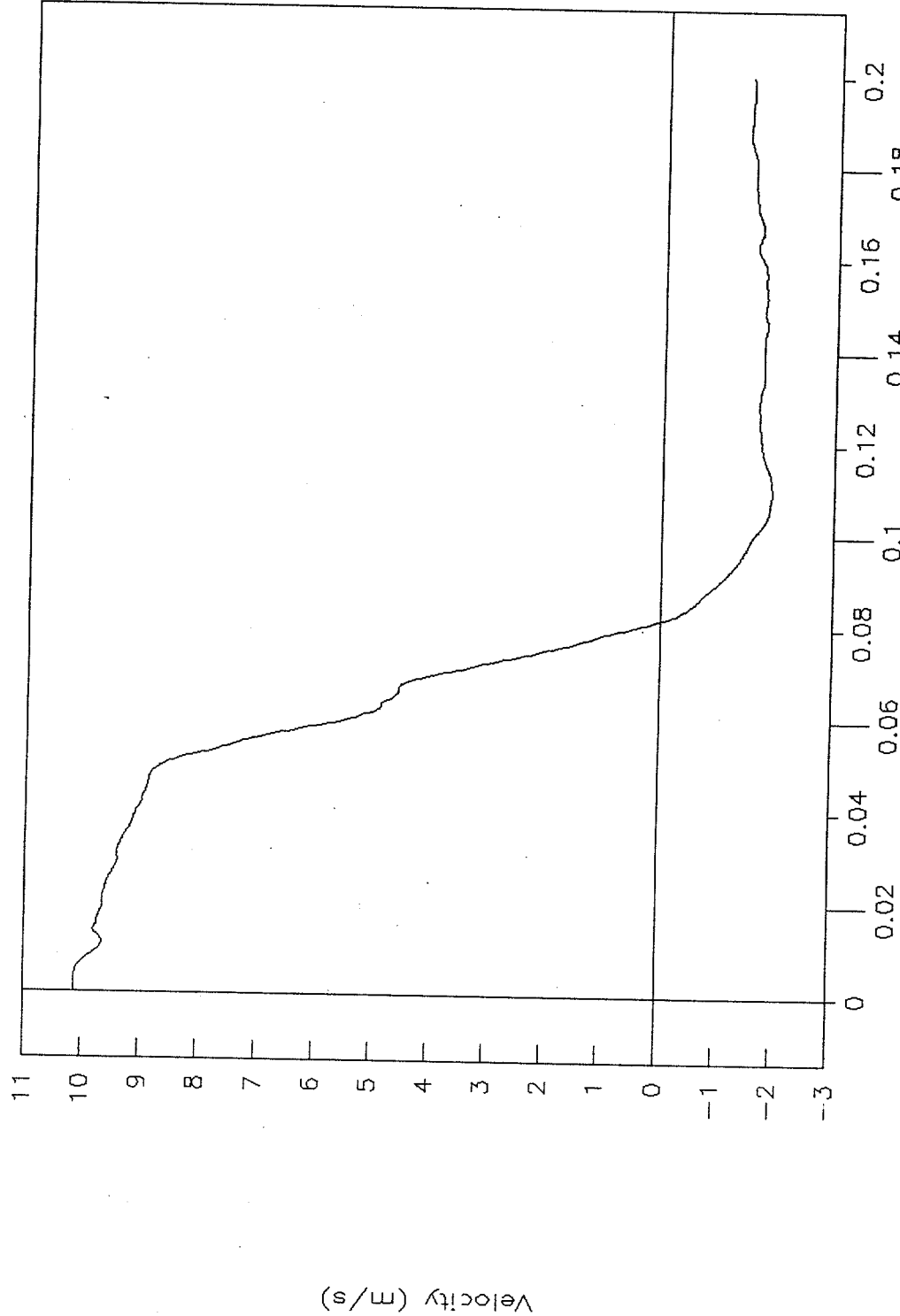


Figure 69. C.g. velocity vs. time, X-axis, test 98F011.



Test No. 98F011
Cg displacement vs. time, X-axis

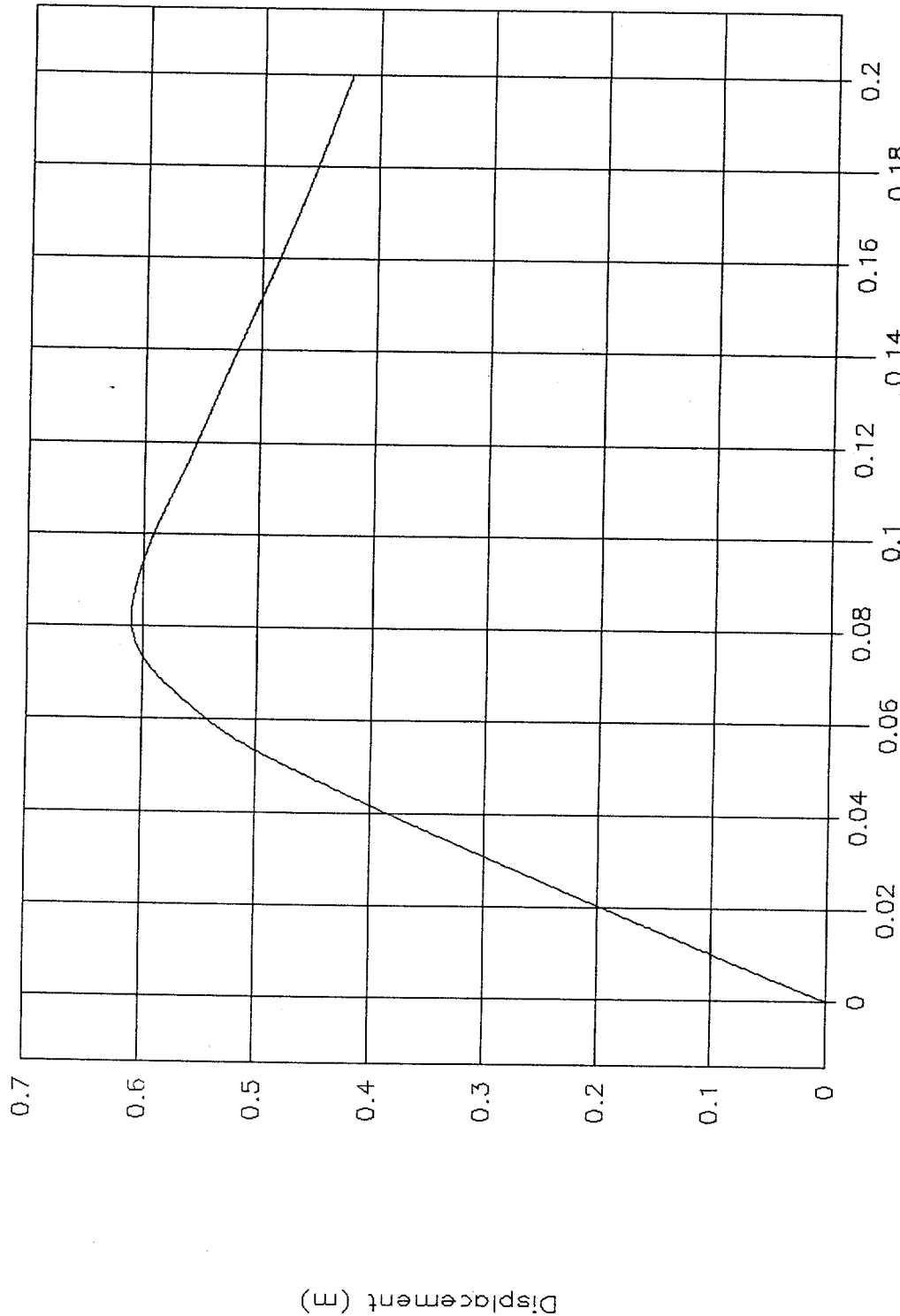


Figure 70. C.g. displacement vs. time, X-axis, test 98F011.



Test No. 98F011
Cg force vs. displacement, X-axis

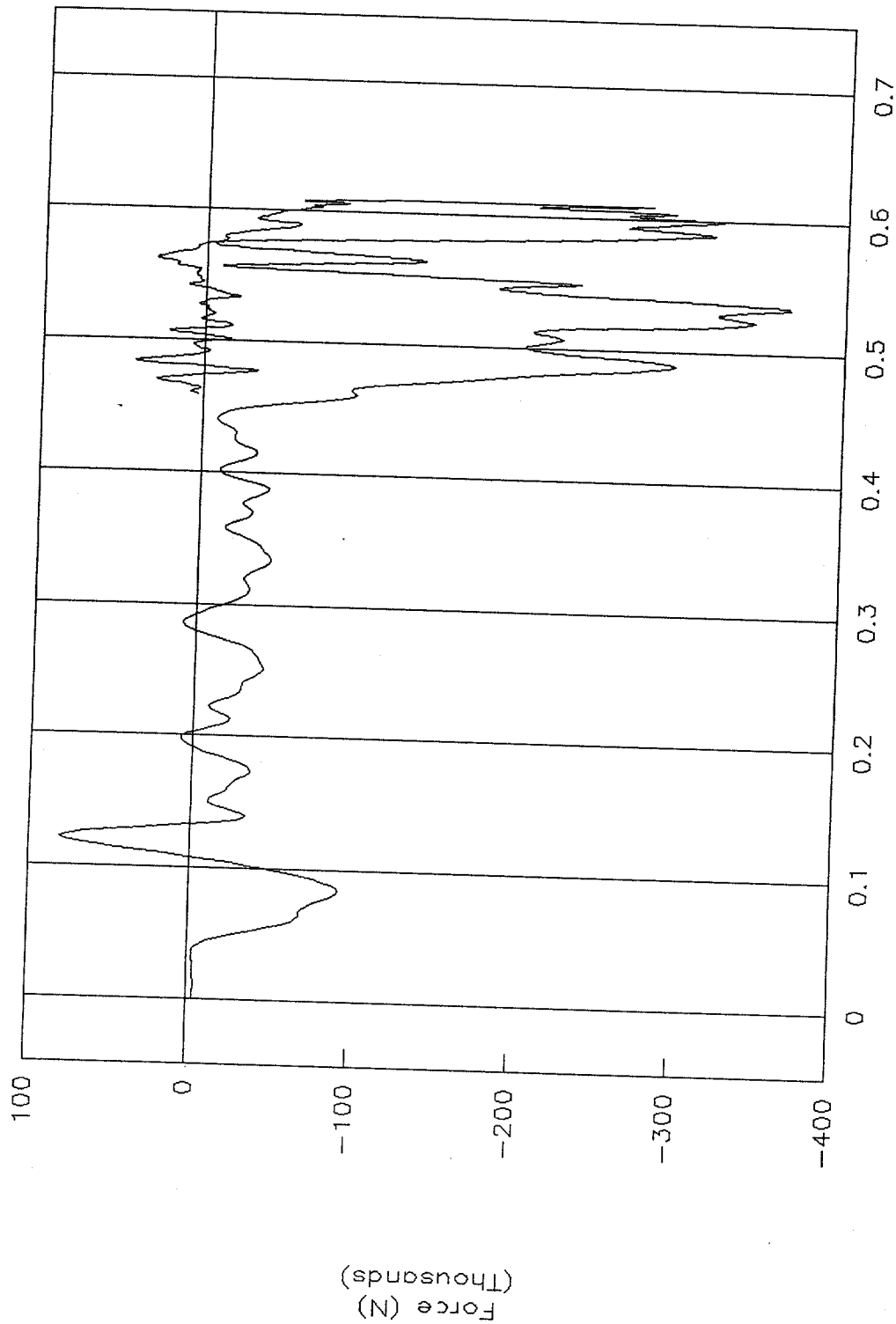


Figure 71. C.g. force vs. displacement, X-axis, test 98F011.



Test No. 98F011
Cg energy vs. displacement, X-axis

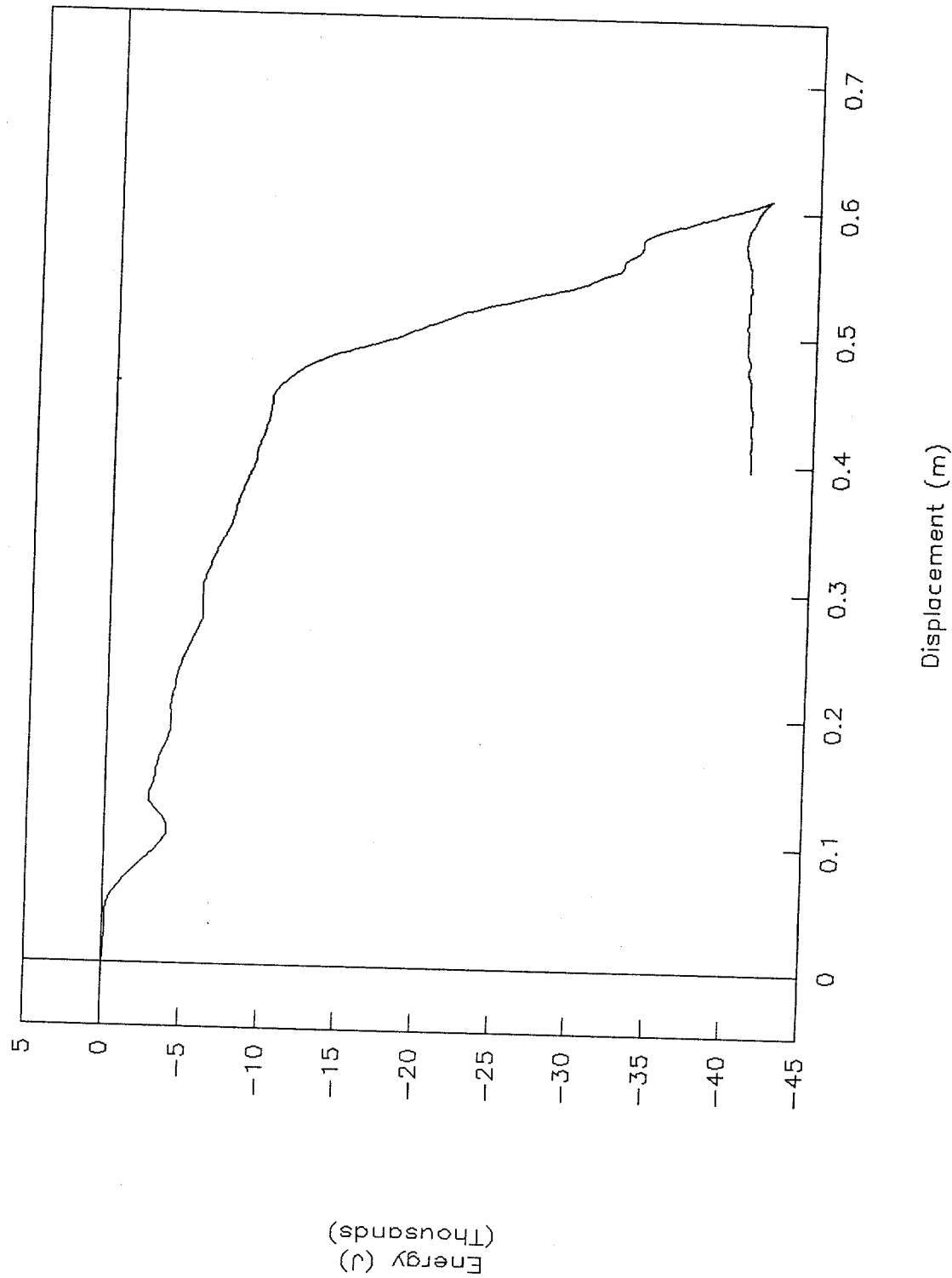


Figure 72. C.g. energy vs. displacement, X-axis, test 98F011.



Test No. 98F011
Cg acceleration vs. time, Y-axis

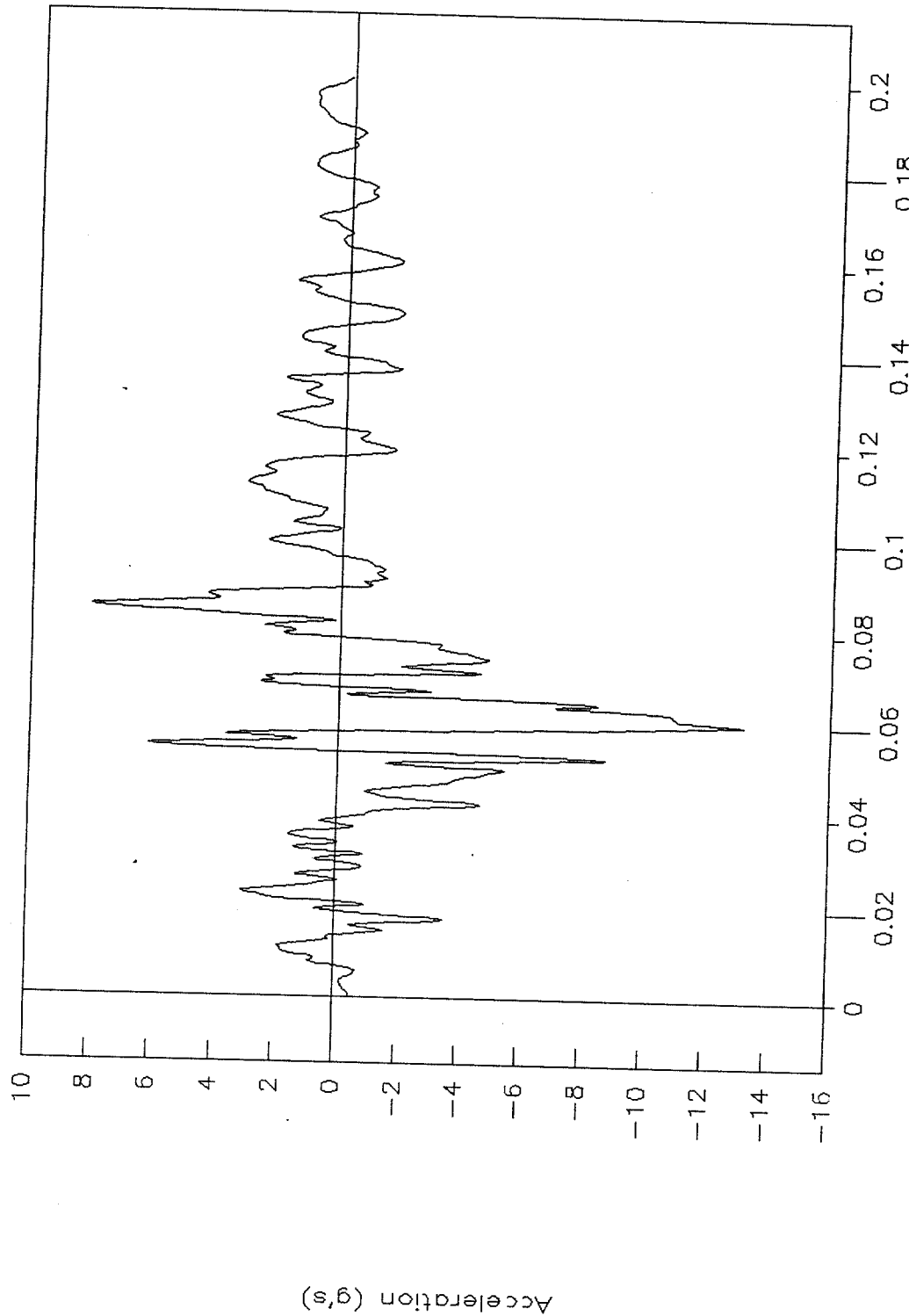


Figure 73. C.g. acceleration vs. time, Y-axis, test 98F011.



Test No. 98F011
Cg acceleration vs. time, Z-axis

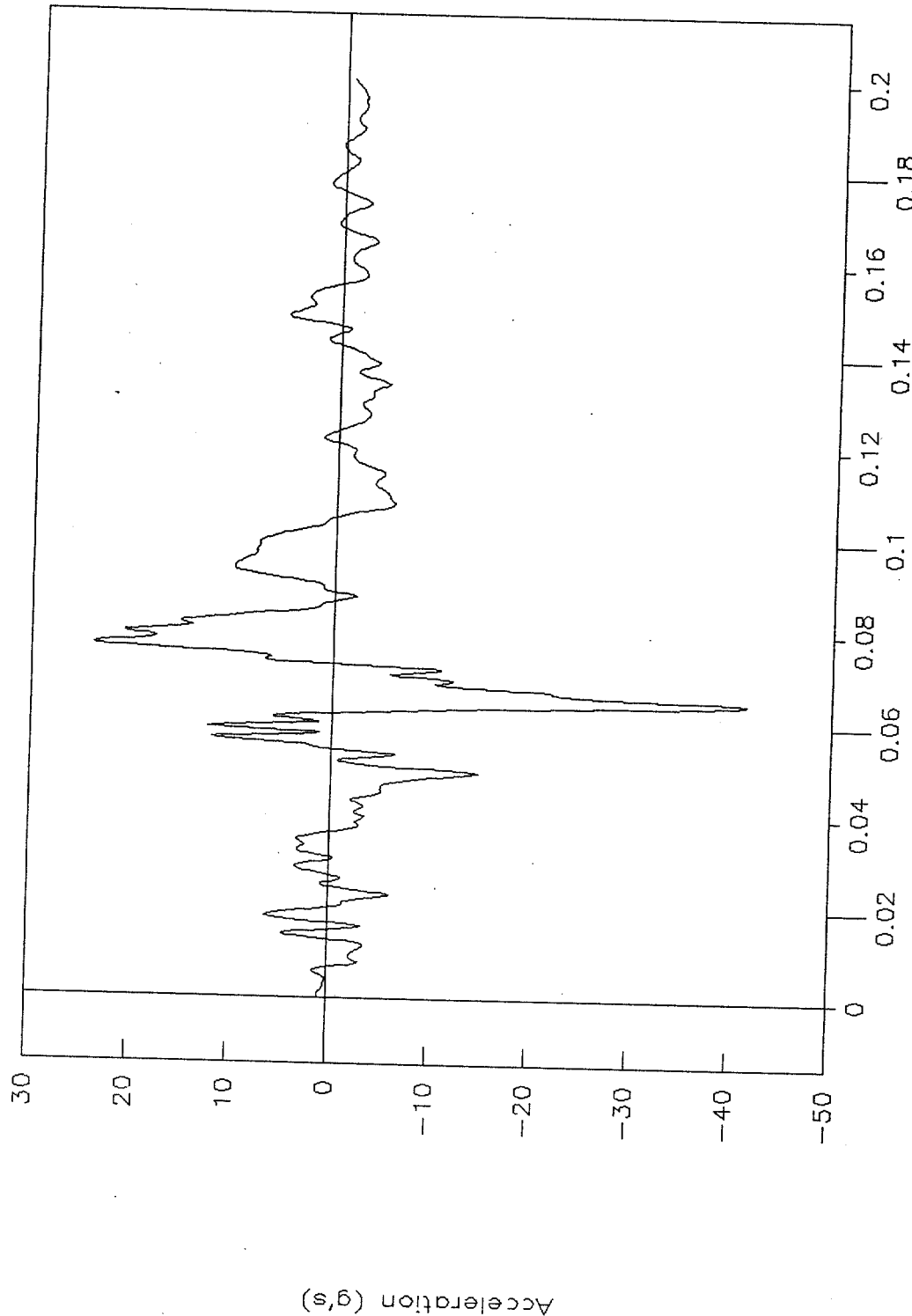


Figure 74. C.g. acceleration vs. time, Z-axis, test 98F011.



Test No. 98F011
Rigid pole, force vs. time

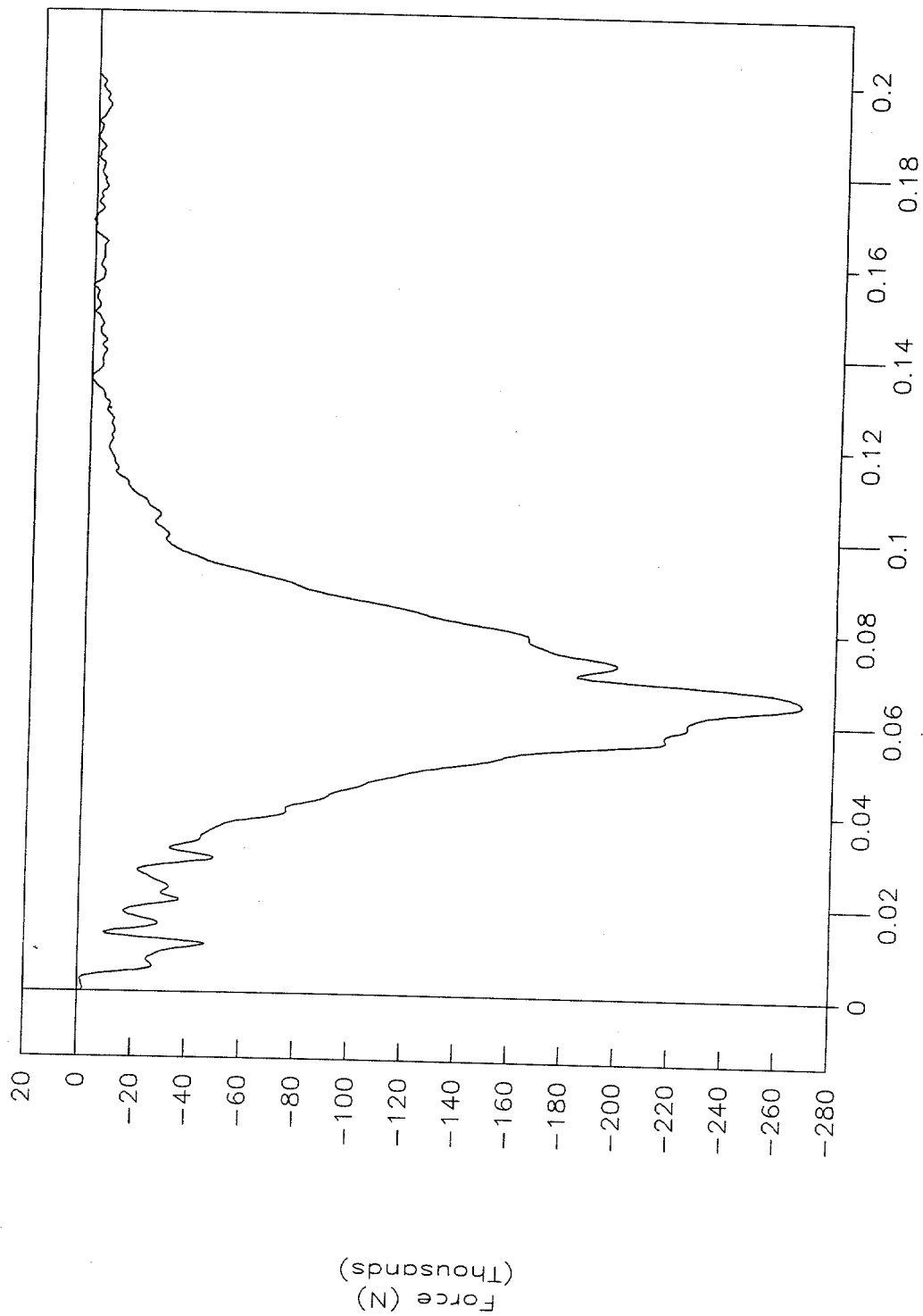


Figure 75. Rigid pole, force vs. time, test 98F011.



Test No. 98F011
Rigid pole, acceleration vs. time

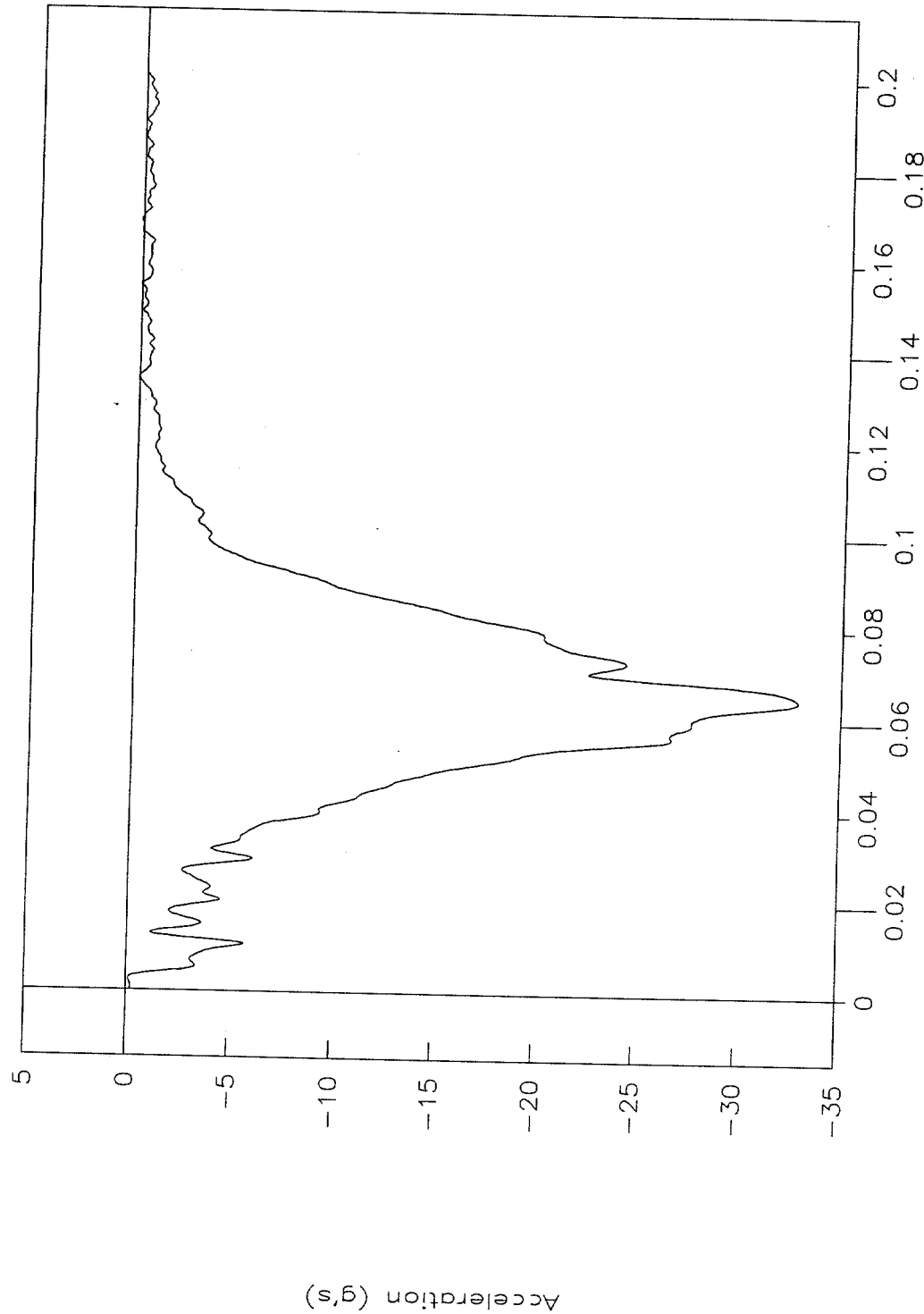


Figure 76. Rigid pole, acceleration vs. time, test 98F011.



Test No. 98F011
Rigid pole, velocity vs. time

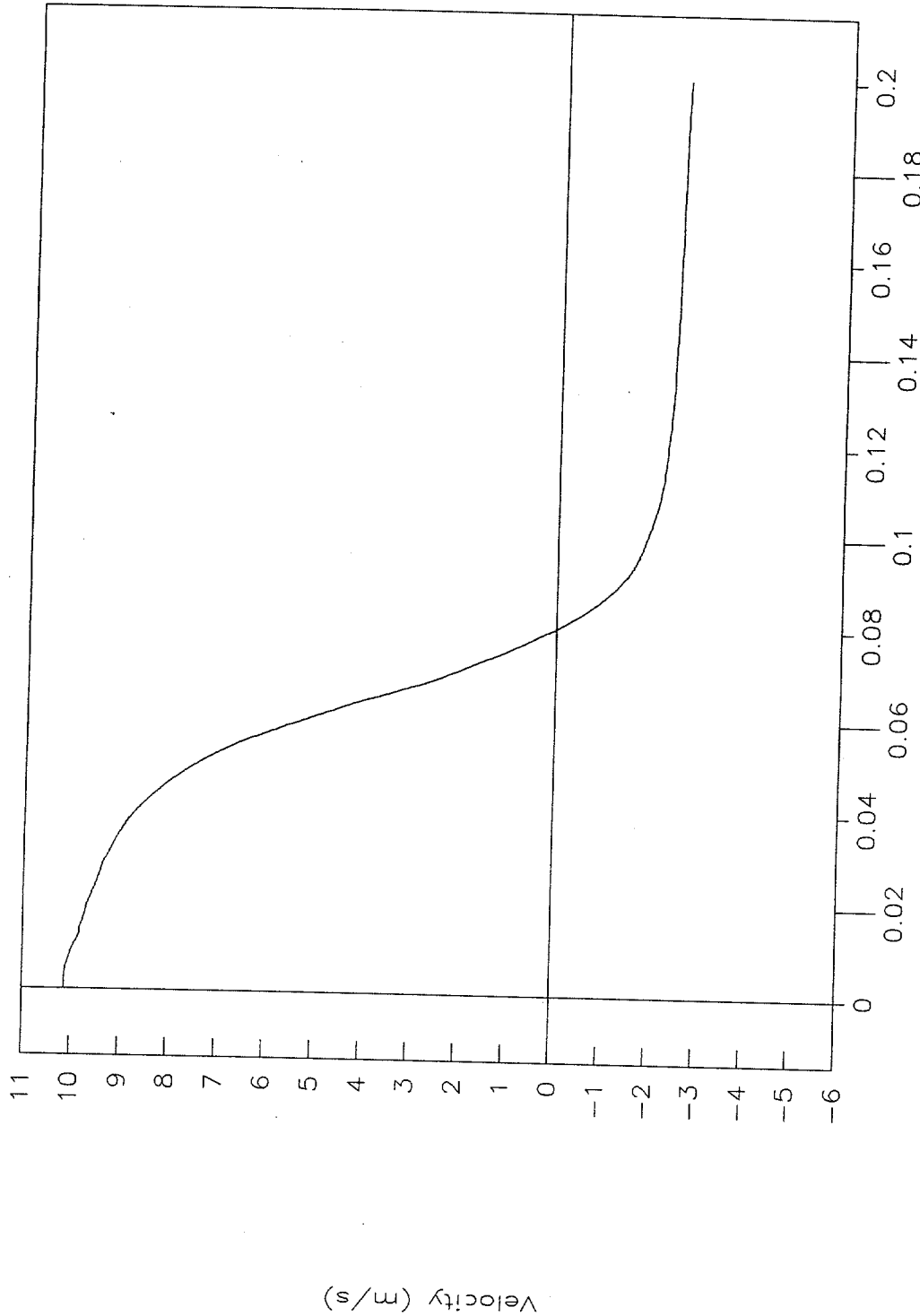


Figure 77. Rigid pole, velocity vs. time, test 98F011.



Test No. 98F011
Rigid pole, displacement vs. time

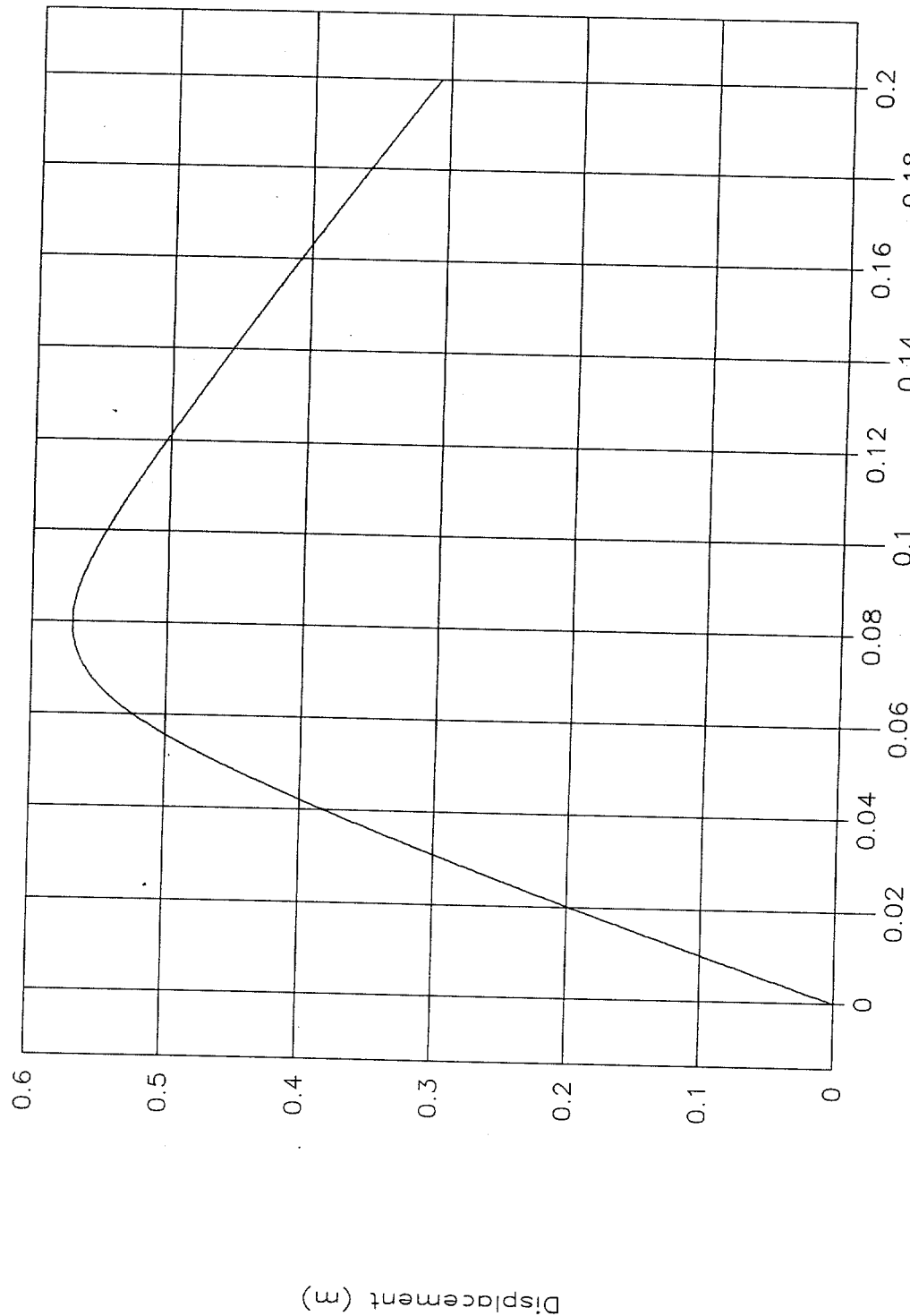


Figure 78. Rigid pole, displacement vs. time, test 98F011.



Test No. 98F011
Rigid pole, force vs. displacement

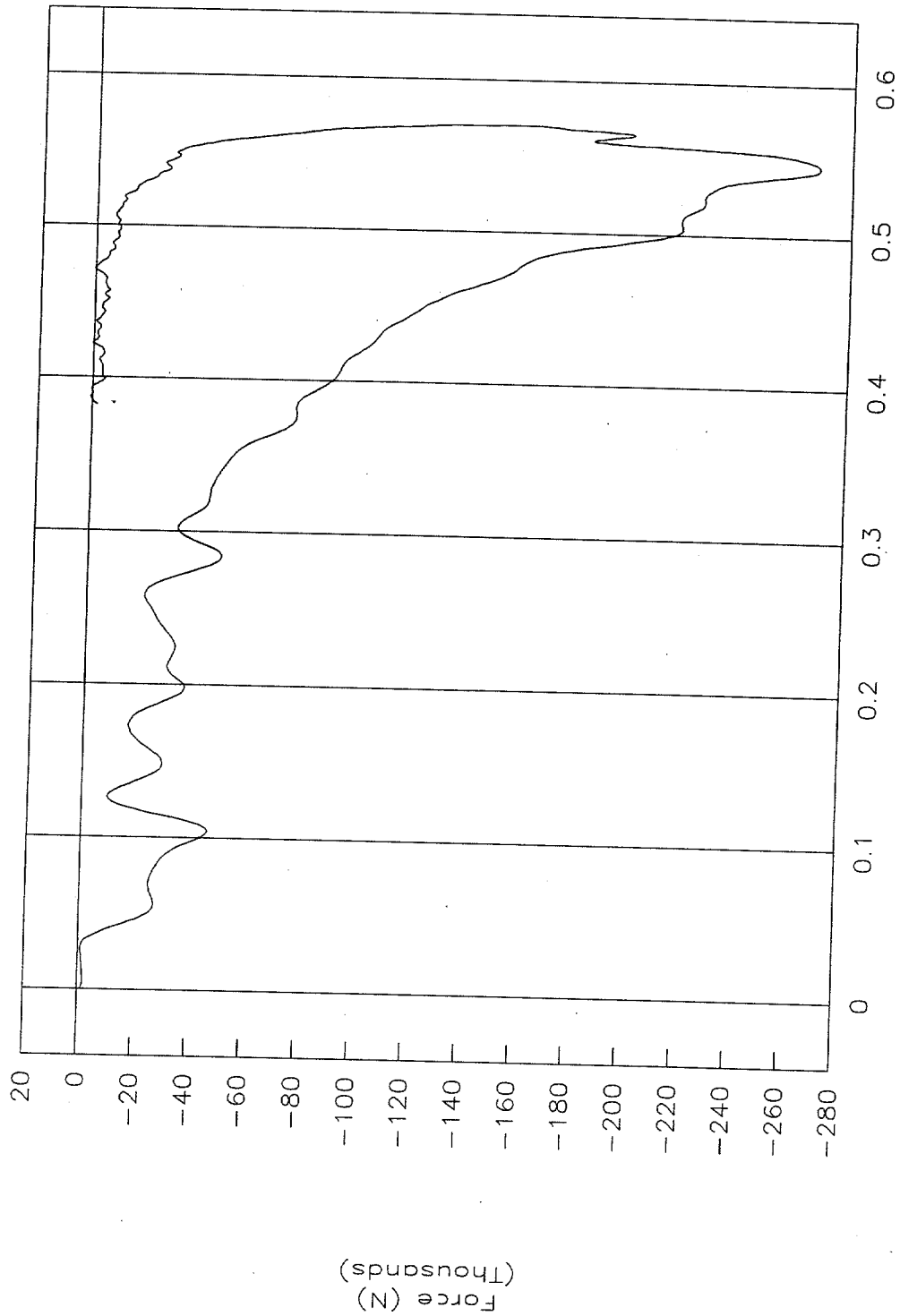


Figure 79. Rigid pole, force vs. displacement, test 98F011.



Test No. 98F011
Rigid pole, energy vs. displacement

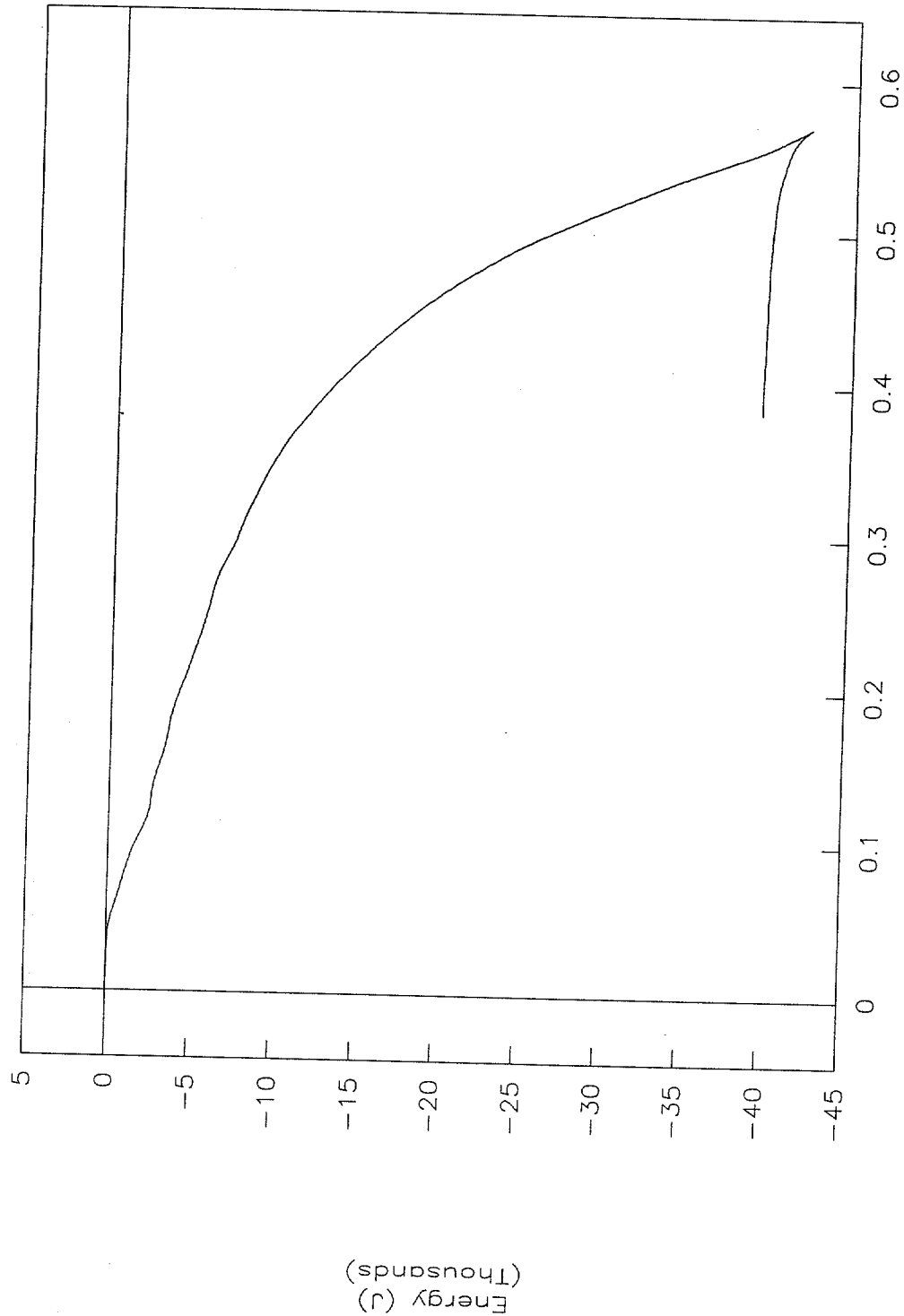


Figure 80. Rigid pole, energy vs. displacement, test 98F011.



Test No. 98F011
Impact force height vs. displacement

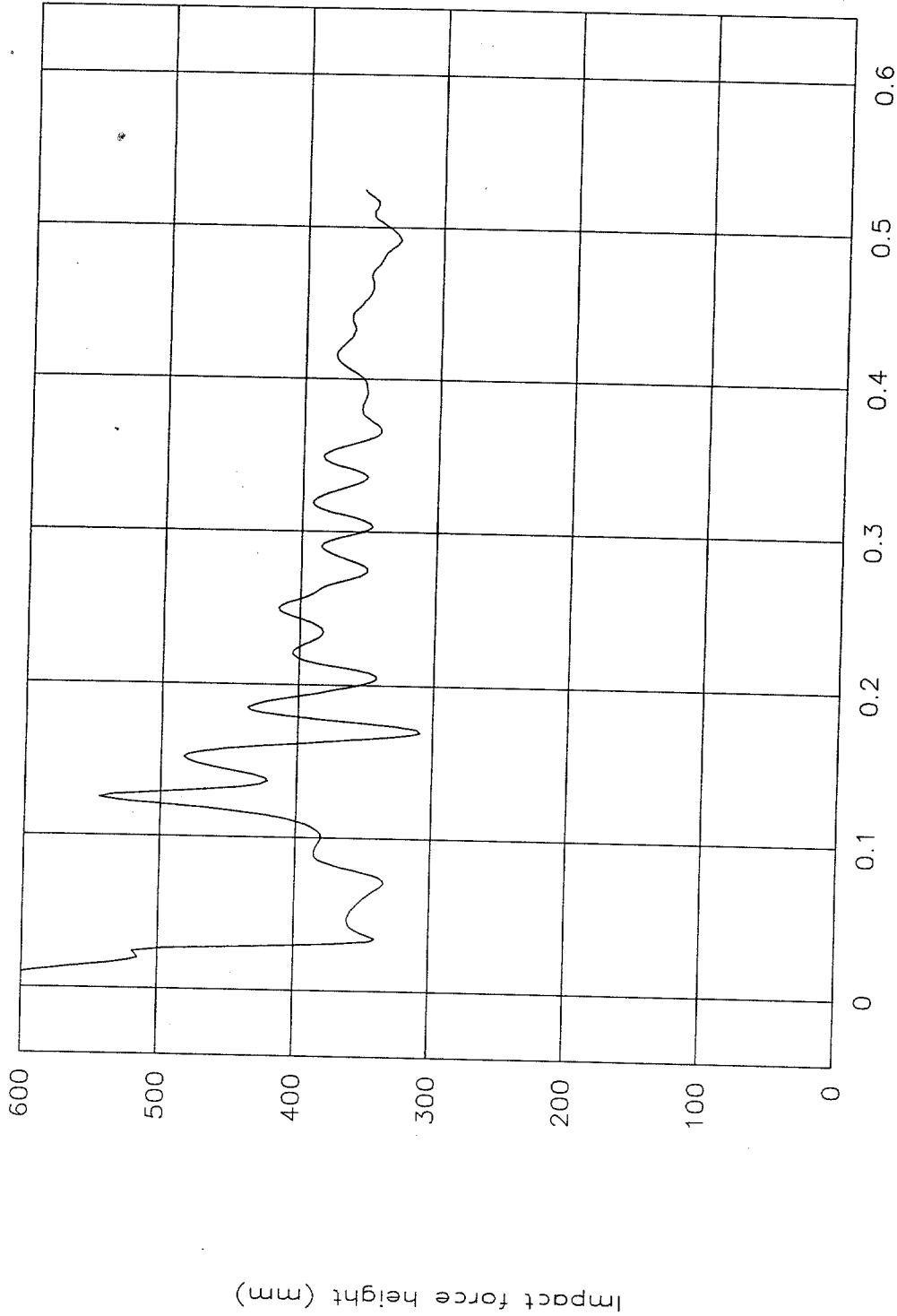


Figure 81. Impact force height vs. displacement, test 98F011.



Test No. 98F011
Top of engine, X-axis

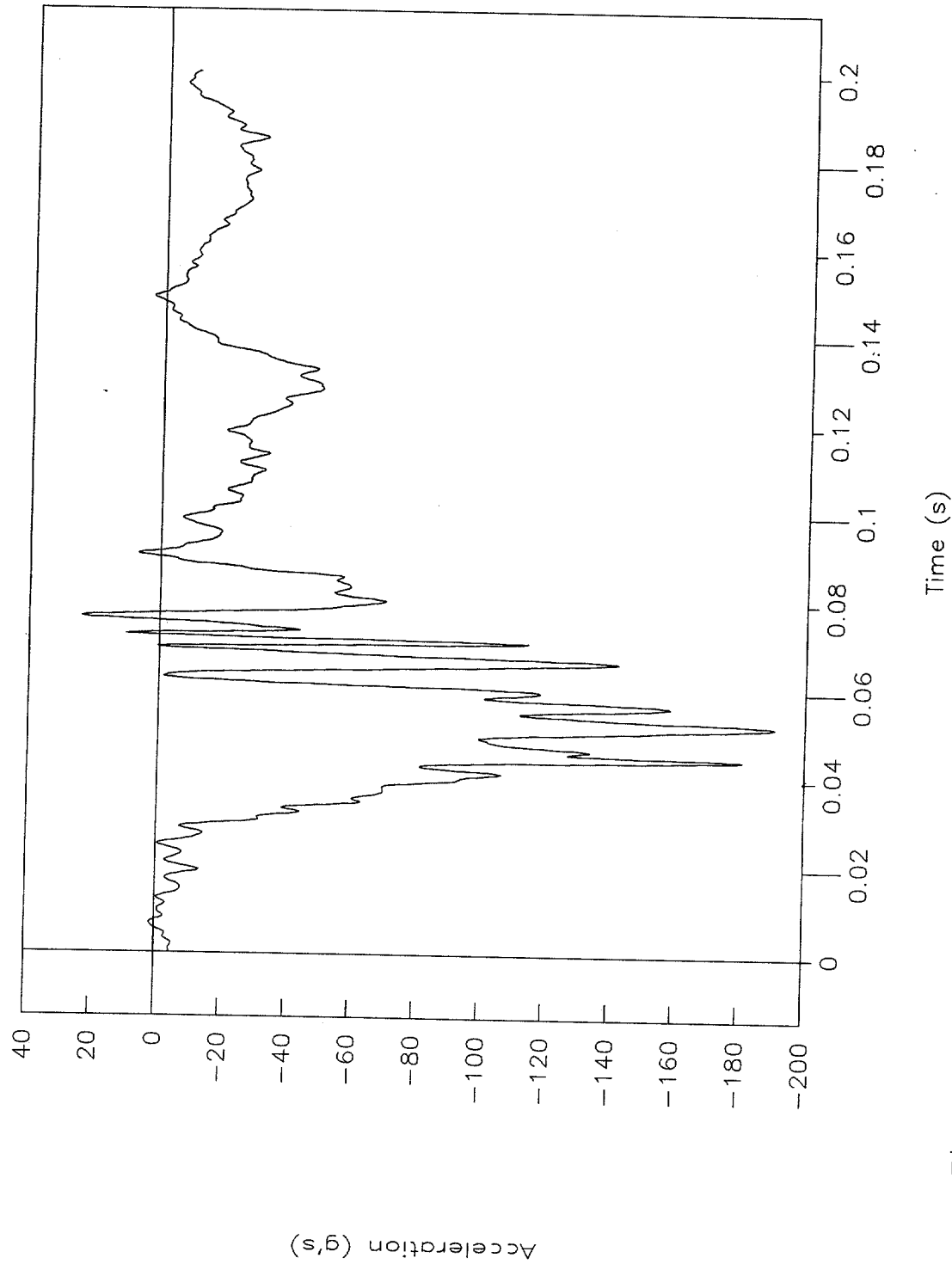


Figure 82. Top of engine acceleration vs. time, X-axis, test 98F011.



Test No. 98F011

Bottom of engine, X-axis

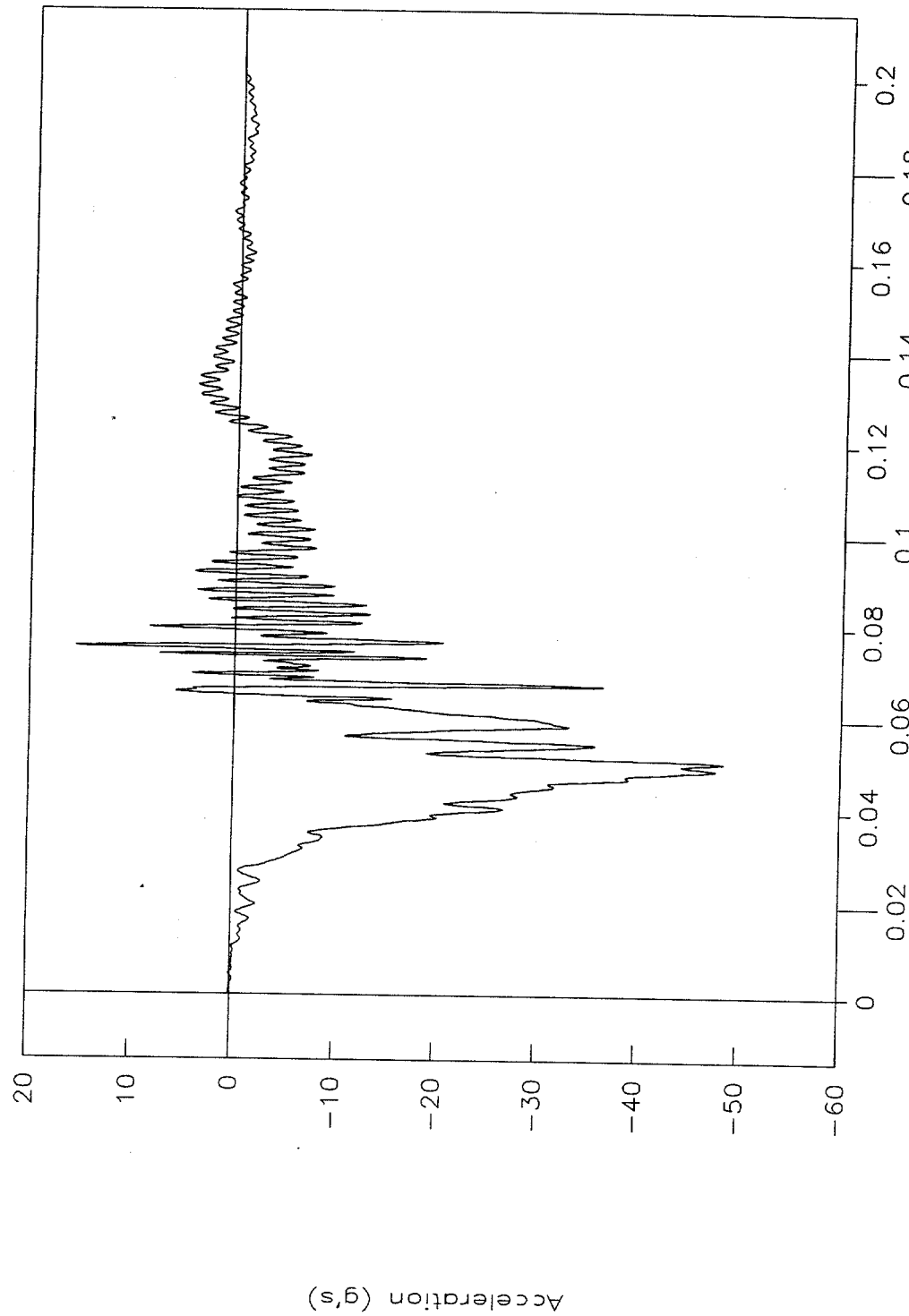


Figure 83. Bottom of engine acceleration vs. time, X-axis, test 98F011.



Test No. 98F011
Left control arm, X-axis

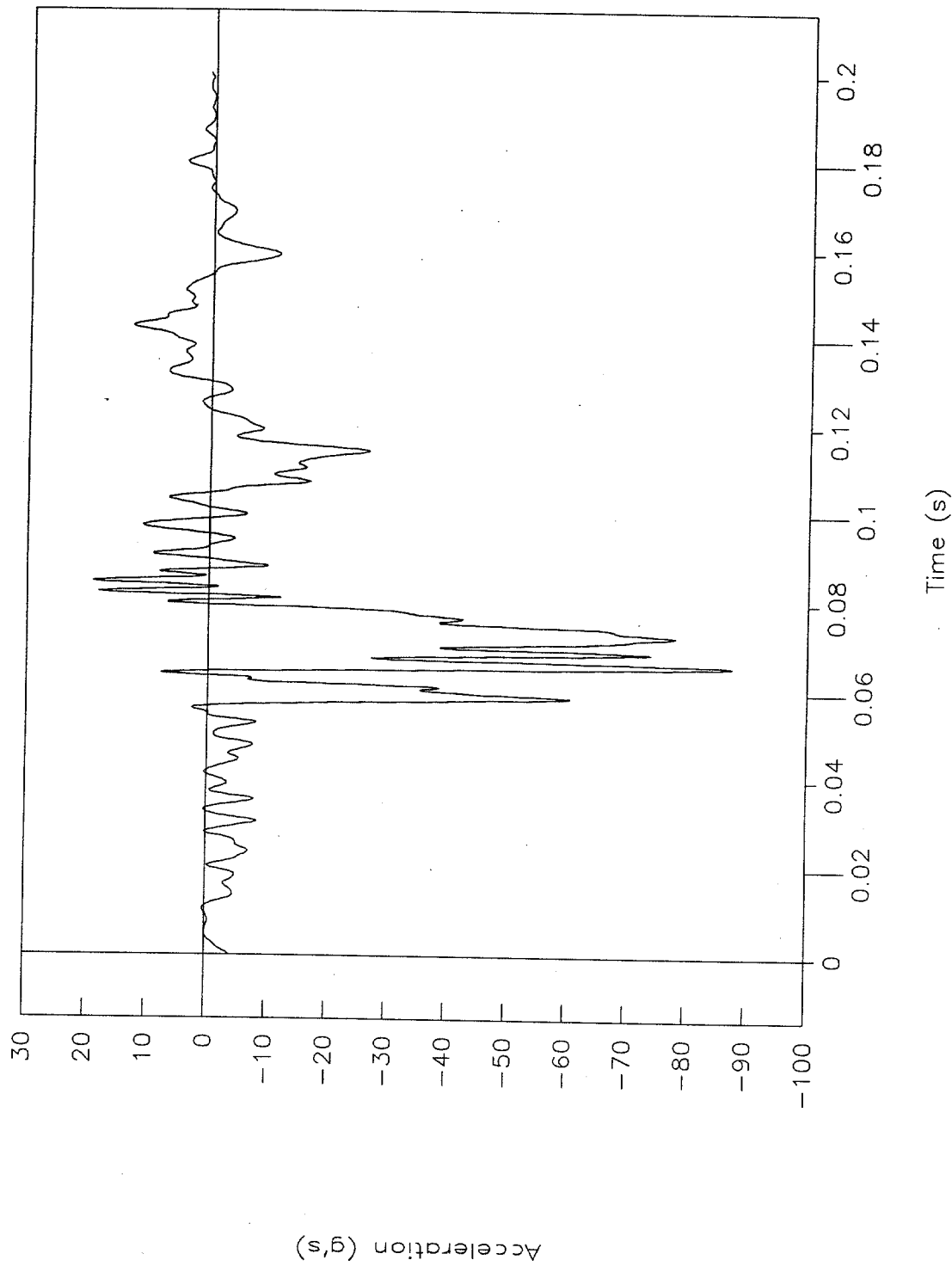


Figure 84. Left control arm acceleration vs. time, X-axis, test 98F011.



Test No. 98F011
Right control arm, X-axis

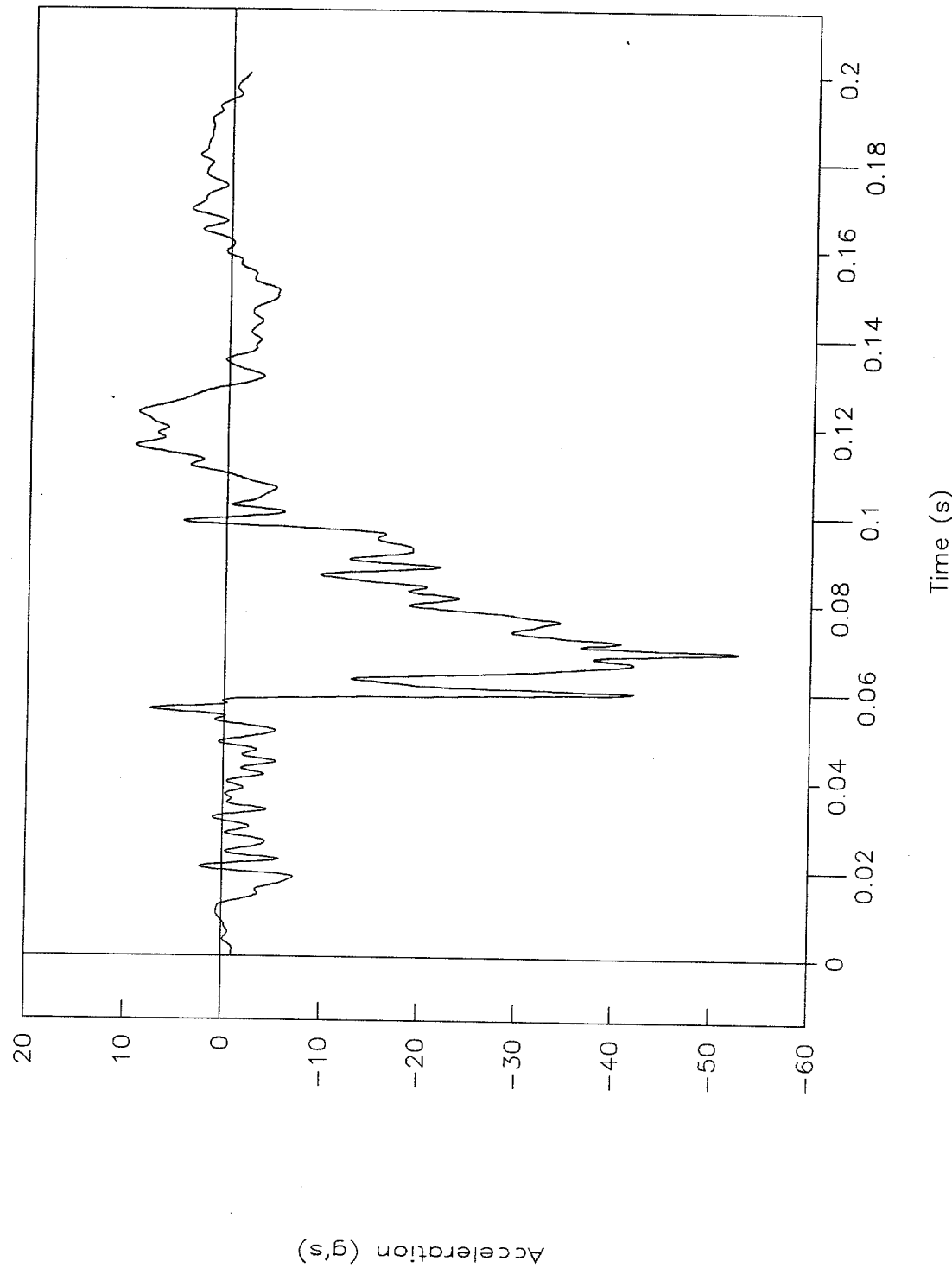


Figure 85. Right control arm acceleration vs. time, X-axis, test 98F011.



Test No. 98F011
Instrument panel, X-axis

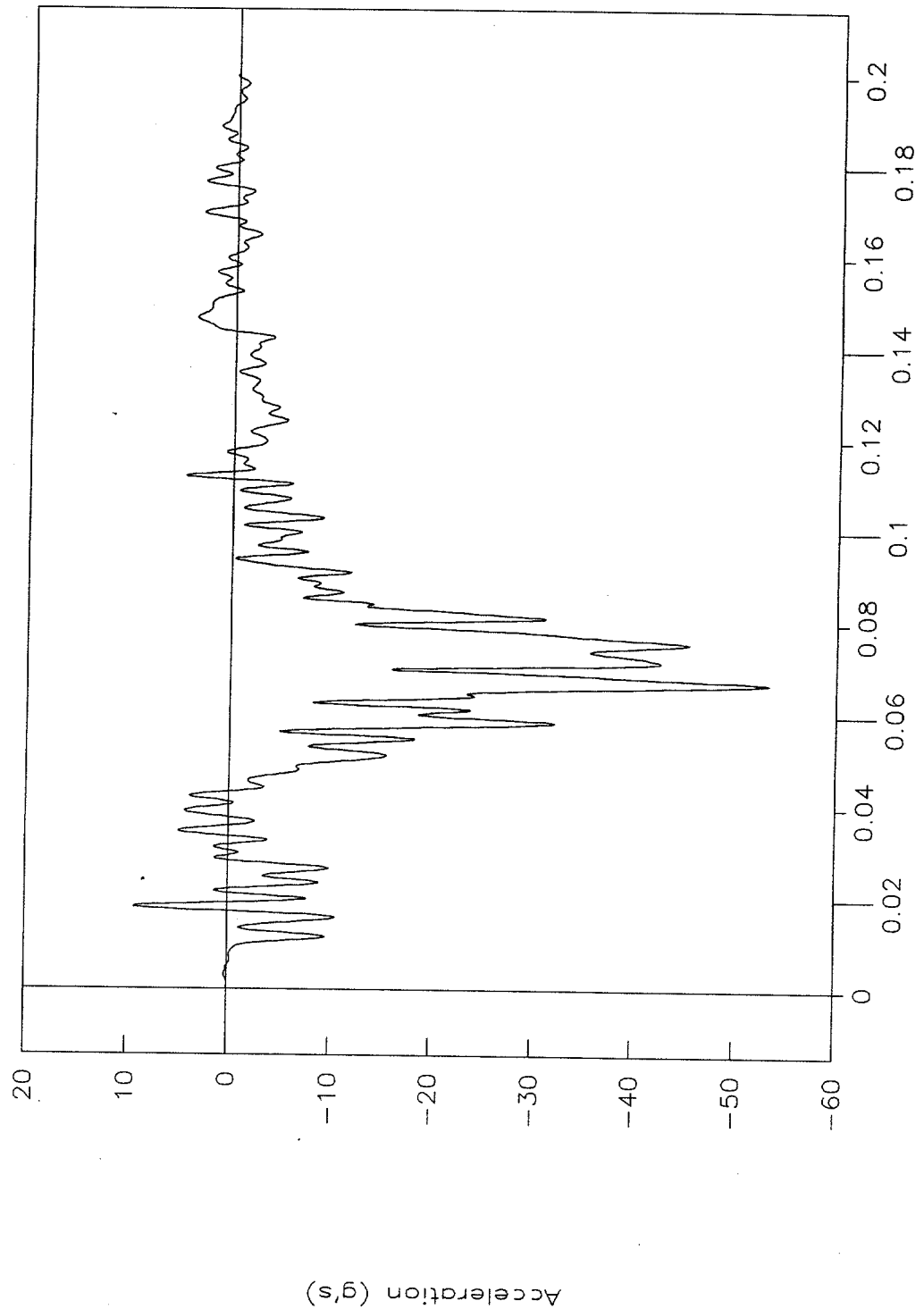


Figure 86. Instrument panel acceleration vs. time, X-axis, test 98F011.



Test No. 98F011
Pitch rate and angle vs. time

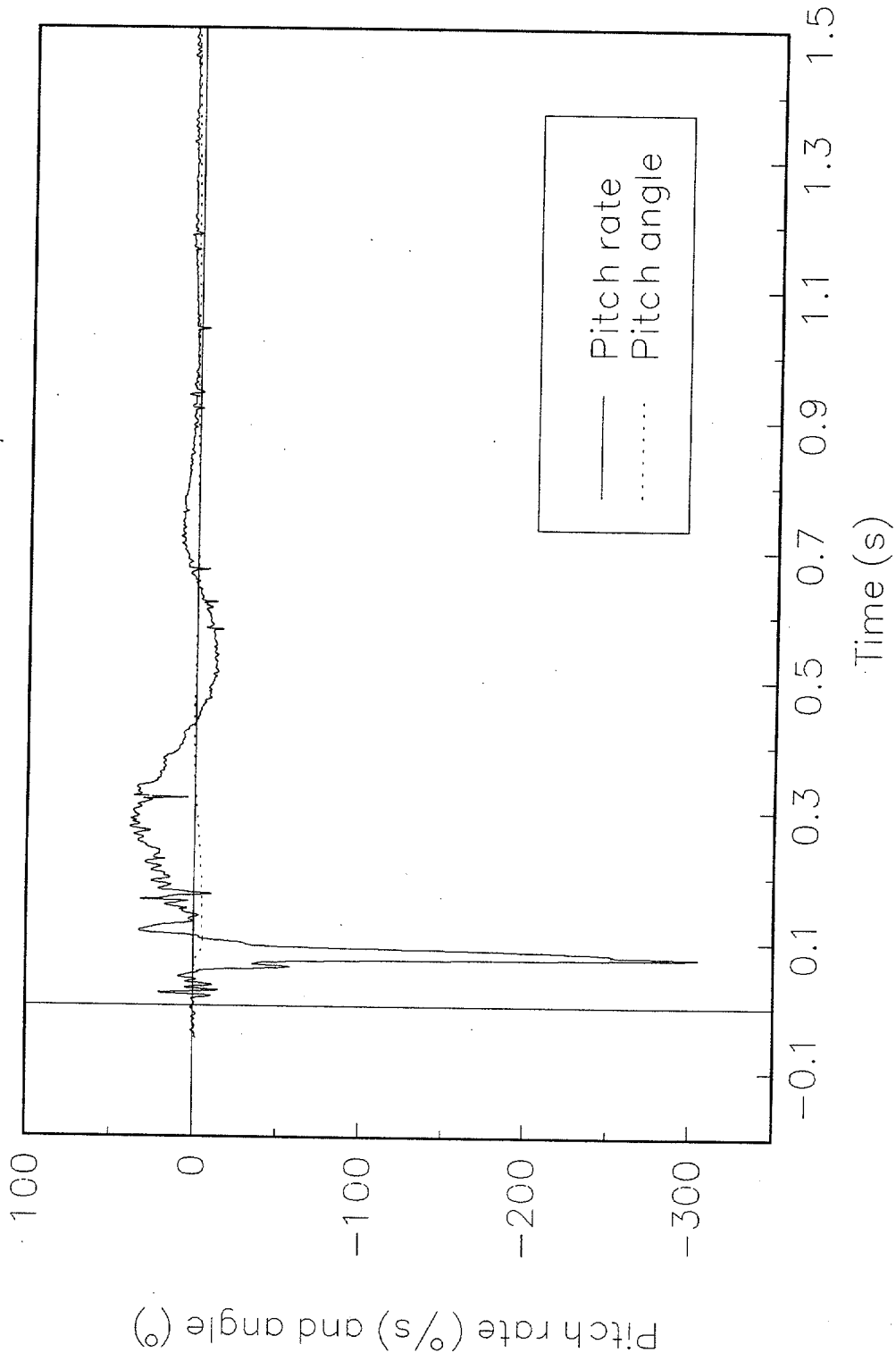


Figure 87. Pitch rate and angle vs. time, test 98F011.



Test No. 98F011
Roll rate and angle vs. time

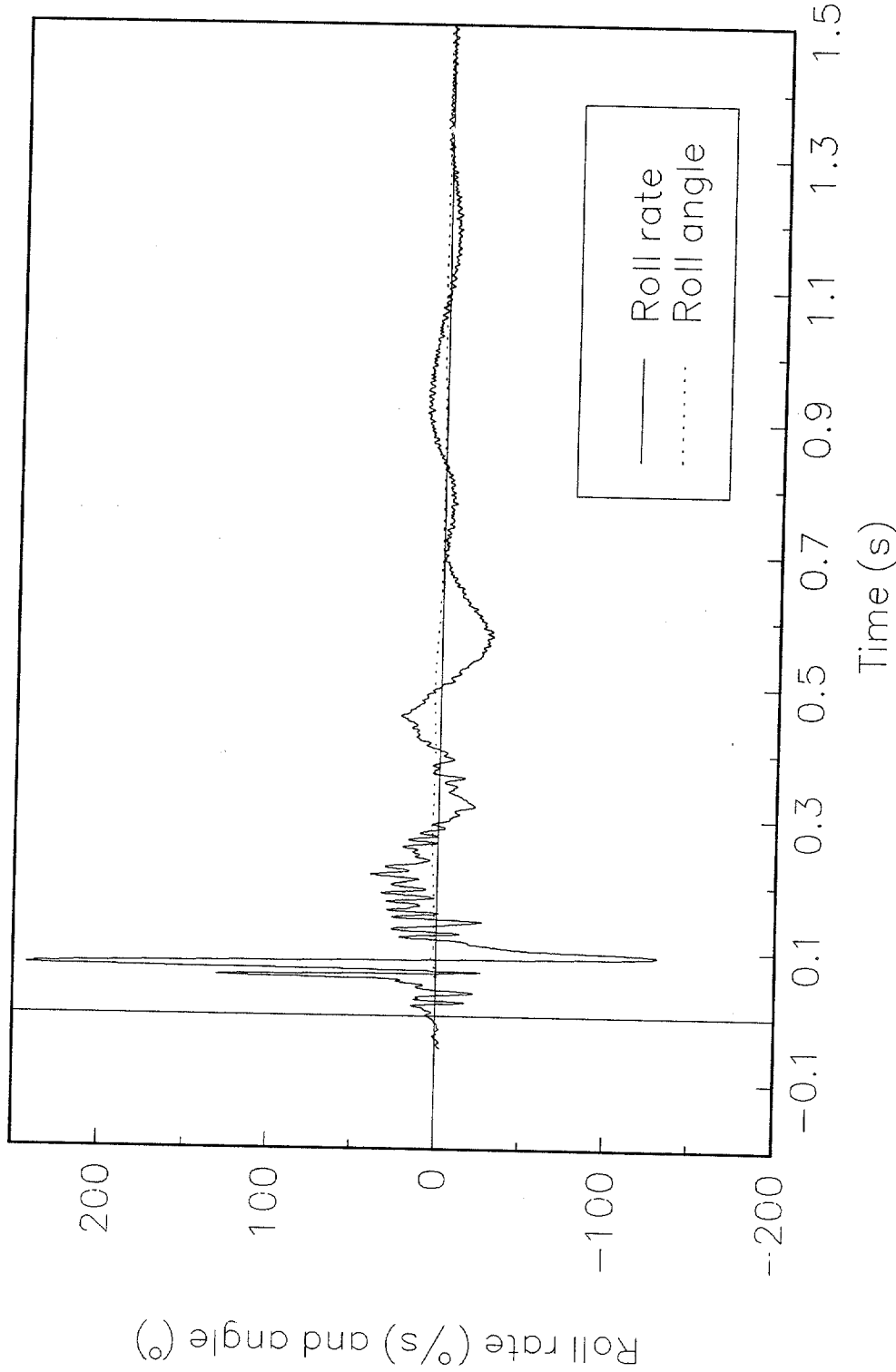


Figure 88. Roll rate and angle vs. time, test 98F011.



Test No. 98F011
Yaw rate and angle vs. time

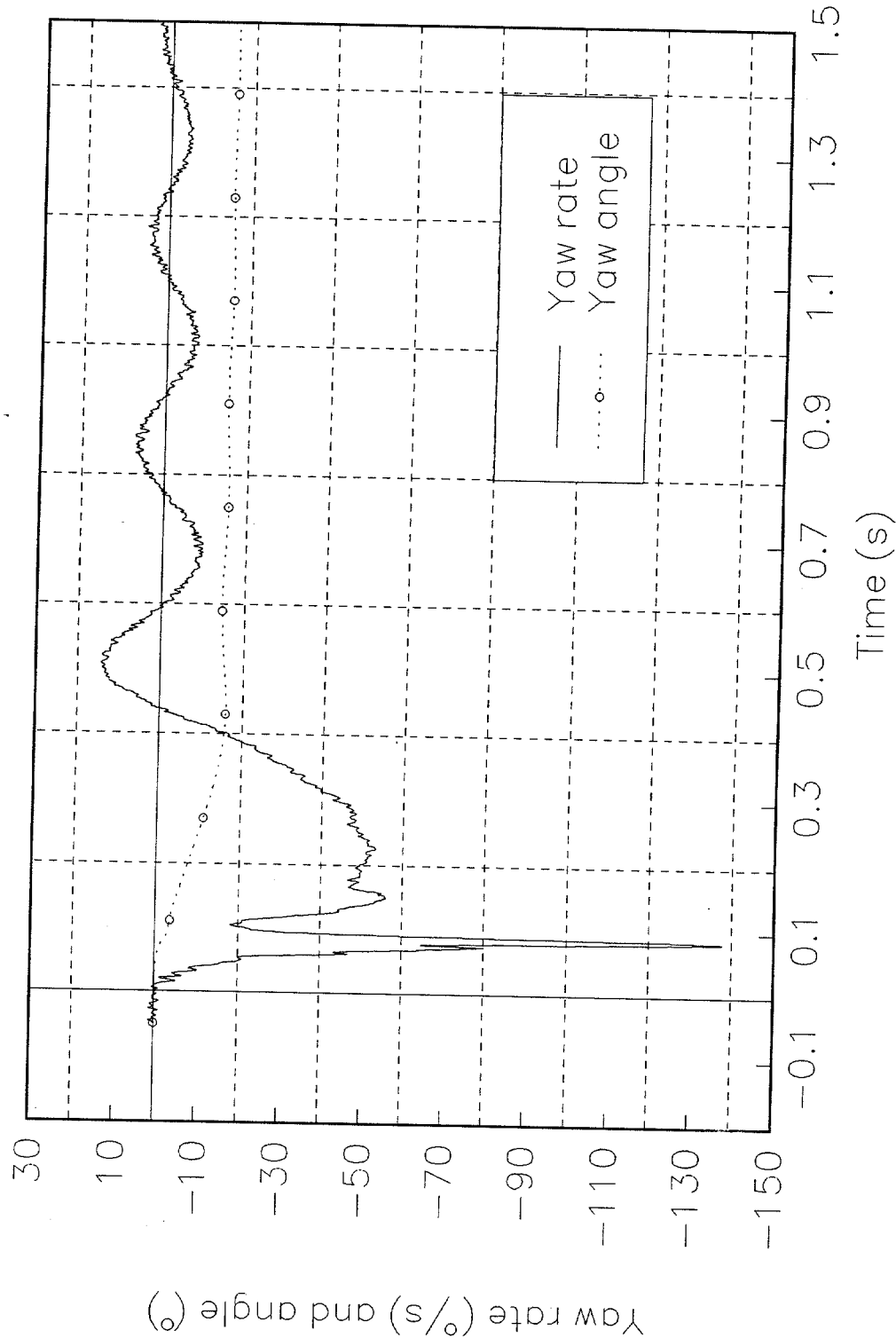


Figure 89. Yaw rate and angle vs. time, test 98F011.



Test No. 98F012

Cg acceleration vs. time, X-axis

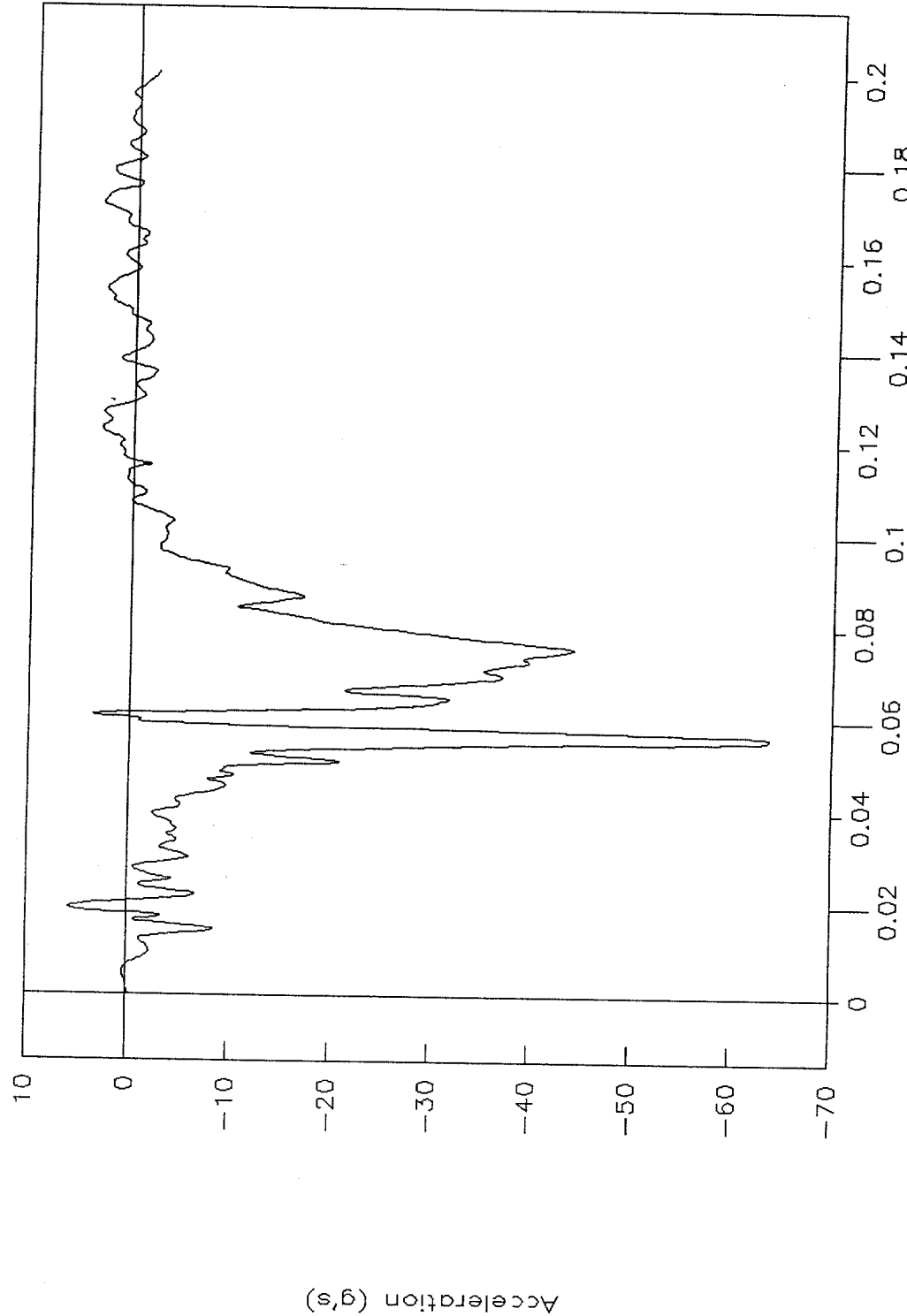


Figure 90. C.g. acceleration vs. time, X-axis, test 98F012.



Test No. 98F012
Cg velocity vs. time, X-axis

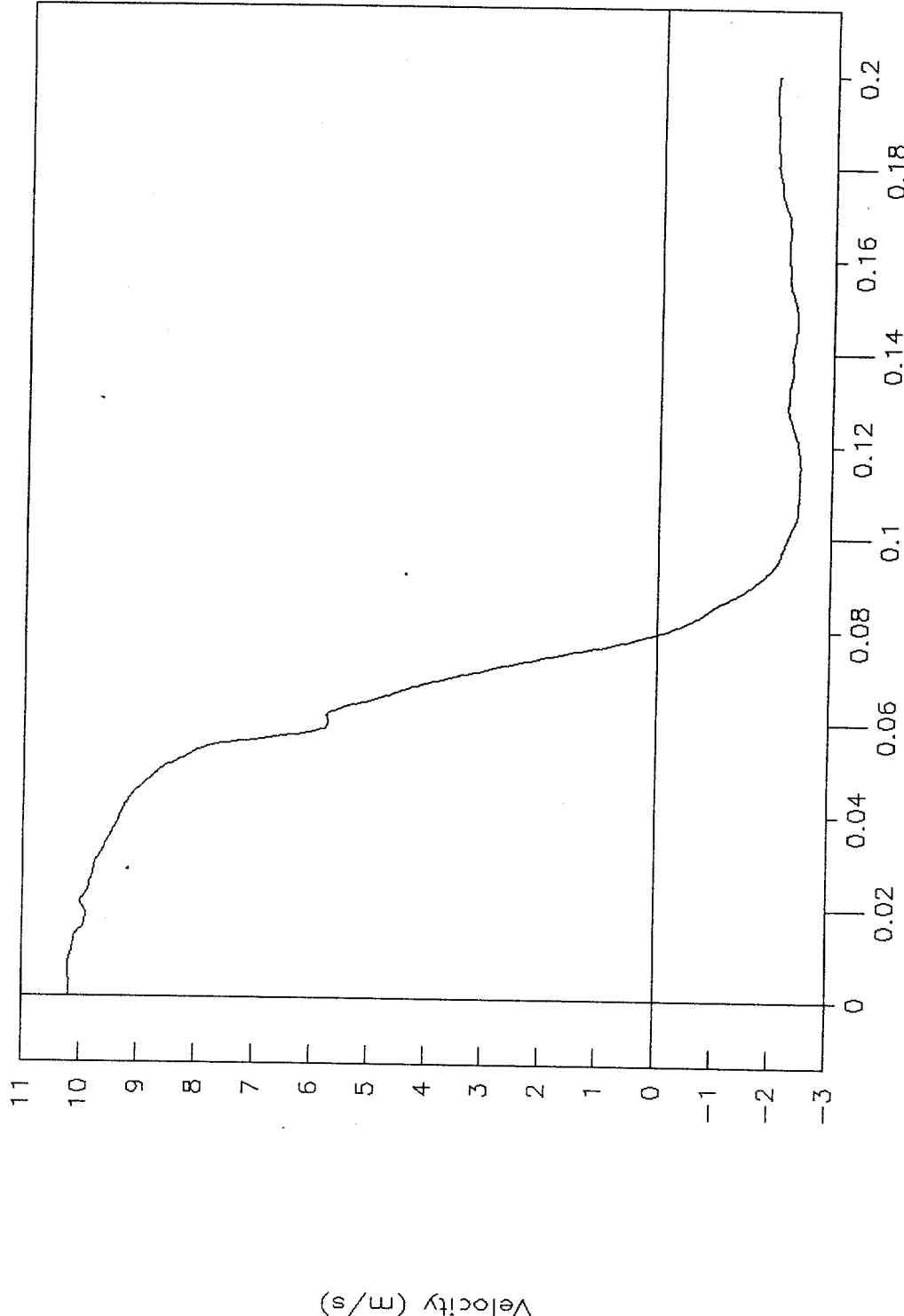


Figure 91. C.g. velocity vs. time, X-axis, test 98F012.



Test No. 98F012
Cg displacement vs. time, X-axis

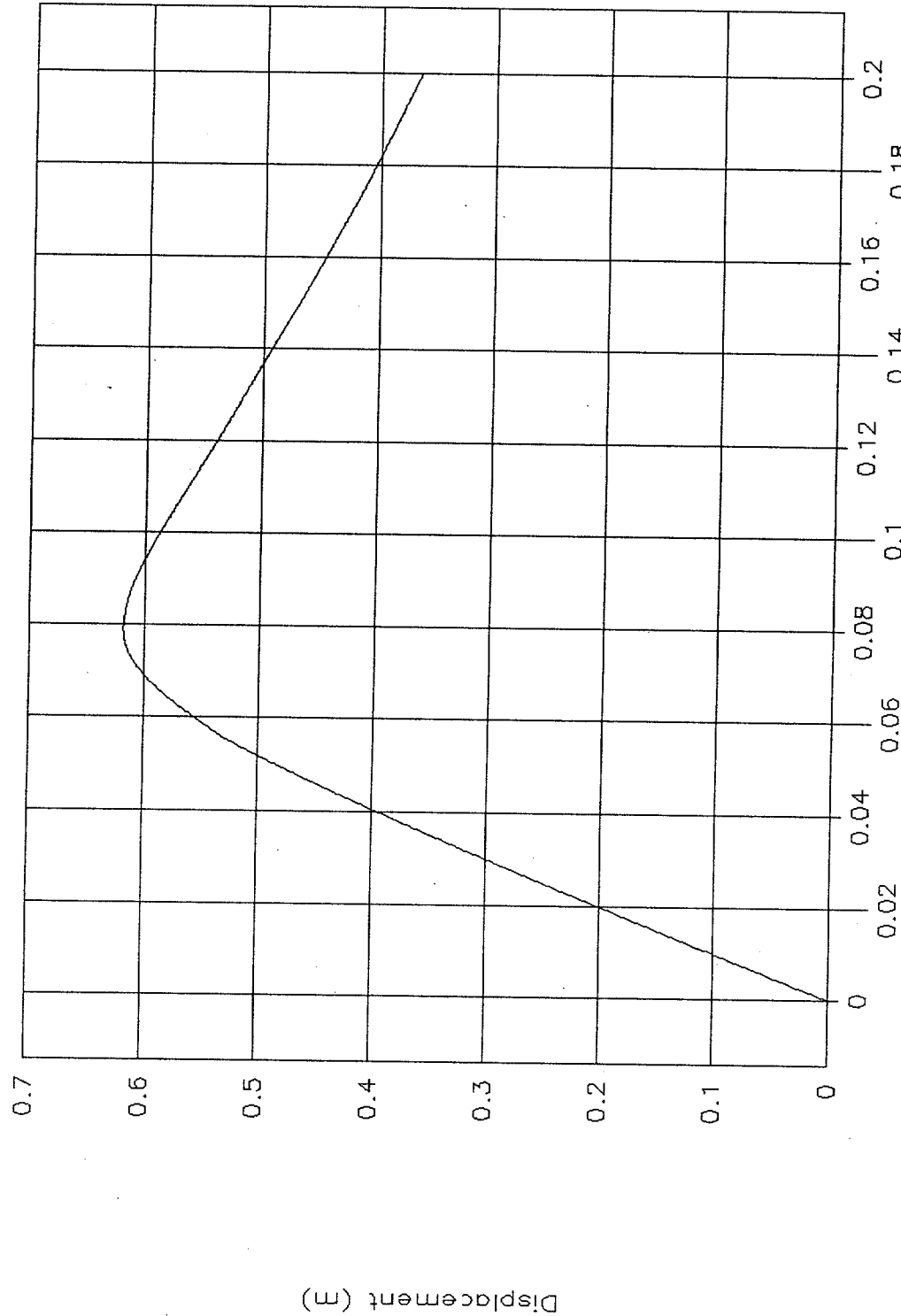


Figure 92. C.g. displacement vs. time, X-axis, test 98F012.



Test No. 98F012
Cg force vs. displacement, X-axis

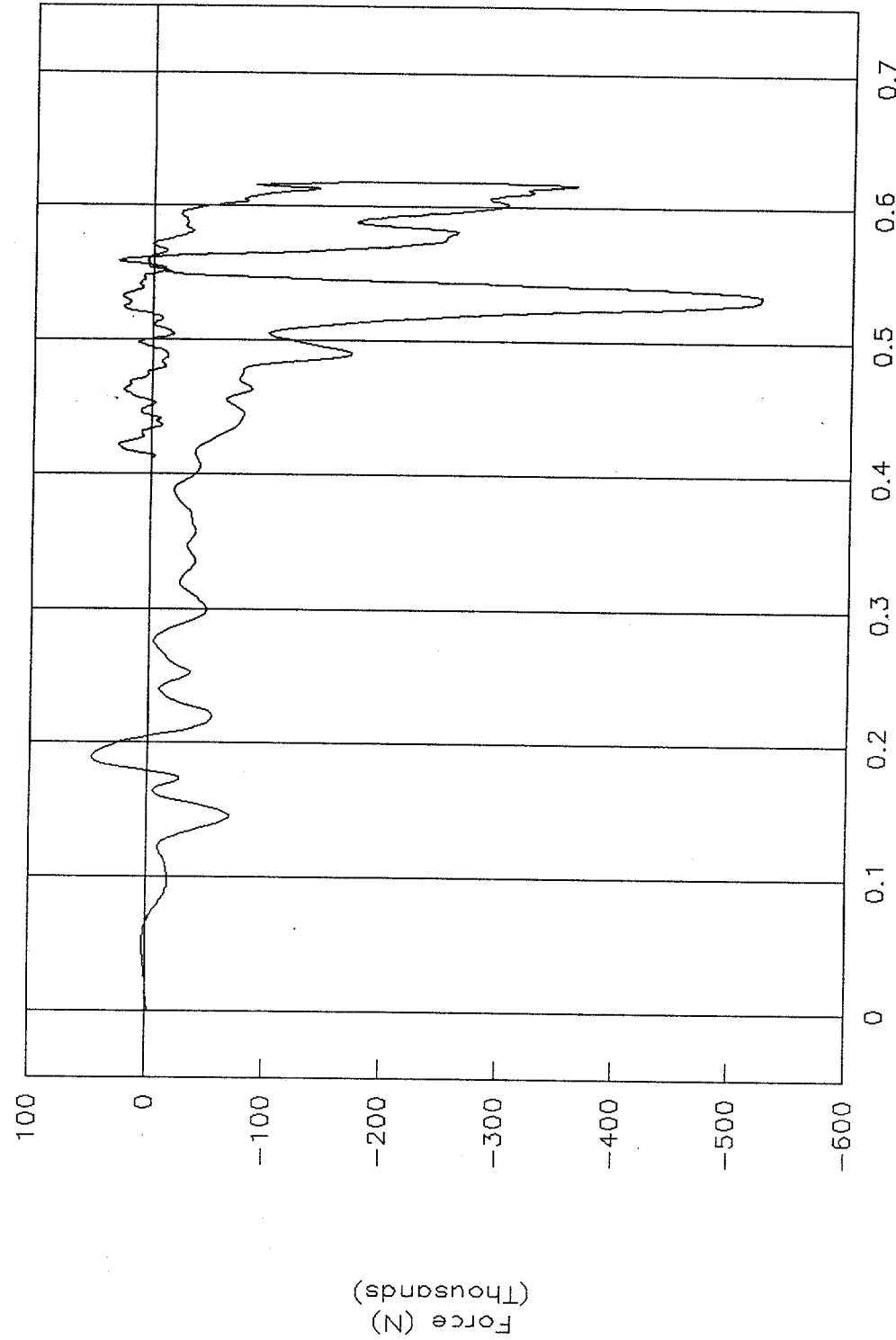


Figure 93. C.g. force vs. displacement, X-axis, test 98F012.



Test No. 98F012
Cg energy vs. displacement, X-axis

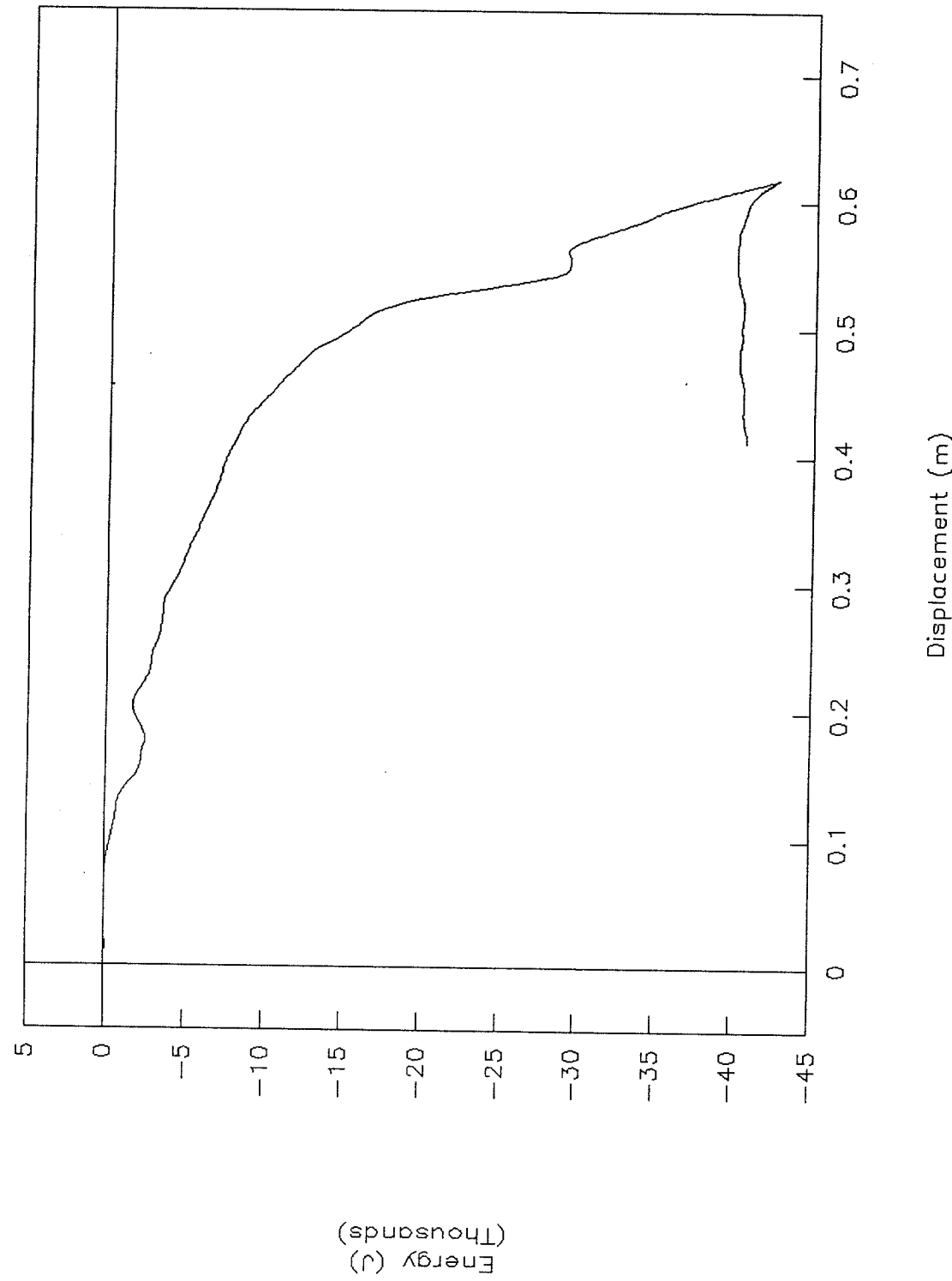


Figure 94. C.g. energy vs. displacement, X-axis, test 98F012.



Test No. 98F012

Cg acceleration vs. time, Y-axis

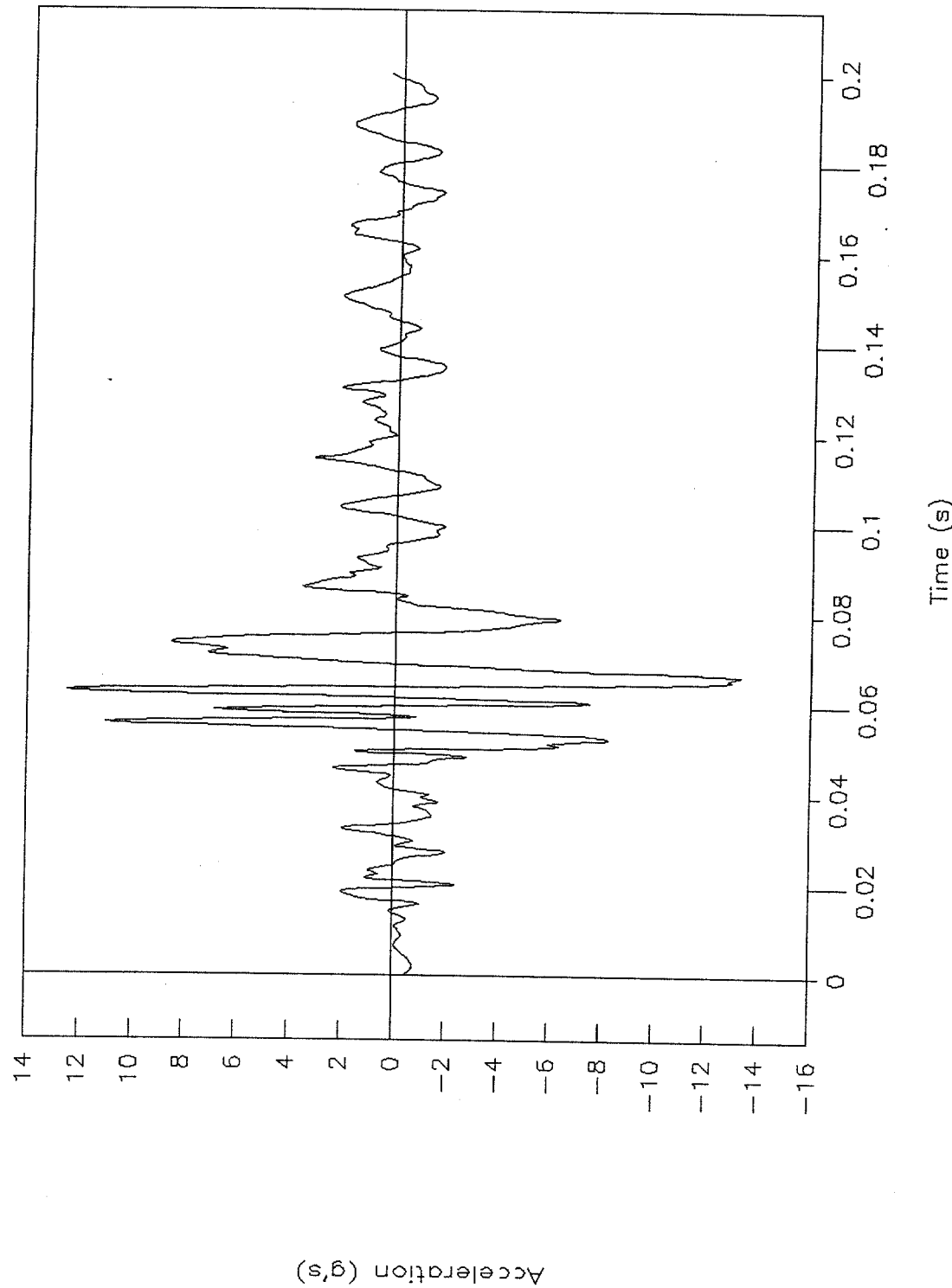


Figure 95. C.g. acceleration vs. time, Y-axis, test 98F012.



Test No. 98F012

Cg acceleration vs. time, Z-axis

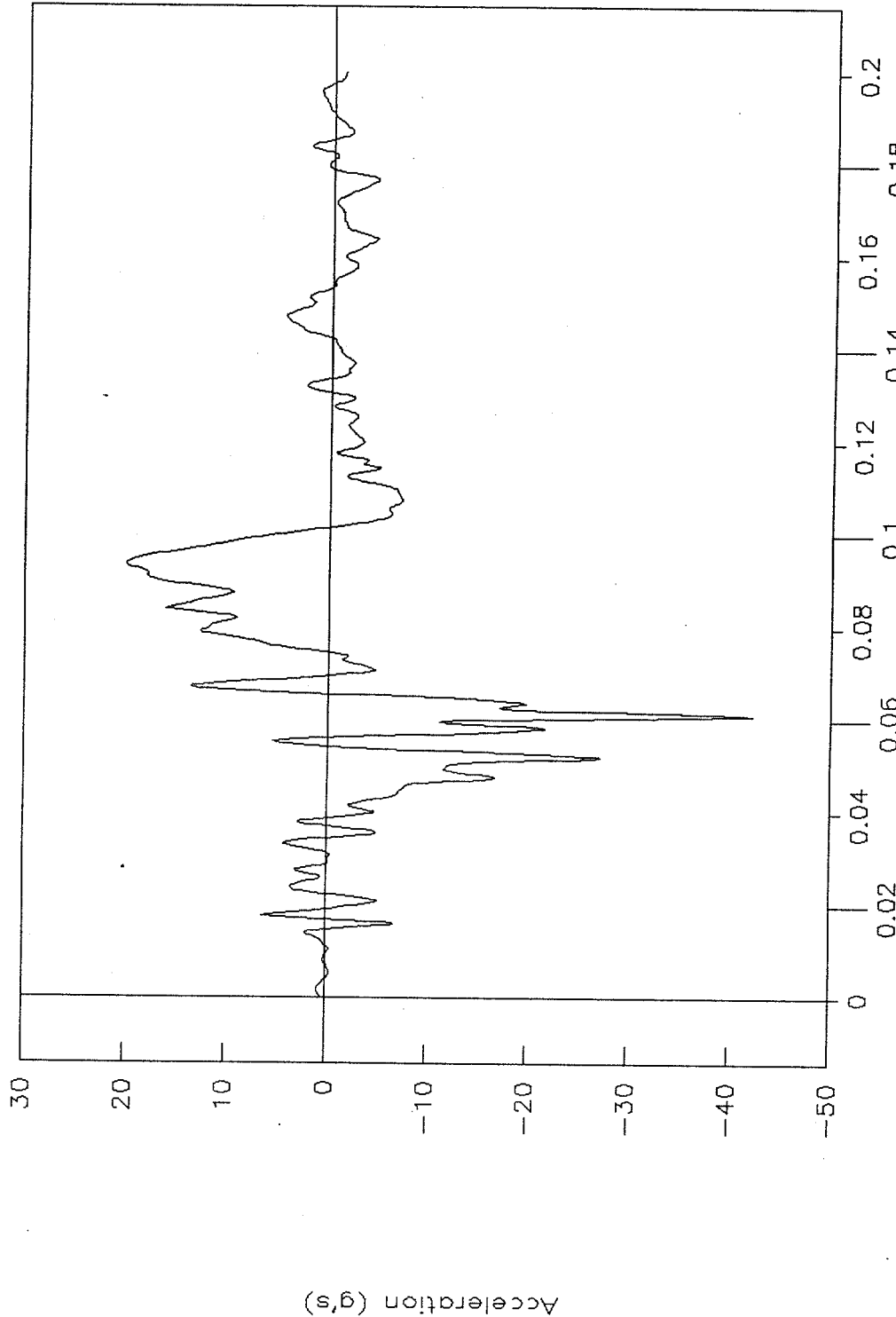


Figure 96. C.g. acceleration vs. time, Z-axis, test 98F012.



Test No. 98F012
Rigid pole, force vs. time

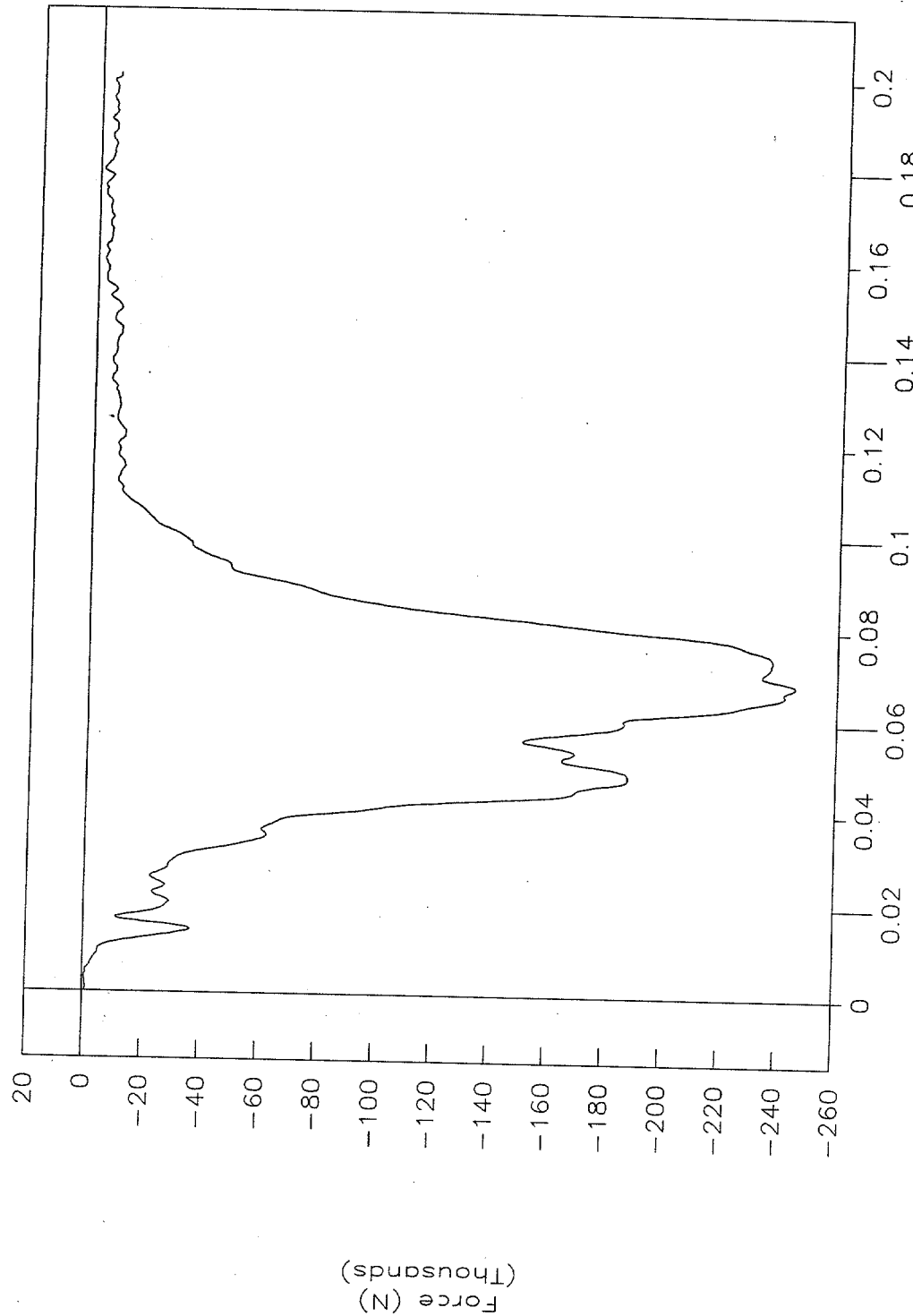


Figure 97. Rigid pole, force vs. time, test 98F012.



Test No. 98F012
Rigid pole, acceleration vs. time

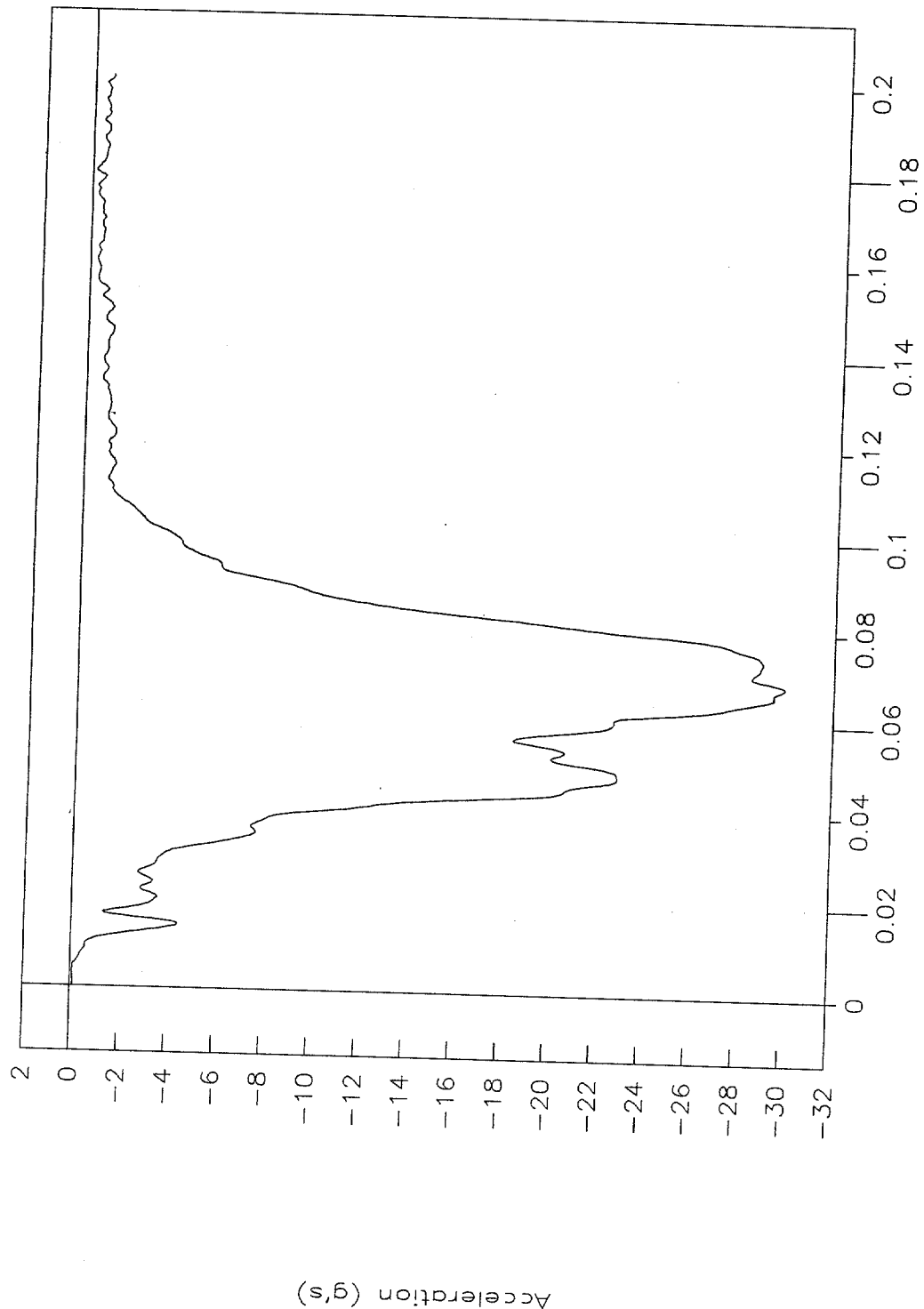


Figure 98. Rigid pole, acceleration vs. time, test 98F012.



Test No. 98F012

Rigid pole, velocity vs. time

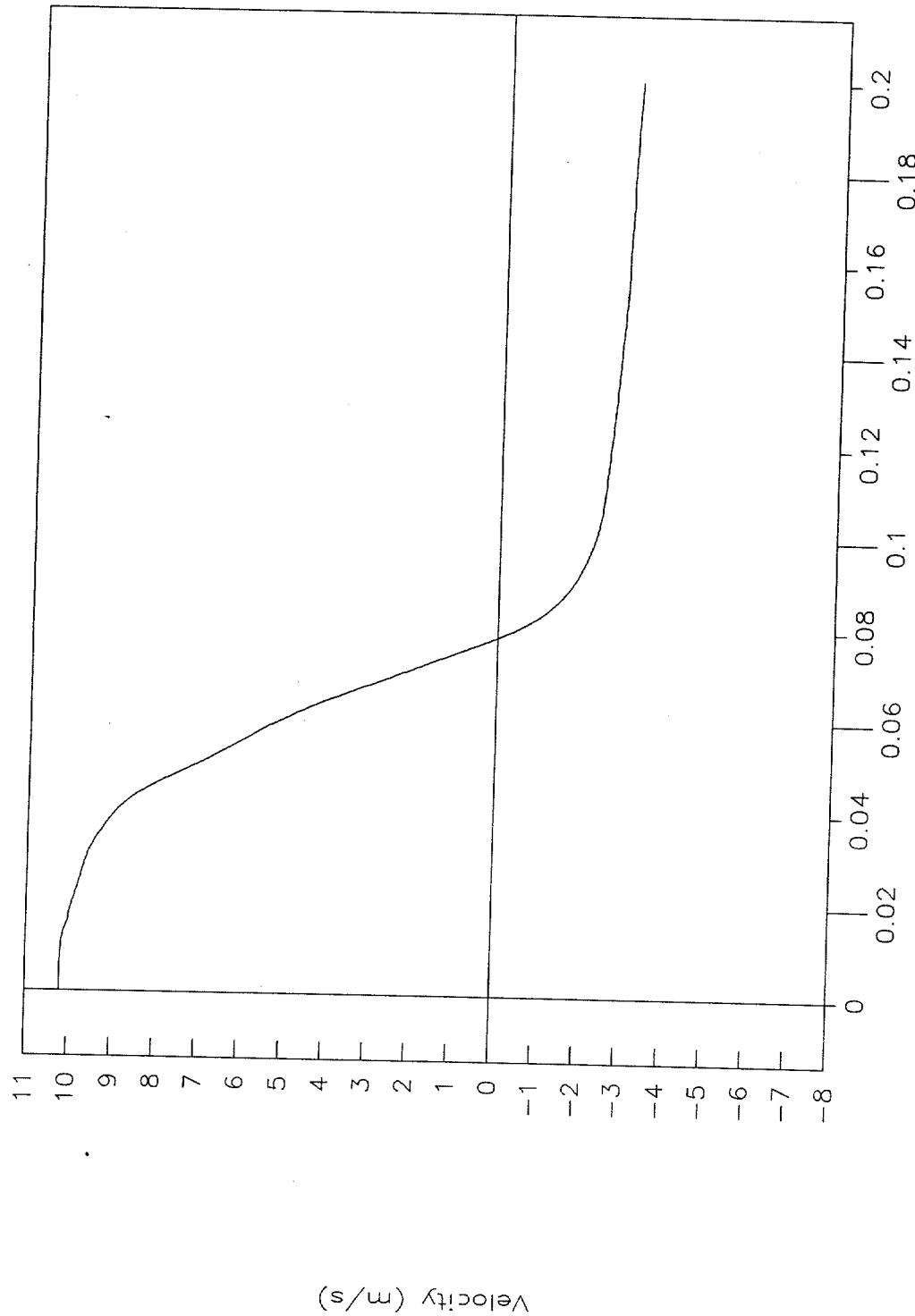


Figure 99. Rigid pole, velocity vs. time, test 98F012.



Test No. 98F012
Rigid pole, displacement vs. time

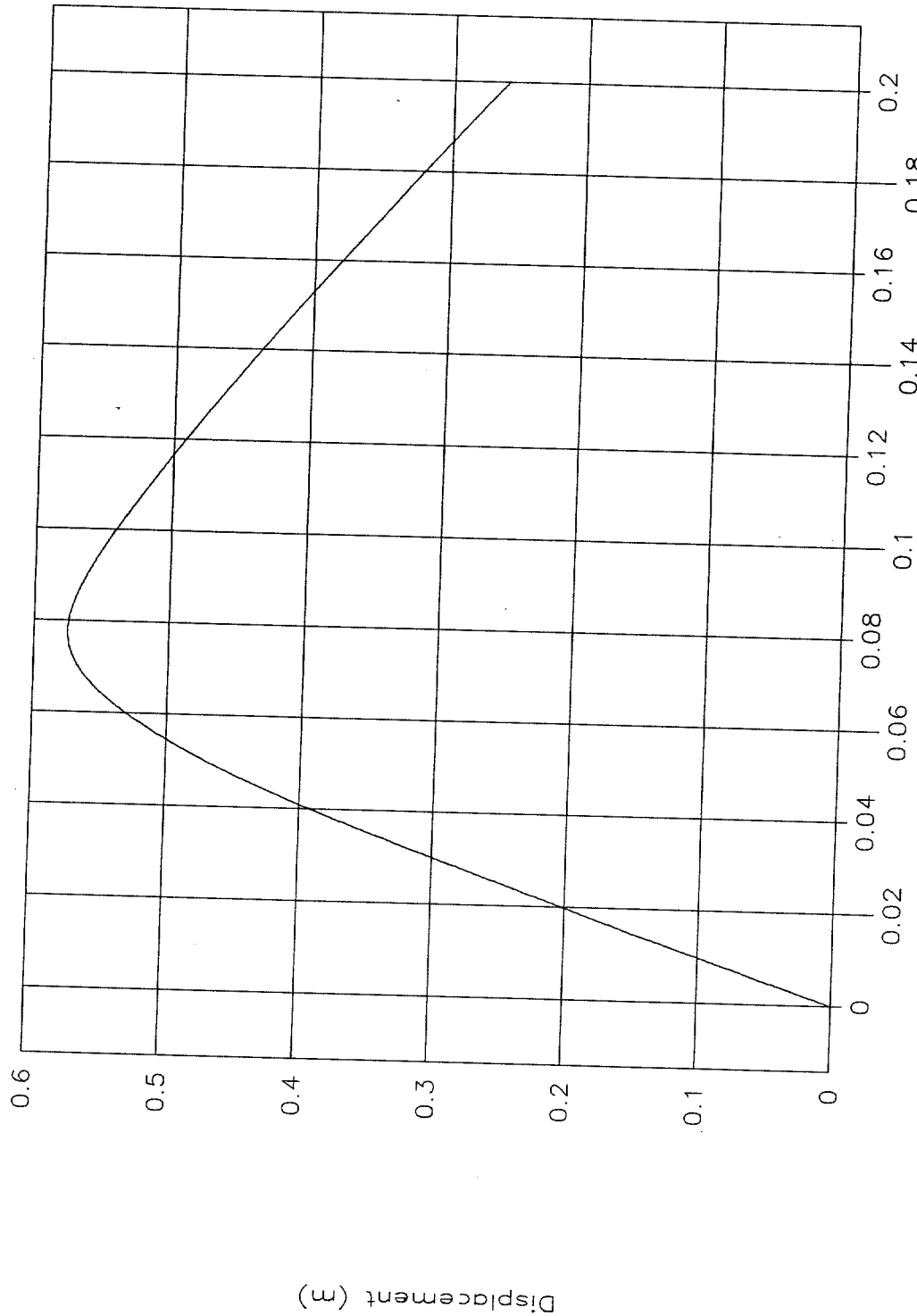


Figure 100. Rigid pole, displacement vs. time, test 98F012.



Test No. 98F012
Rigid pole, force vs. displacement

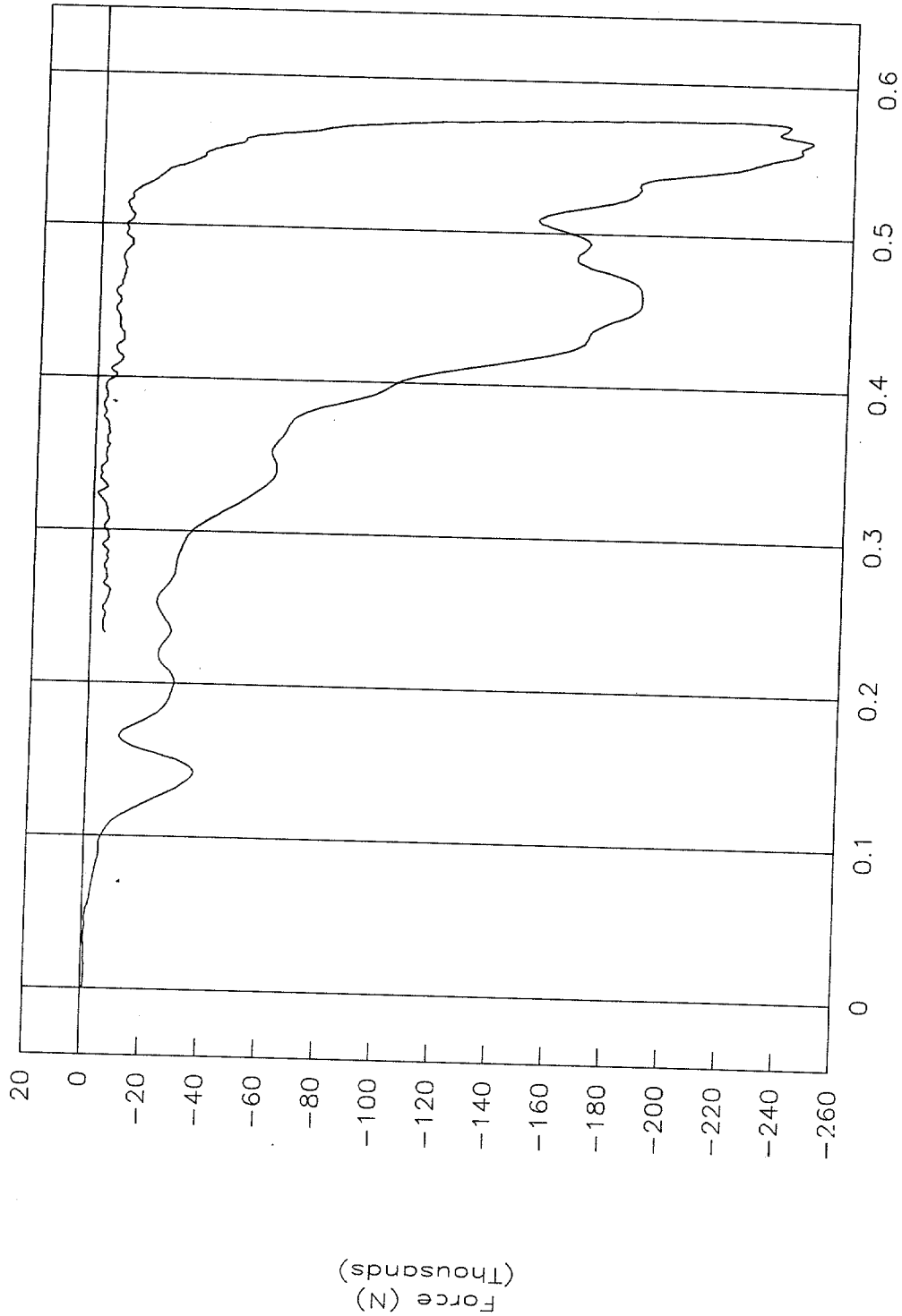


Figure 101. Rigid pole, force vs. displacement, test 98F012.



Test No. 98F012
Rigid pole, energy vs. displacement

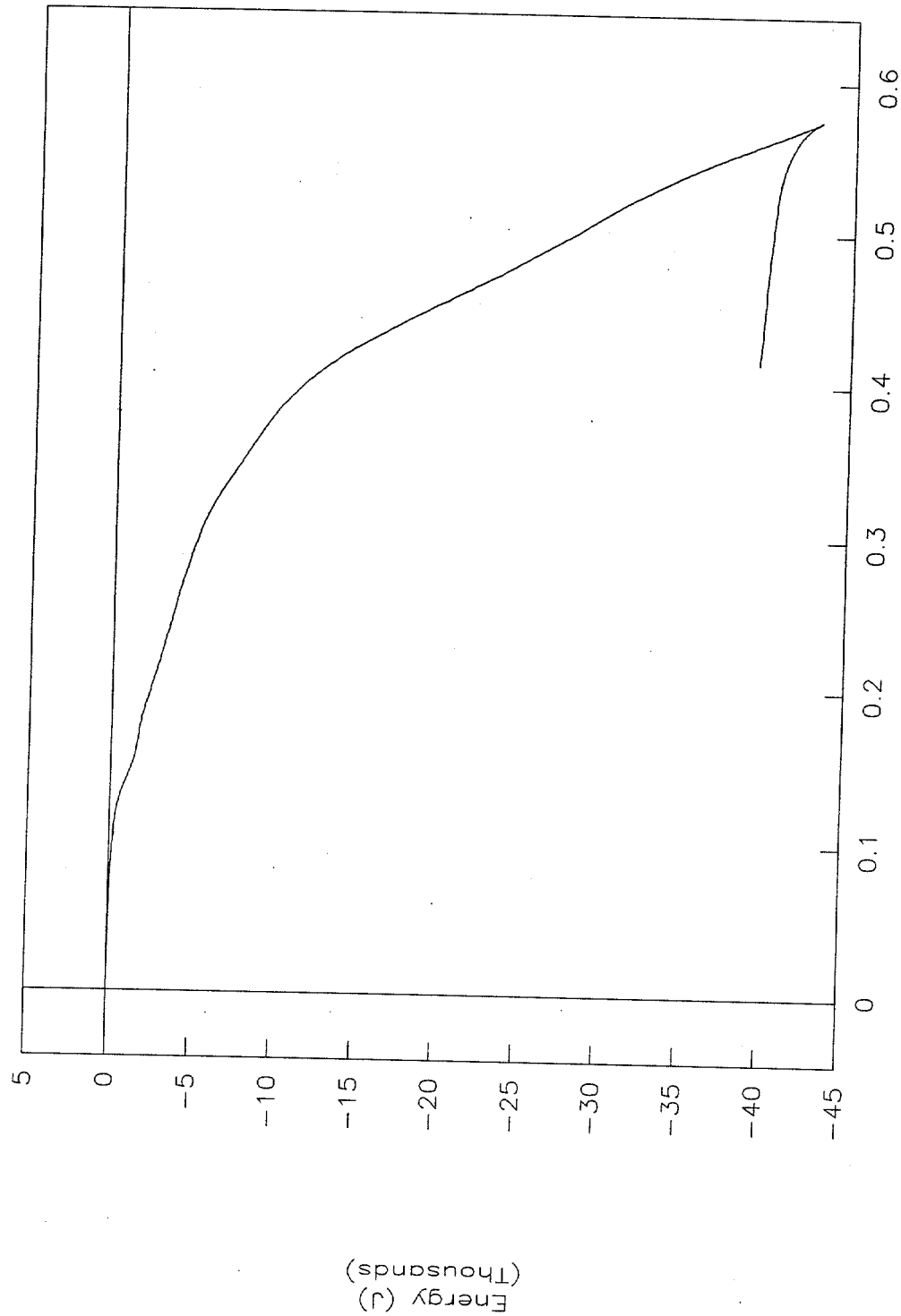


Figure 102. Rigid pole, energy vs. displacement, test 98F012.



Test No. 98F012
Impact force height vs. displacement

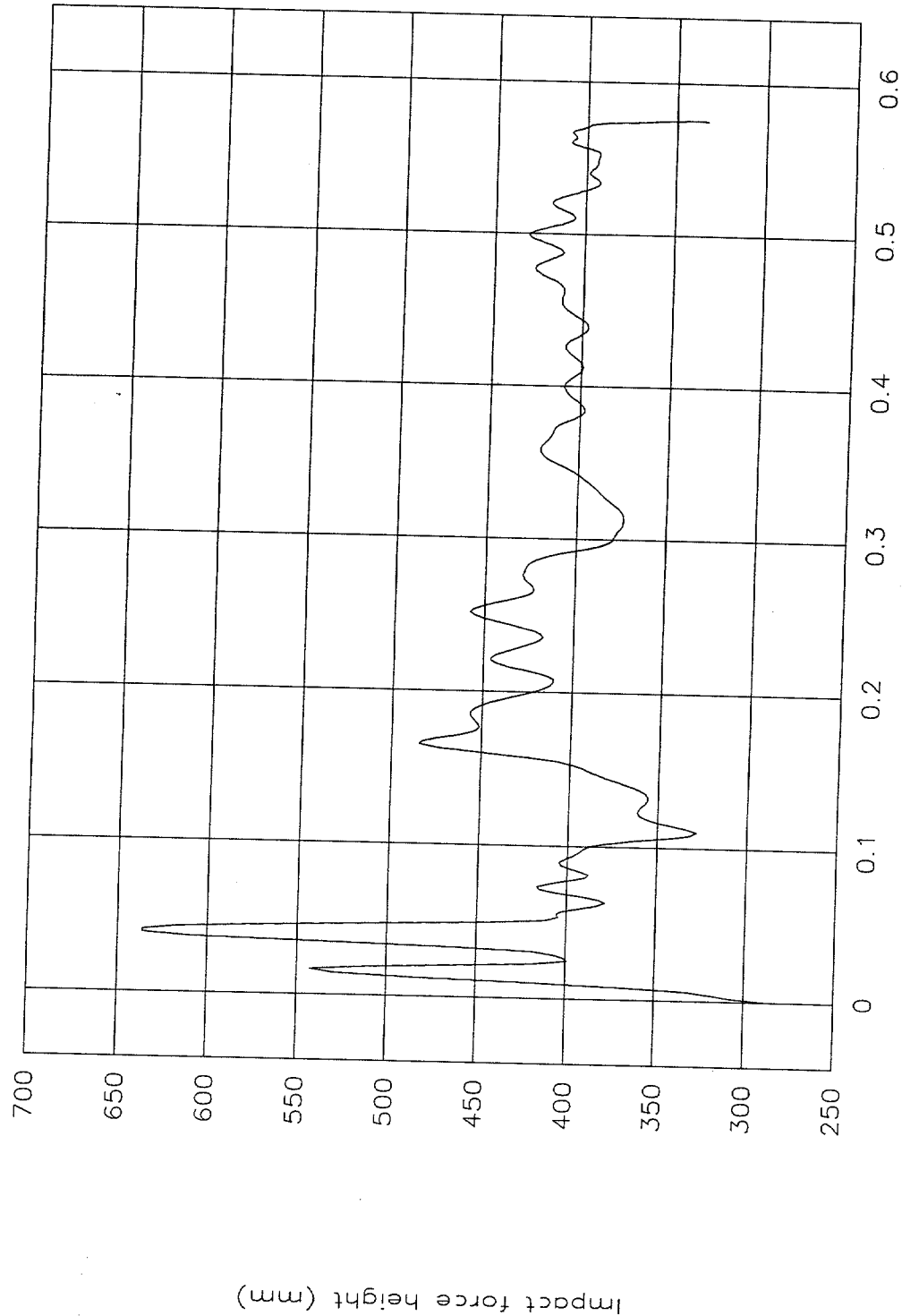


Figure 103. Impact force height vs. displacement, test 98F012.



Test No. 98F012
Top of engine, X-axis

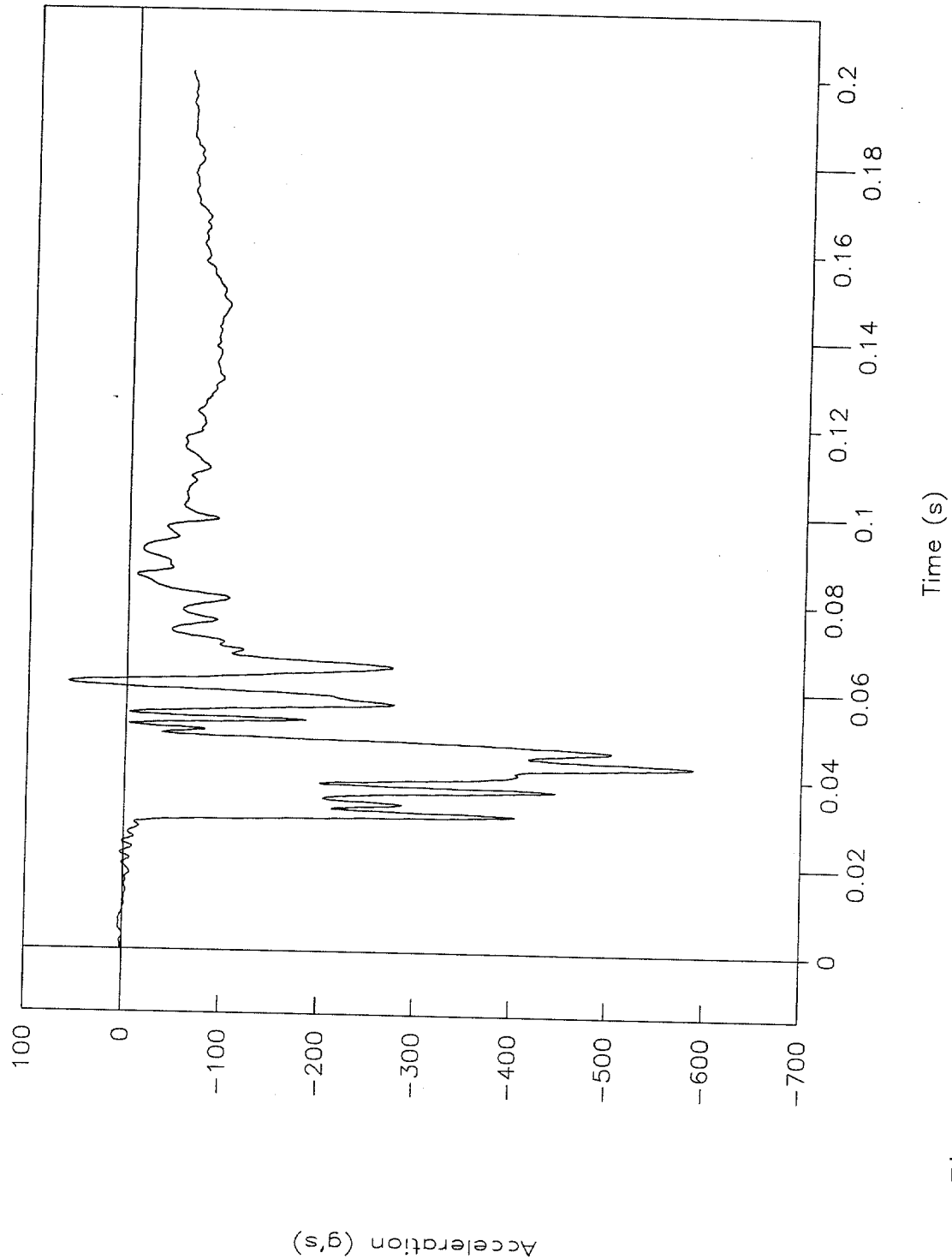


Figure 104. Top of engine acceleration vs. time, X-axis, test 98F012.



Test No. 98F012
Bottom of engine, X-axis

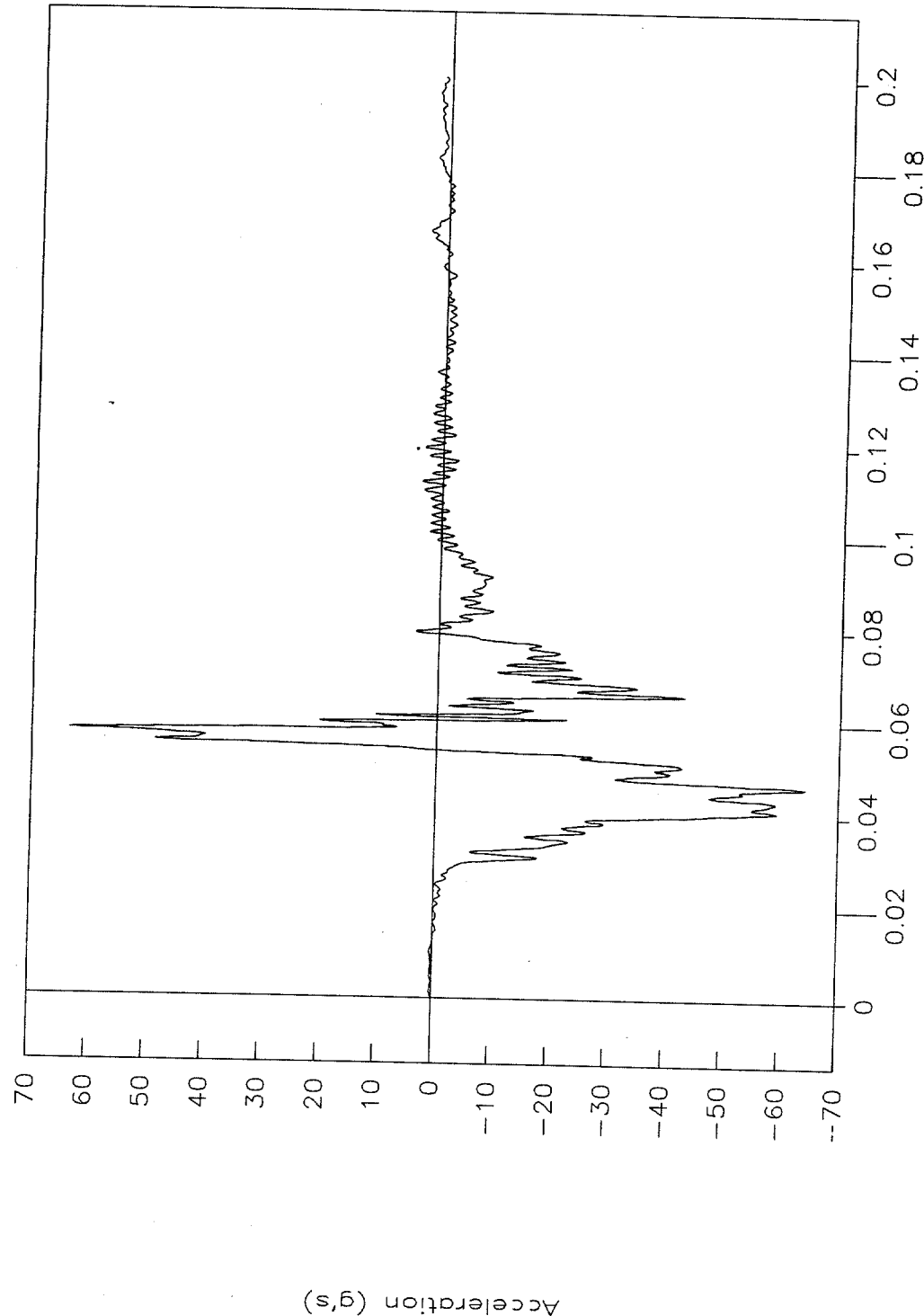


Figure 105. Bottom of engine acceleration vs. time, X-axis, test 98F012.



Test No. 98F012

Left control arm, X-axis

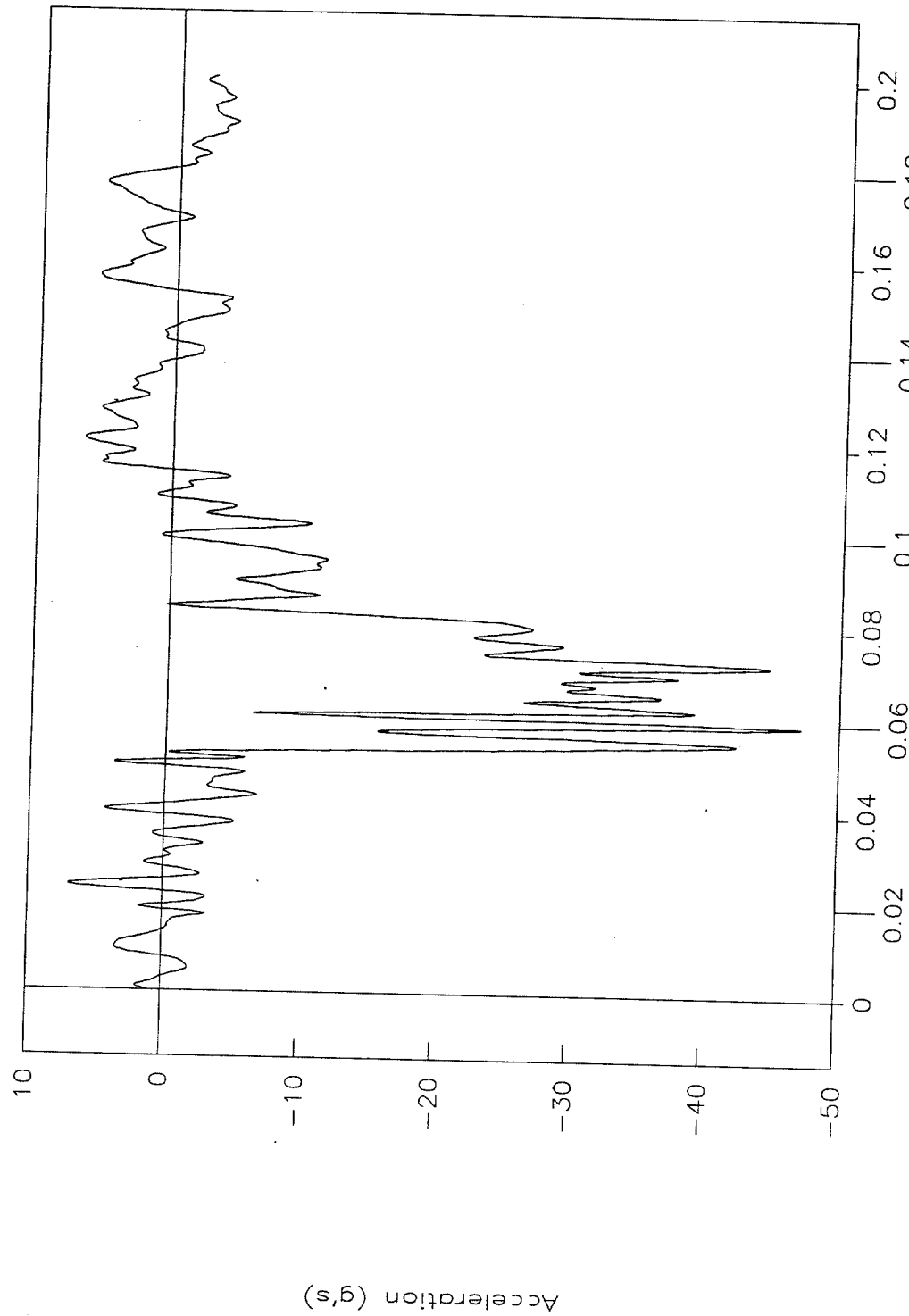


Figure 106. Left control arm acceleration vs. time, X-axis, test 98F012.



Test No. 98F012
Right control arm, X-axis

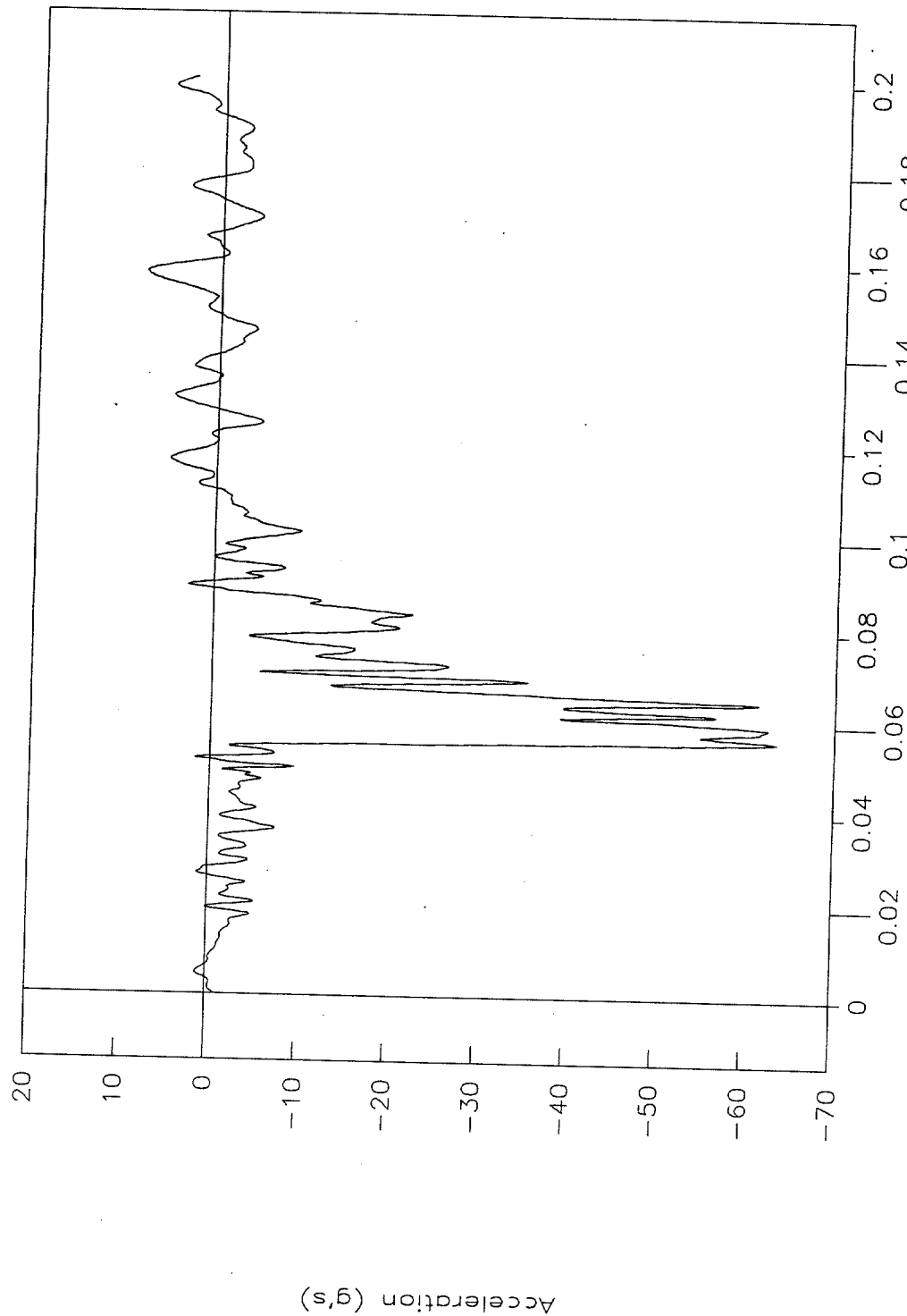


Figure 107. Right control arm acceleration vs. time, X-axis, test 98F012.



Test No. 98F012

Instrument panel, X-axis

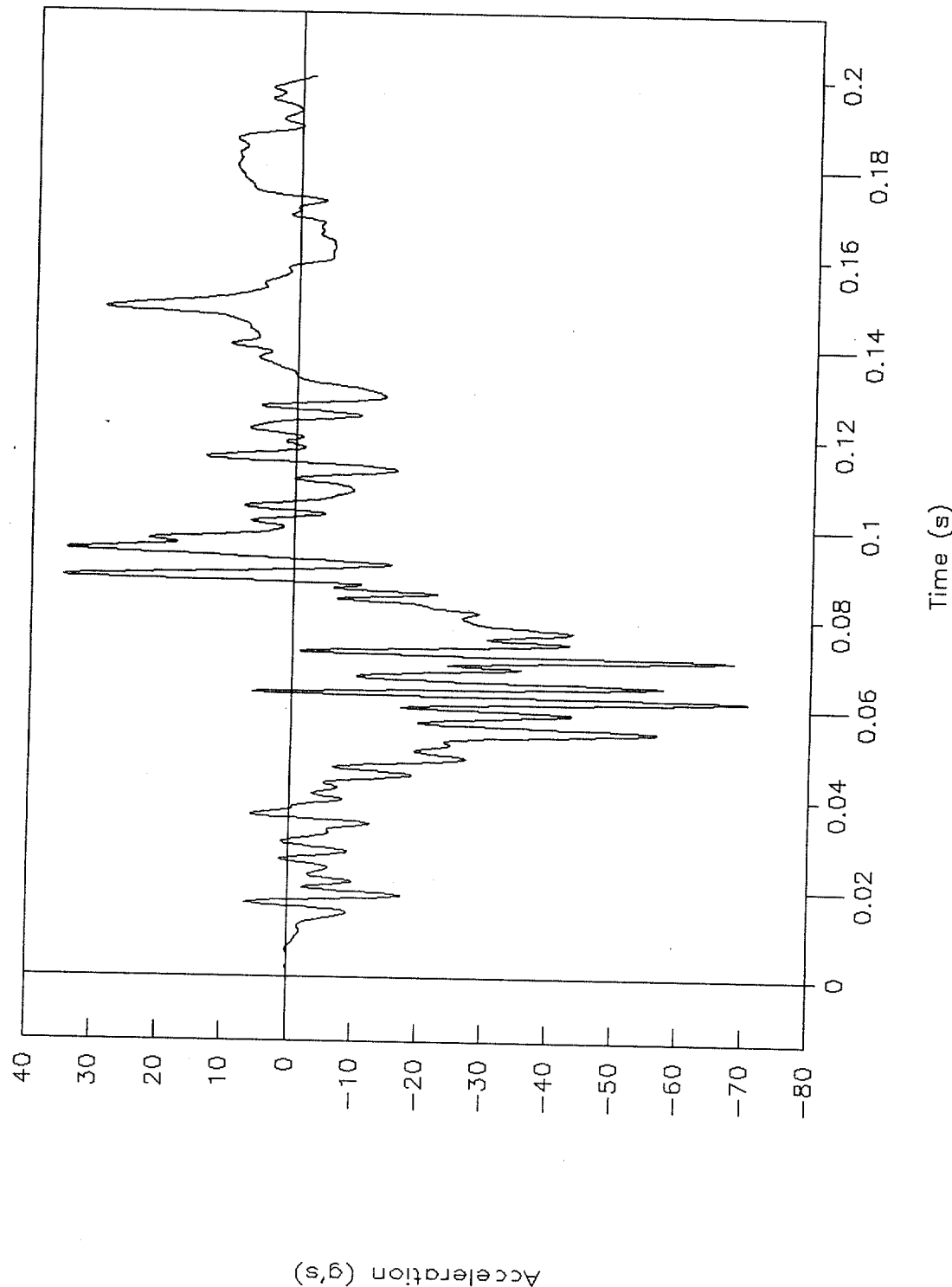


Figure 108. Instrument panel acceleration vs. time, X-axis, test 98F012.



Test No. 98F012
Pitch rate and angle vs. time

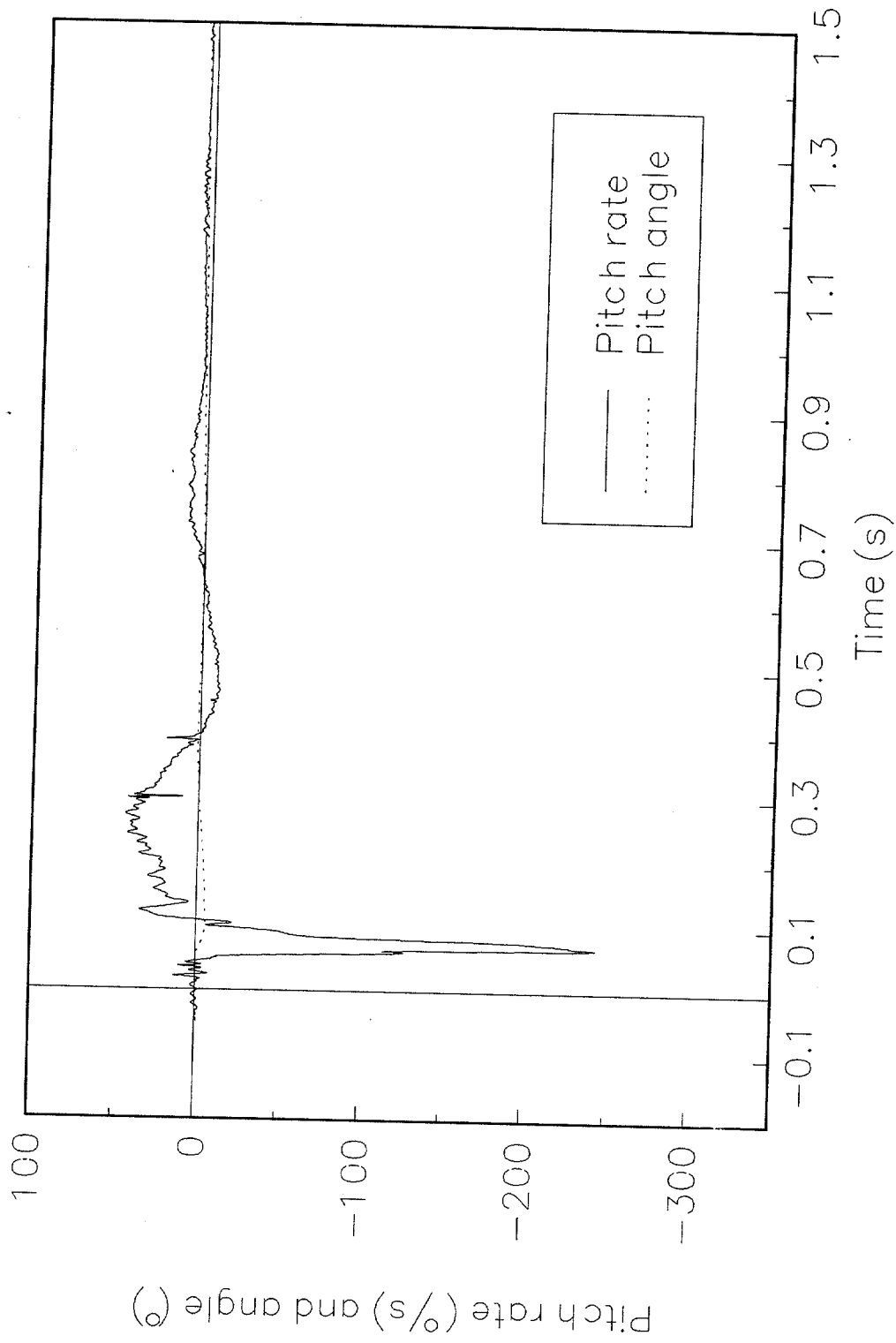


Figure 109. Pitch rate and angle vs. time, test 98F012.



Test No. 98F012
Roll rate and angle vs. time

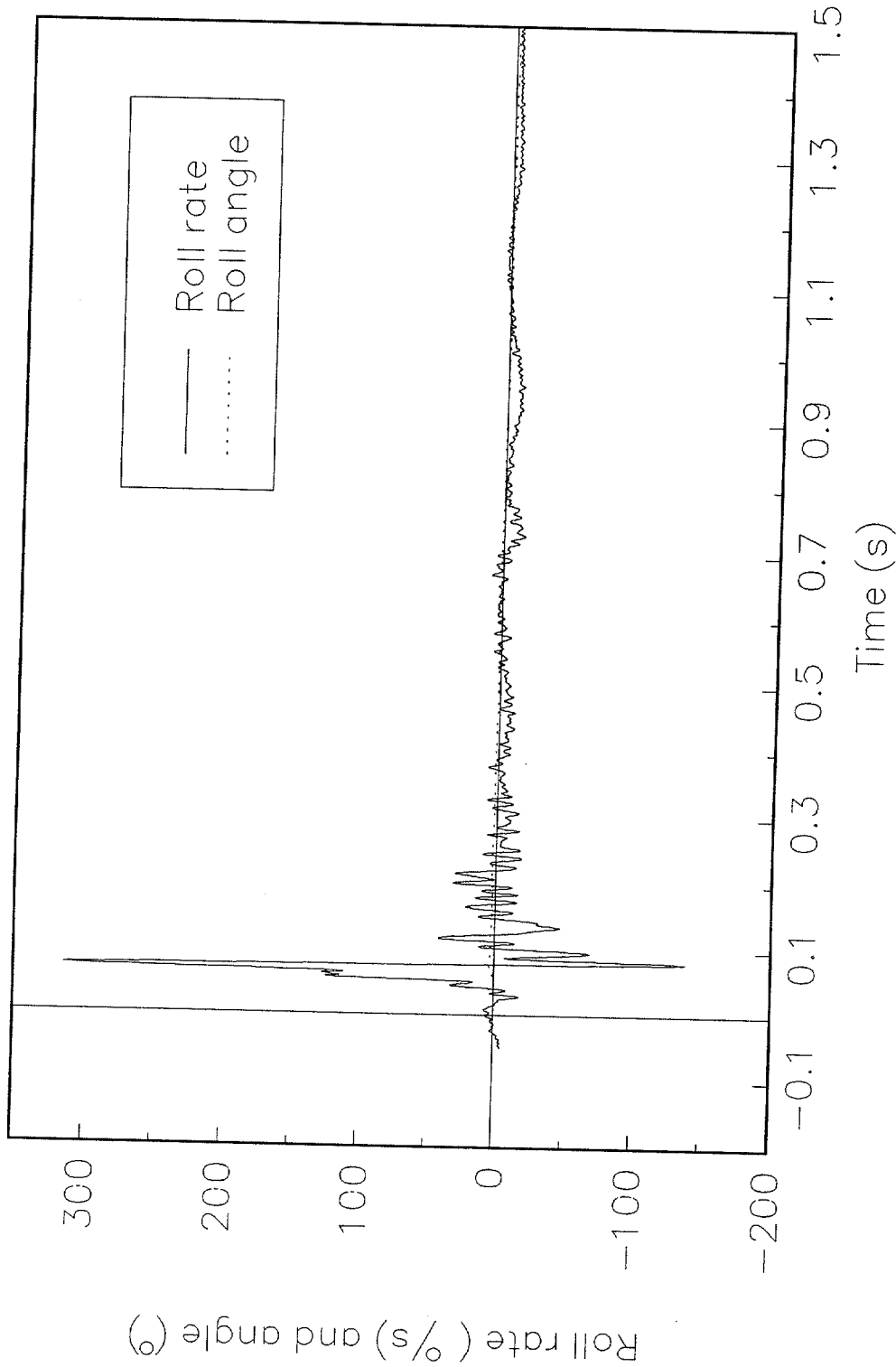


Figure 110. Roll rate and angle vs. time, test 98F012.



Test No. 98F012
Yaw rate and angle vs. time

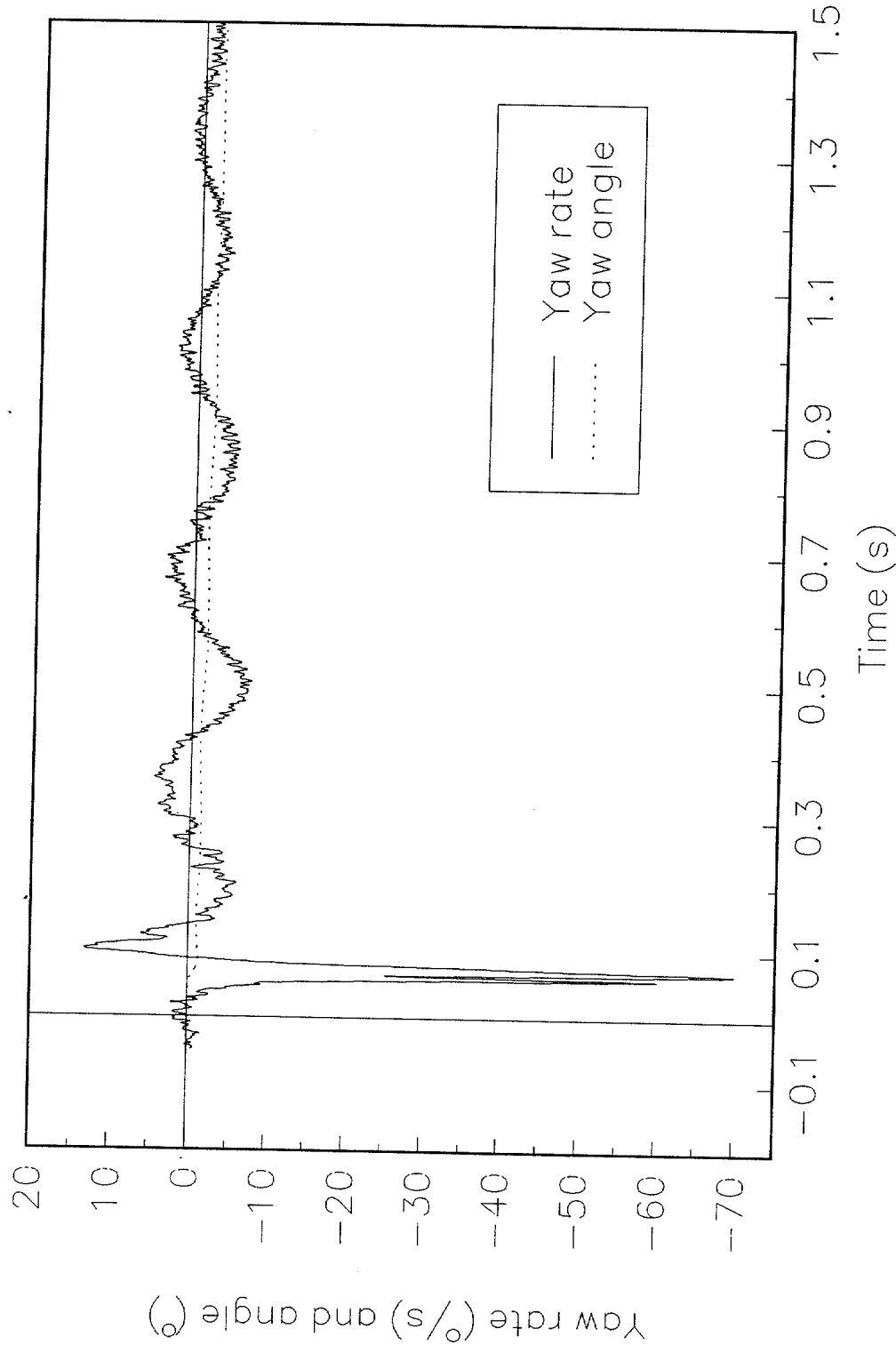


Figure 111. Yaw rate and angle vs. time, test 98F012.



Test No. 98F014
Cg acceleration vs. time, X-axis

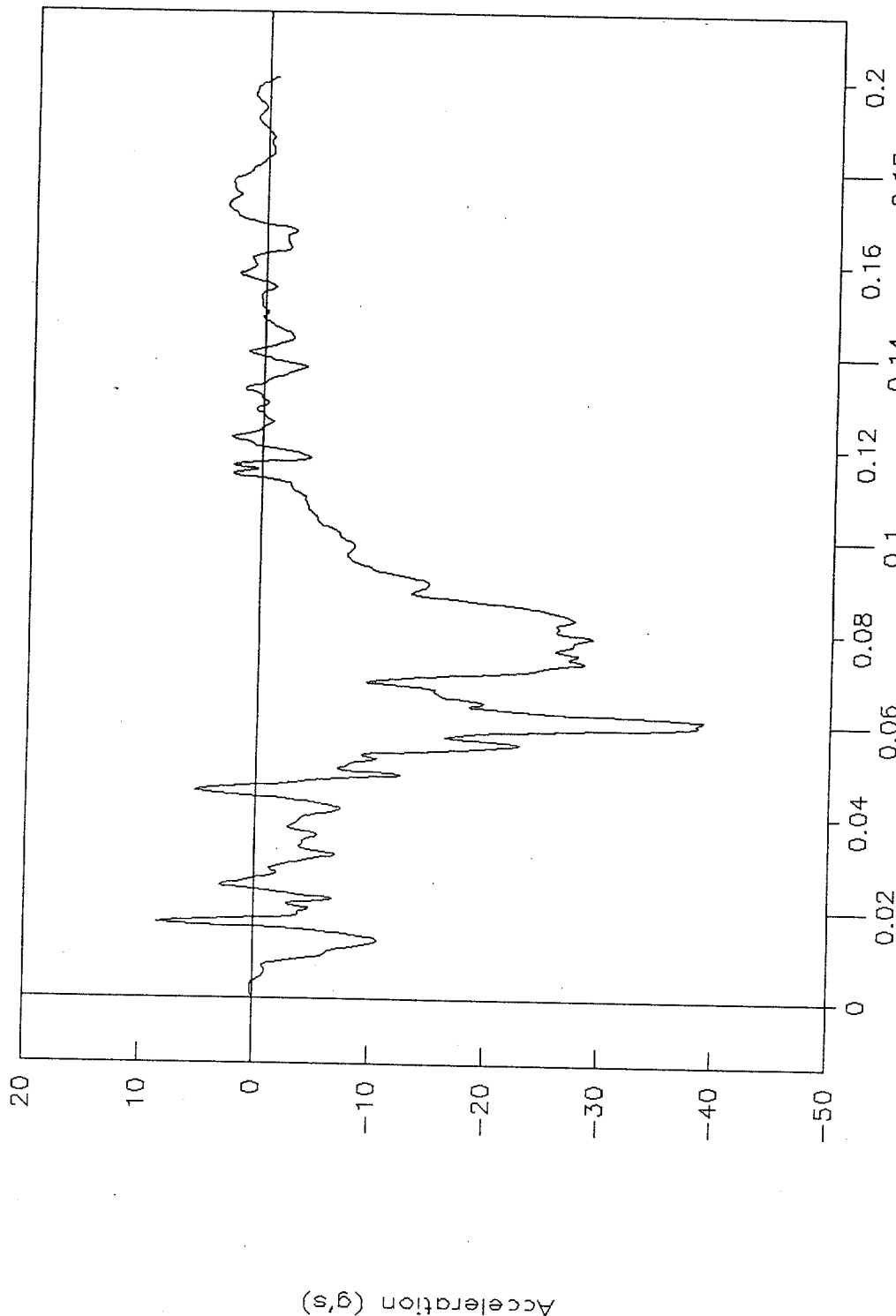


Figure 112. C.g. acceleration vs. time, X-axis, test 98F014.



Test No. 98F014
Cg velocity vs. time, X-axis

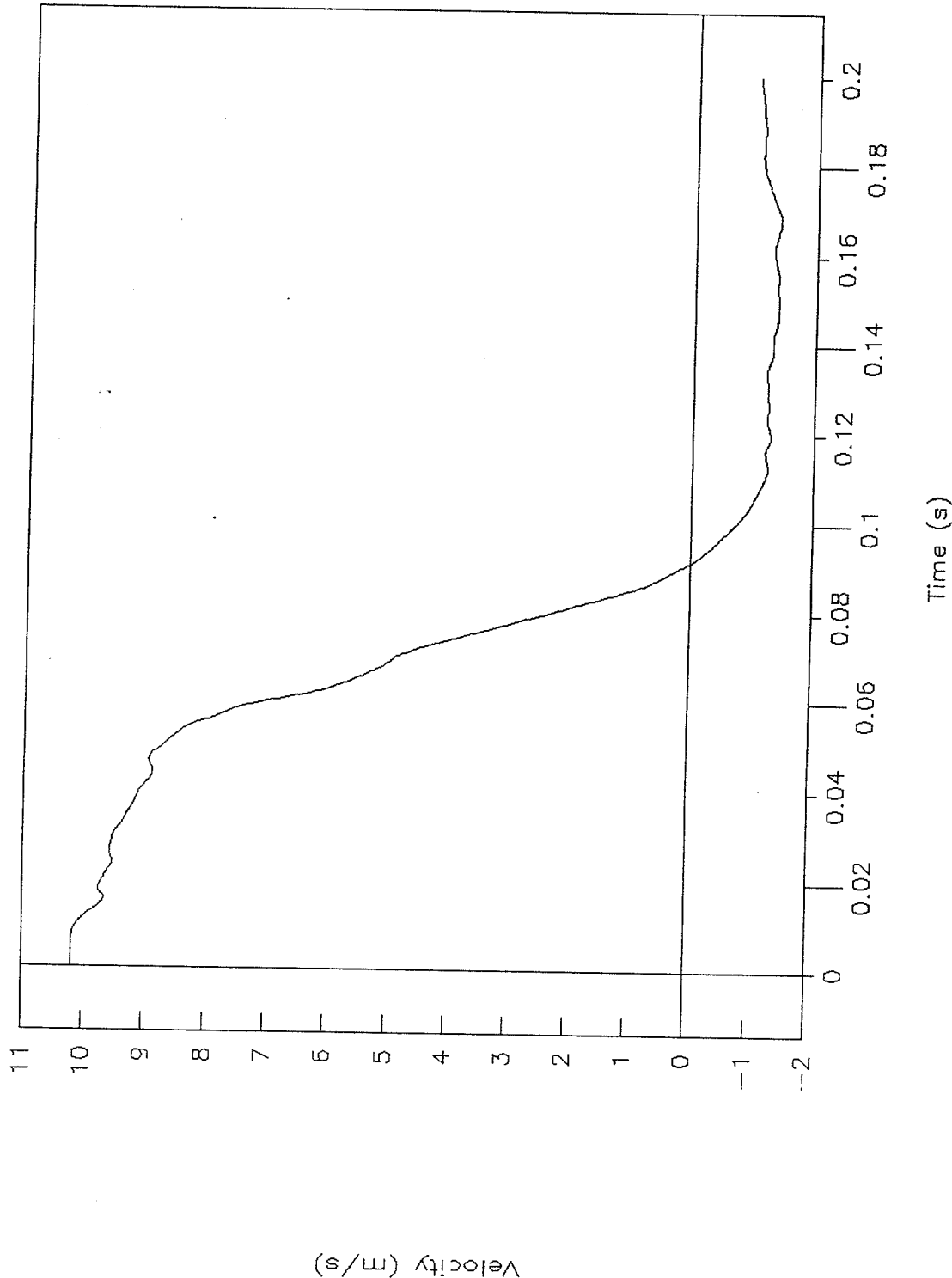


Figure 113. C.g. velocity vs. time, X-axis, test 98F014.



Test No. 98F014
Cg displacement vs. time, X-axis

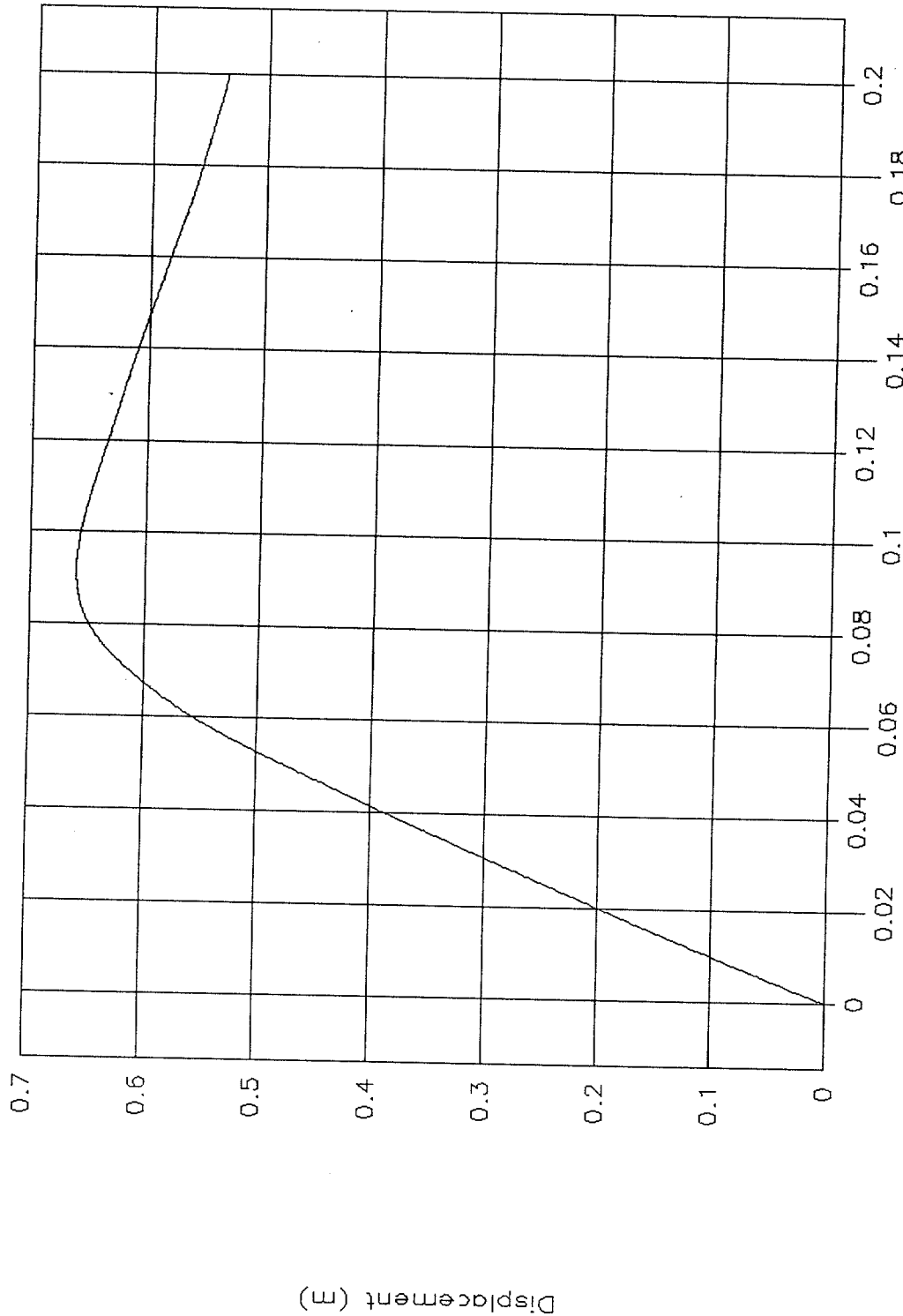


Figure 114. C.g. displacement vs. time, X-axis, test 98F014.



Test No. 98F014
Cg force vs. displacement, X-axis

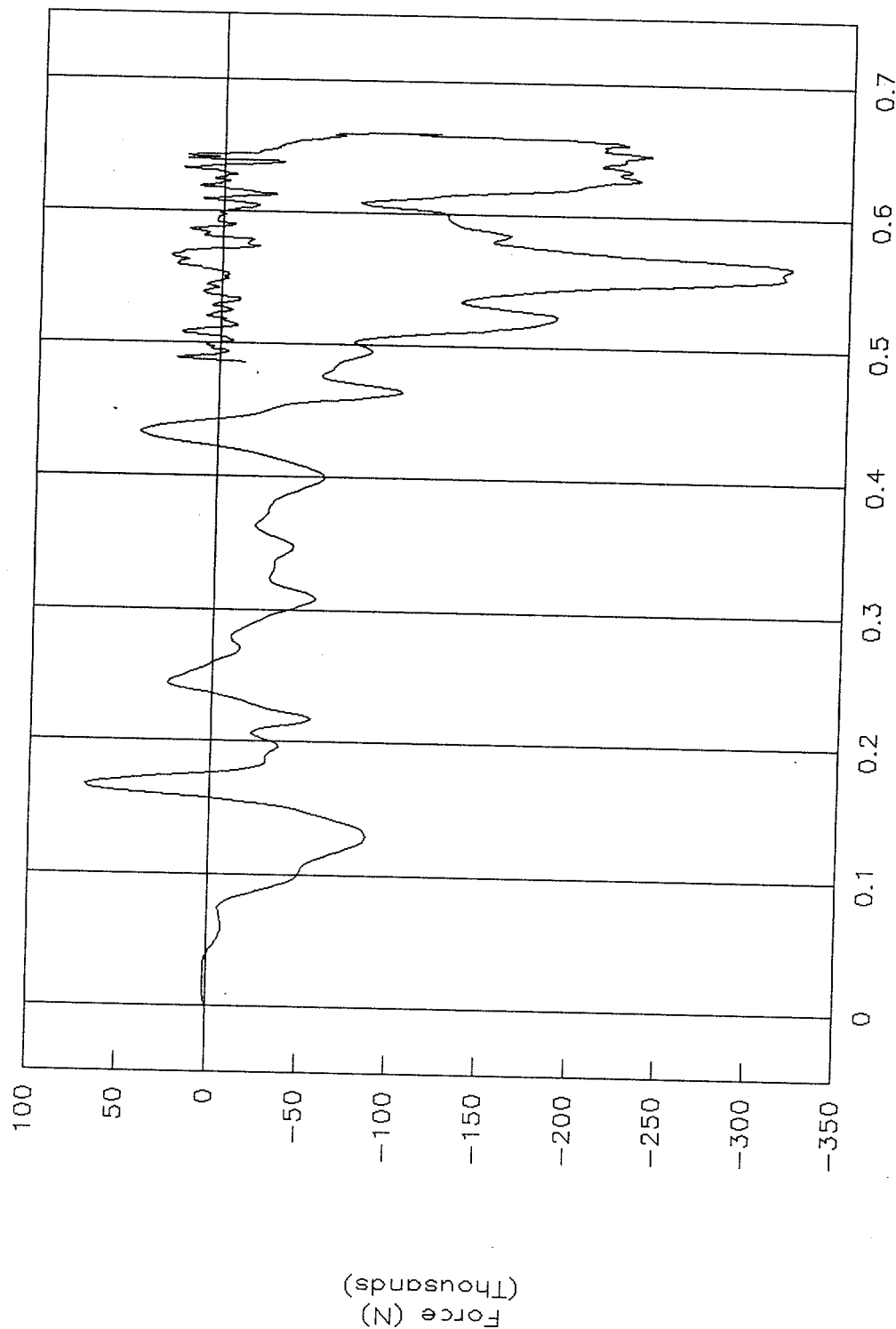
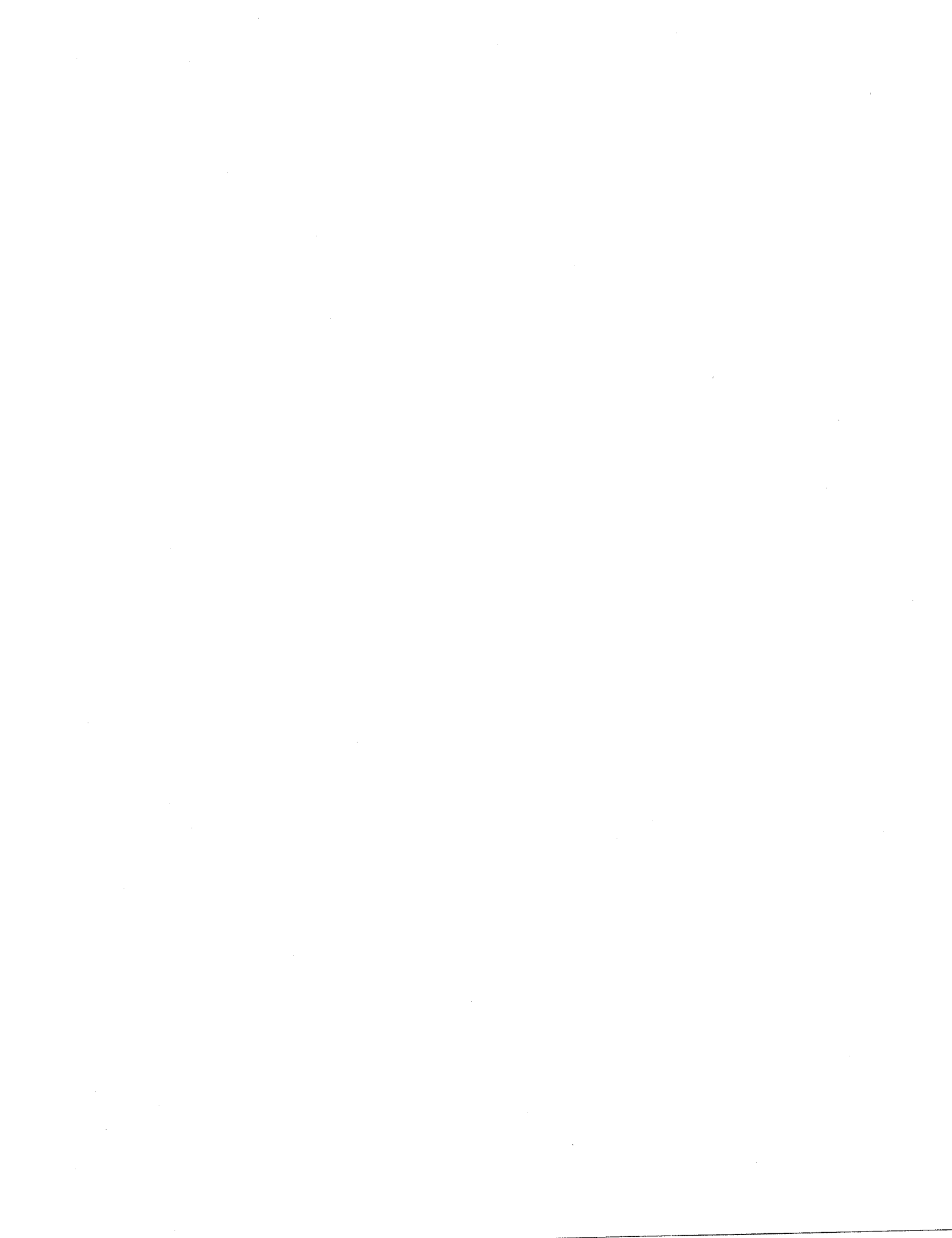


Figure 115. C.g. force vs. displacement, X-axis, test 98F014.



Test No. 98F014
Cg energy vs. displacement, X-axis

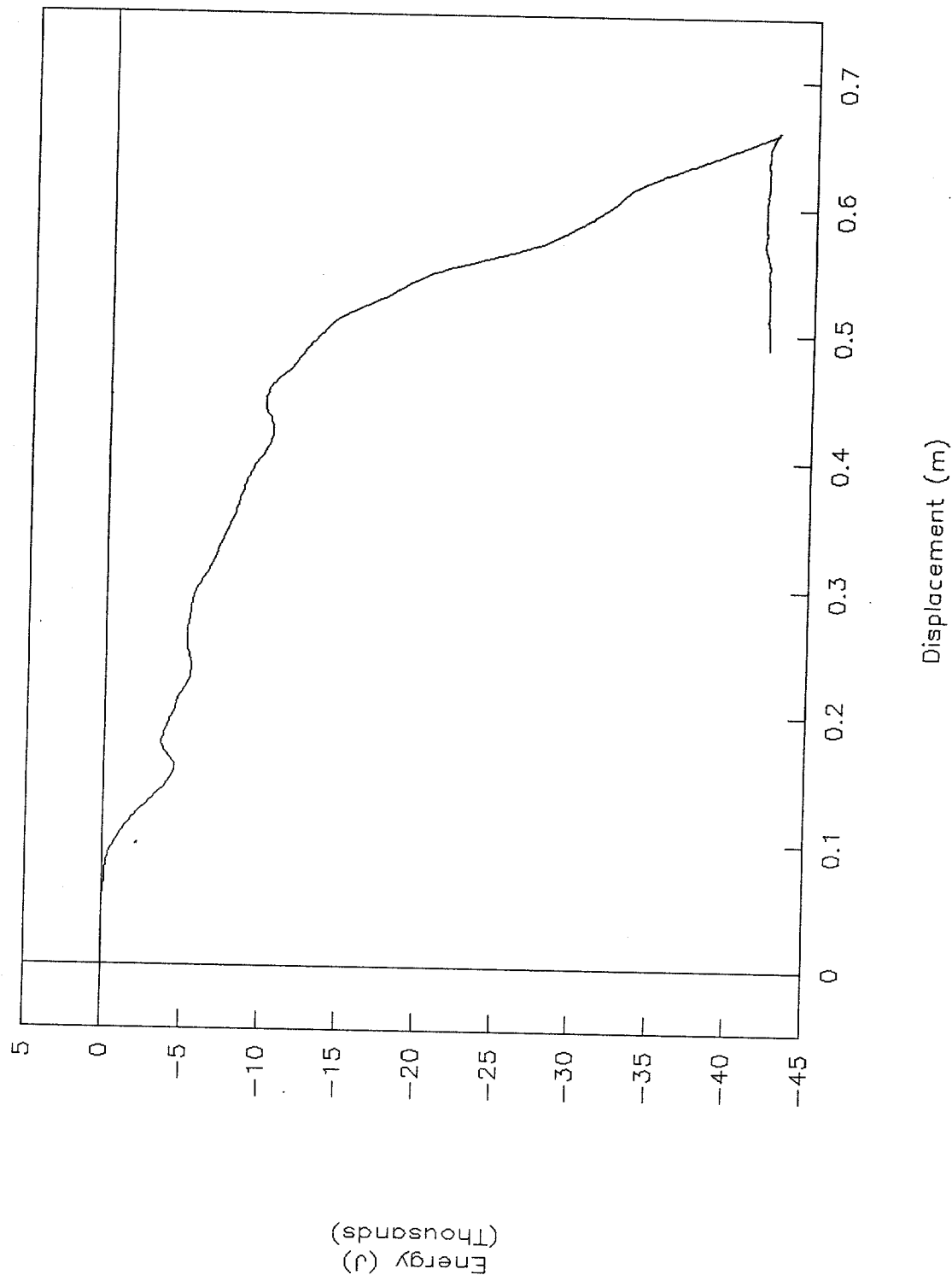


Figure 116. C.g. energy vs. displacement, X-axis, test 98F014.



Test No. 98F014
Cg acceleration vs. time, Y-axis

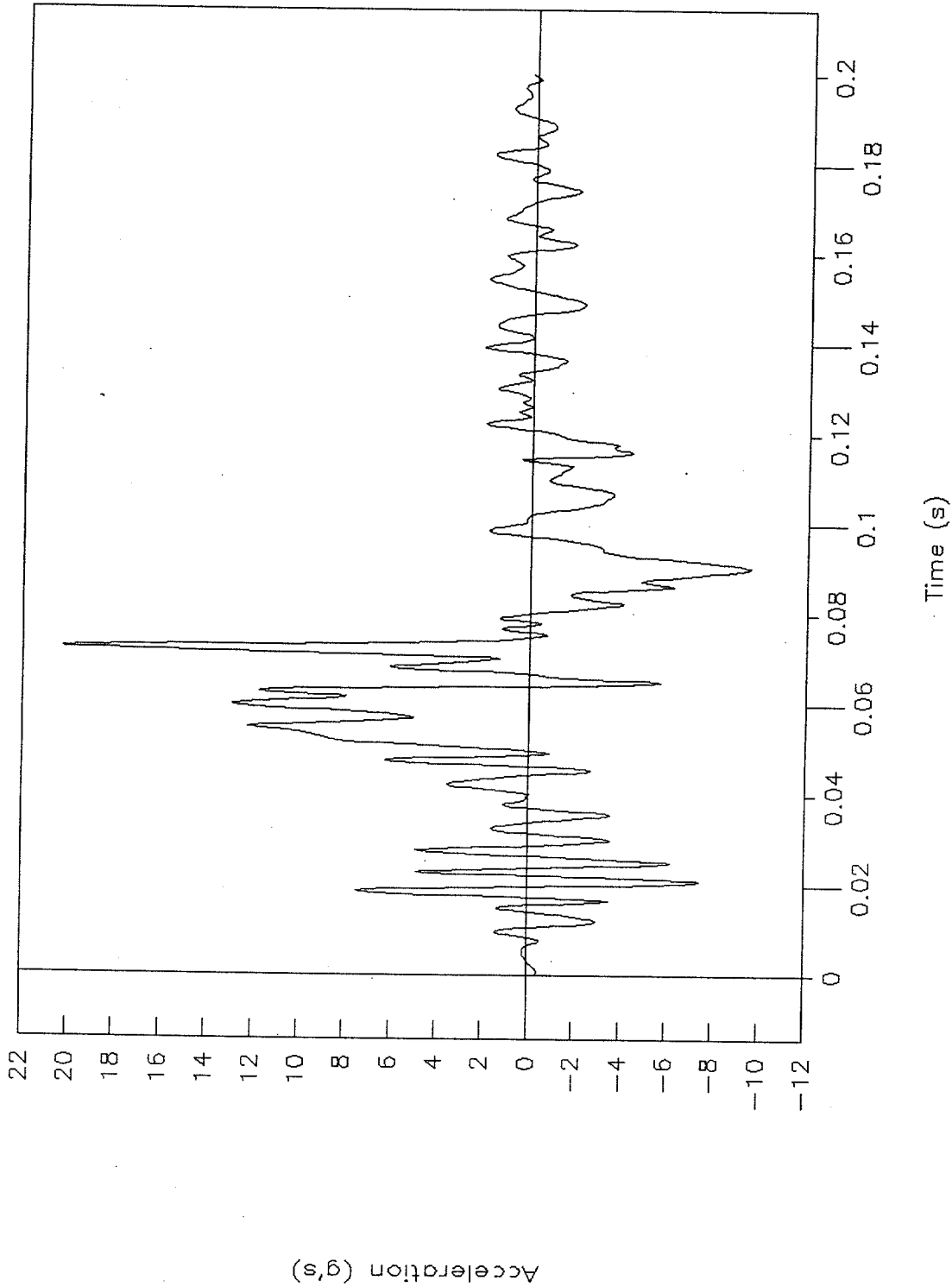


Figure 117. C.g. acceleration vs. time, Y-axis, test 98F014.



Test No. 98F014
Cg acceleration vs. time, Z-axis

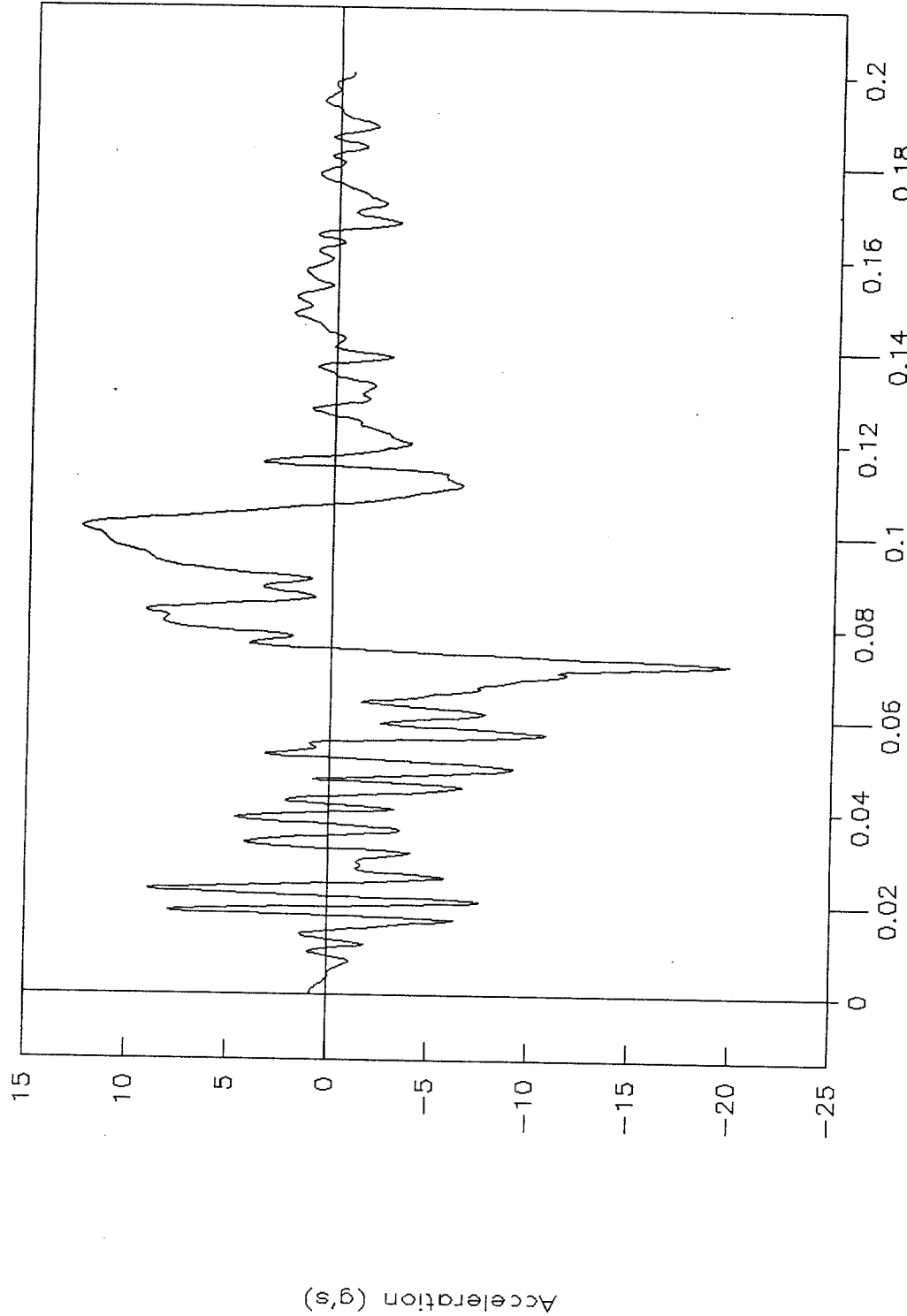


Figure 118. C.g. acceleration vs. time, Z-axis, test 98F014.



Test No. 98F014
Rigid pole, force vs. time

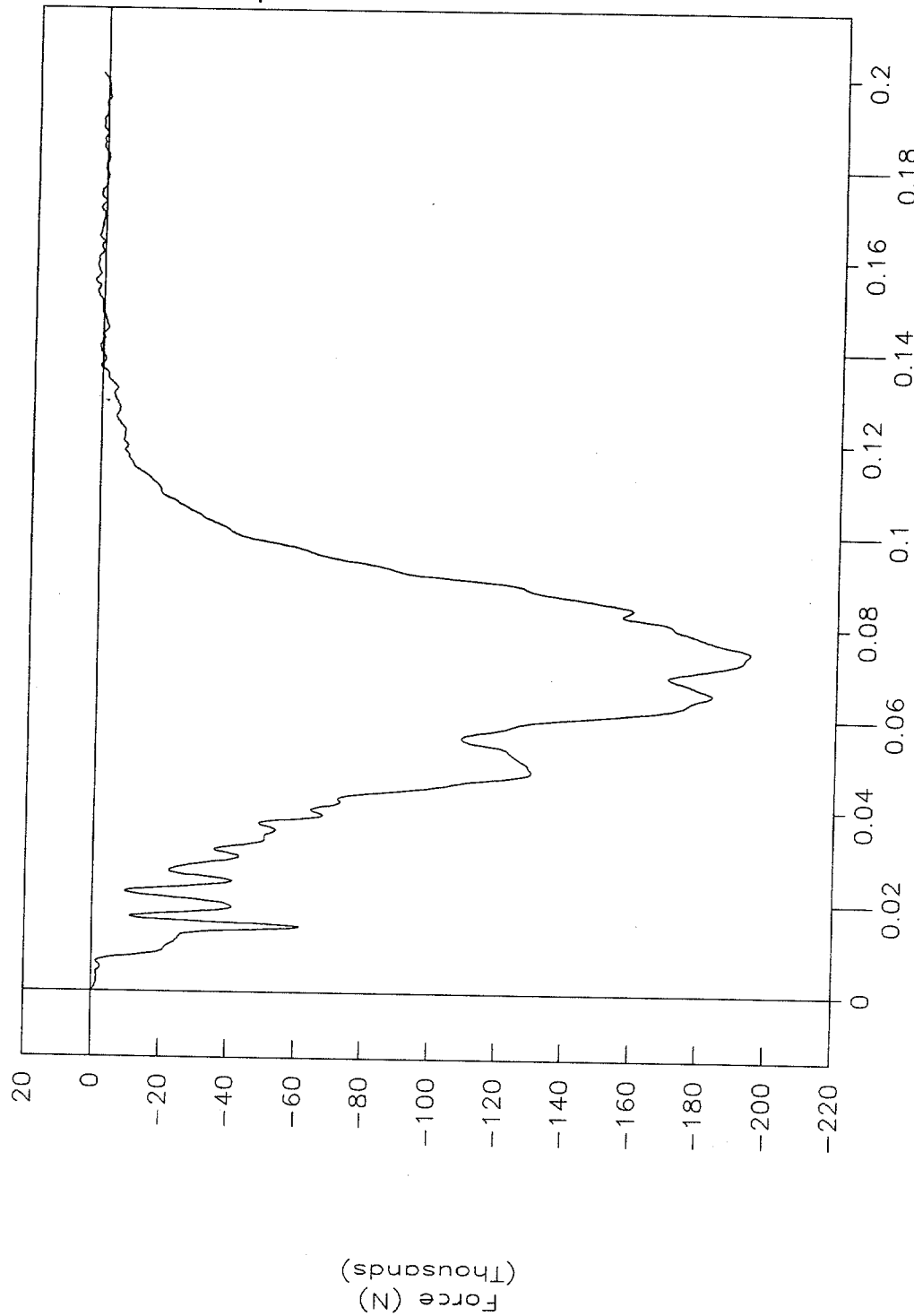


Figure 119. Rigid pole, force vs. time, test 98F014.



Test No. 98F014
Rigid pole, acceleration vs. time

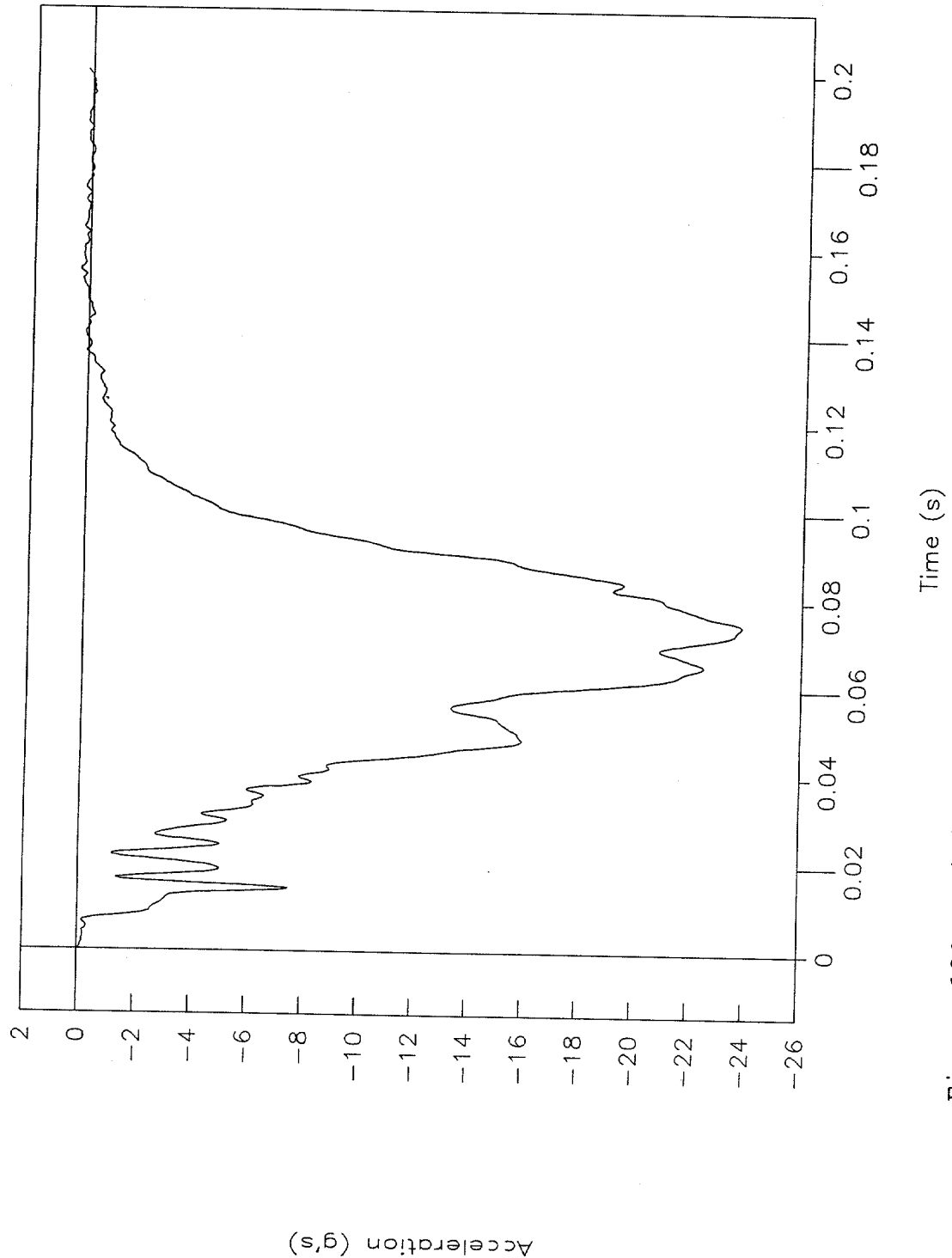


Figure 120. Rigid pole, acceleration vs. time, test 98F014.



Test No. 98F014
Rigid pole, velocity vs. time

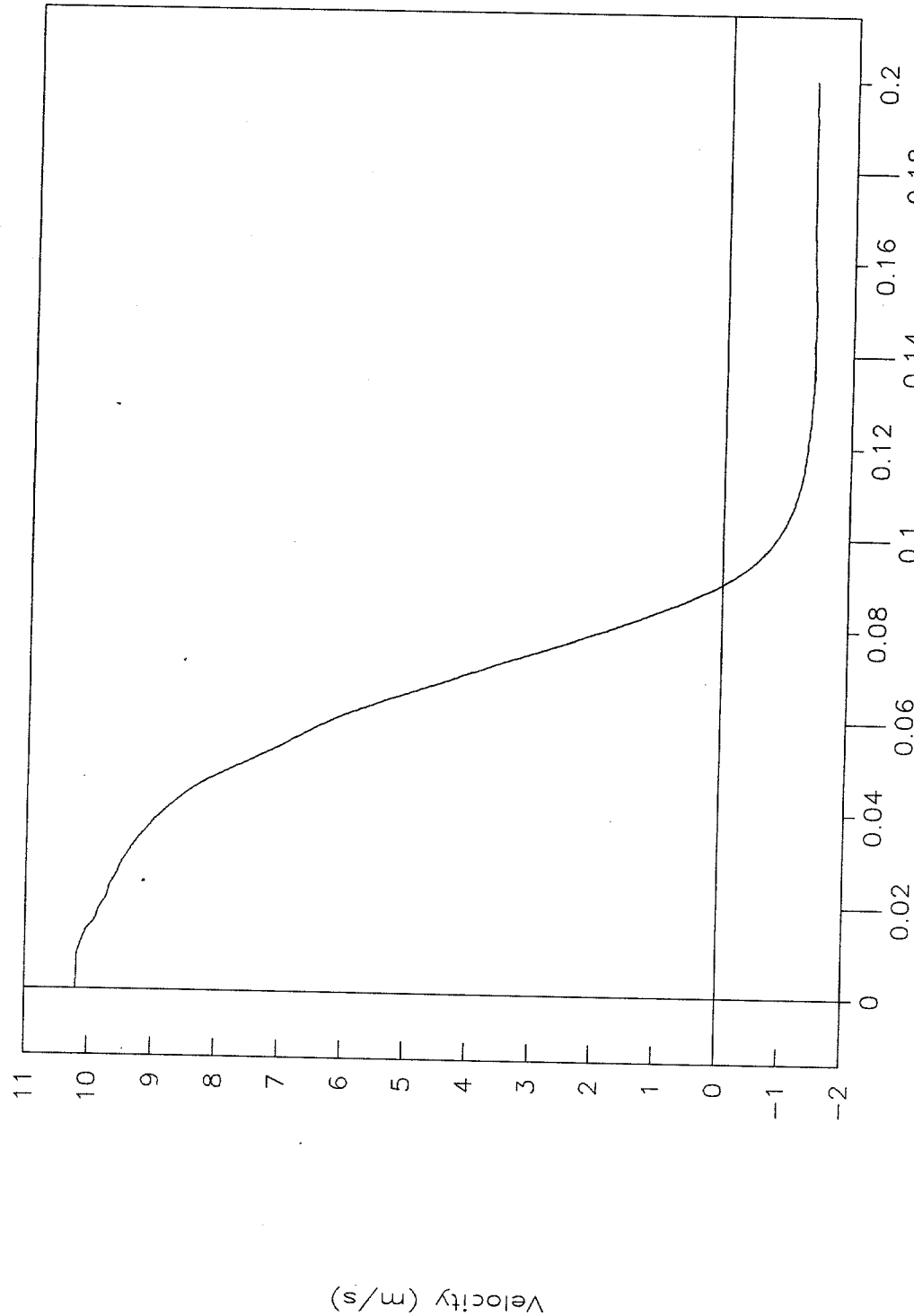


Figure 121. Rigid pole, velocity vs. time, test 98F014.



Test No. 98F014
Rigid pole, displacement vs time

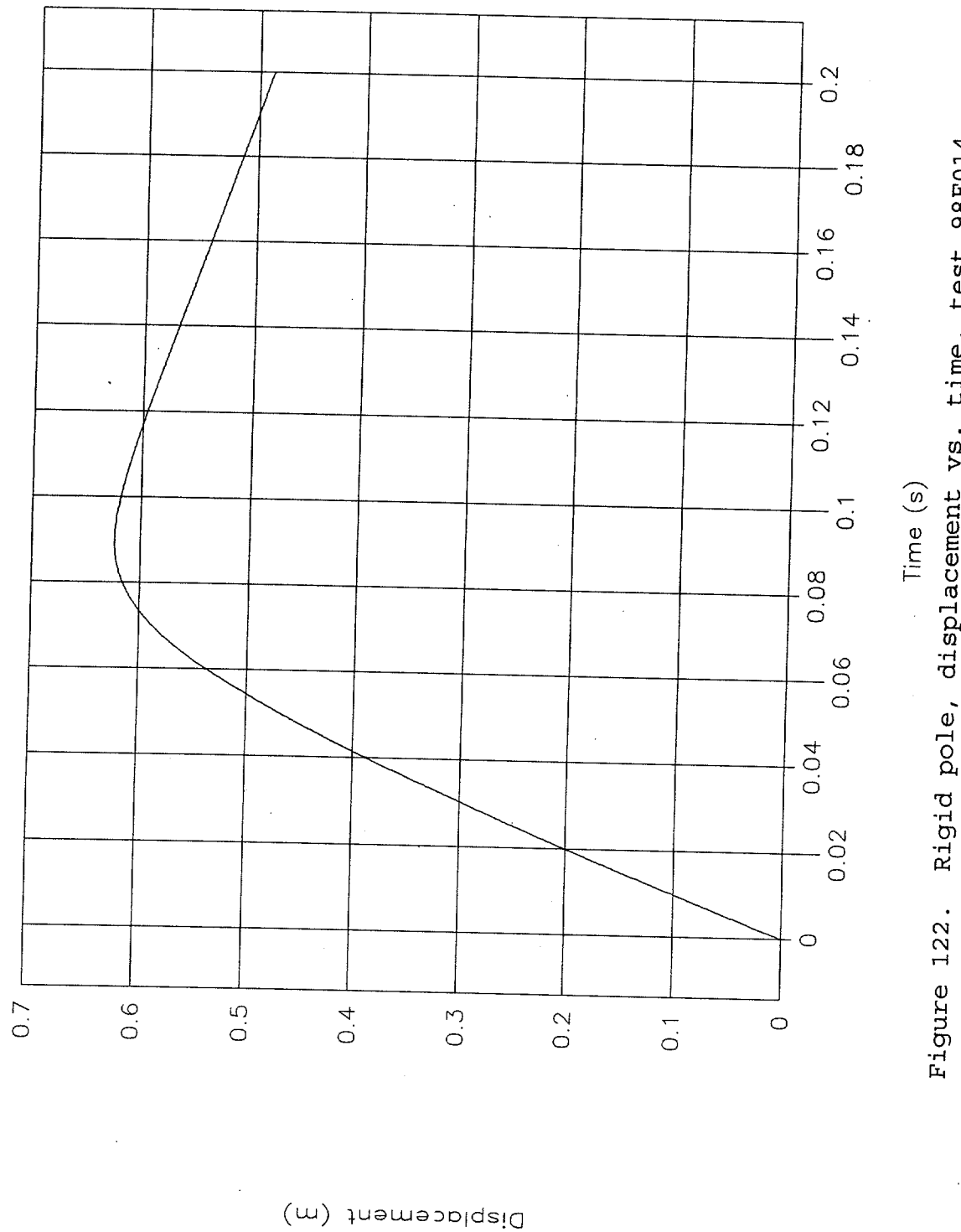


Figure 122. Rigid pole, displacement vs. time, test 98F014.



Test No. 98F014
Rigid pole, force vs. displacement

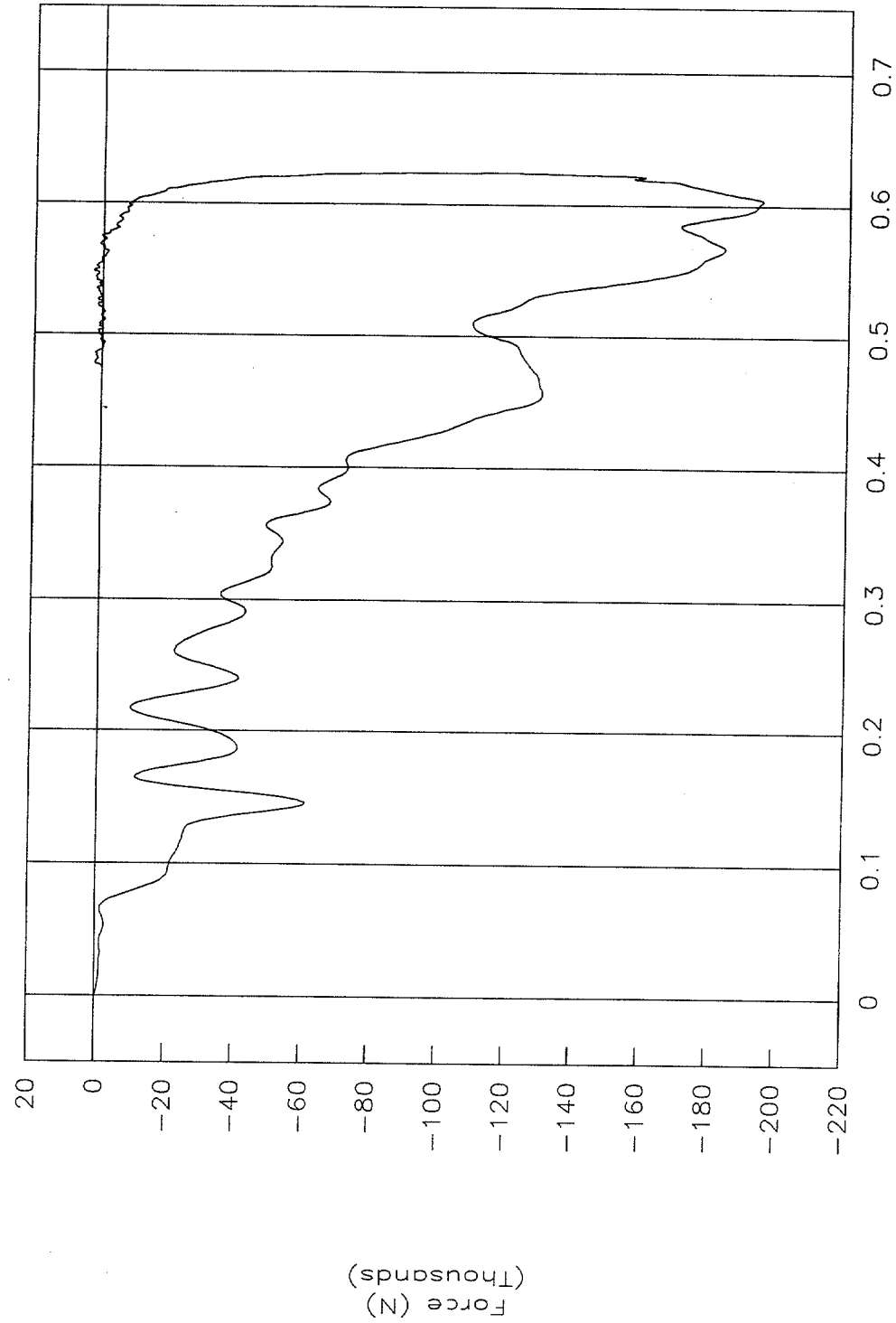


Figure 123. Rigid pole, force vs. displacement, test 98F014.



Test No. 98F014
Rigid pole, energy vs. displacement

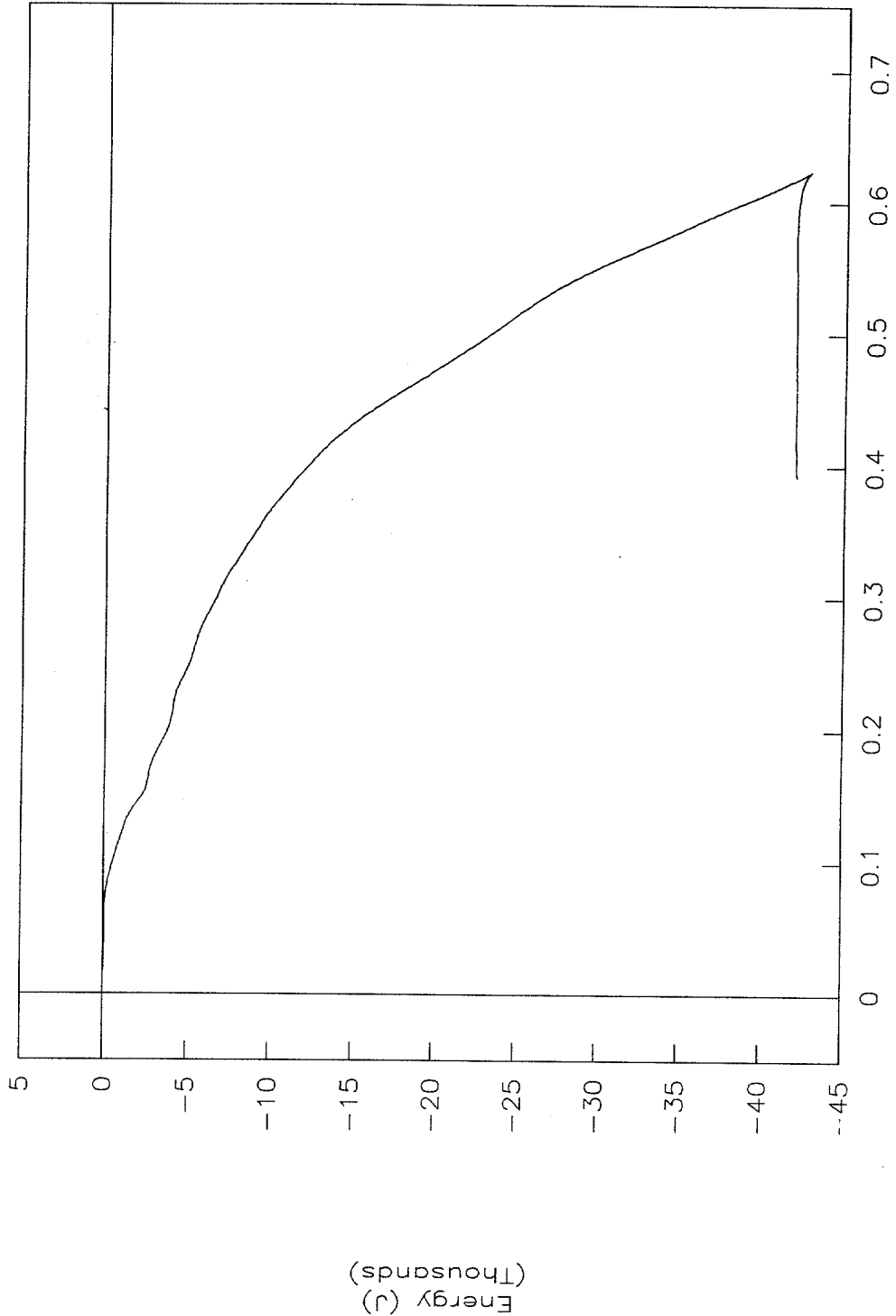


Figure 124. Rigid pole, energy vs. displacement, test 98F014.



Test No. 98F014

Impact force height vs. displacement

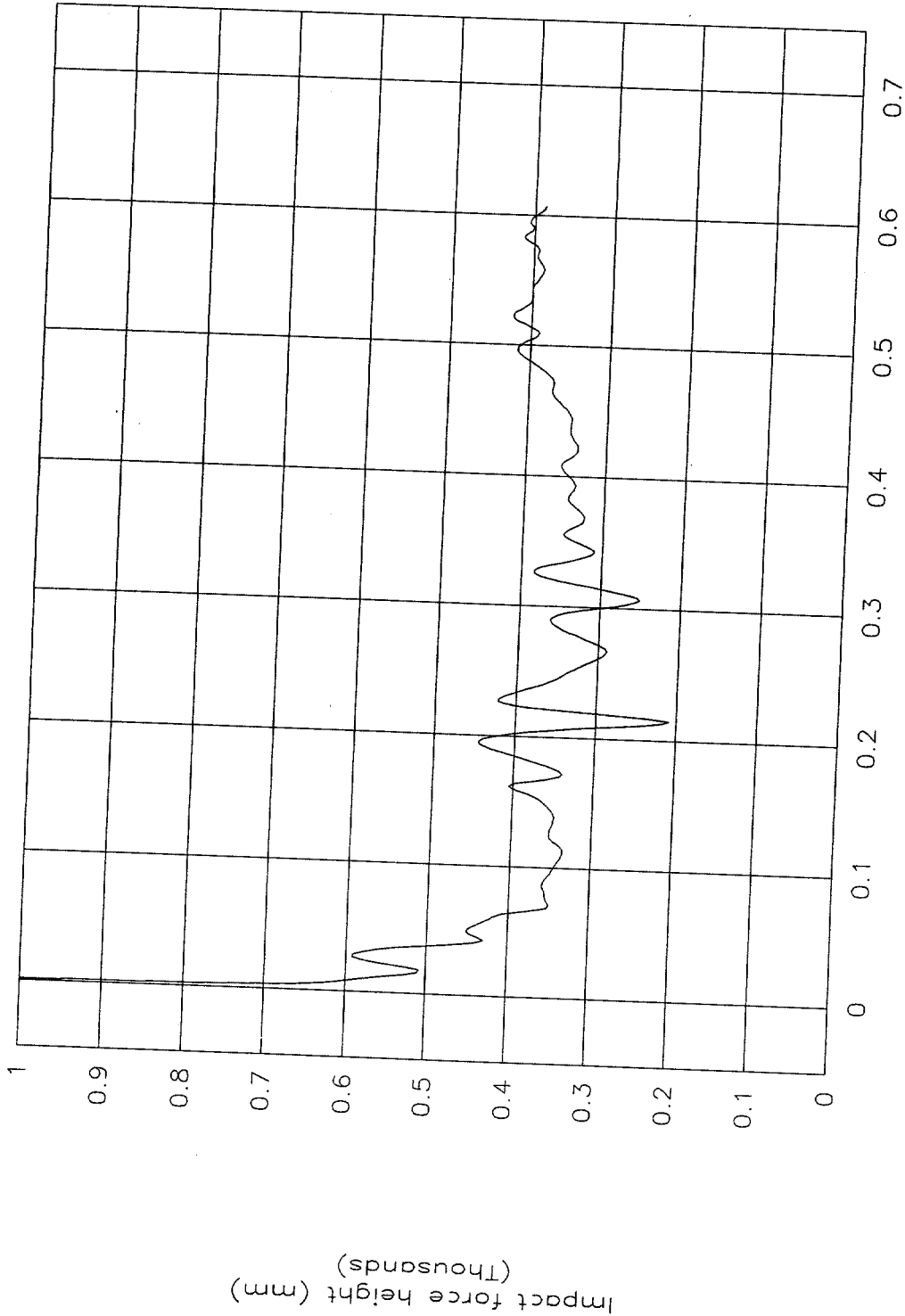


Figure 125. Impact force height vs. displacement, test 98F014.



Test No. 98F014
Top of engine, X-axis

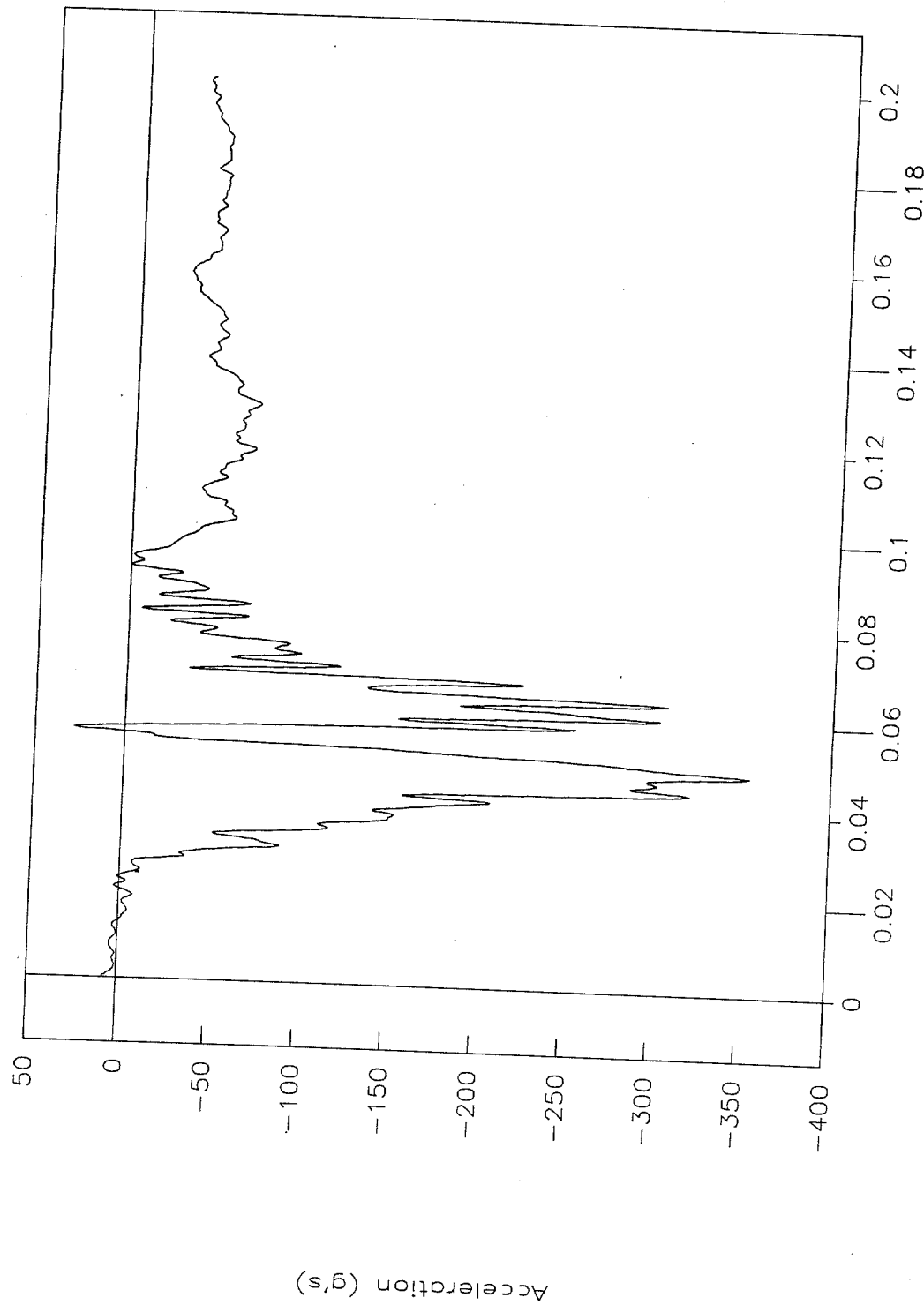


Figure 126. Top of engine acceleration vs. time, X-axis, test 98F014.



Test No. 98F014
Bottom of engine, X-axis

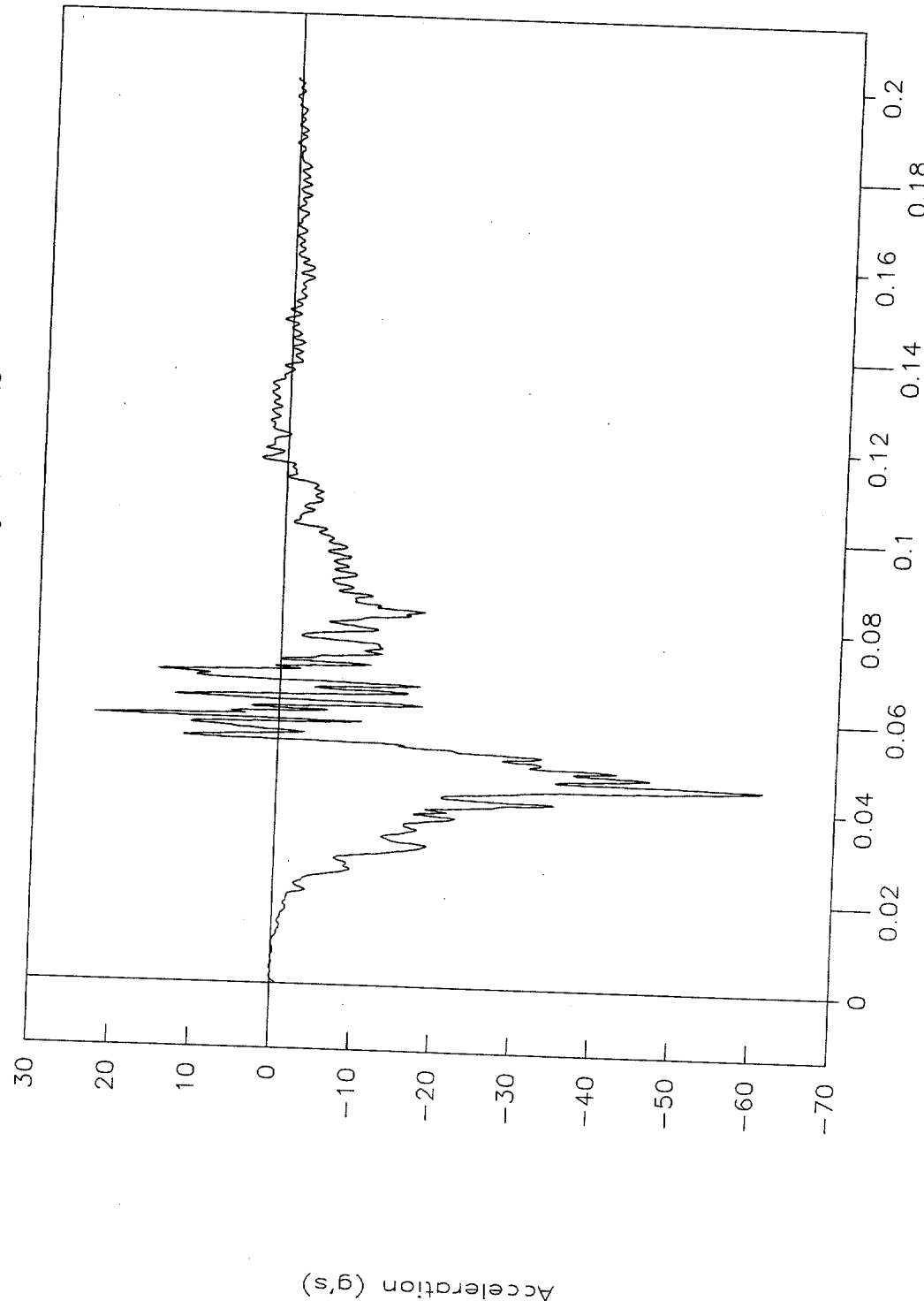


Figure 127. Bottom of engine acceleration vs. time, X-axis, test 98F014.



Test No. 98F014

Left control arm, X-axis

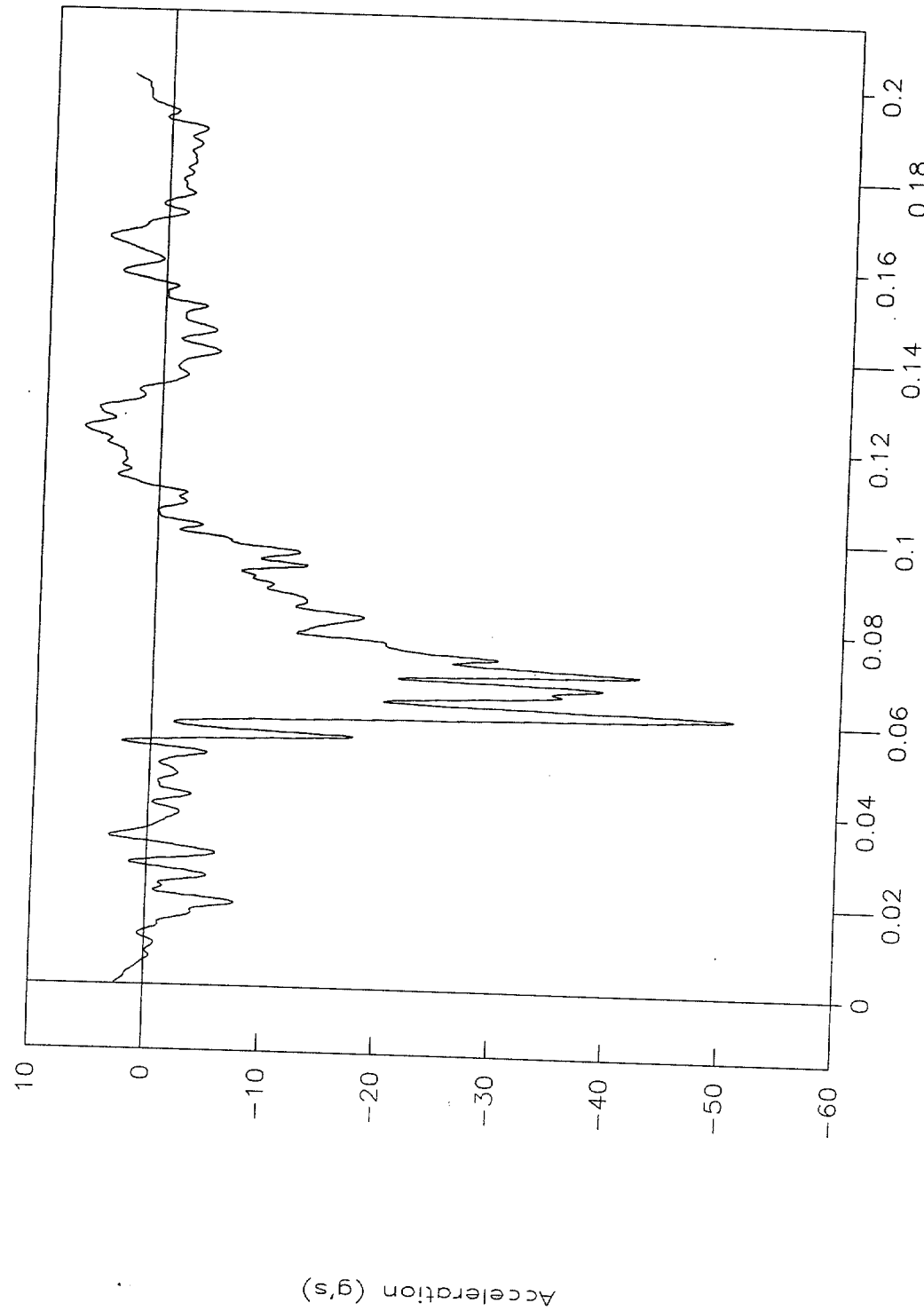


Figure 128. Left control arm acceleration vs. time, X-axis, test 98F014.



Test No. 98F014
Right control arm, X-axis

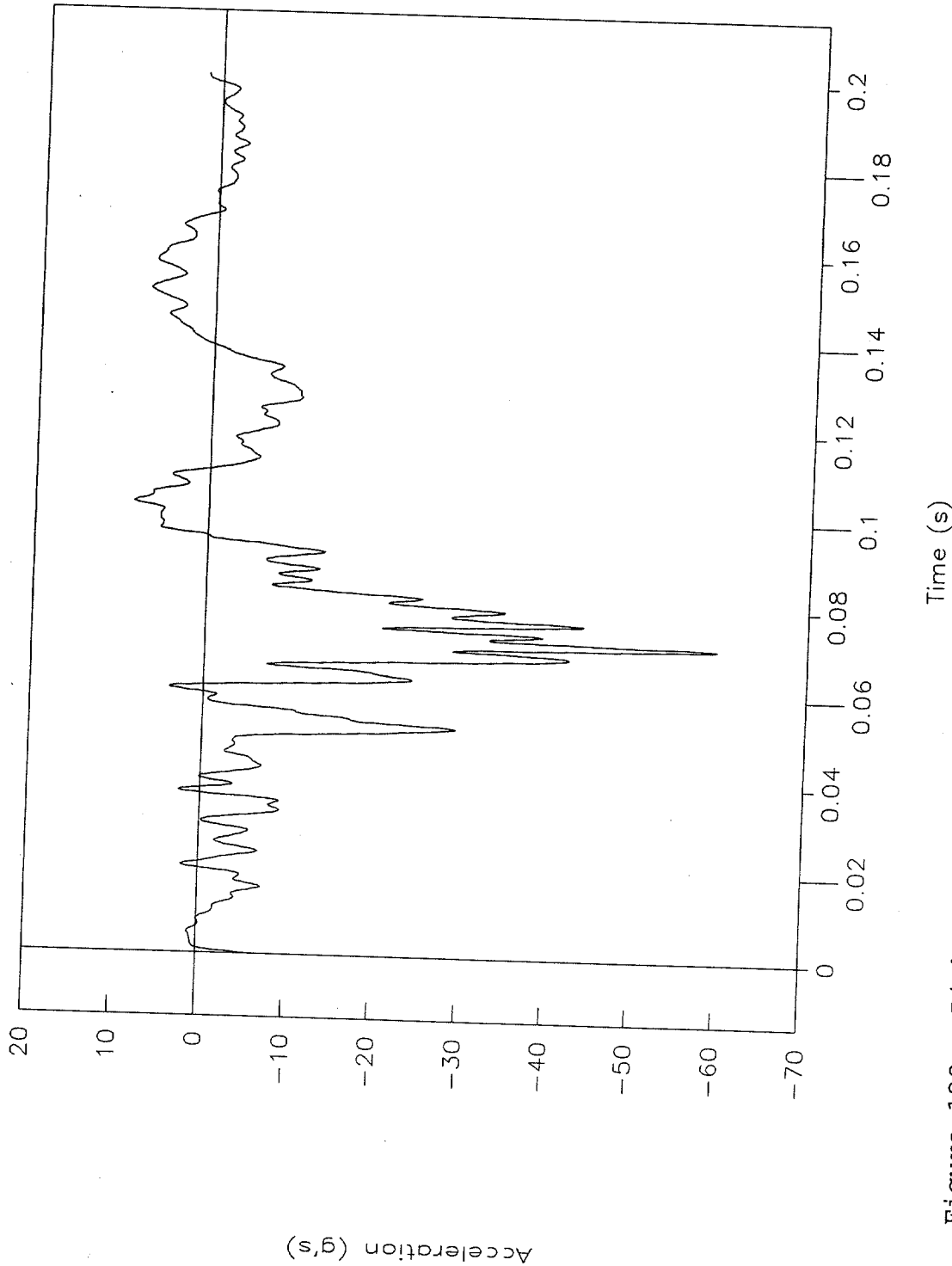


Figure 129. Right control arm acceleration vs. time, X-axis, test 98F014.



Test No. 98F014
Pitch rate and angle vs. time

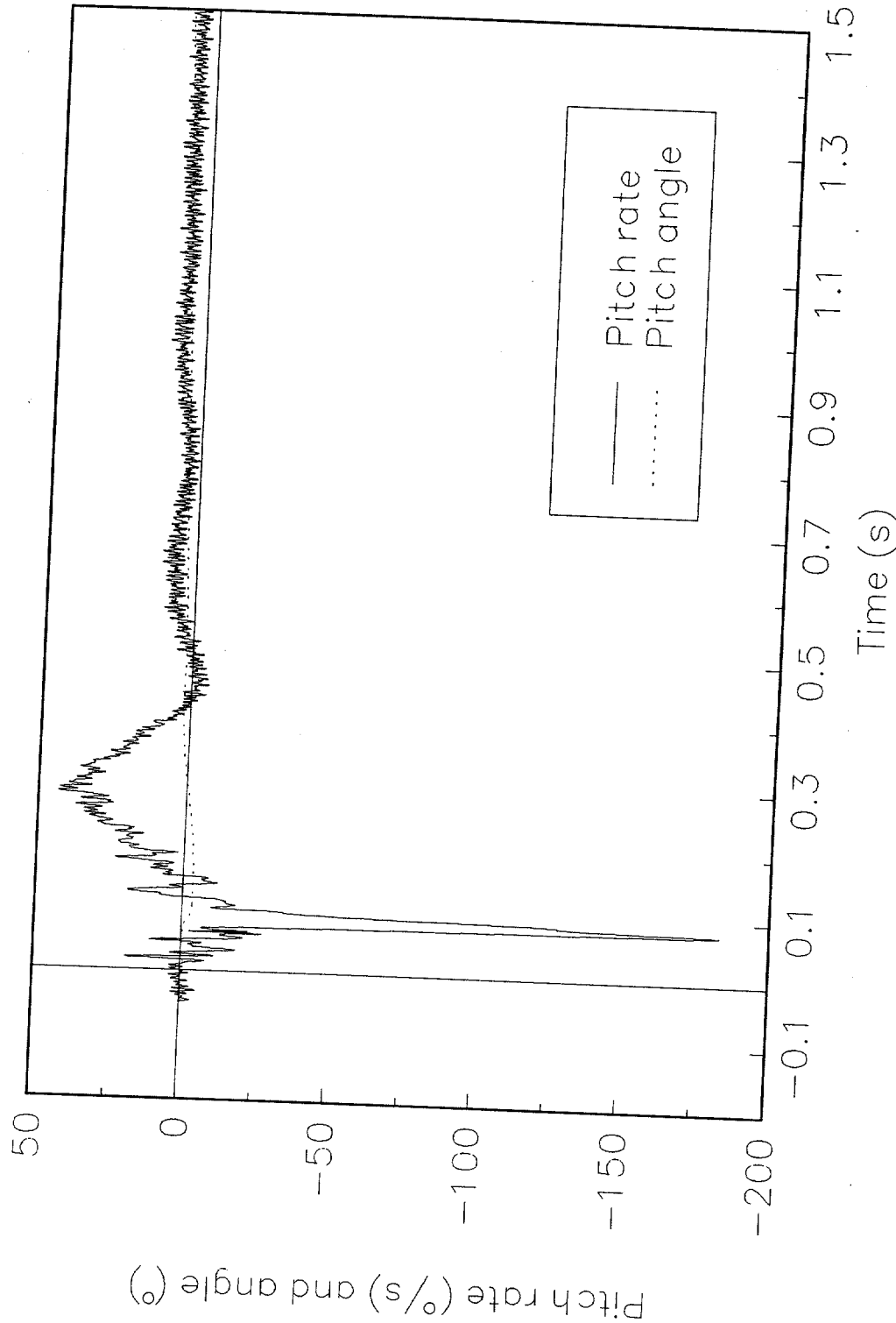


Figure 130. Pitch rate and angle vs. time, test 98F014.



Test No. 98F014
Roll rate and angle vs. time

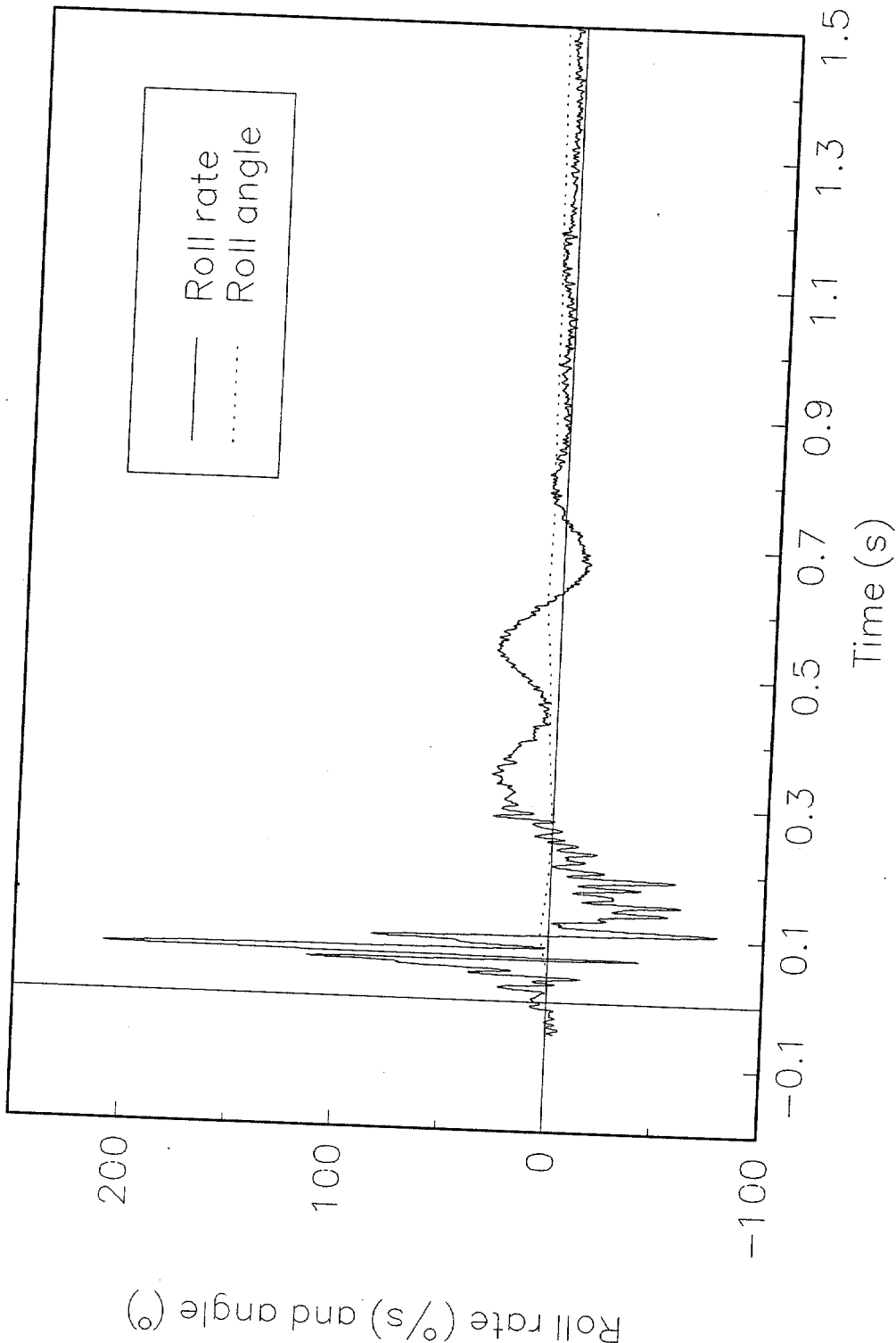


Figure 131. Roll rate and angle vs. time, test 98F014.



Test No. 98F014
Yaw rate and angle vs. time

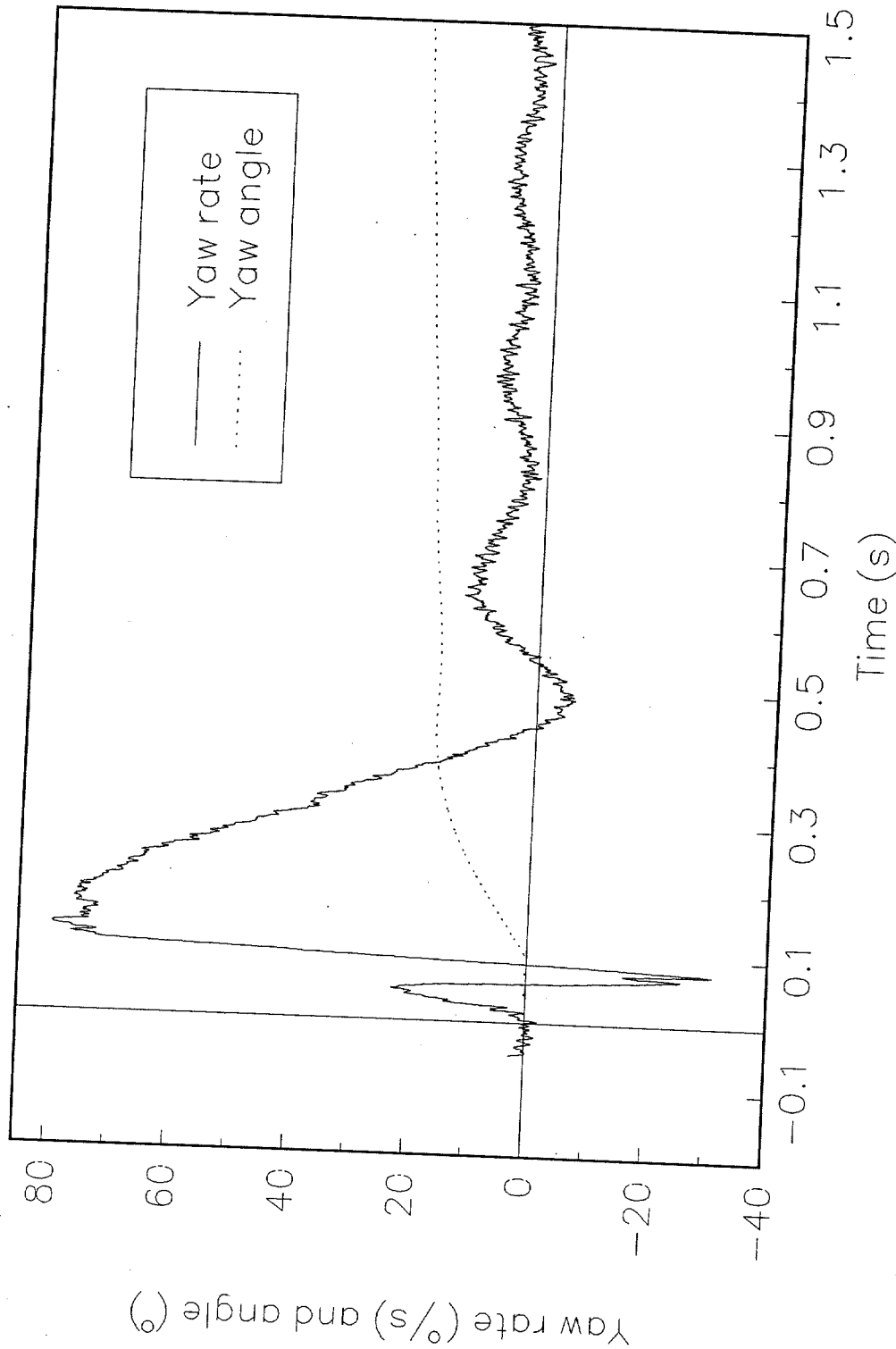


Figure 132. Yaw rate and angle vs. time, test 98F014.



Test No. 98F015
Cg acceleration vs. time, X-axis

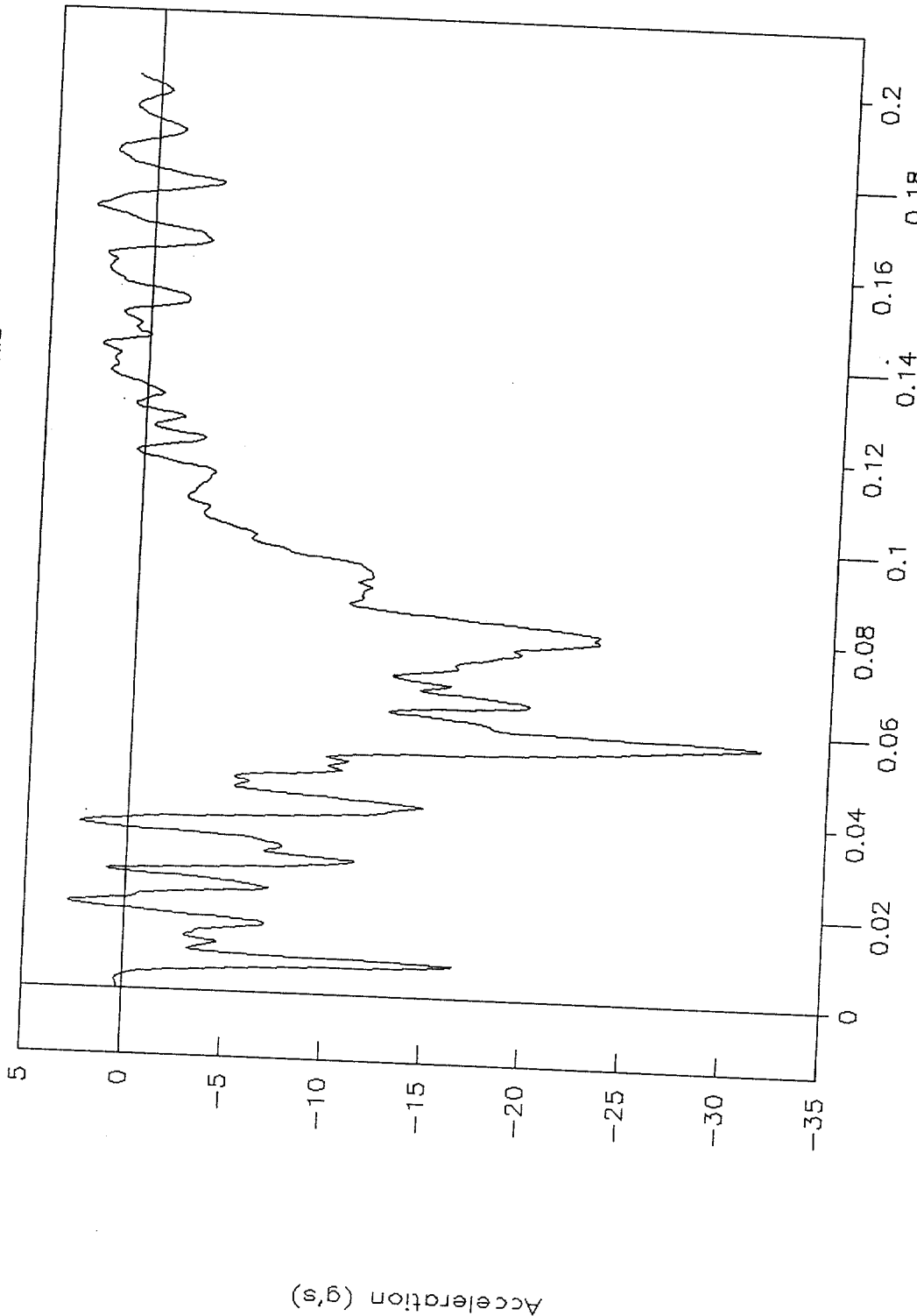


Figure 133. C.g. acceleration vs. time, X-axis, test 98F015.



Test No. 98F015
Cg velocity vs. time, X-axis

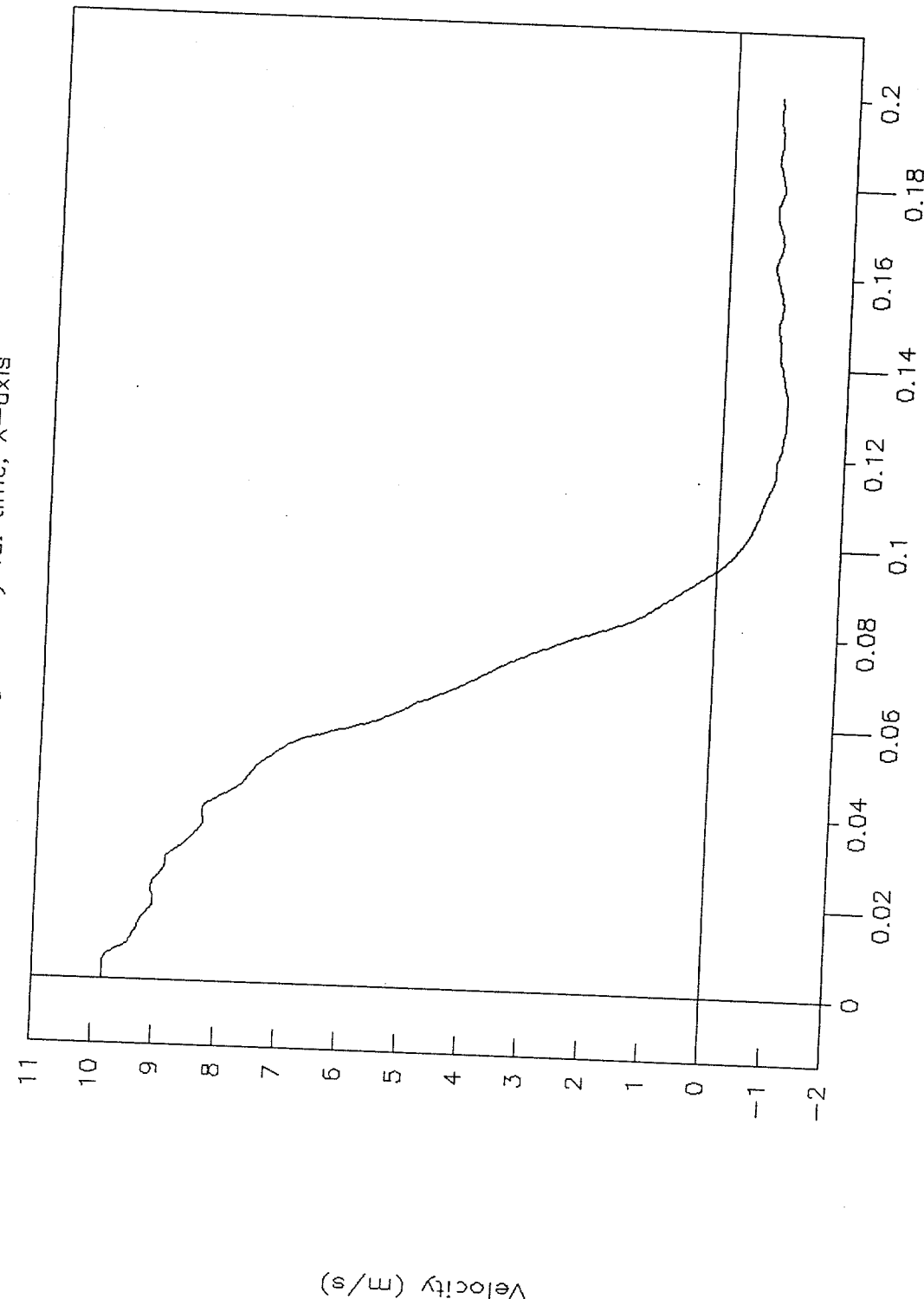


Figure 134. C.g. velocity vs. time, X-axis, test 98F015.



Test No. 98F015
Cg displacement vs. time, X-axis

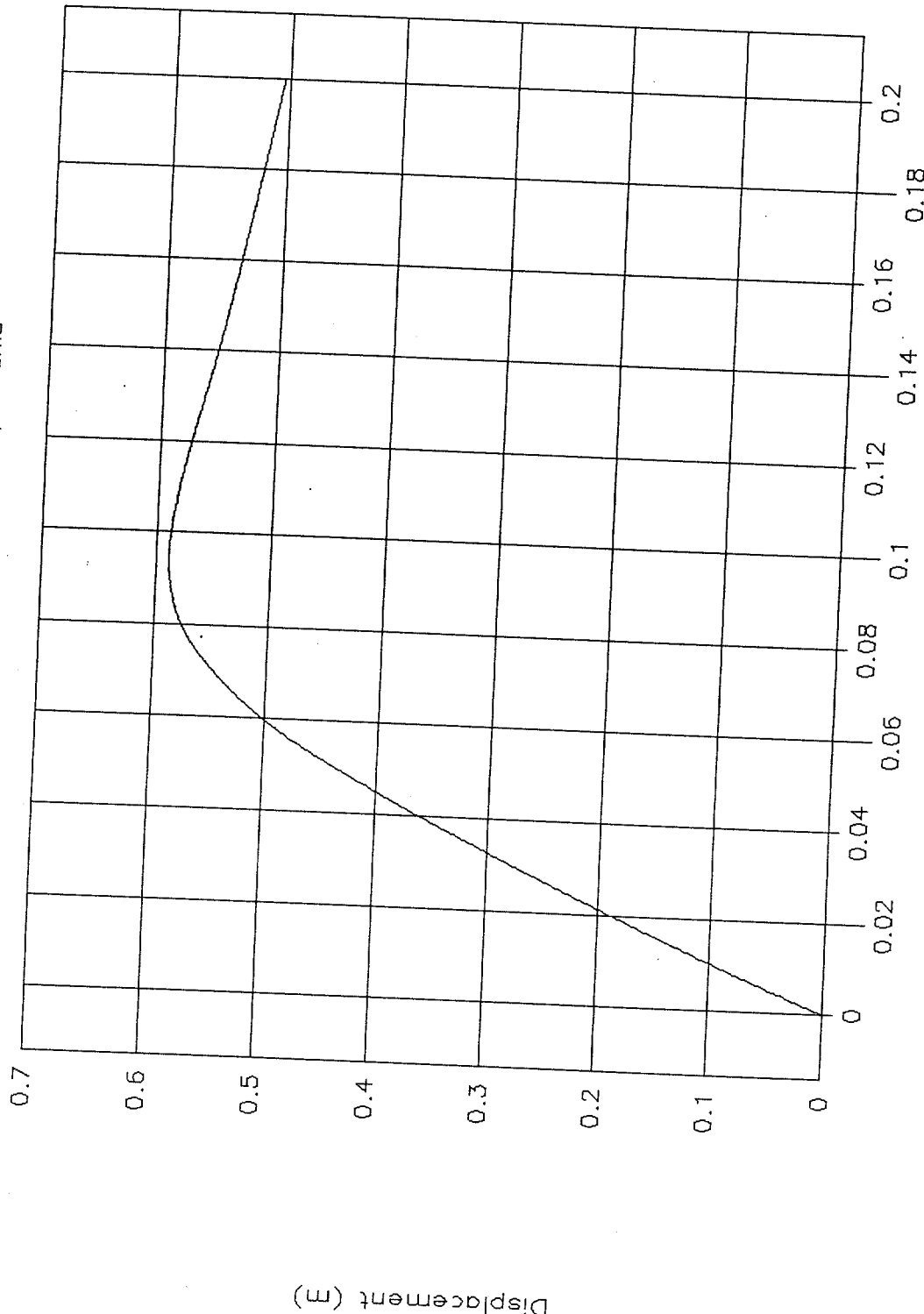


Figure 135. C.g. displacement vs. time, X-axis, test 98F015.



Test No. 98F015
Cg force vs. displacement, X-axis

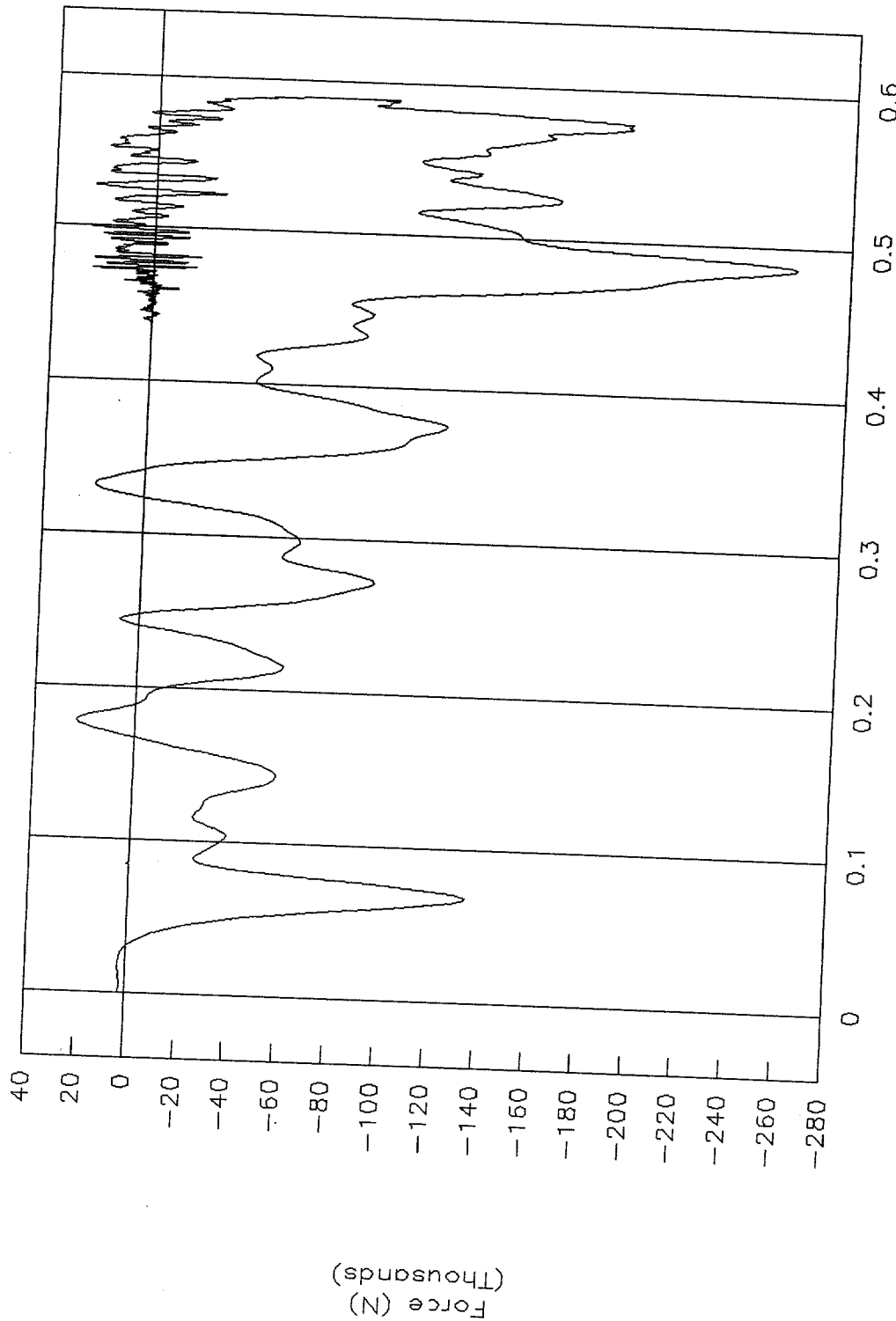


Figure 136. C.g. force vs. displacement, X-axis, test 98F015.



Test No. 98F015
Cg energy vs. displacement, X-axis

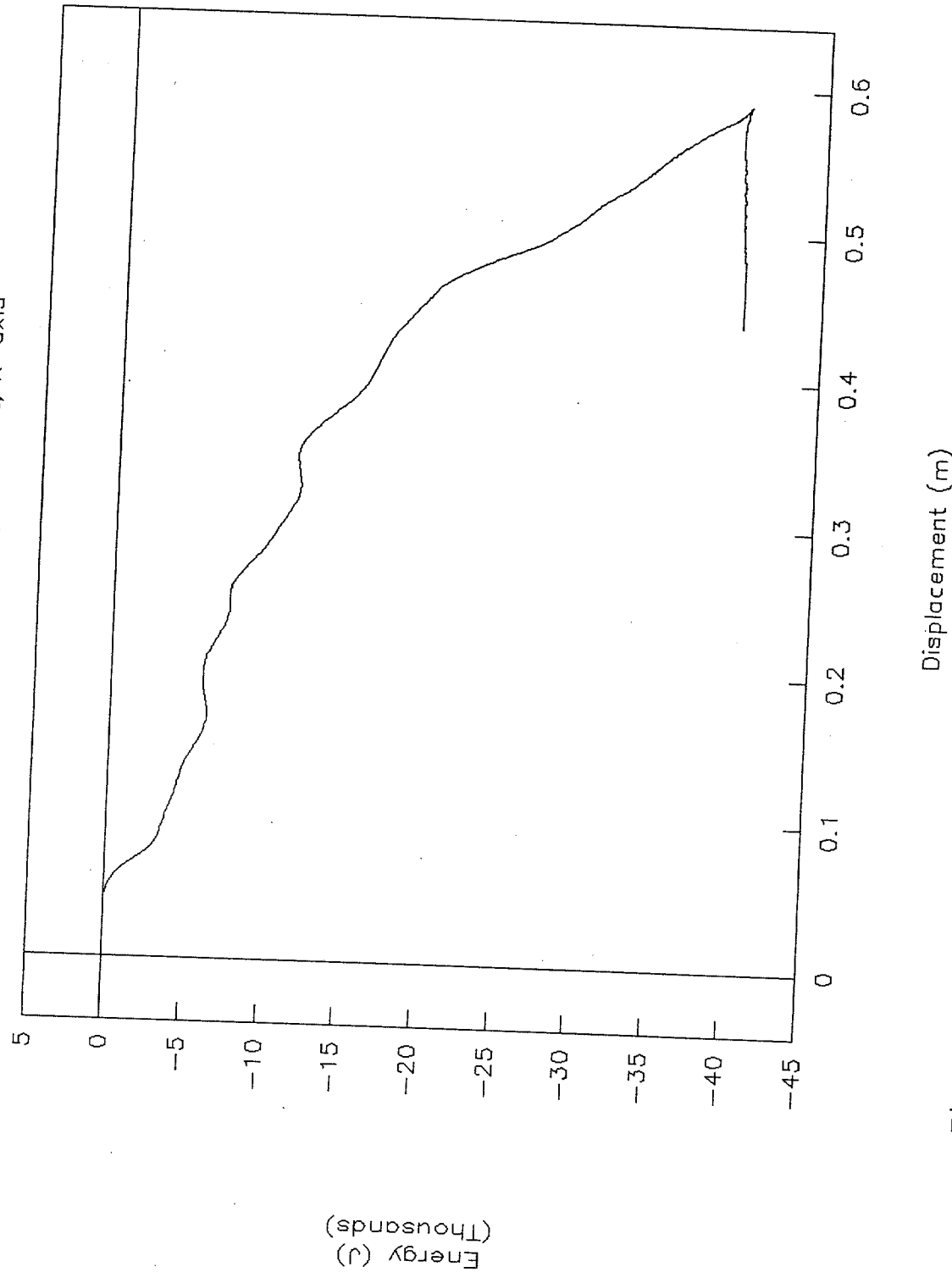


Figure 137. C.g. energy vs. displacement, X-axis, test 98F015.



Test No. 98F015
Cg acceleration vs. time, Y-axis

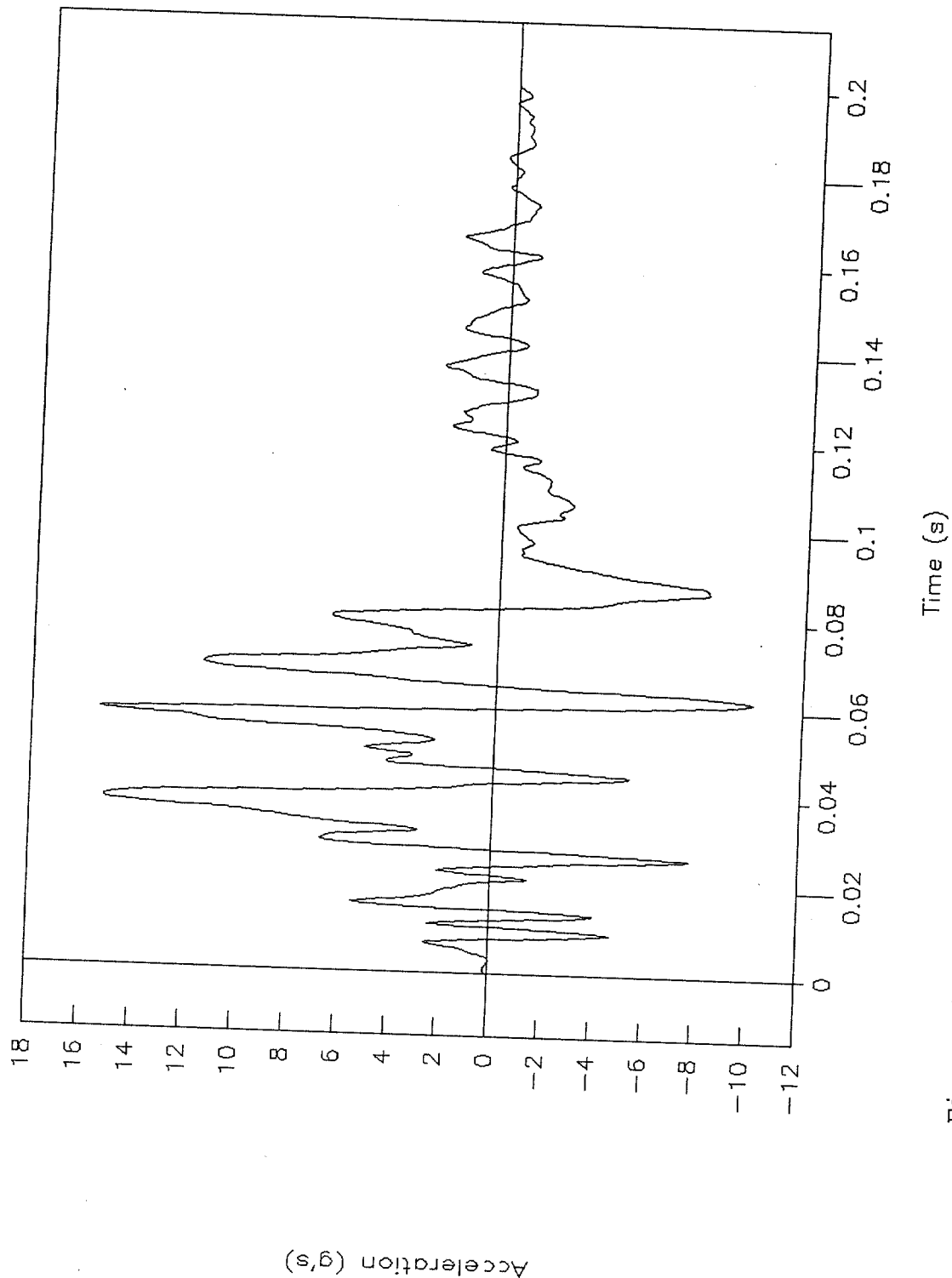


Figure 138. C.g. acceleration vs. time, Y-axis, Test 98F015.



Test No. 98F015
Cg acceleration vs. time, Z-axis

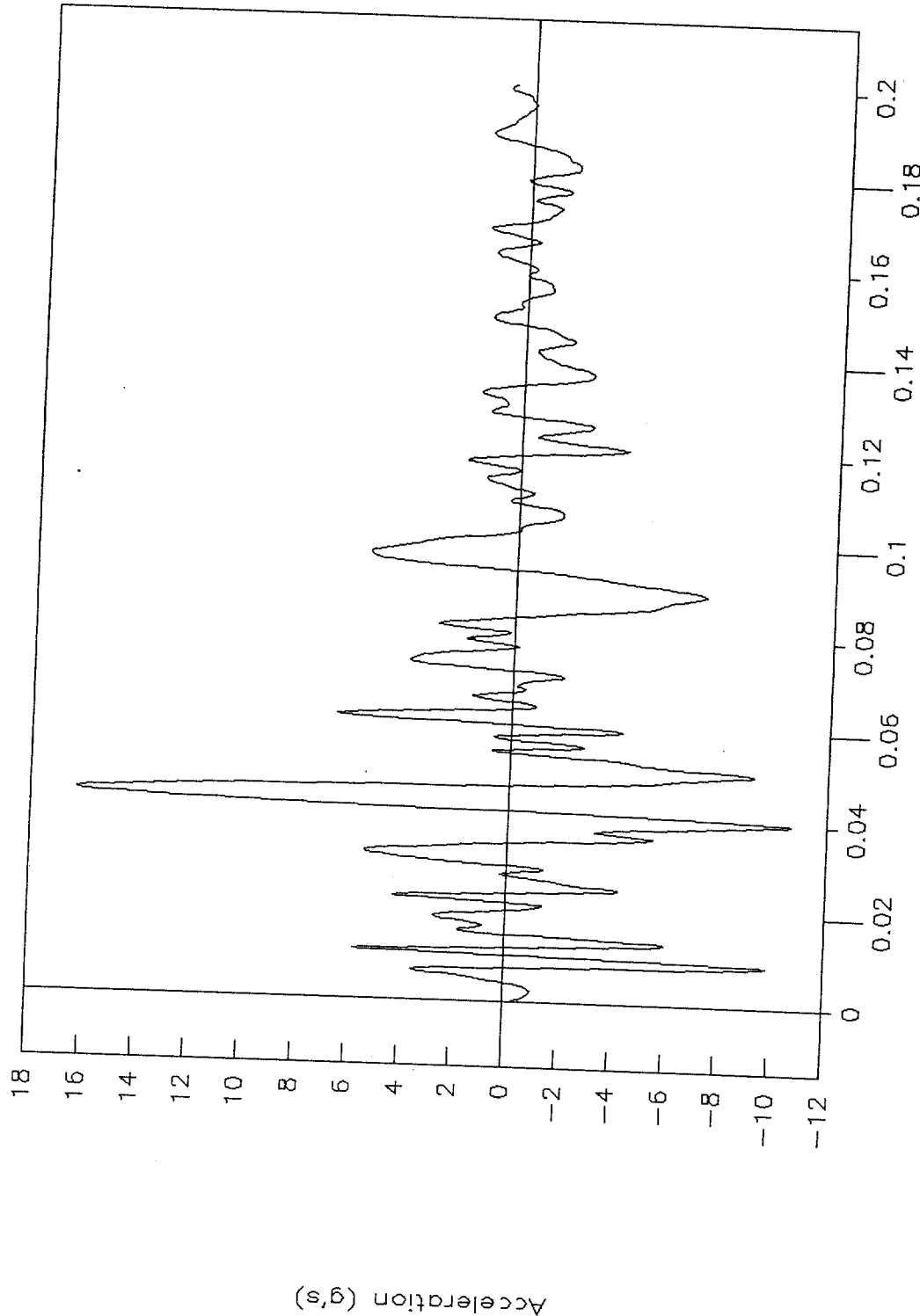


Figure 139. C.g. acceleration vs. time, Z-axis, test 98F015.



Test No. 98F015
Rigid pole, force vs. time

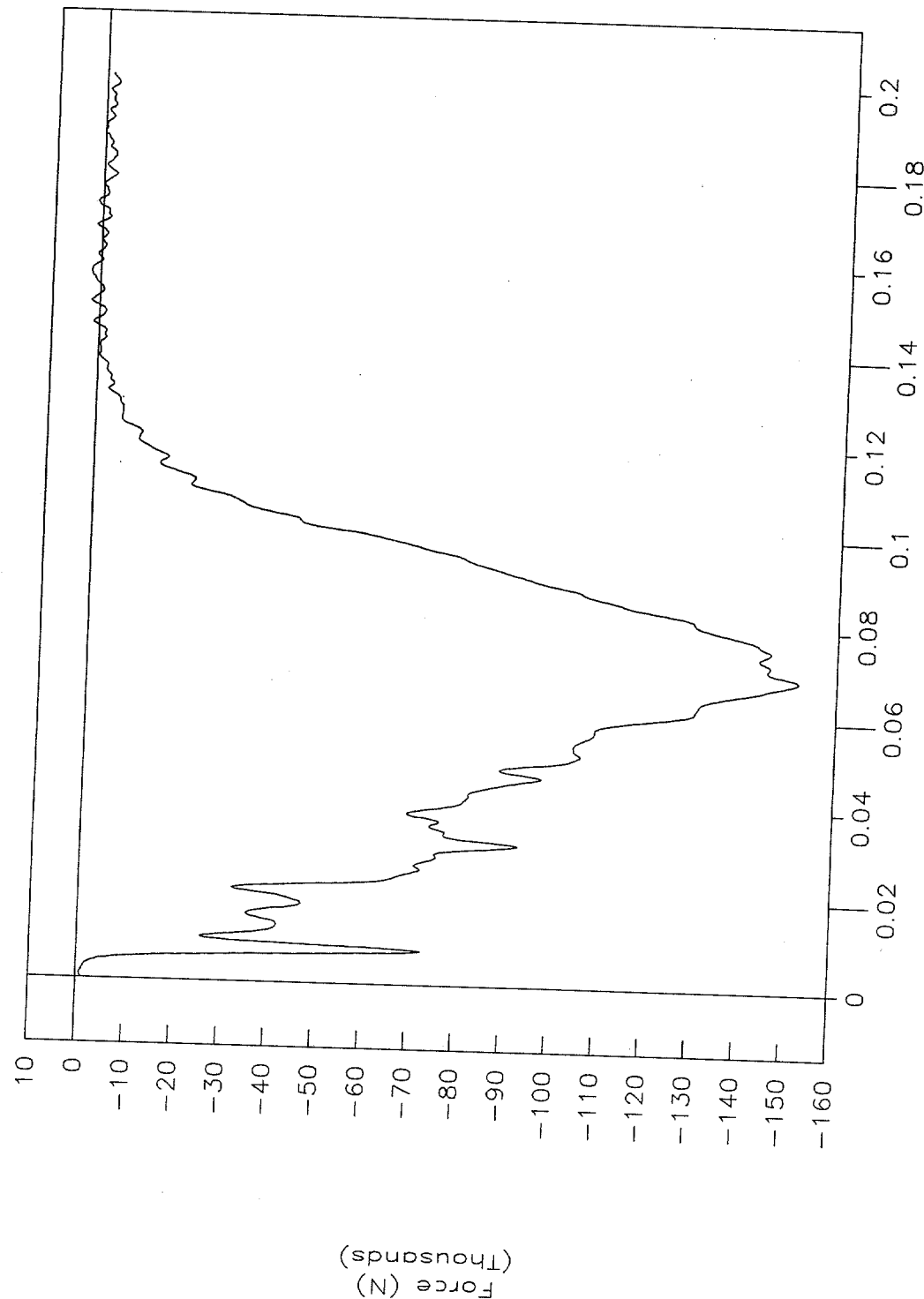


Figure 140. Rigid pole, force vs. time, test 98F015.



Test No. 98F015
Rigid pole, acceleration vs. time

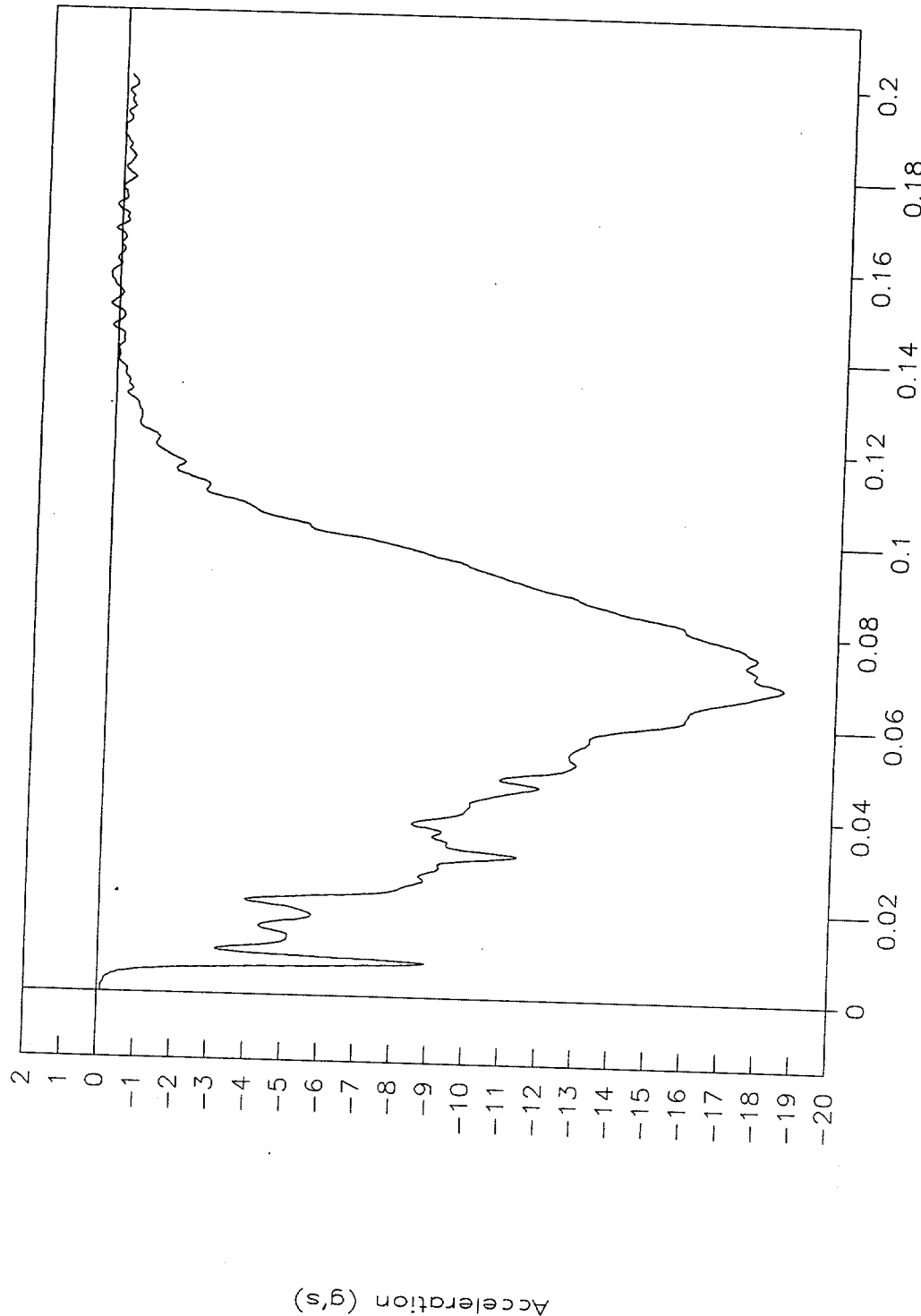


Figure 141. Rigid pole, acceleration vs. time, test 98F015.



Test No. 98F015
Rigid pole, velocity vs. time

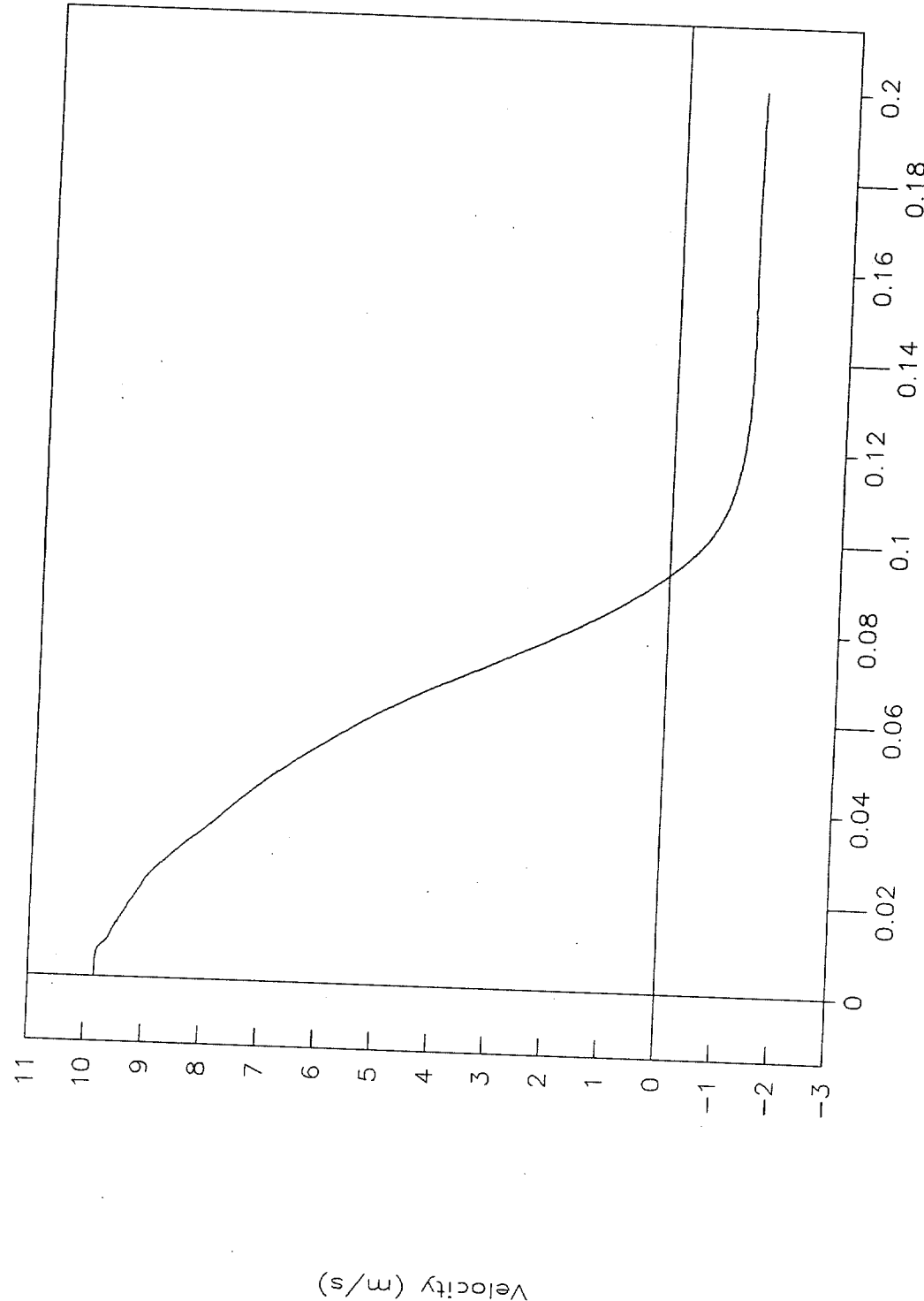


Figure 142. Rigid pole, velocity vs. time, test 98F015.



Test No. 98F015
Rigid pole, displacement vs. time

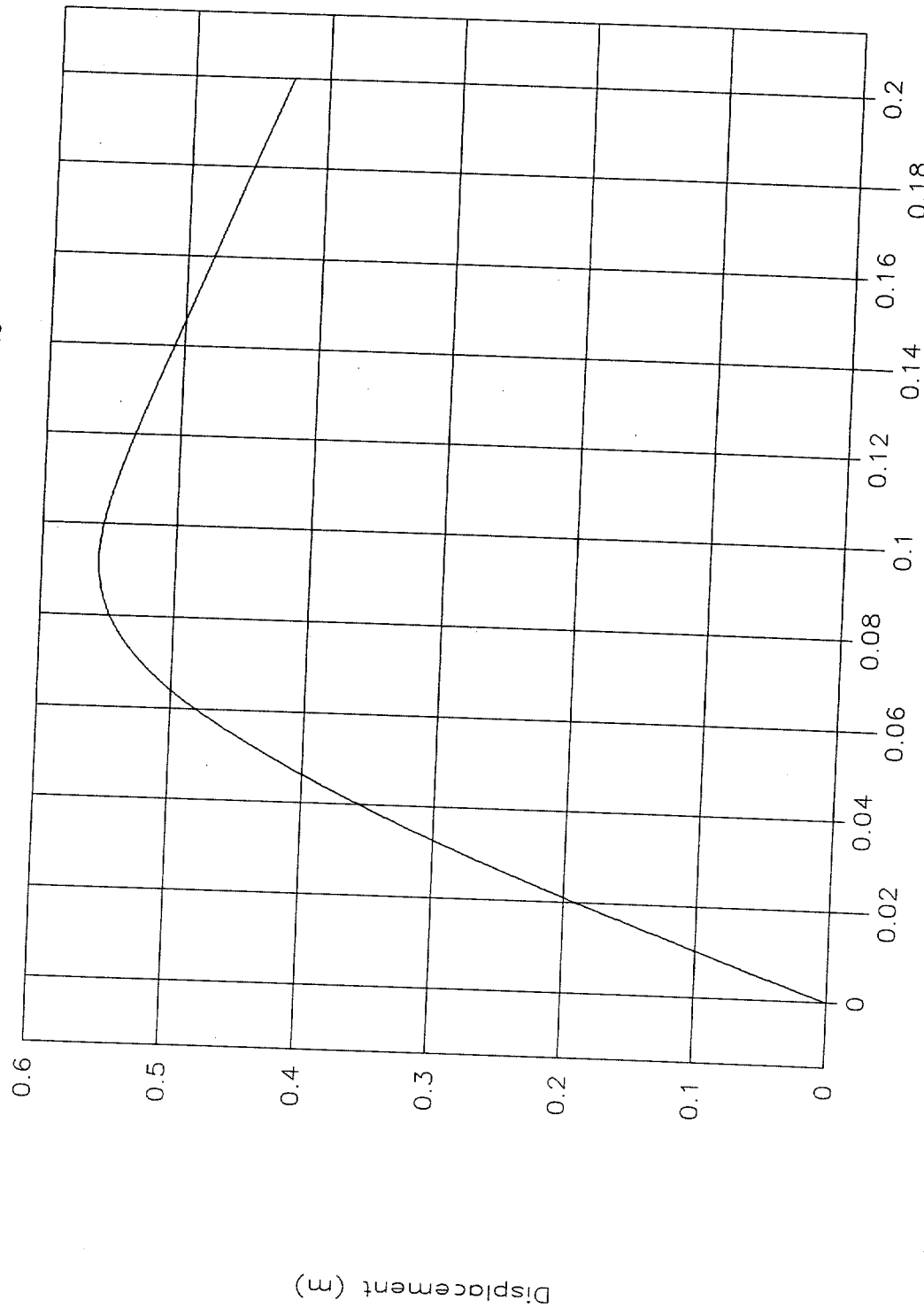


Figure 143. Rigid pole, displacement vs. time, test 98F015.



Test No. 98F015
Rigid pole, force vs. displacement

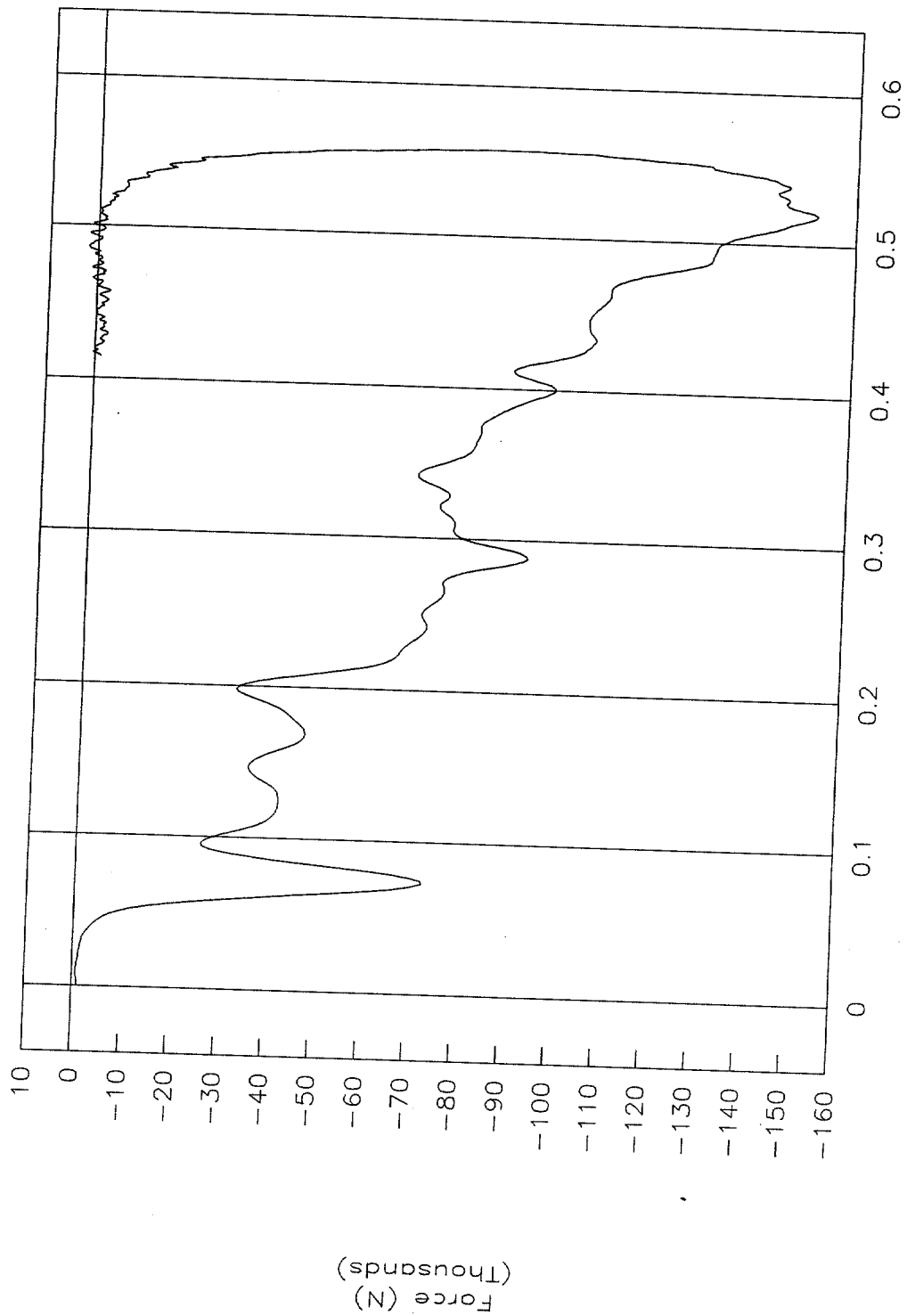


Figure 144. Rigid pole, force vs. displacement, test 98F015.



Test No. 98F015
Rigid pole, energy vs. displacement

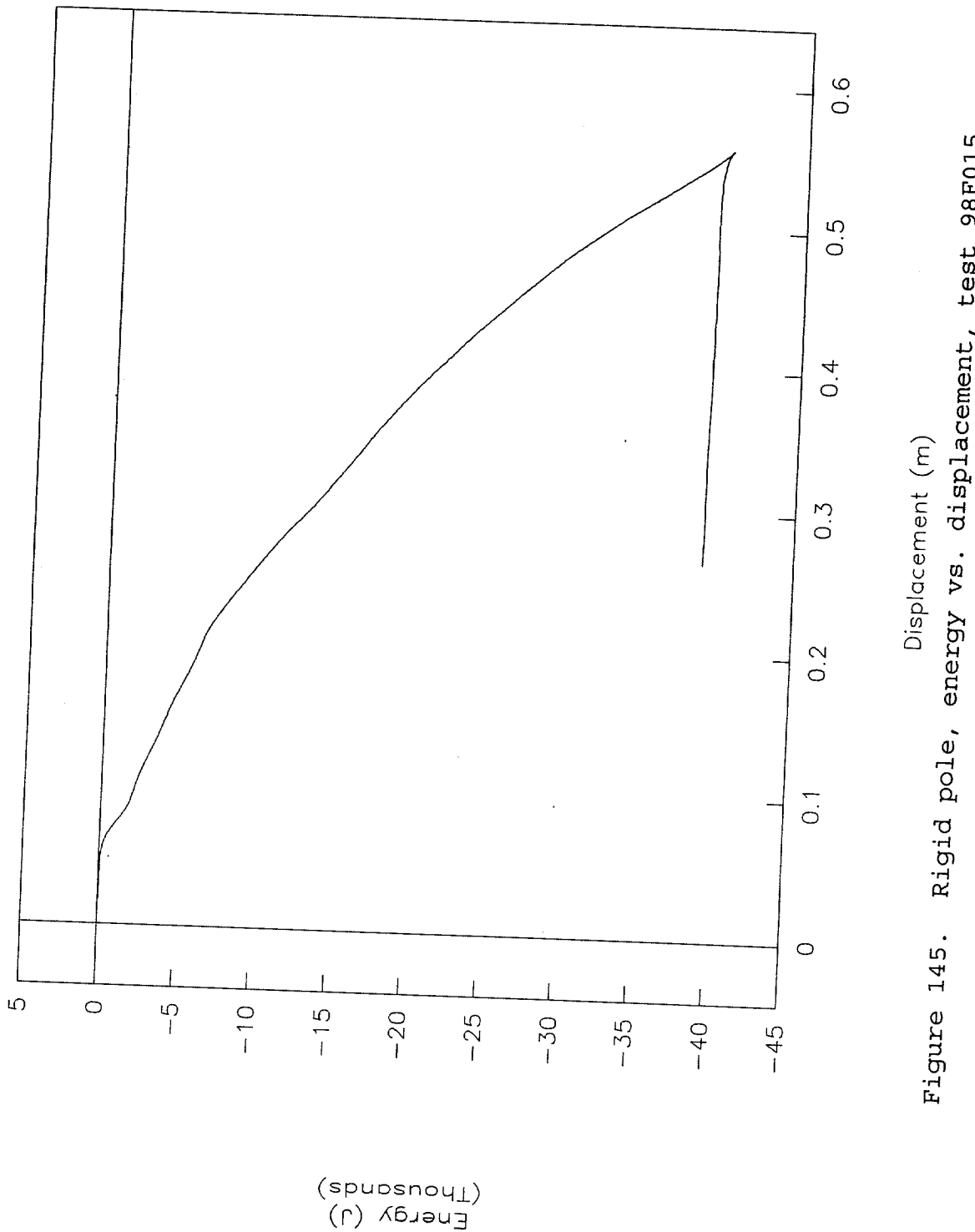


Figure 145. Rigid pole, energy vs. displacement, test 98F015.



Test No. 98F015

Impact force height vs. displacement

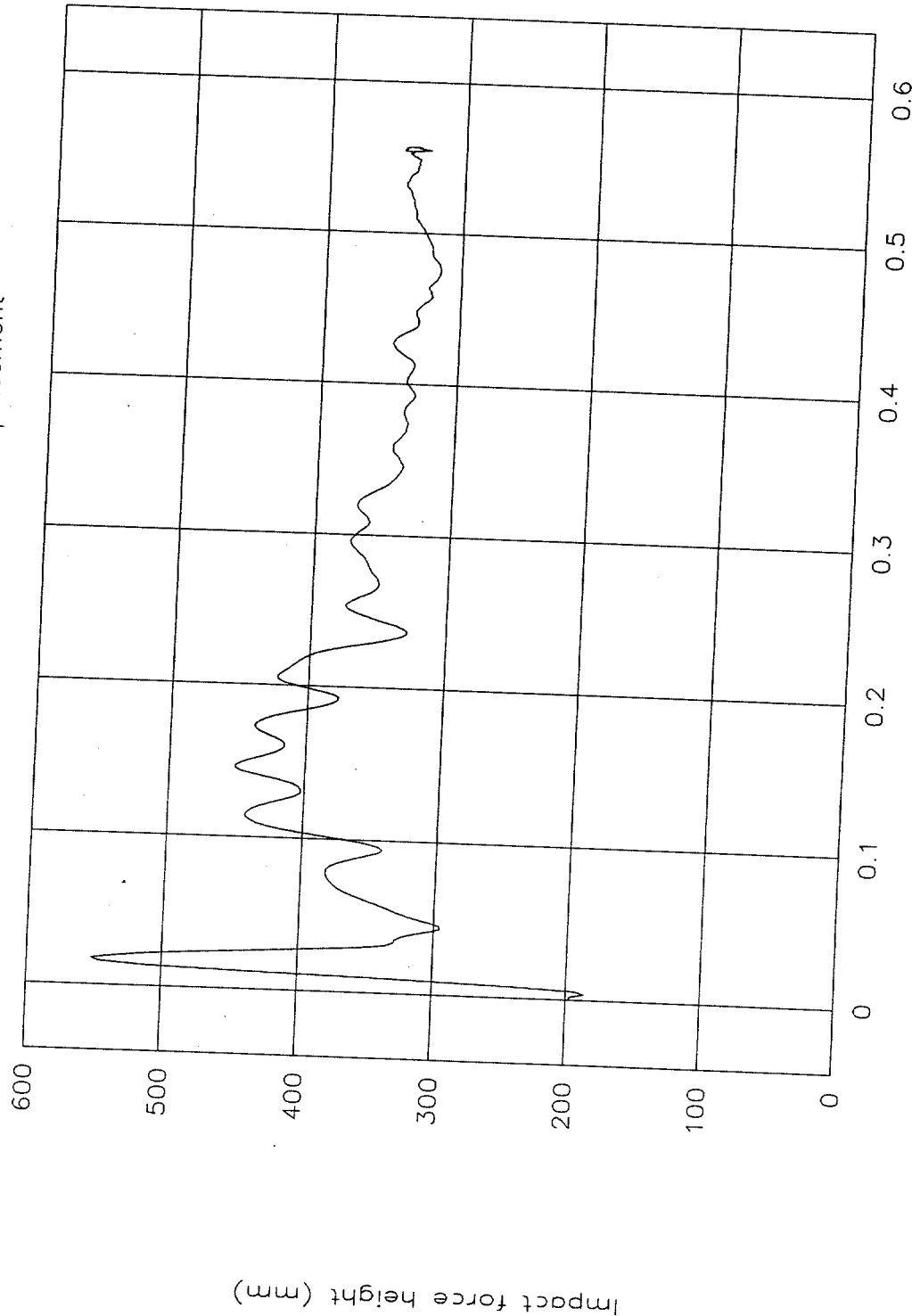


Figure 146. Impact force height vs. displacement, test 98F015.



Test No. 98F015
Top of engine, X-axis

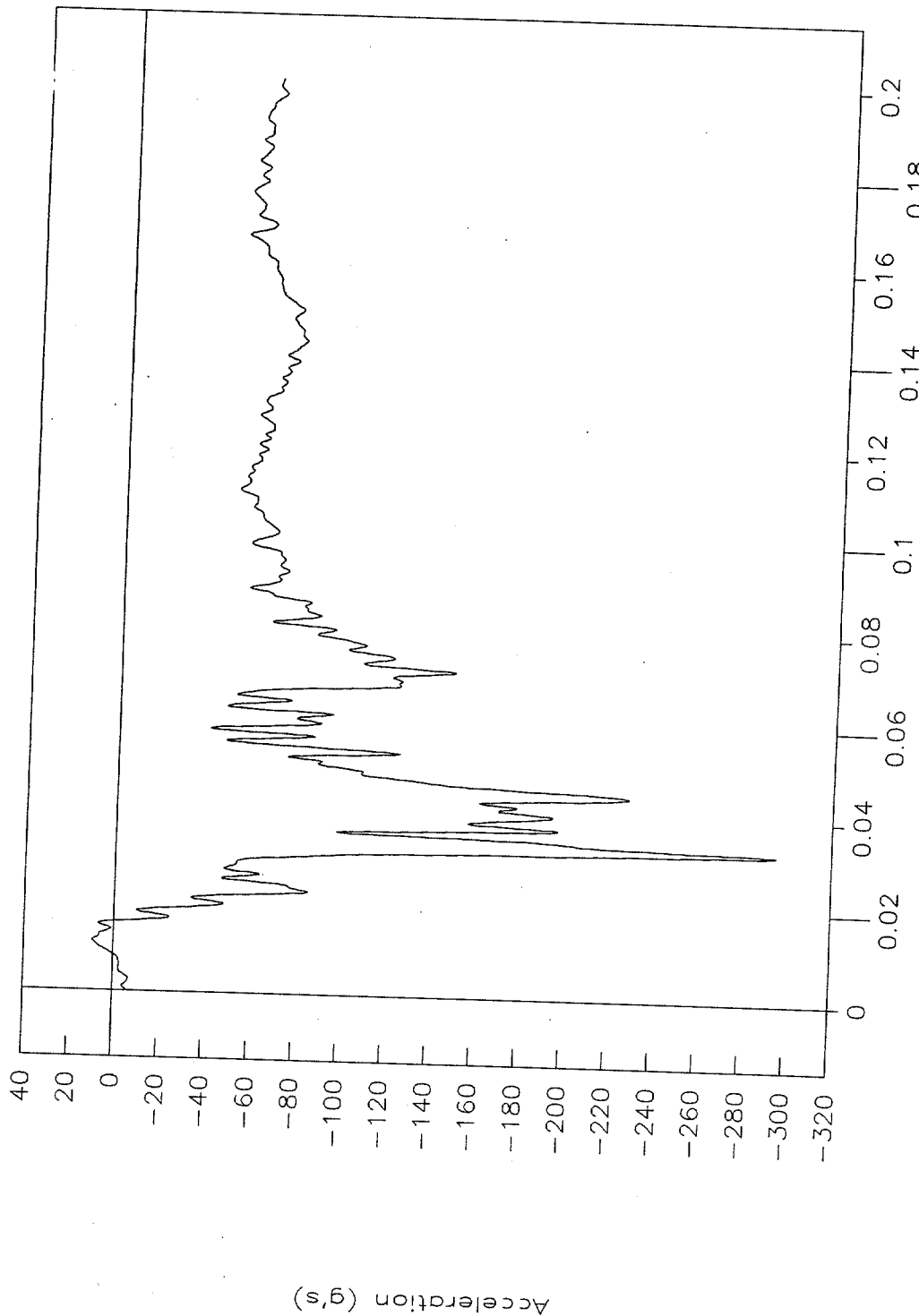


Figure 147. Top of engine acceleration vs. time, X-axis, test 98F015.



Test No. 98F015
Bottom of engine, X-axis

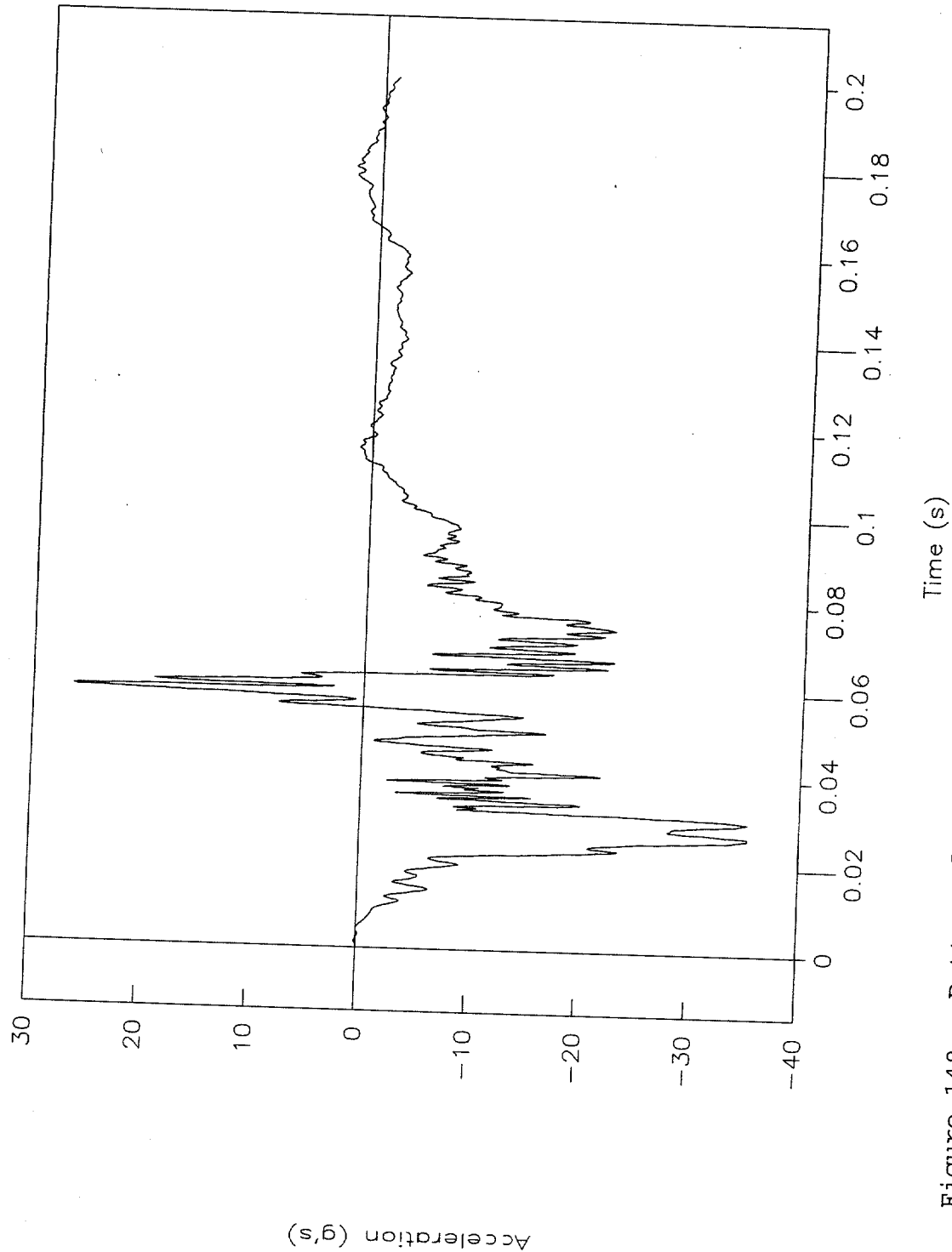


Figure 148. Bottom of engine acceleration vs. time, X-axis, test 98F015.



Test No. 98F015

Left control arm, X-axis

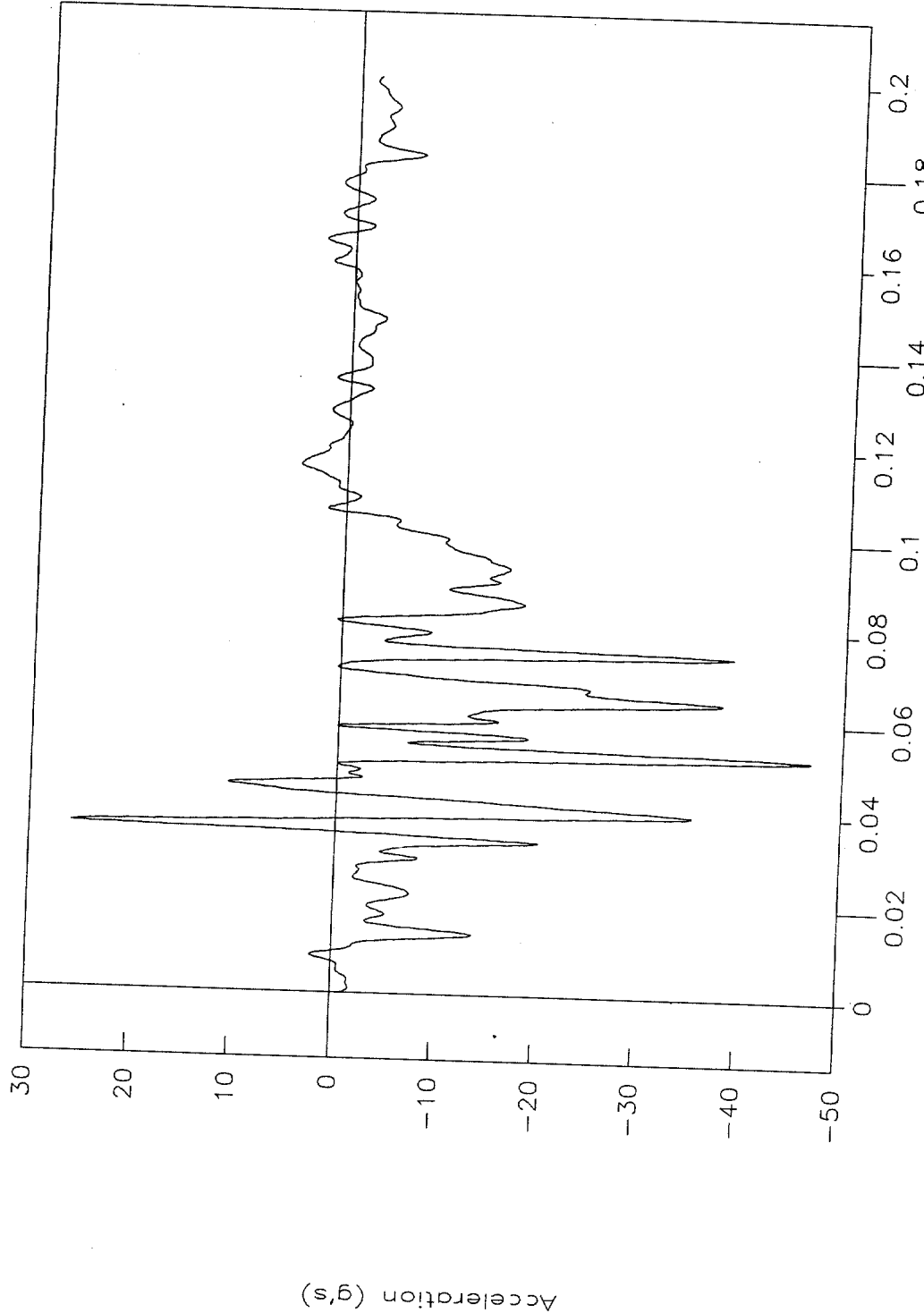


Figure 149. Left control arm acceleration vs. time, X-axis, test 98F015.



Test No. 98F015
Right control arm, X-axis

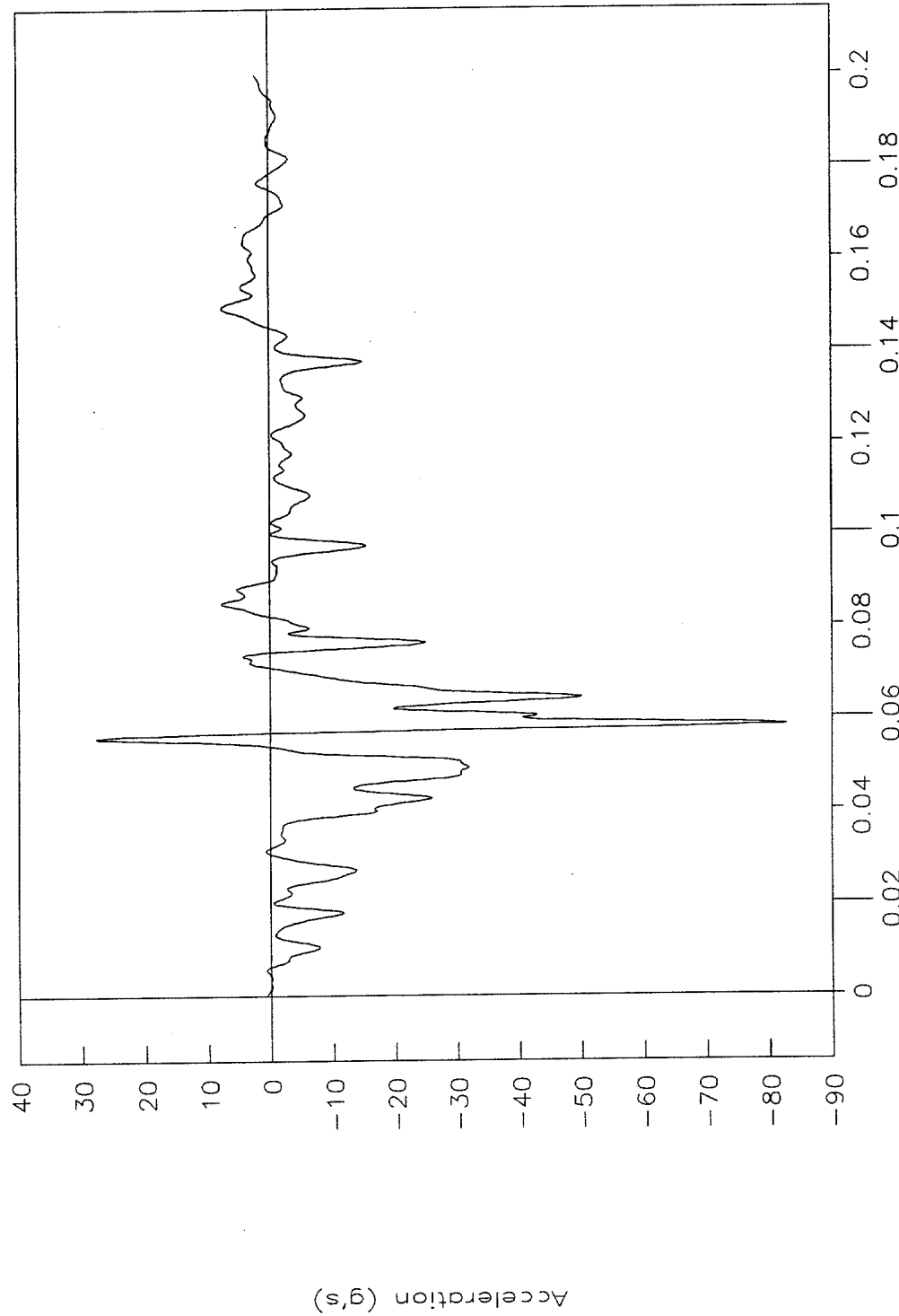


Figure 150. Right control arm acceleration vs. time, X-axis, test 98F015.

Test No. 98F015
Pitch rate and angle vs. time

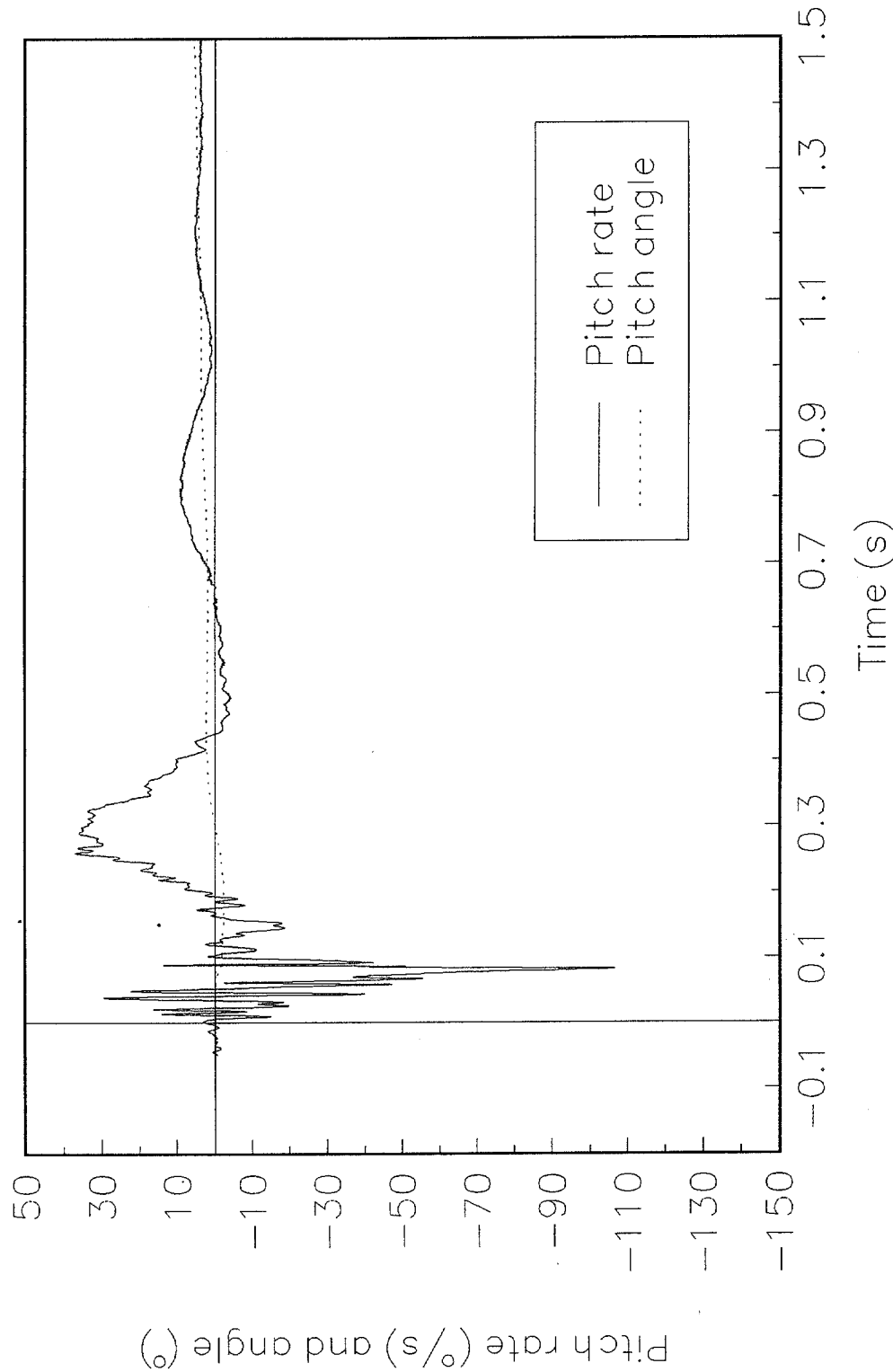


Figure 151. Pitch rate and angle vs. time, test 98F015.

Test No. 98F015
Roll rate and angle vs. time

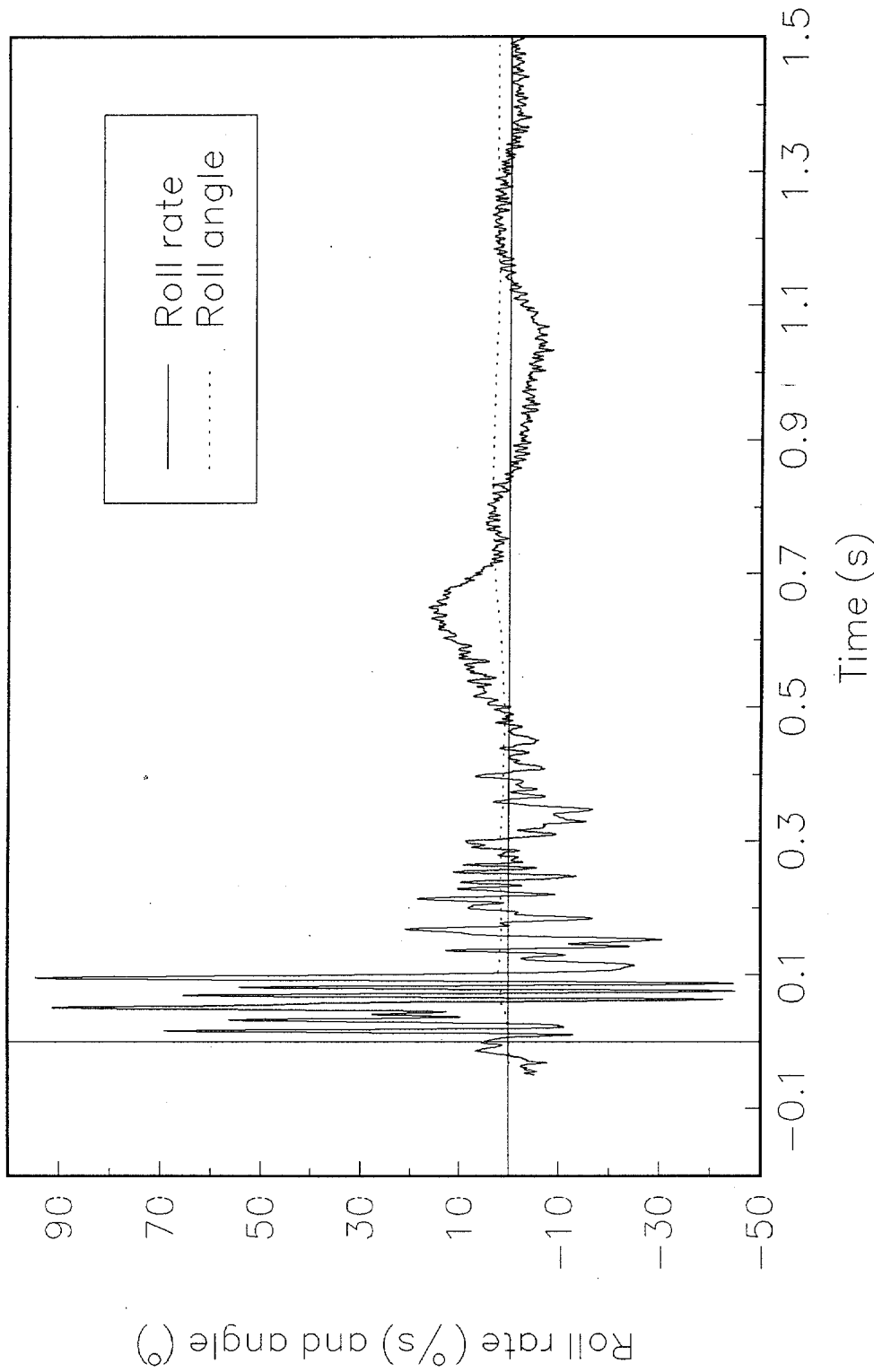


Figure 152. Roll rate and angle vs. time, test 98F015.

Test No. 98F015
Yaw rate and angle vs. time

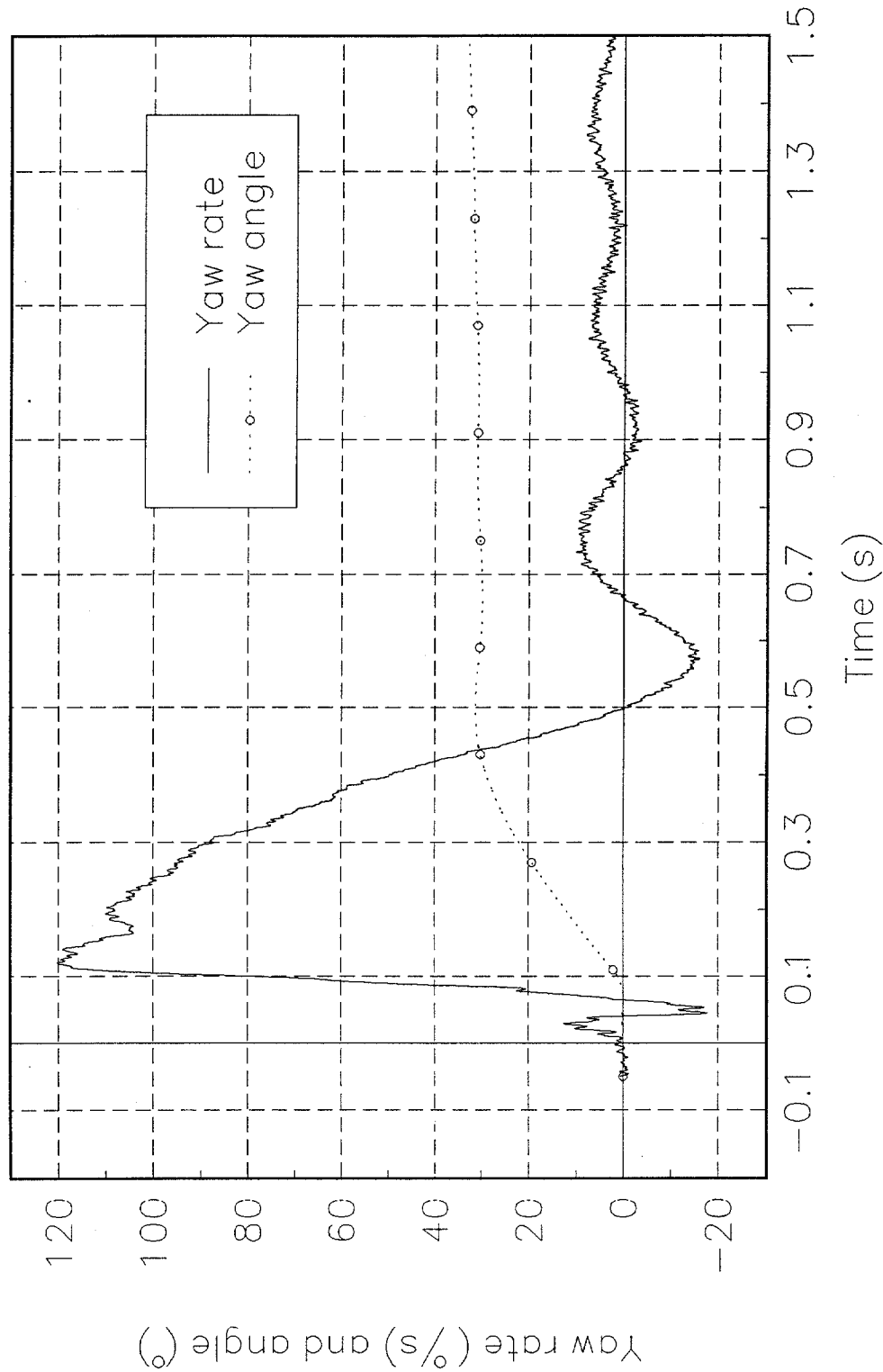
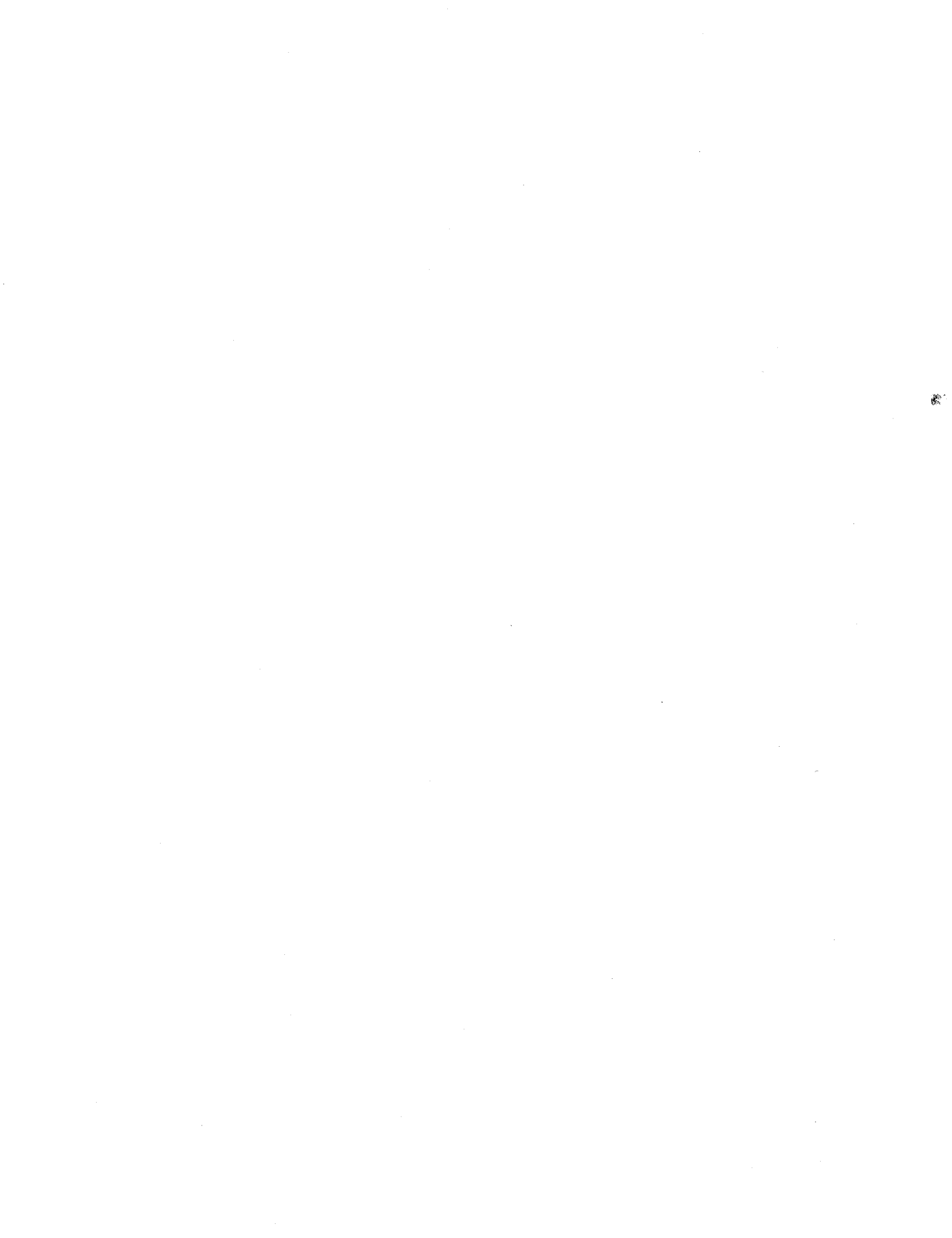


Figure 153. Yaw rate and angle vs. time, test 98F015.



Test No. 99S001
Cg acceleration vs. time, Y-axis

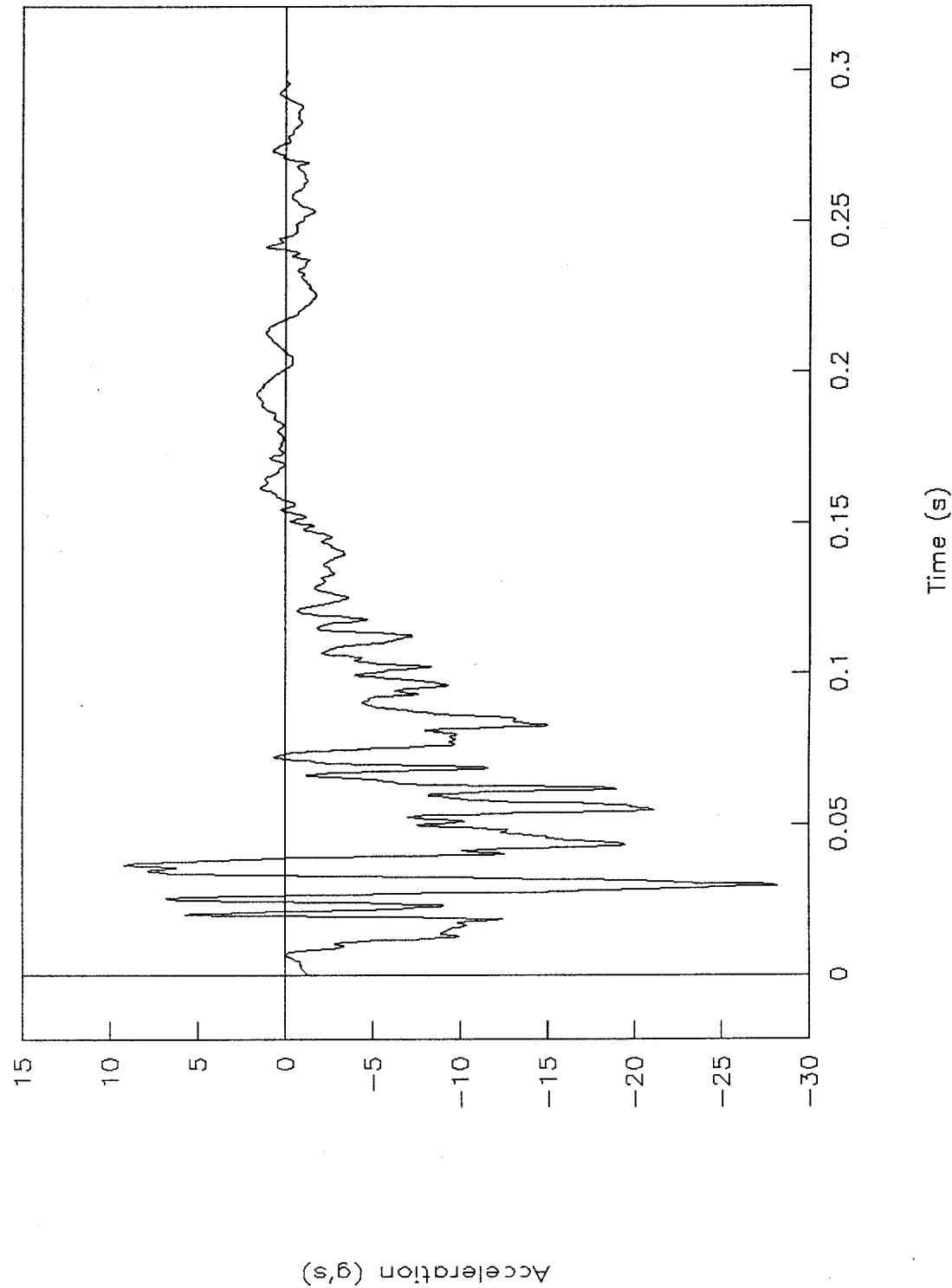


Figure 154. C.g. acceleration vs. time, Y-axis, test 99S001.

Test No. 99S001
Cg. velocity vs. time, Y-axis

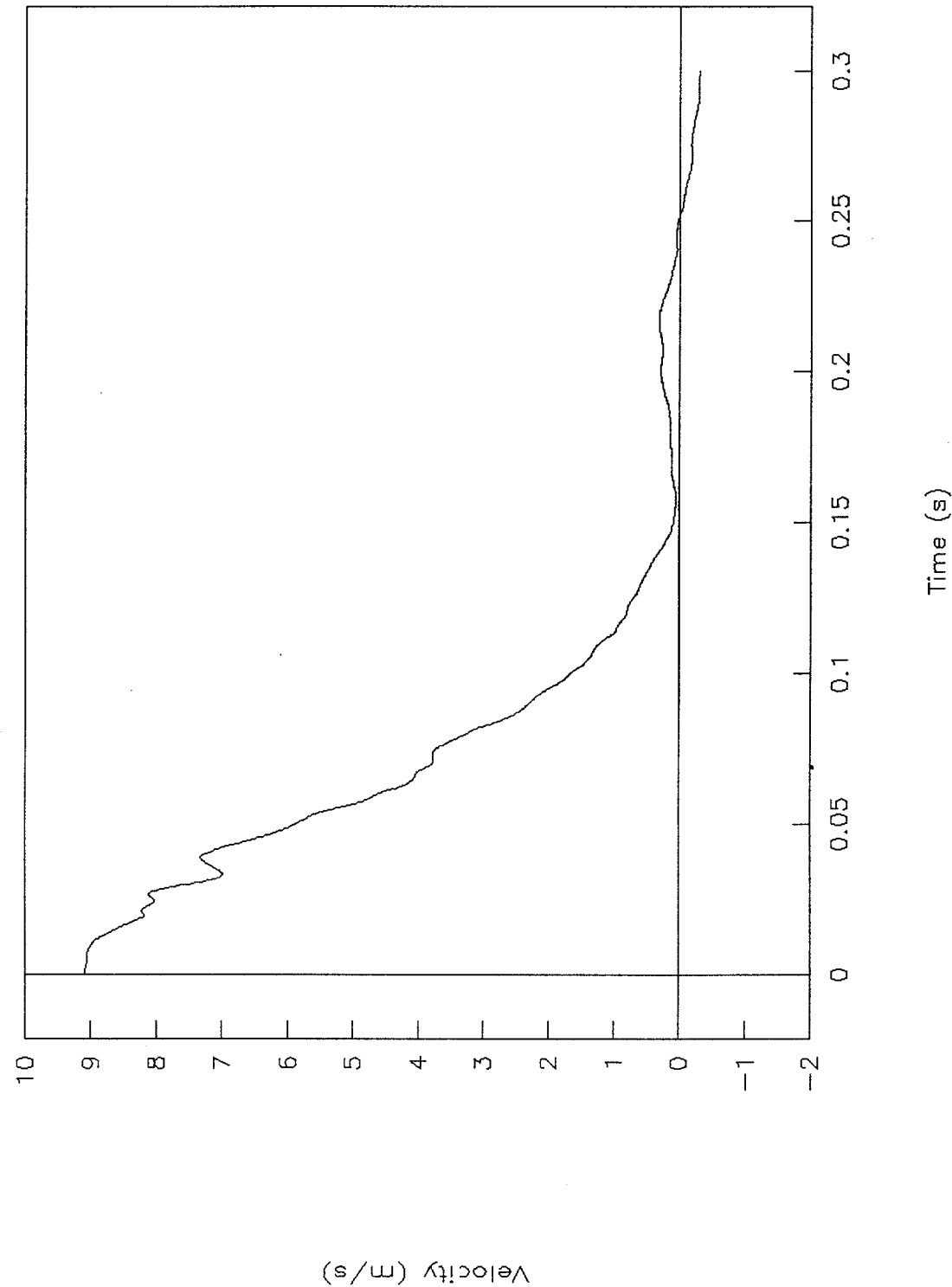


Figure 155. C.g. velocity vs. time, Y-axis, test 99S001.

Test No. 99S001

Cg displacement vs. time, Y-axis

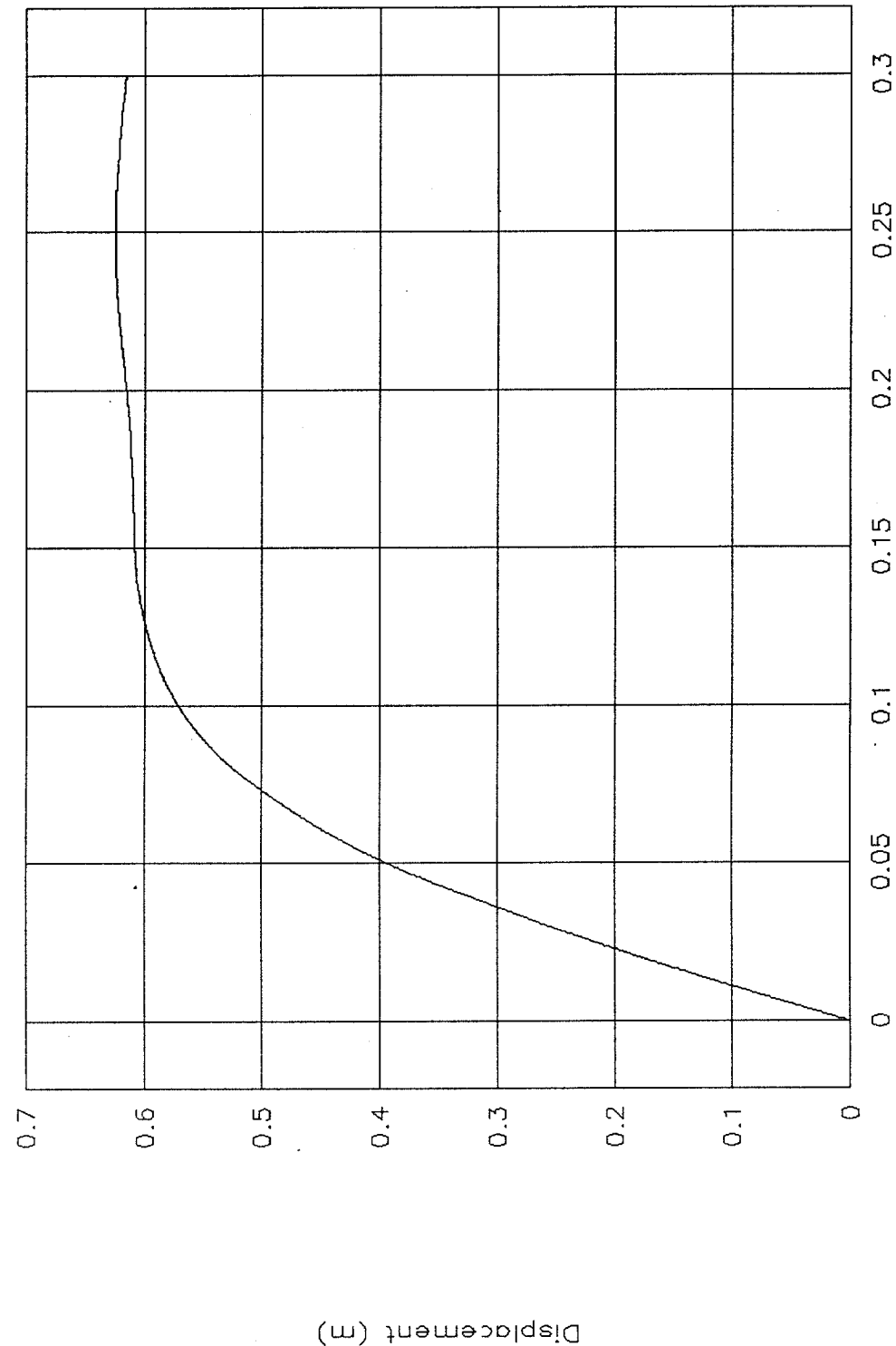


Figure 156. C.g. displacement vs. time, Y-axis, test 99S001.

Test No. 99S001
Cg force vs. displacement, Y-axis

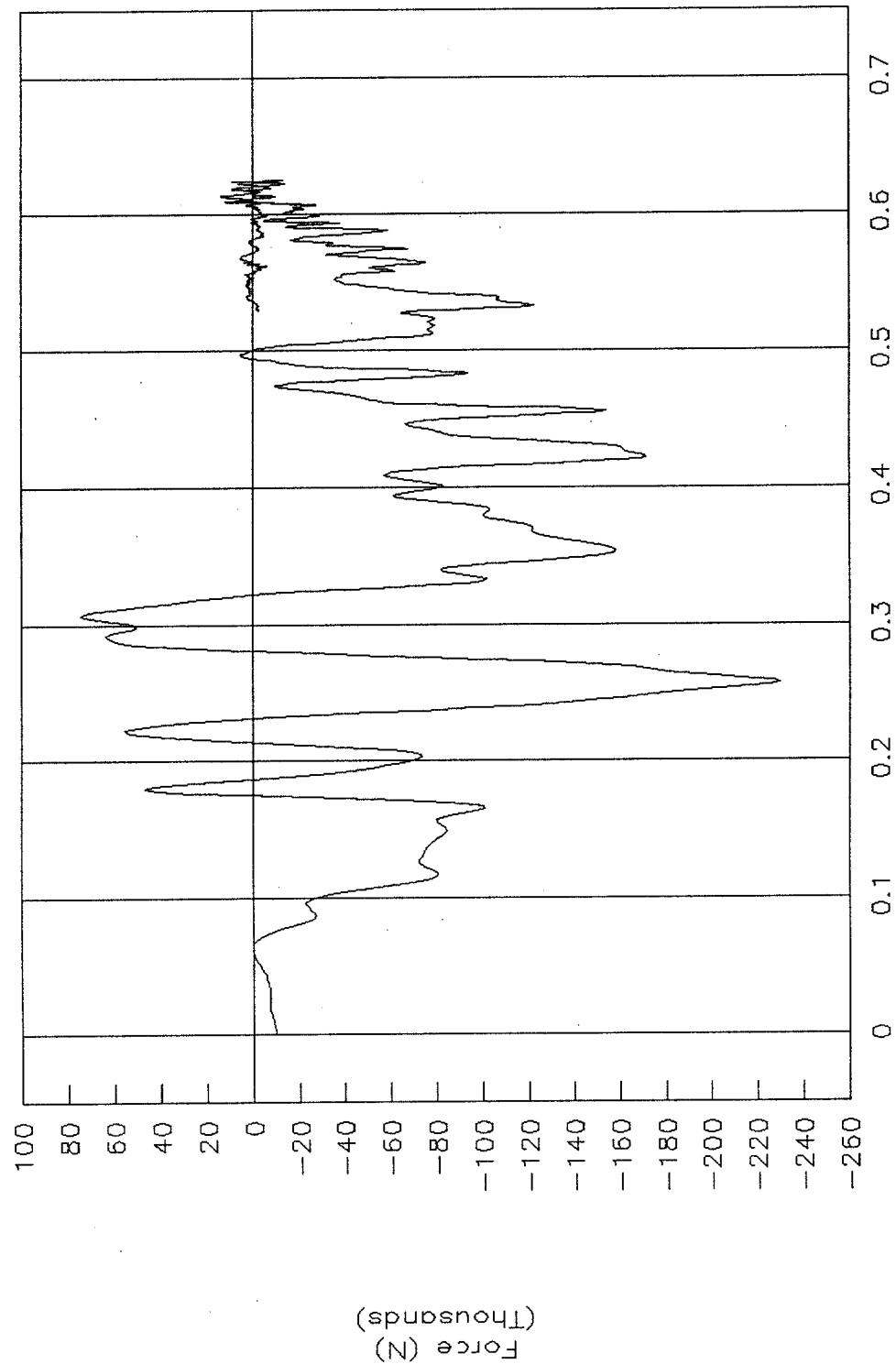


Figure 157. C.g. force vs. displacement, Y-axis, test 99S001.

Test No. 99S001
Cg energy vs. displacement, Y-axis

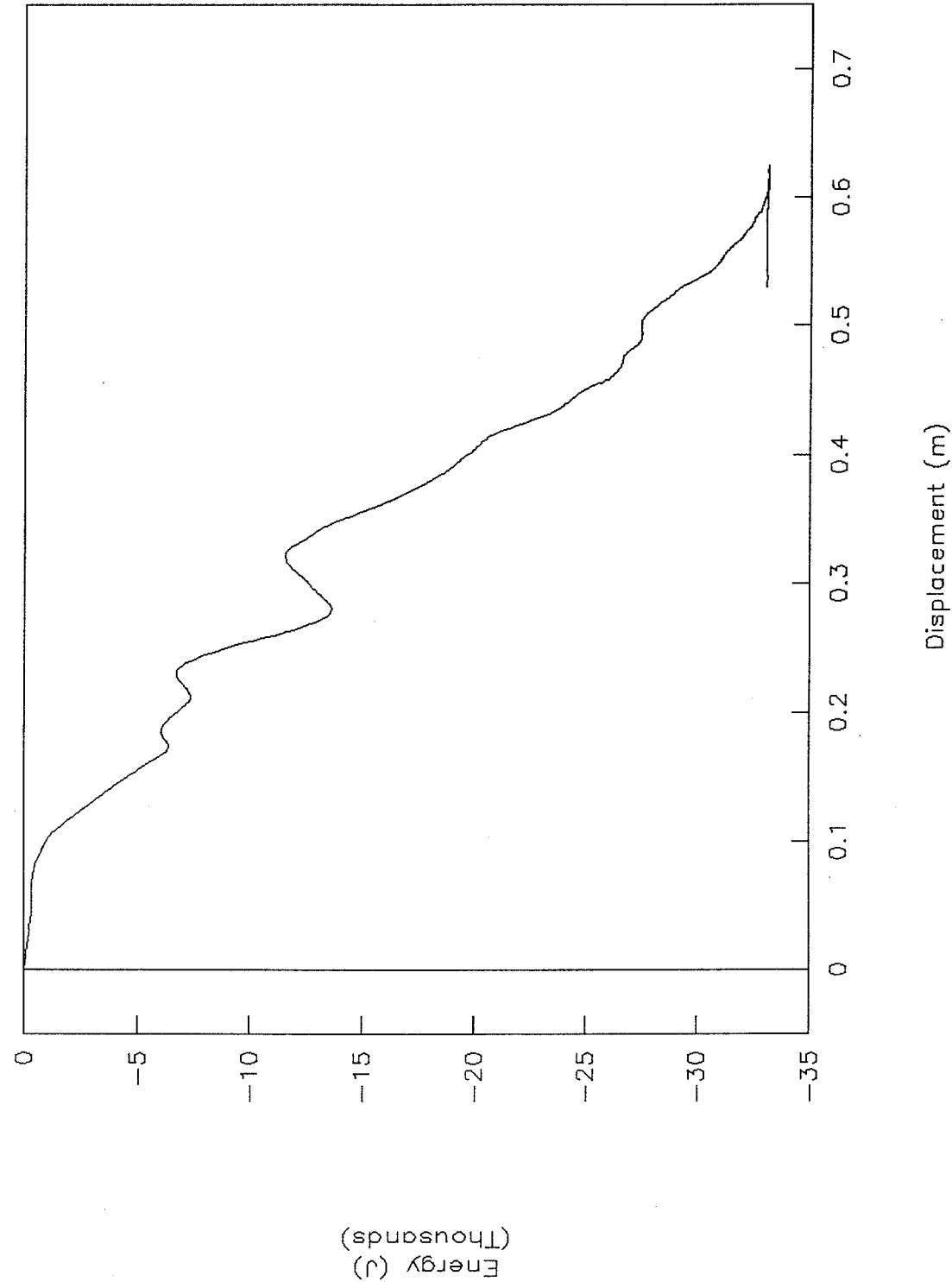


Figure 158. C.g. energy vs. displacement, Y-axis, test 99S001.

Test No. 99S001
Cg acceleration vs. time, X-axis

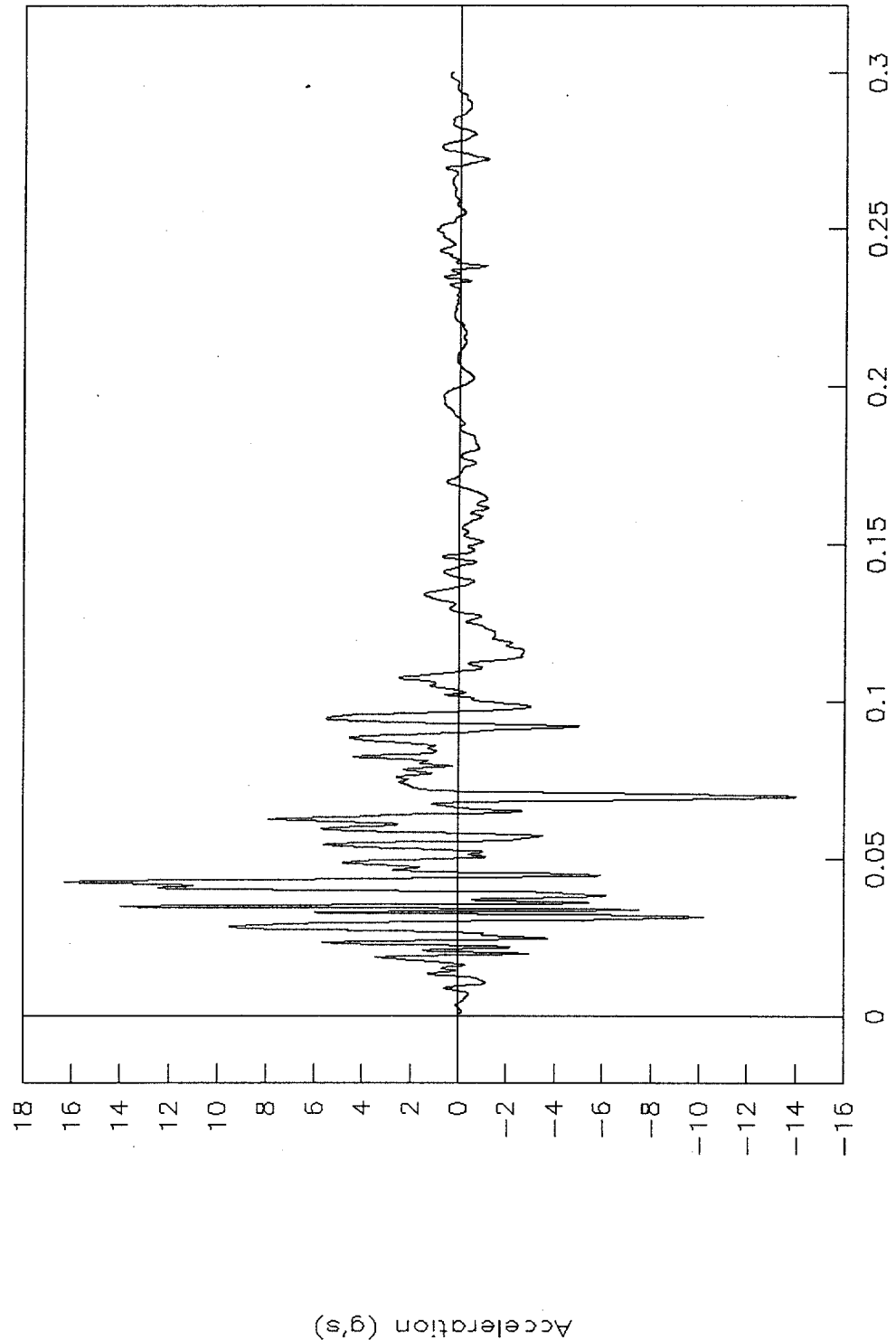


Figure 159. C.g. acceleration vs. time, X-axis, test 99S001.

Test No. 99S001
Cg acceleration vs. time, Z-axis

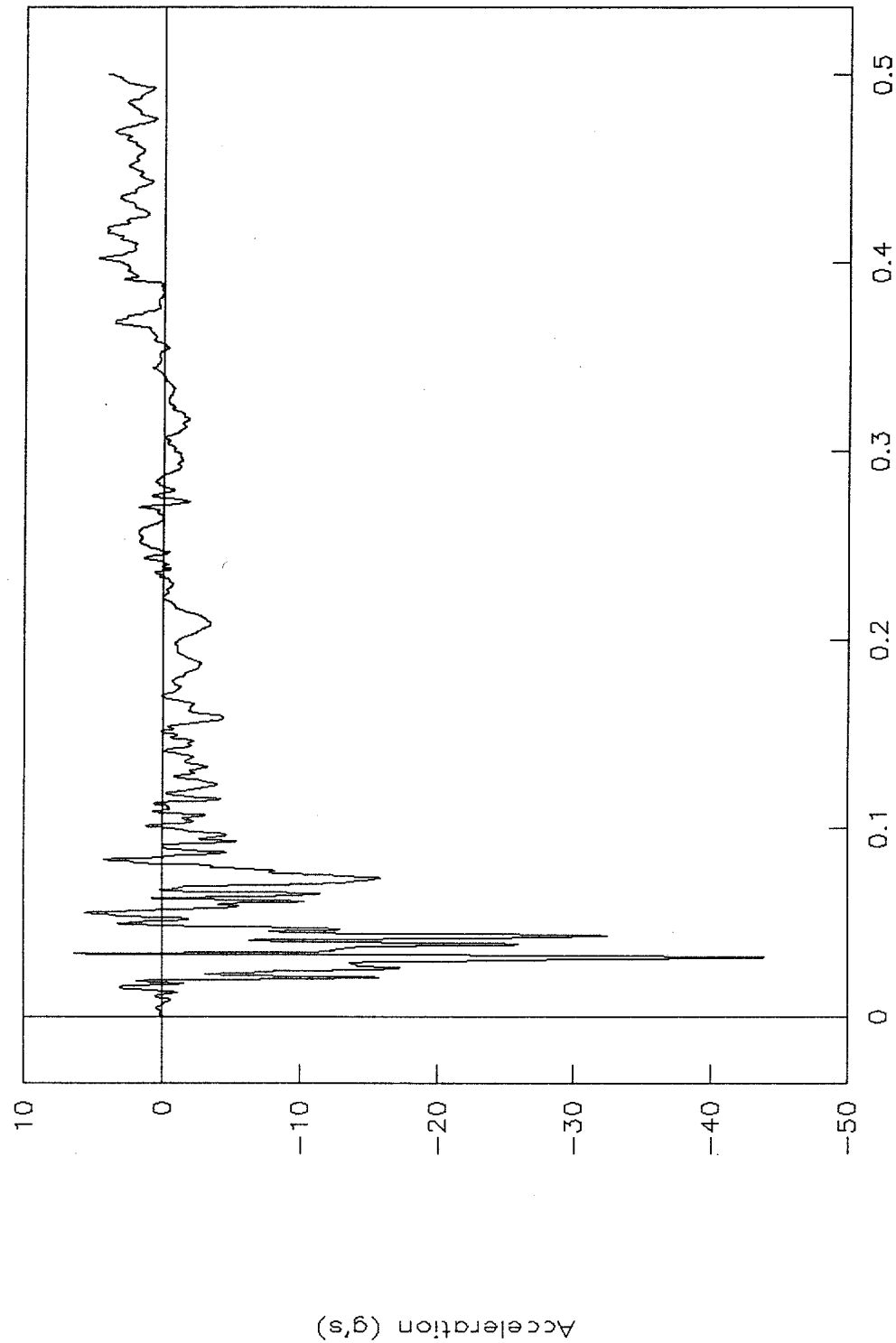


Figure 160. C.g. acceleration vs. time, Z-axis, test 99S001.

Test No. 99S001
Rigid pole, force vs. time

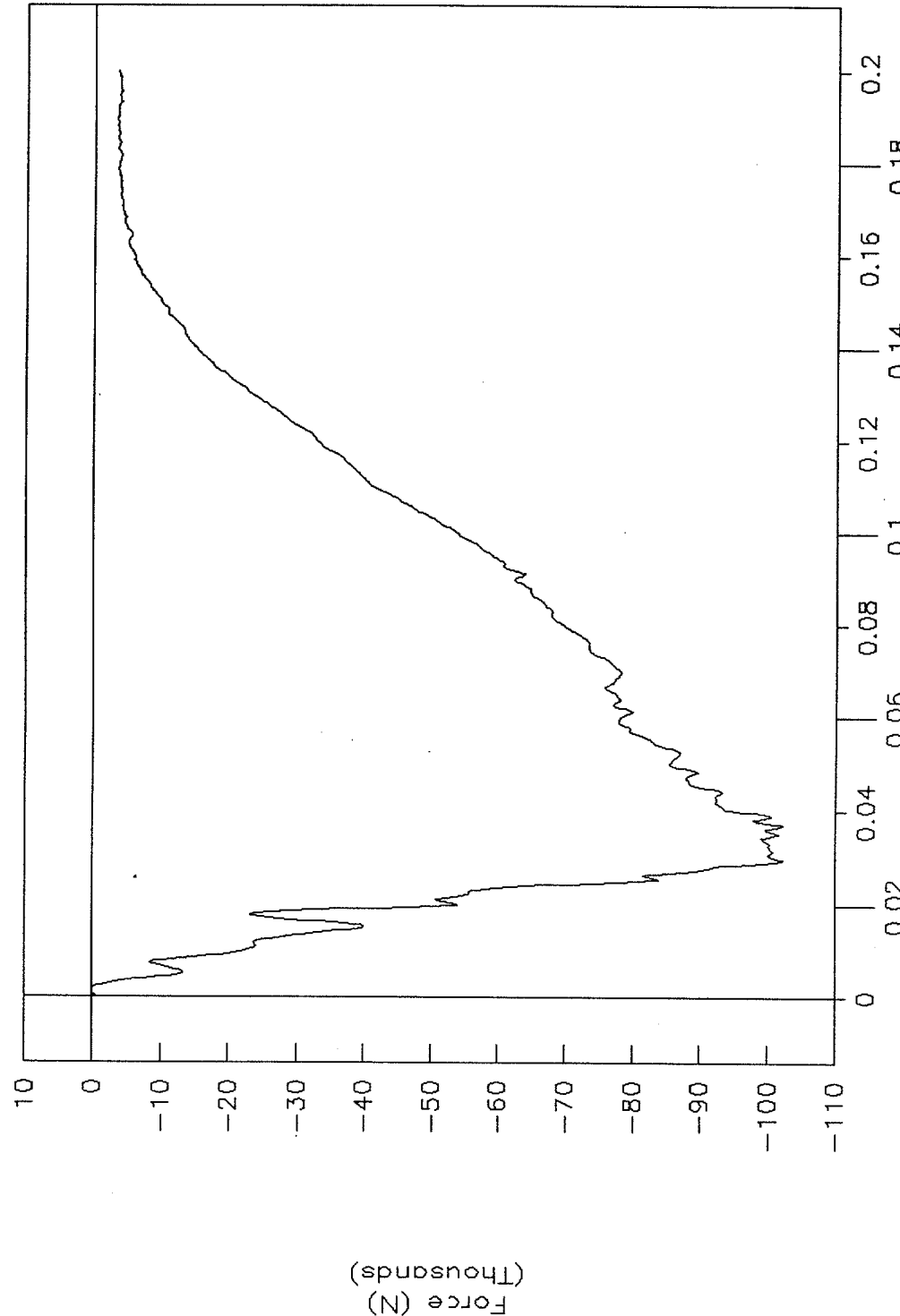


Figure 161. Rigid pole, force vs. time, test 99S001.

Test No. 99S001

Rigid pole, acceleration vs. time

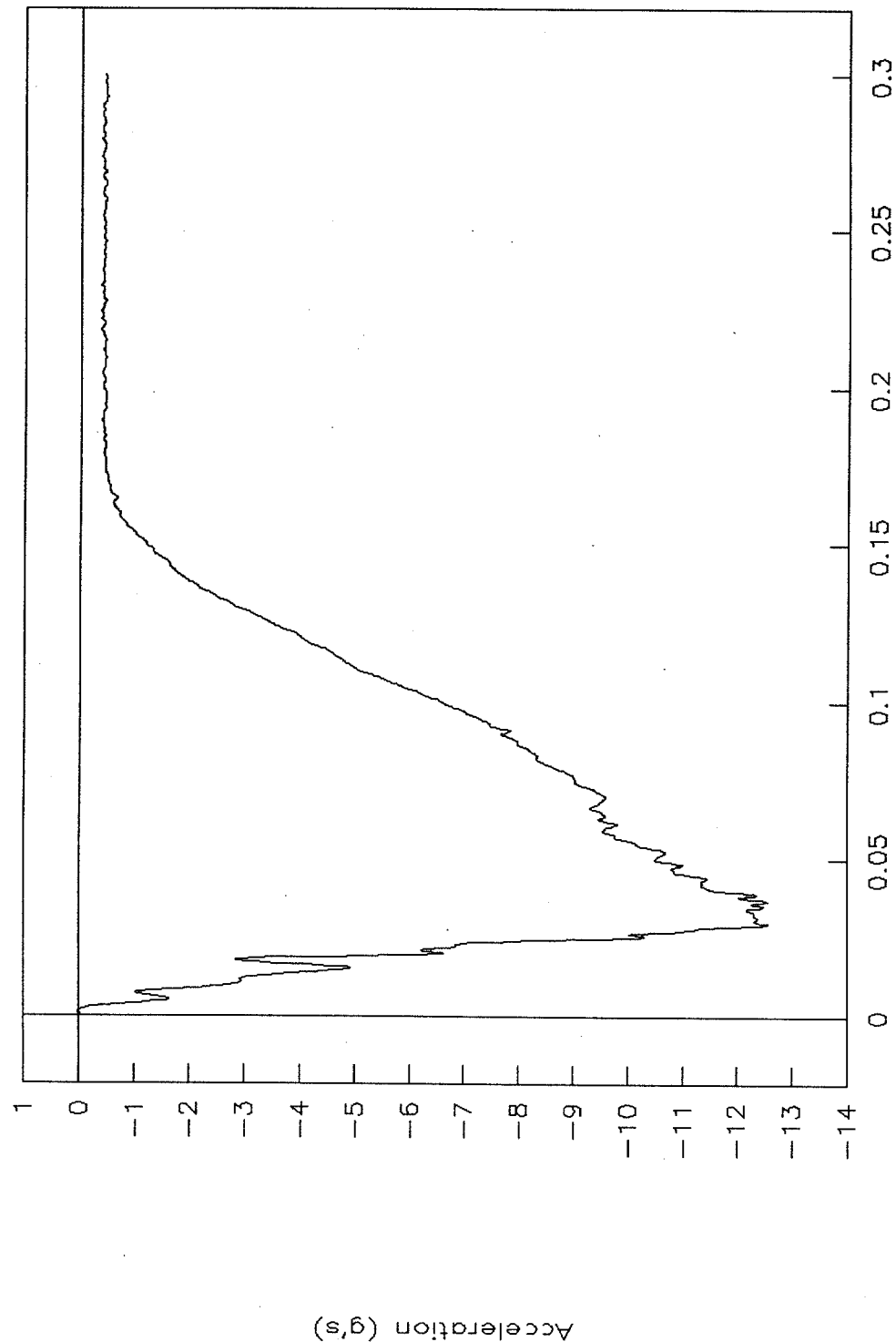


Figure 162. Rigid pole, acceleration vs. time, test 99S001.

Test No. 99S001
Rigid pole, velocity vs. time

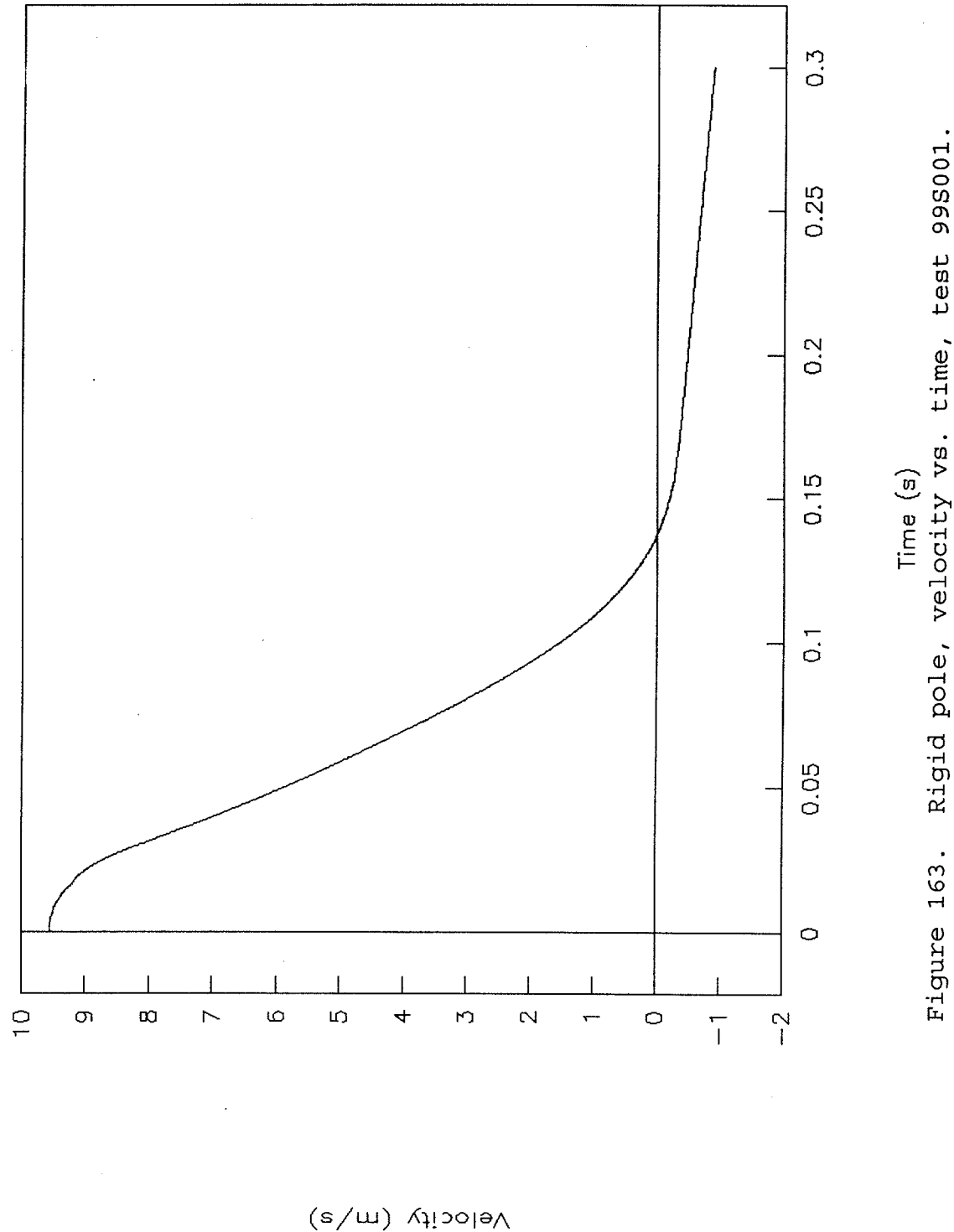


Figure 163. Rigid pole, velocity vs. time, test 99S001.

Test No. 99S001
Rigid pole, displacement vs. time

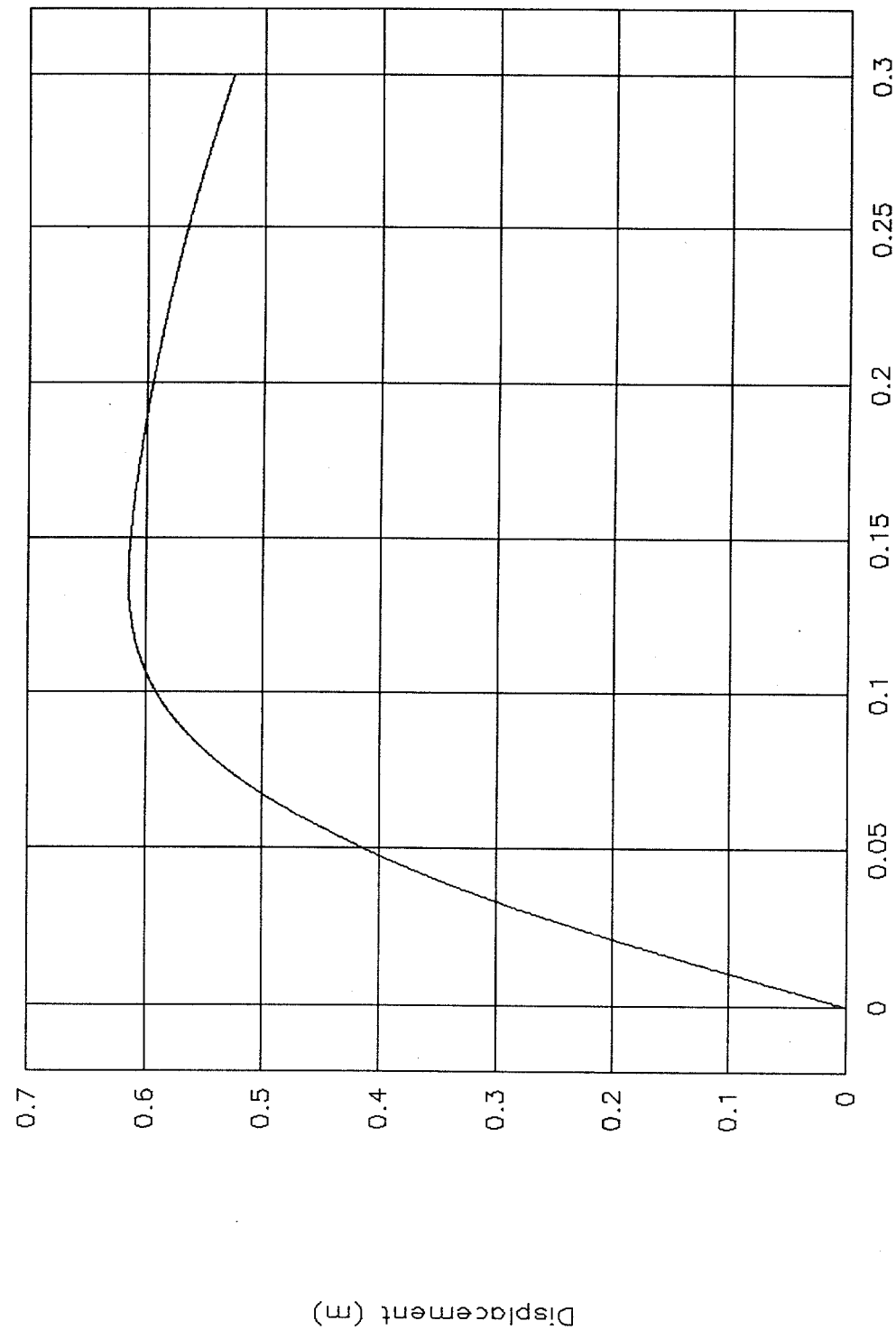


Figure 164. Rigid pole, displacement vs. time, test 99S001.

Test No. 99S001
Rigid pole, force vs. displacement

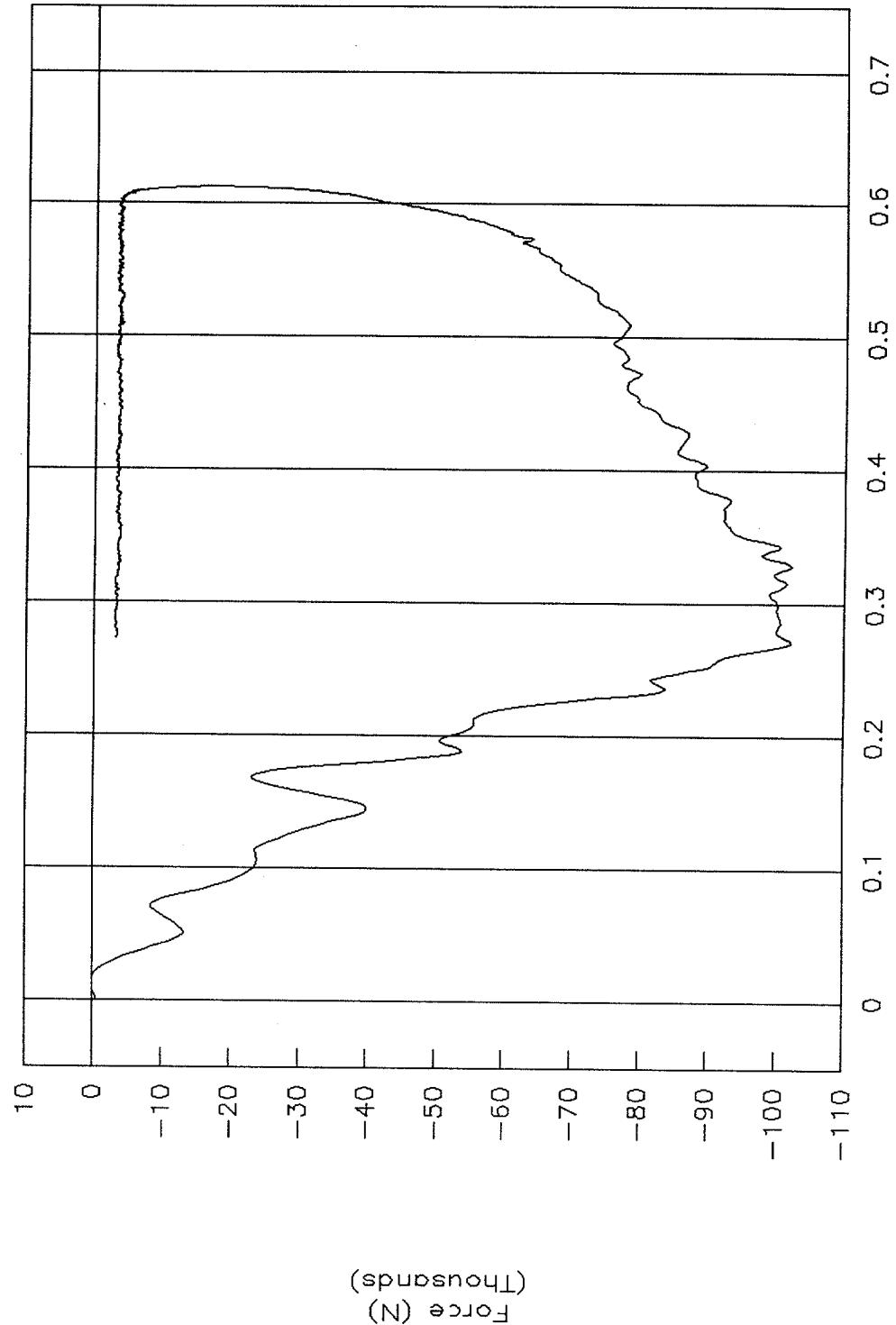


Figure 165. Rigid pole, force vs. displacement, test 99S001.



Test No. 99S001

Rigid pole, energy vs. displacement

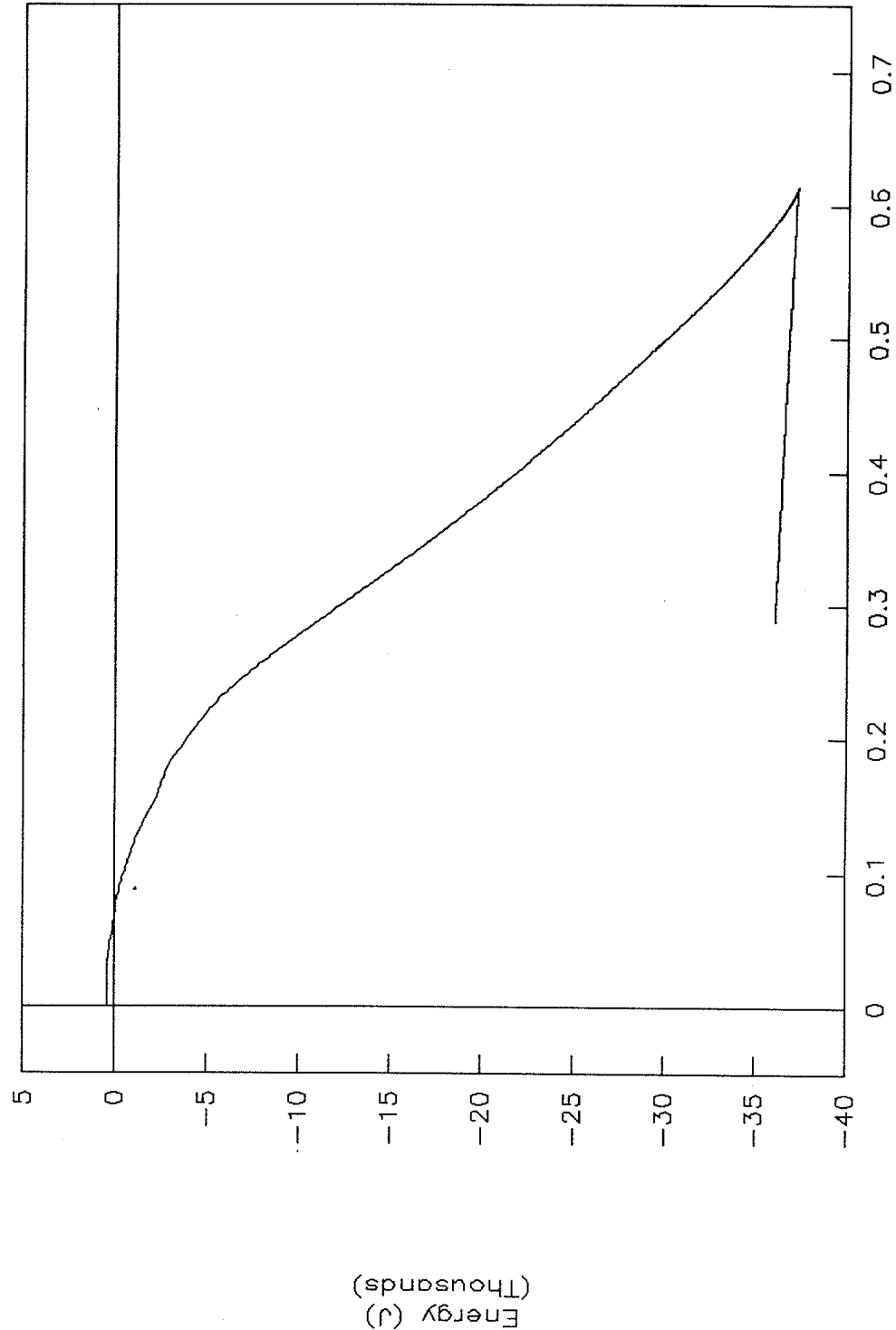


Figure 166. Rigid pole, energy vs. displacement, test 99S001.

Test No. 99S001

Outer door-skin, acceleration vs. time

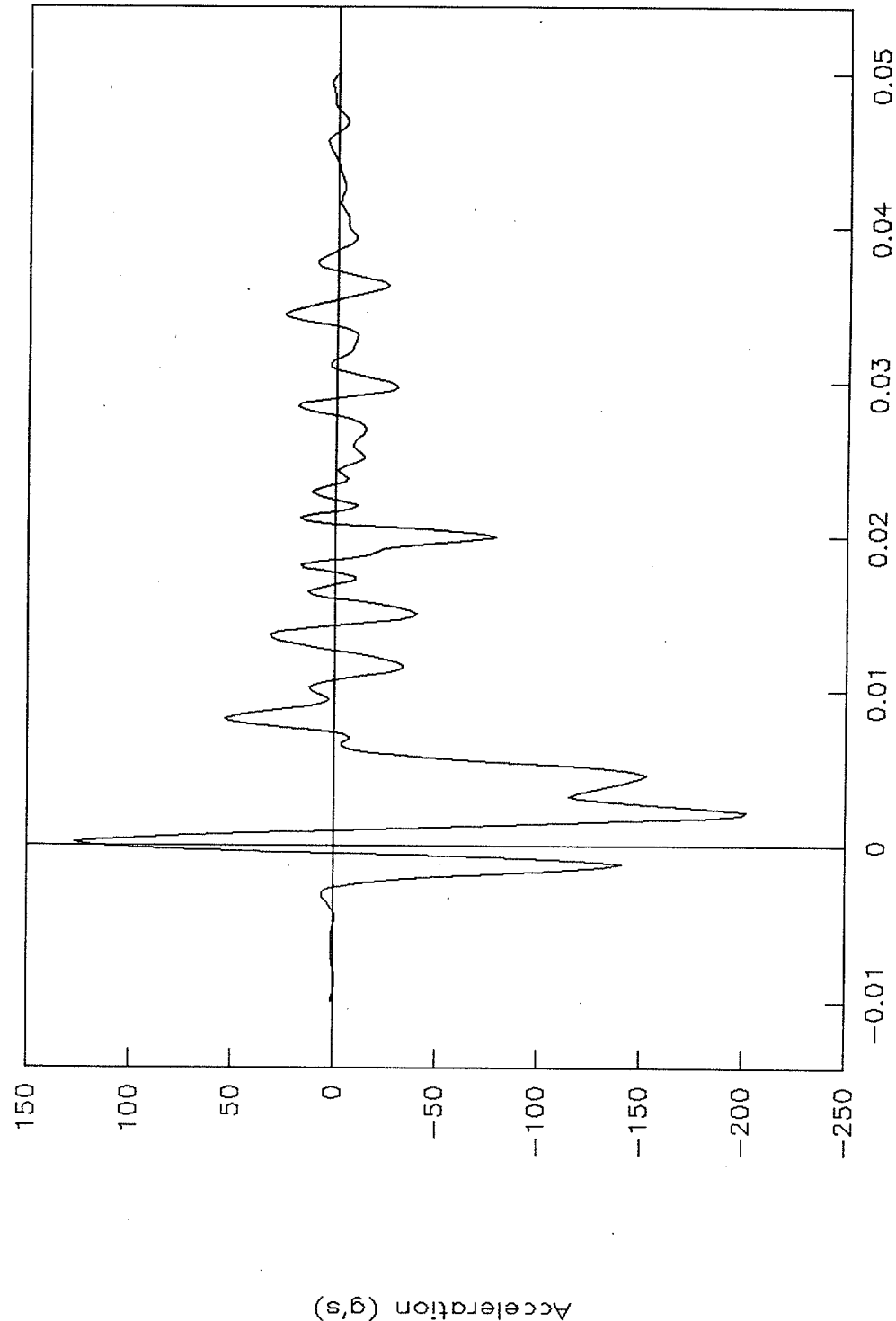


Figure 167. Outer door-skin, acceleration vs. time, test 99S001.



Test No. 99S001
Top of engine, Y-axis

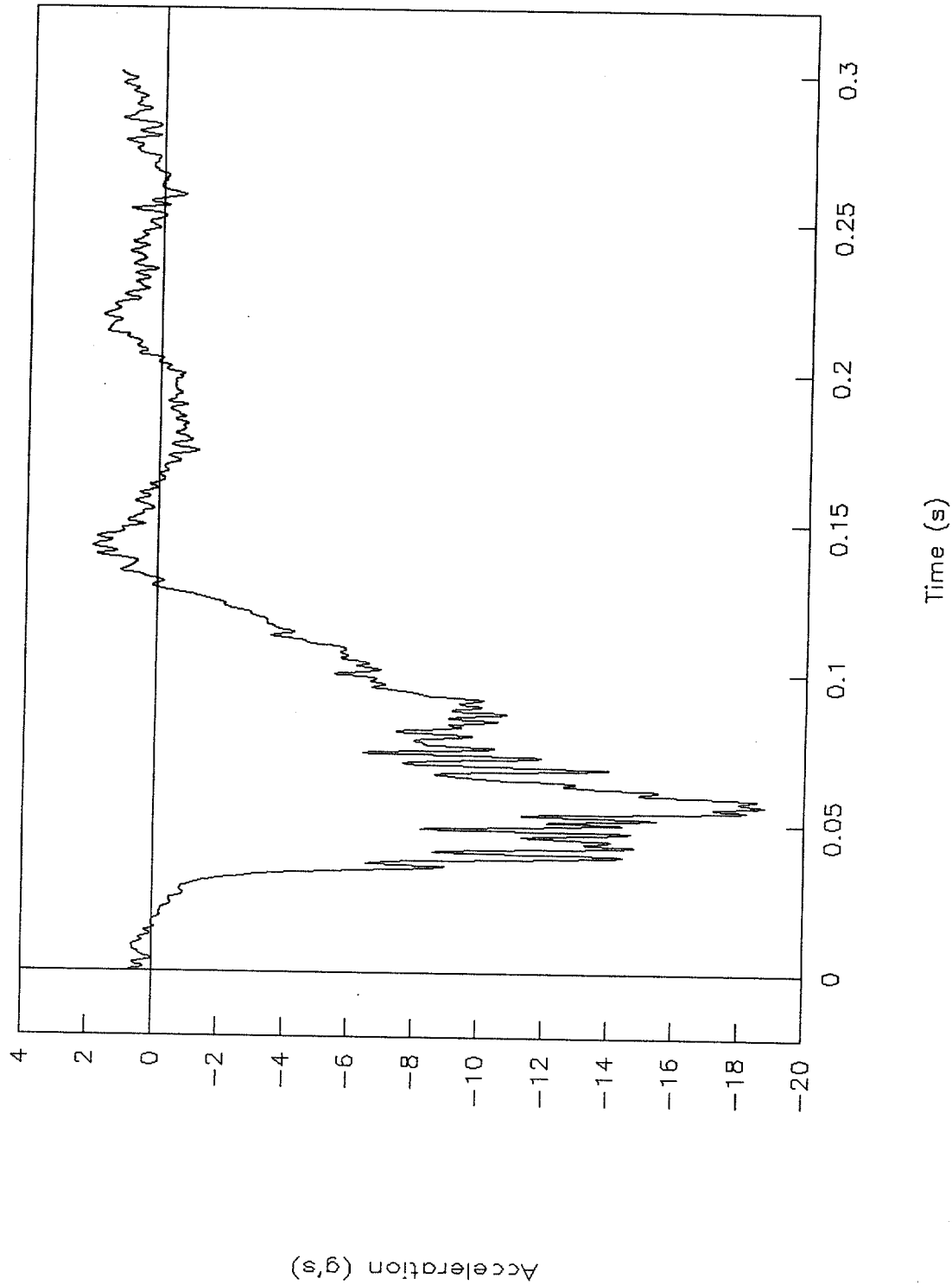


Figure 169. Top of engine acceleration vs. time, Y-axis, test 99S001.



Test No. 99S001
Top of engine, X-axis

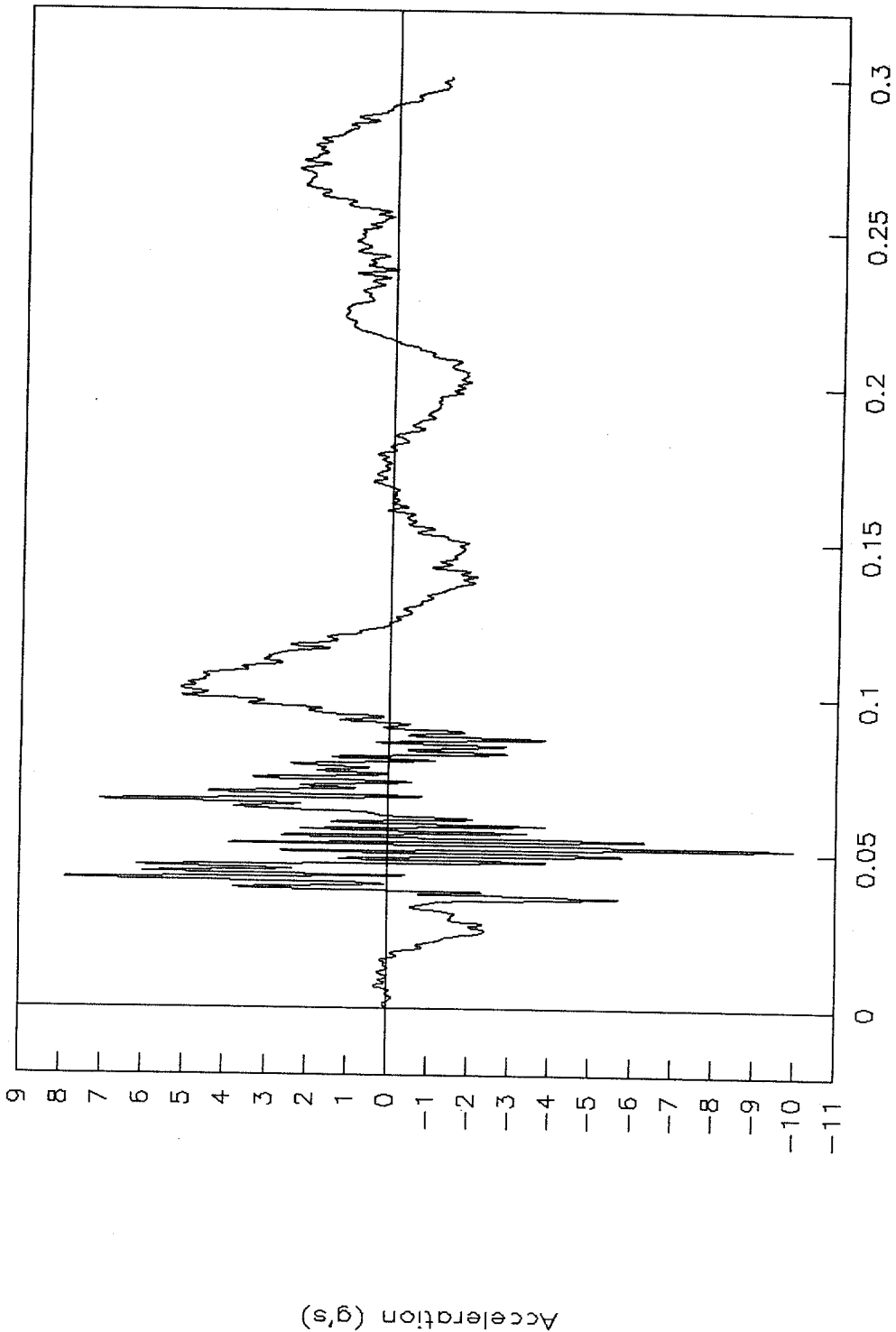


Figure 170. Top of engine acceleration vs. time, X-axis, test 99S001.



Test No. 99S001
Seat track, Y-axis

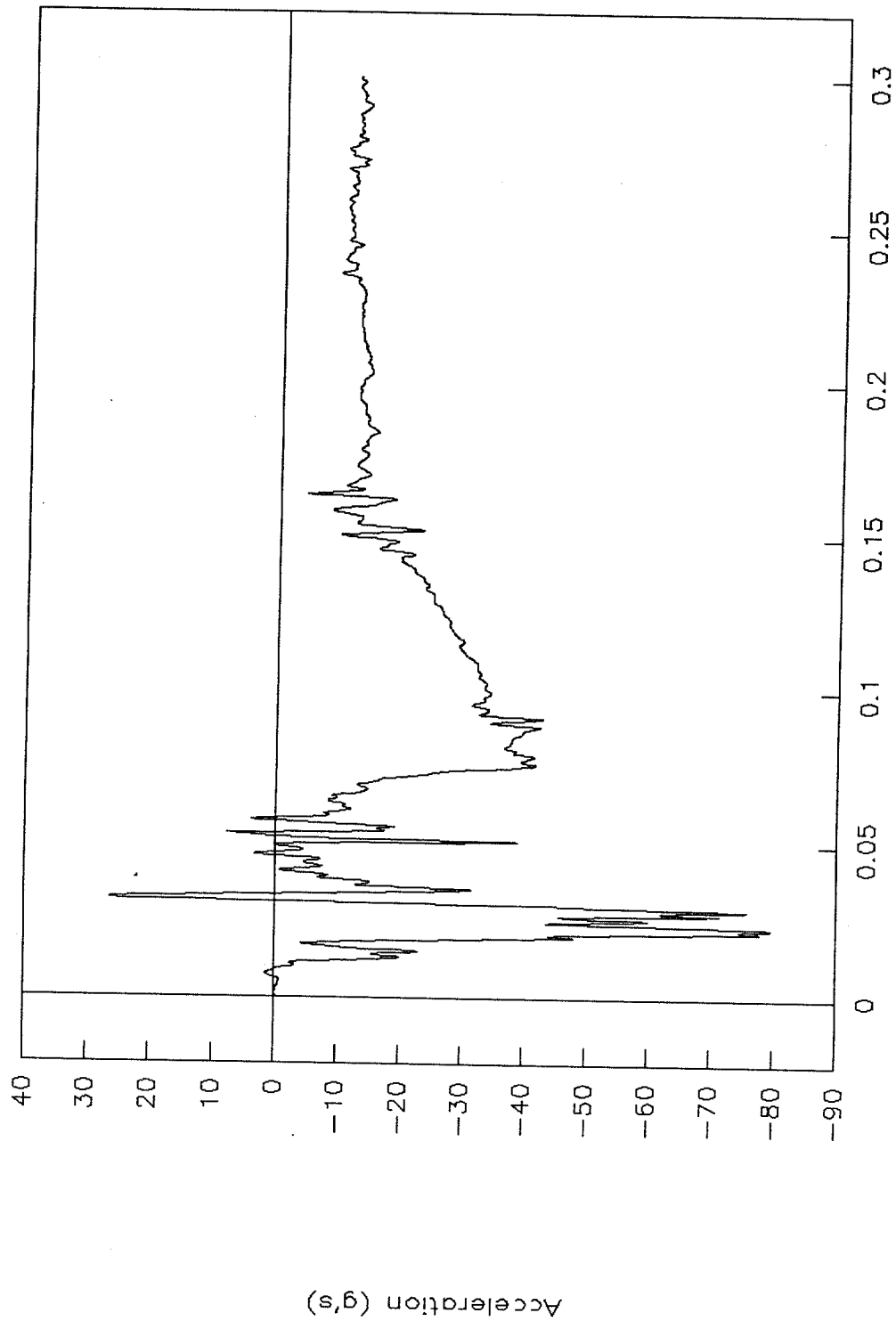


Figure 171. Seat track acceleration vs. time, Y-axis, test 99S001.



Test No. 99S001
Passenger side roof sill, Y-axis

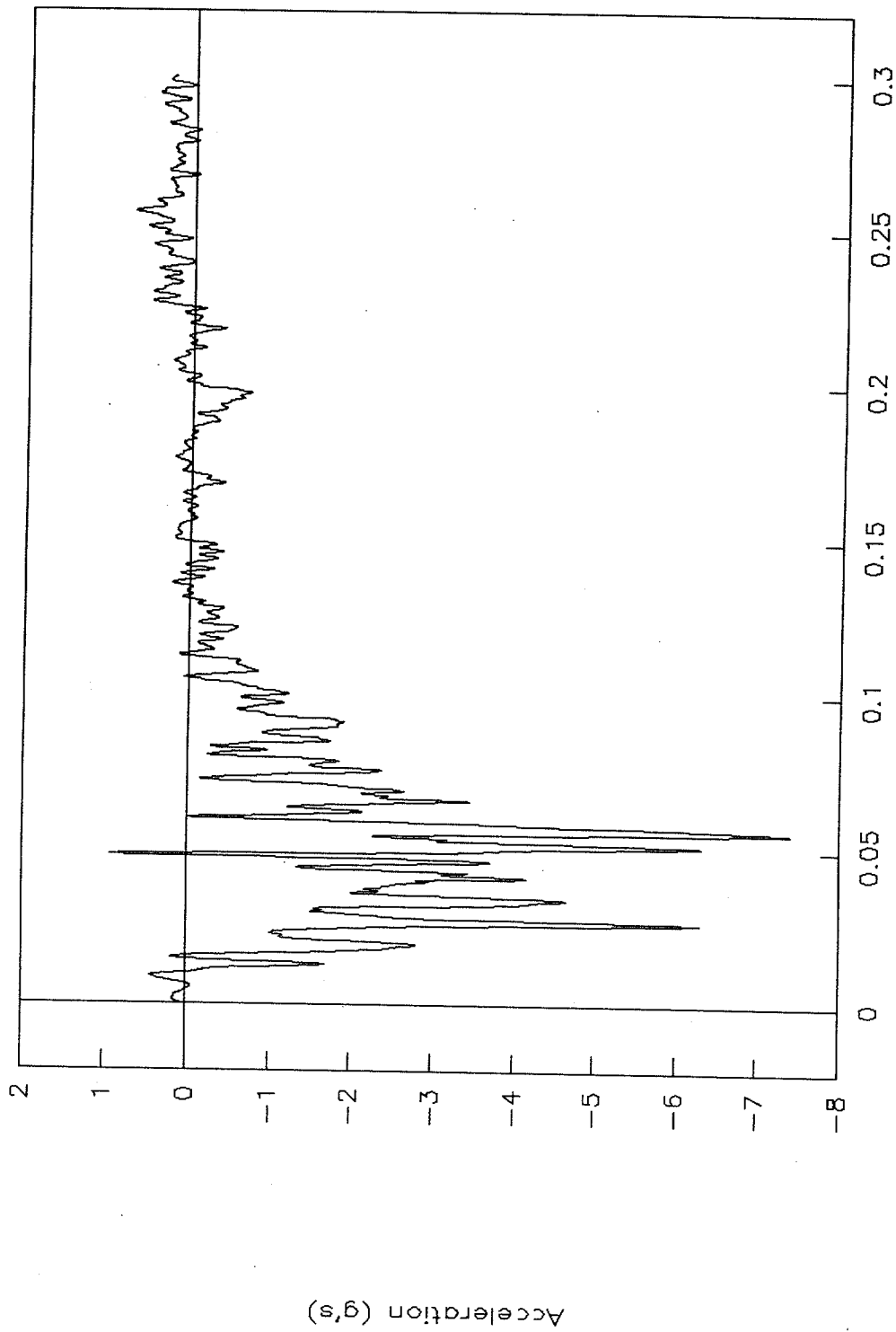


Figure 172. Passenger side roof-sill acceleration vs. time, Y-axis, test 99S001.



Test No. 99S001
Passenger side floor sill, Y-axis

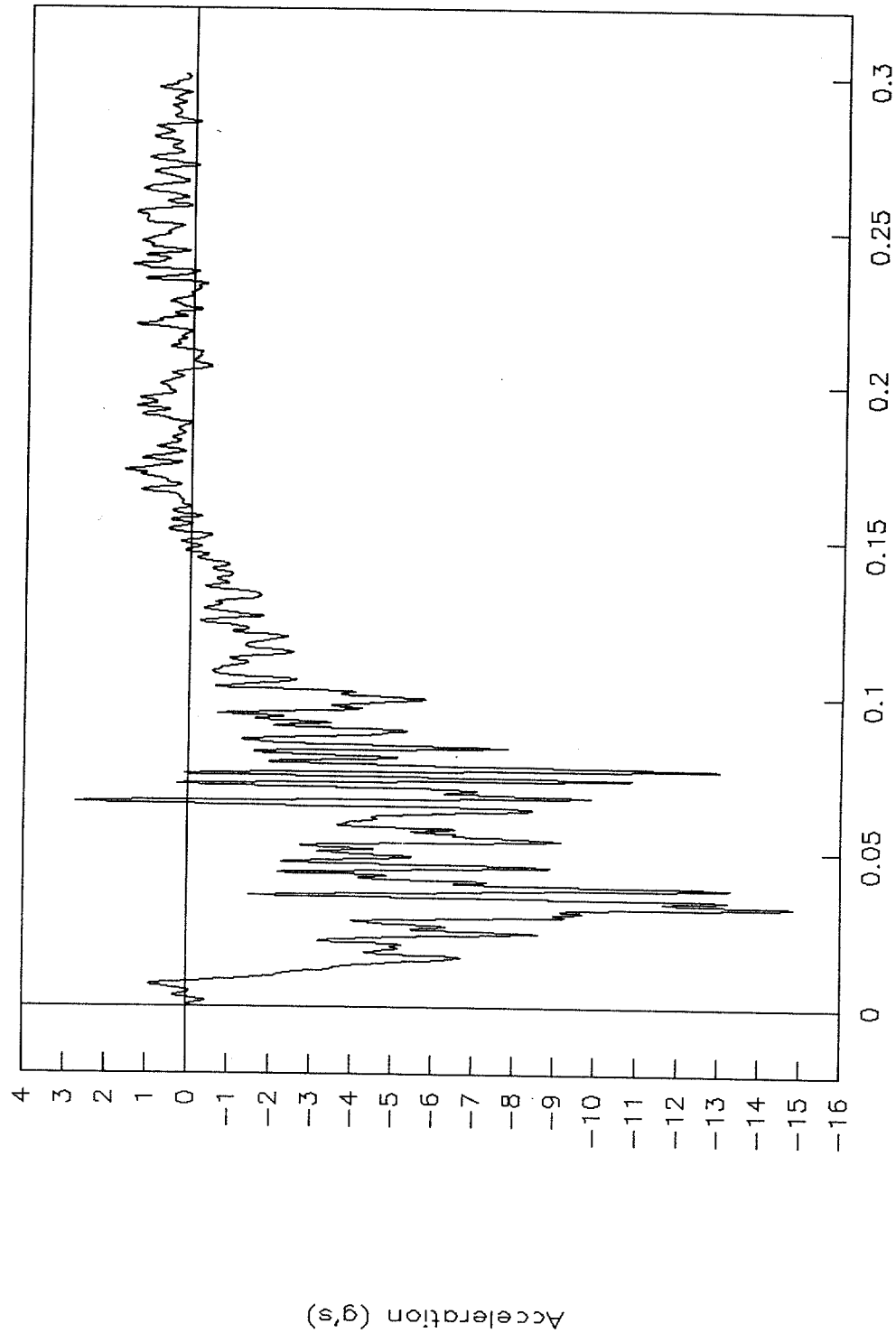


Figure 173. Passenger side floor-sill acceleration vs. time, Y-axis, test 99S001.



Test No. 99S001
Acceleration above rear axle, Y-axis

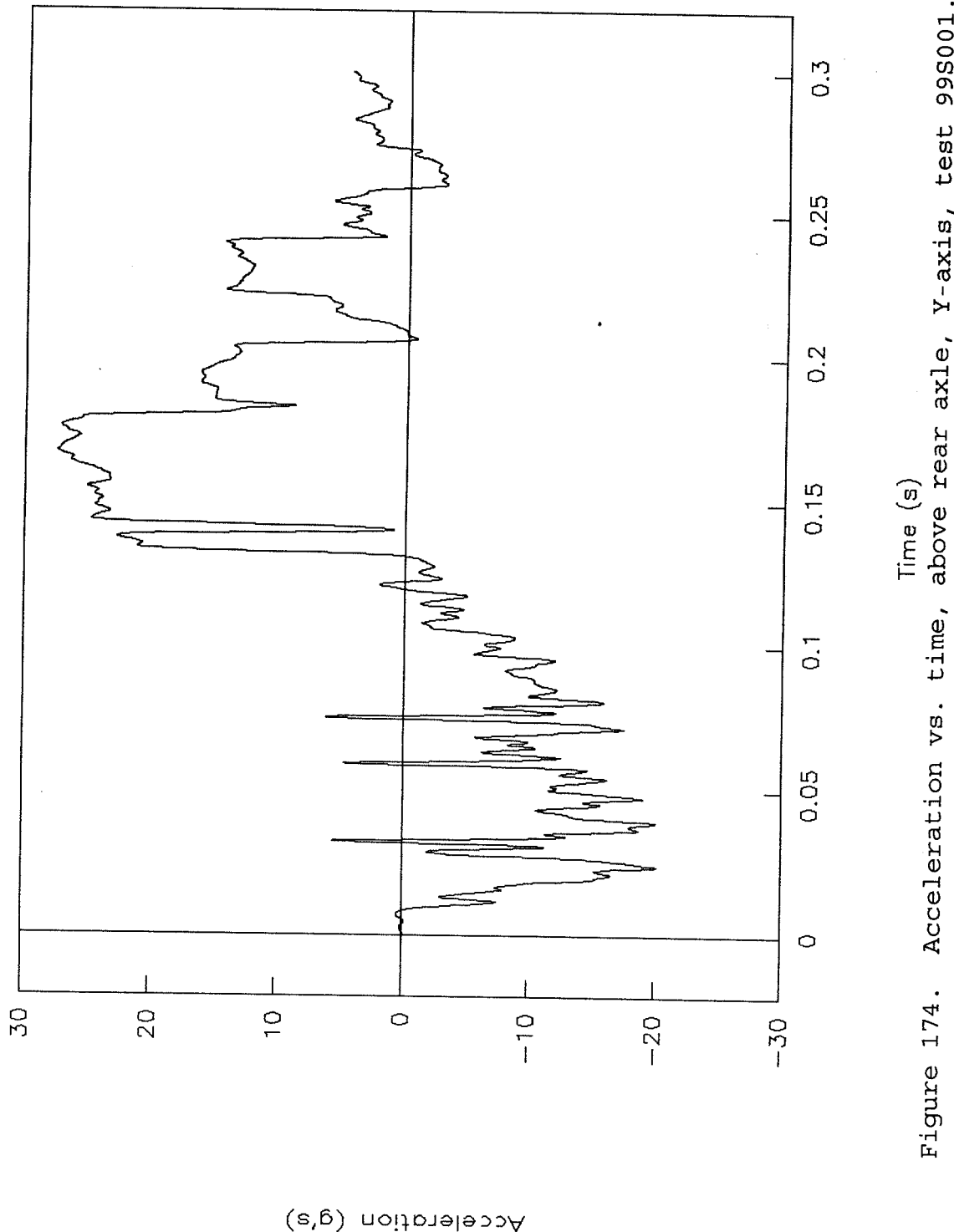


Figure 174. Acceleration vs. time, above rear axle, Y-axis, test 99S001.



Test No. 99S001
Acceleration above rear axle, X-axis

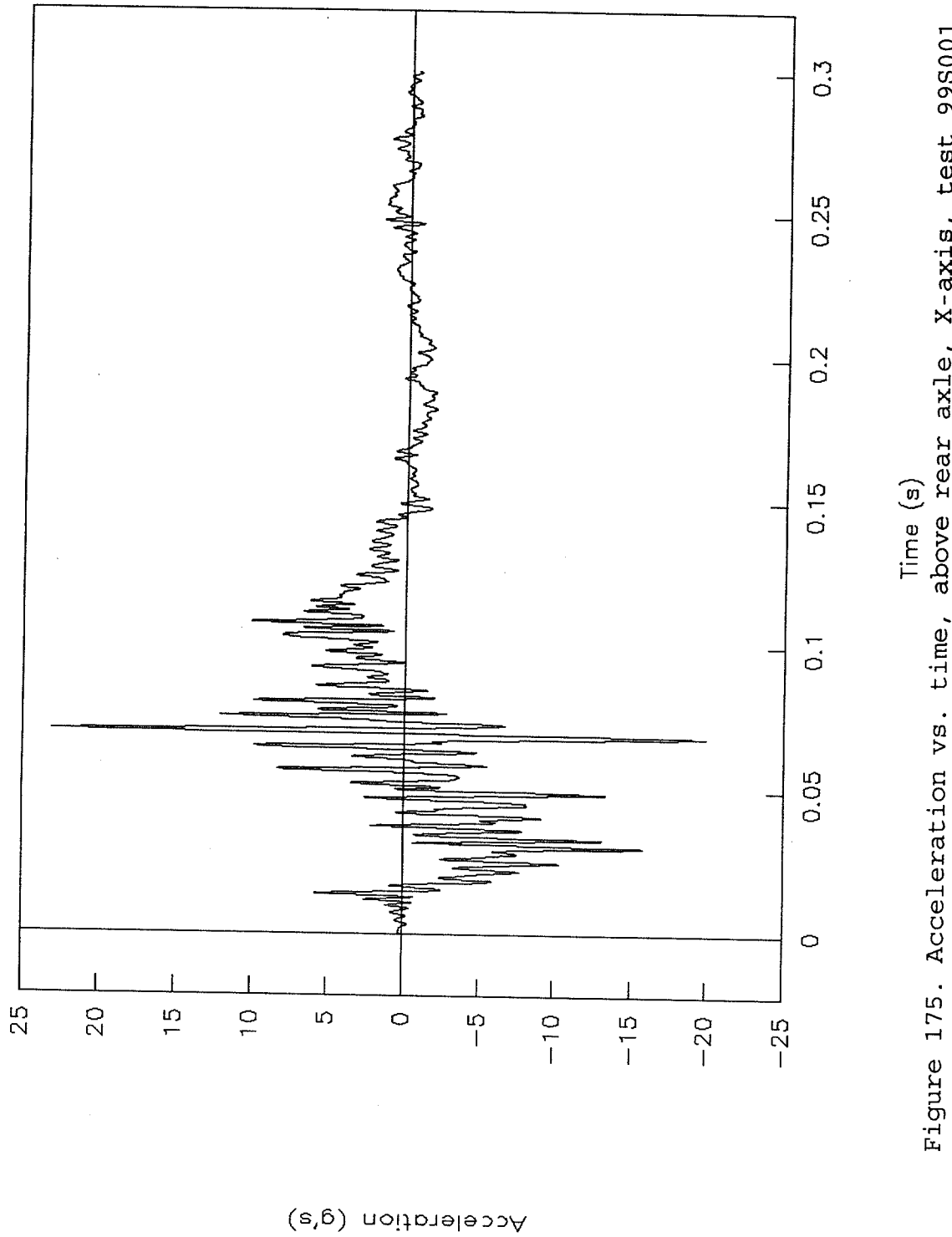


Figure 175. Acceleration vs. time, above rear axle, X-axis, test 99S001.



Test No. 99S001
Pitch rate and angle vs. time

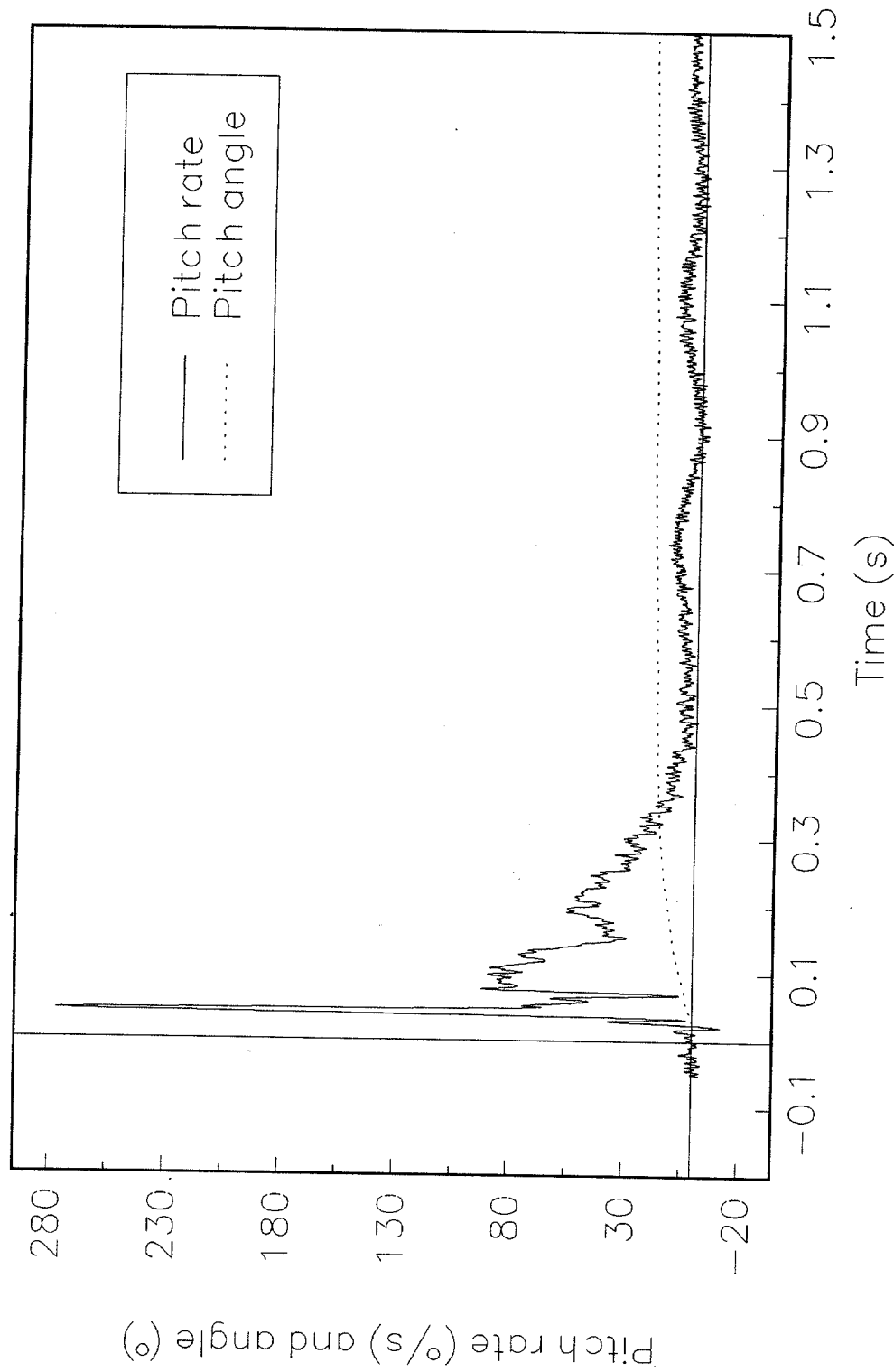
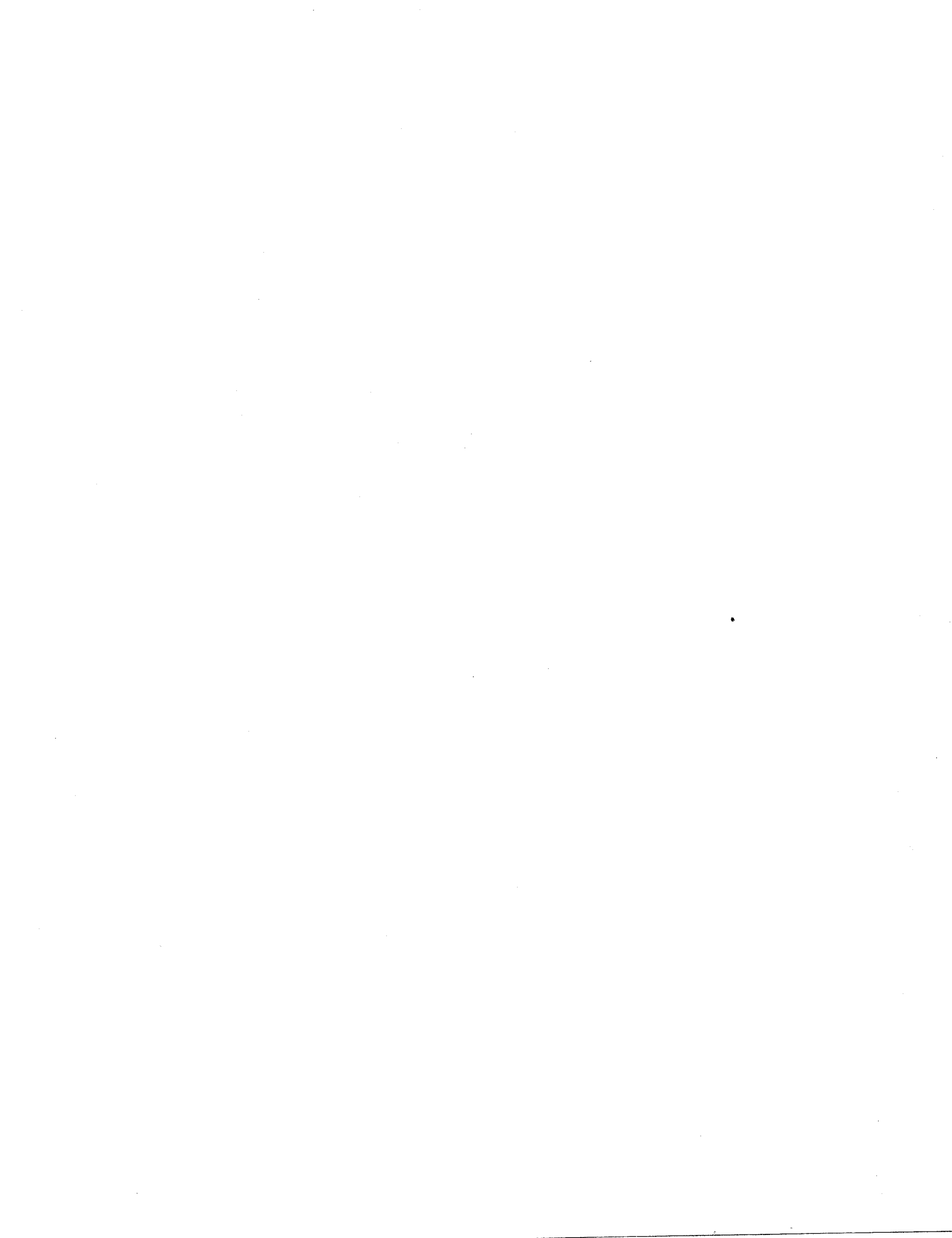


Figure 176. Pitch rate and angle vs. time, test 99S001.



Test No. 99S001
Roll rate and angle vs. time

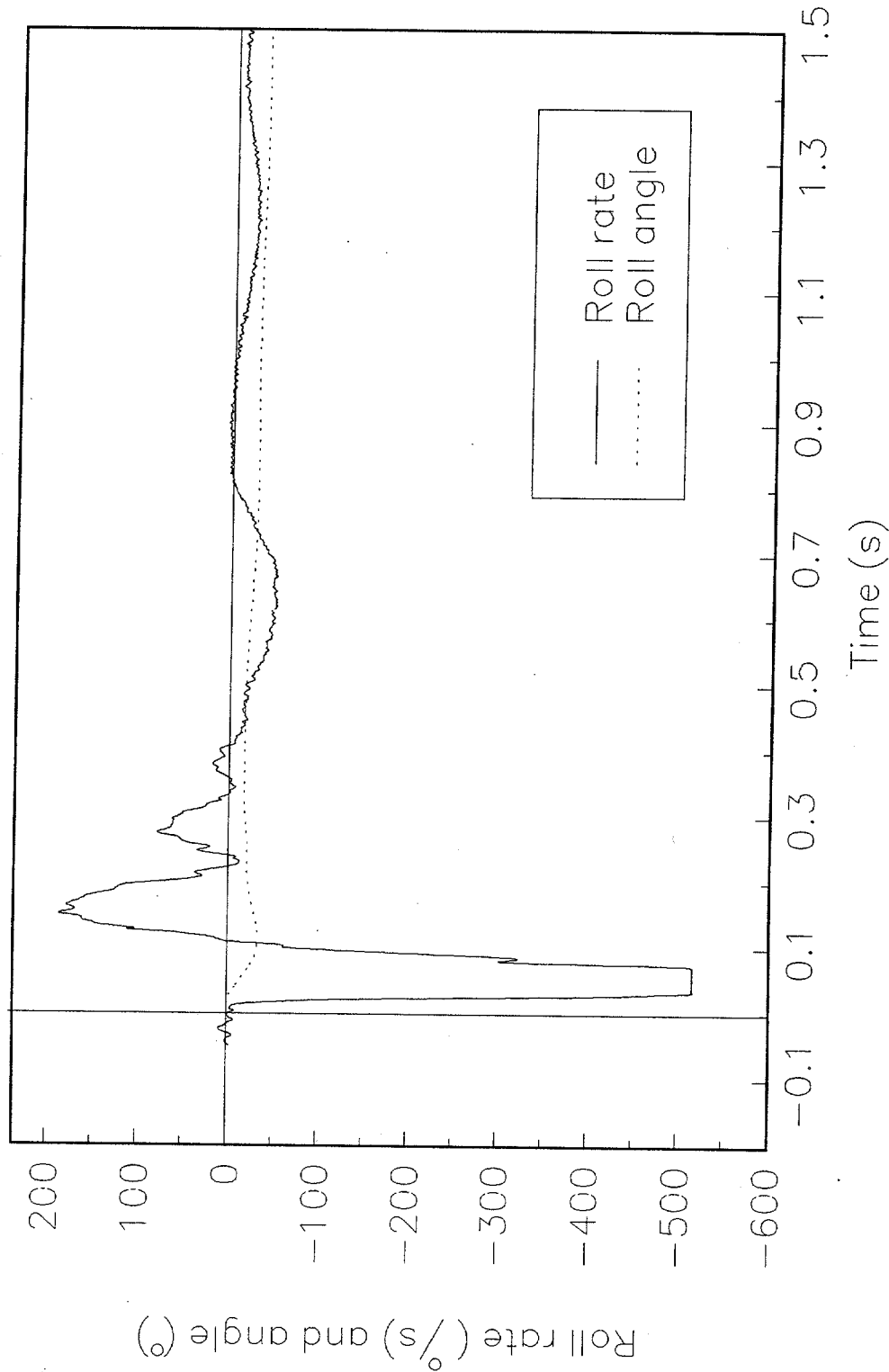


Figure 177. Roll rate and angle vs. time, test 99S001.



Test No. 99S001
Yaw rate and angle vs. time

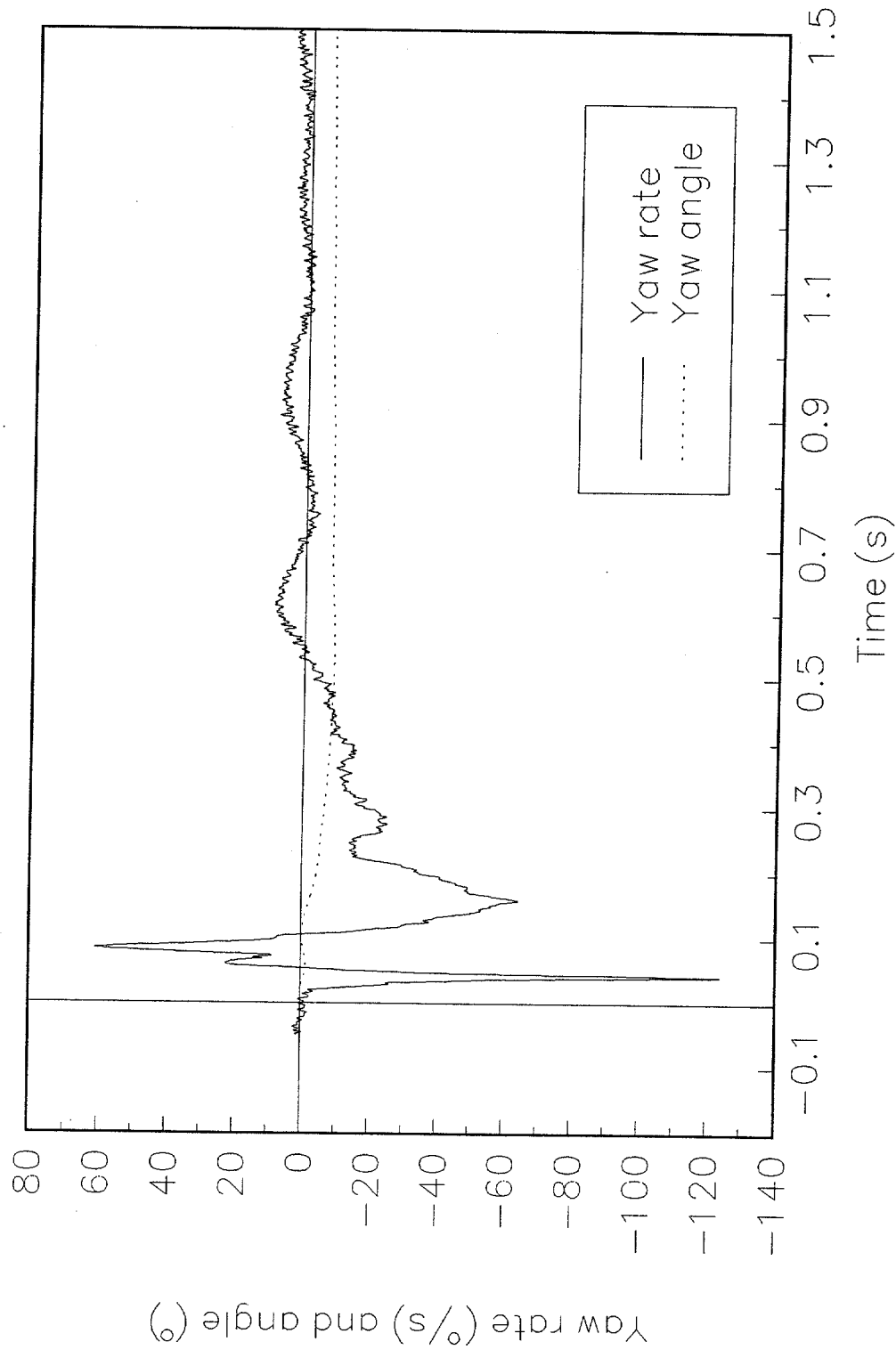


Figure 178. Yaw rate and angle vs. time, test 99S001.



REFERENCES

- (1) Ross, H. E. Jr., Sicking, D. L., Zimmer, R. A., and Michie, J.D., *Recommended Procedures for the Safety Performance Evaluation of Highway Features*, NCHRP Report 350, National Cooperative Highway Research Program, Transportation Research Board, Washington, DC, 1993.
- (2) NHTSA. *Laboratory Test Procedures for Federal Motor Vehicle Safety Standard 208*, National Highway Traffic Administration, Washington, DC, May 1992.

